The University of Hull

Development and Integration of Simplified Real-World to Chip Interfaces for Use in the Detection of Infectious Diseases

Being a Thesis submitted for the degree of Doctor of Philosophy at the University of Hull

by

Christopher Birch
MCHEM (University of Hull)

June 2014

Abstract

Bacterial-based infectious disease, such as sexually transmitted infections and hospital-acquired infections, present a worldwide burden on healthcare issues. To control the spread of infection and to inform clinical treatment, rapid point of care (POC) diagnosis is required. Although some are currently available, these are commonly limited by a requirement for sample processing prior to analysis and a requirement for user intervention. Novel real world-to-chip interfaces are required which can receive a sample with little or no pre-processing and should be manufactured with minimal cost. In addition, manufacturing protocols should ideally be developed to allow easy adjustment of design for customising to process a wide variety of sample types and volumes.

Here, focussing on bacterial-based POC diagnostics, a microfluidic platform has been developed which holds the potential to receive a variety of sample types for the detection of infectious organisms by implementing multiple sample-to-chip interfaces. The platform consists of a glass microfluidic device which is incorporated in to a custom-made integrated genetic analyser (IGA) for sample processing.

A series of interfacing substrates were investigated using two types of porous silica and the biopolymer chitosan (α(1→4)-linked 2-amino-2-deoxy-β-D-glucopyranose) as contributing materials. For analysis of urine samples, a porous silica monolith, synthesised from tetramethyl orthosilicate, was developed, capable of receiving and processing human urine samples (≈ 150 µl) for DNA capture and purification. Due to the nature of synthesis, these monoliths hold the potential for resizing and shaping, dependent on the sample volume and for integration to downstream steps, such as polymerase chain reaction (PCR) amplification. The monolith was first optimised structurally using flow systems made from monoliths encased in heat shrink wrap and was incorporated in to a microfluidic device by way of disk. The latter was achieved by sealing the monolith in place with a sondary porous silica phase synthesised from potassium silicate, creating a dual porous silica (DPS) real world interface. The DNA extraction efficiencies of monolithic flow systems and the DPS system were 51 % and 44 % respectively. The DPS was shown to provide DNA of sufficient quality and integrity to support PCR amplification for both *Chlamydia trachomatis* and *Neisseria gonorrhoea* target sequences. The system

did however lack sensitivity (1.3×10^{-3} ng DNA μl^{-1} urine), when compared with systems of similar applications in the literature, likely due to large elution volumes (> 20 µl) and/or ethanol carryover. In addition, chitosan was introduced to the silica surface of the monolith as an alternative methodology for DNA extraction by anion exchange. The system provided DNA extraction efficiencies of 40 % and DNA was subsequently amplified by PCR.

Using an alternative application, an investigation was also carried out in to the analysis of small volume blood samples (≤ 6 µl) for use in the same system. This was achieved by implementing a Phusion® blood direct kit in to a glass microfluidic device to amplify gDNA of bacterial target, methicillin resistant *Staphylococcus aureus* (MRSA). The system was shown to amplify DNA in 6 µl blood (0.083 ng μl^{-1}) off-chip. It was then demonstrated to work on-chip in a 12.5 µl glass chamber, using a Peltier system for thermal cycling.

For use in conjunction with all interfaces, an IGA with a built in DNA separation/ detection system, based on plug injection, capillary electrophoresis separation and fluorescence detection has been shown to reproducibly report the presence of target DNA sequences, against that of a custom-made size ladder. The detection of a 107 bp generic *Staphylococcus aureus* marker and 532 bp sequence from the *mecA* gene unique to MRSA were detected in 20 and 25 min, respectively. Importantly, the detection system is designed to integrate directly to upstream steps and has a Peltier element fitted for thermal cycling.

The work described here contributes towards a platform which offers the opportunity to tackle a number of diagnostic applications in one fit-for-all instrument.

Acknowledgements

I would like to thank my supervisors, Dr Charlotte Dyer and Professor Stephen Haswell for their guidance throughout this project.

I would like to thank Mrs Chris Murphy for sharing her knowledge in the field.

I would like to thank Dr Steve Clark and Dr Mohammadmehdi Nasr Esfahani for the fabrication of all microfluidic devices used throughout this project.

In addition I am very grateful for all the help and advice given by everyone else in the Analytical Chemistry group and also by my colleagues in the Department of Biology.

I would like to thank Dr Jay Wadhawan for all his support and motivational advice.

I would like to show huge appreciation to my parents for all their love and support over the last 4 years. During the very challenging times, I don't think I could have done without them.

Finally, thank you to Deana Barone, who has been there for me every day over the last 18 months. Her warmth and support has been indispensable.

List of Abbreviations

BP- Base pairs

BSA- Bovine serum albumin

CCSB- Chitosan coated silica beads

CS- Chaotropic salt

CE- Capillary electrophoresis

DNA- Deoxyribonucleic acid

dNTP- Deoxynucleotide triphosphate

DPS- Dual porous silica

dsDNA- Double stranded DNA

EDTA- Ethylenediaminetetracetic acid

EOF- Electroosmotic flow

EOP- Electroosmotic pumping

ETFE- Ethylenetetrafluoroethylene

GNP- Gold nanoparticles

GuHCl- Guanidine hydrochloride

HDA- Helicase-dependant amplification

HIV- Human immunodeficiency virus

hgDNA- Human genomic DNA

HSW- Heat shrink wrap

IGA- Integrated genetic analyser

IFAST- Immiscible filtration assisted surface tension

IR- Infrared

LIF- Lateral flow immunochromatography

MALDI-TOF- Matrix assisted laser desorption ionisation- time of flight

MES- 2-(*N*-morpholino)ethanesulfonic acid

NAAT- Nucleic acid amplification test

PCR- Polymerase chain reaction

PDMS- Polydimethylsiloxane

PEO- Polyethylene oxide

PG- Picogreen

POC - Point of care

PS- Porous silica

PSM- Porous silica monolith

PTFE- Polytetrafluoroethylene

RT-PCR- Reverse transcriptase-polymerase chain reaction

SEM- Scanning electron microscopy

SPE- Solid phase extraction

TAE- Tris, acetic acid, EDTA

TEOS- Tetraethylorthosilicate

TMOS- Tetramethylorthosilicate

Table of Contents

Table of Figures

List of Tables

List of Equations

1 Introduction

1.1 Infectious disease

At present infectious disease places a significant burden on the world, both socially and economically. During the last decade, it has been reported that 15 million deaths a year worldwide are due to infectious disease. Of this, infectious disease-related deaths in the developed world account for ≈ 5 % of all deaths, while in the developing world this is estimated at > 50 % ((Yager *et al*, 2006). The US alone spends $16 billion on treatment related to sexually transmitted infectious disease (e.g. *Chlamydia trachomatis*, human immunodeficiency virus (HIV)), along with an estimated $28-45 billion cost due to hospital acquired infections (Stone, 2009; Owusu-Edusei *et al* 2013). Due to the high prevalence of life-threatening diseases, such as HIV, developing countries have also suffered further economic burden, due to a decrease in output or "gross national product". It was estimated in 1999 that the worst affected countries saw the economy decrease by up to 12%, due to infectious disease (Fonkwo, 2008). It has been acknowledged that infectious disease must be tackled aggressively in order to abate these issues and as etiological understanding of human disease has increased, so has the scope for development of diagnostic tools.

Records of human problems associated with infection can be dated back to the prehistoric era (Moellering, 1995). Malaria is thought to have been present since the beginning of the species (Joy *et al*, 2003). Tuberculosis was dated as early as 2400 BC and small pox was first dated in 1500 BC (Nerlich *et al*, 2007). The plague, in its three subtypes (pneumonic, bubonic and septicaemia) (*Yersinia pestis*), was first recorded in 400 BC and continued to ravage civilisations for the following 2000 years (Martin *et al*, 2006). Earliest reports of typhoid fever can be dated back to an early plague around 430 BC (Papagrigorakis *et al*, 2006). The devastating and ongoing effects of other well known diseases, such as yellow fever and cholera have been documented heavily over the last 500 years (McNeill, 2004; Sack *et al*, 2004).

Over the last few decades, clinical diagnostics has directed much of its attention to bacterial sexually transmitted infections (STI), such as *C. trachomatis* and *Neisseria gonorrhoea* (Peeling *et* al, 2006; Peeling and Ronald, 2009; Baron and Tenover, 2012) and bacterial nosocomial infections, such as methicillin resistant *Staphylococcus aureus (MRSA)* and *Clostridium difficile* (Okada, 2005; Baron and

Tenover, 2012). Diagnostic measures for STIs must be rigorous, as the disease is often asymptomatic and can thus spread through populations unnoticed. Considering *C. trachomatis,* for example, although individuals can be asymptomatic, it is also responsible for sequelae, such as non gonoccal urethritis and pelvic inflammatory disease (Lewis, 1998). In addition, susceptibility to more serious viral infections, such as HIV is also increased 5-fold when a *C. trachomatis* infection is present (Van Dyck *et al*, 2001). Today, STIs account for a large proportion of reported infectious diseases globally with cases of *C. trachomatis* infections and *N. gonorrhoea* being reported at over 1 million new cases each year (Greer and Wendel Jr, 2008, Mania-Pramanik, 2012).

S. aureus is a gram positive coccal bacterium, commonly found to colonise humans. It is estimated that one third of the human population carry *S. aureus* in the groin, nose, nasopharynx and/or perineum. However, those with compromised immunity, such as hospital patients and those with open wounds are found to be more susceptible to infection (Raygada and Levine, 2009). In addition, groups in close contact, such as sports teams sharing showers and towels, along with younger children interacting with one another are often susceptible. More and more frequently, cases such as these and others appearing outside hospital environments (community-associated) are being reported (Mediavilla *et al*, 2012). *S. aureus* has been receiving increasing attention over the last 70 years, due to the ongoing struggle for containment with antibiotic treatment. Advances in the 1940s, saw the emergence of penicillin, an antibiotic which contained a beta-lactam ring (Figure 1.1), shown to interfere with *S. aureus* and inhibit its ability to generate cell walls, thus incapacitating the organism from spreading (Lim, 2002).

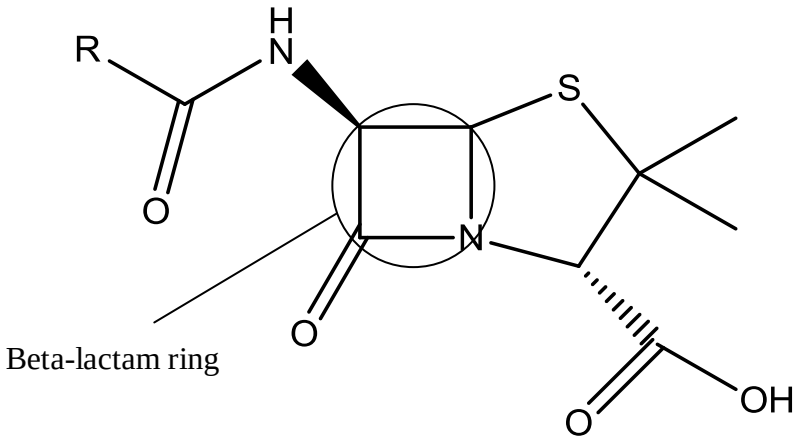

Figure 1.1: Molecular image of the drug penicillin.

Image highlights beta lactam ring, responsible for disabling *S. aureus* by inhibiting cell wall production. Molecule was drawn using Chemdraw software.

Within a decade, *S. aureus*, developed resistance to penicillin, with the production of beta lactamase, an enzyme capable of breaking down the beta lactam ring, thus rendering the drug ineffective. Following this, a derivative of penicillin was introduced called methicillin, which possessed the same beta-lactam ring with additional surrounding groups providing protection from the beta lactamase. The use of methicillin saw a sharp decline in *S. aureus*-related infections following its introduction in 1959, until *S. aureus* again developed resistance. In this instance, a mobile genetic element containing the *mecA* gene had an additional mechanism, which affected a reduced affinity to methicillin preventing the drug from attaching to the cell wall, again rendering it ineffective. While "methicillin" is used to name methicillin resistant *S. aureus* (MRSA), the label "methicillin resistant" actually describes the resistance to a broad variety of derivatives such as oxacillin, amoxicillin and the beta lactams already described (Chatterjee, 2013). Now it is estimated that 44% of hospital-acquired infections are MRSA-related with an increasing number of community-associated cases also being reported. The latter is attributed to habits of personal hygiene, as well as compromised skin barrier, as already discussed. While, simple colonisation is generally asymptomatic, a diagnosed infection can be associated with mild-to-severe skin and tissue infection and in more extreme cases, dermatitis necrotising pneumonia, endocartitis and bloodstream infections. Due to this

and the increasing resistance to antibiotics, it is becoming increasingly important to diagnose *S. aureus* rapidly (Rasmussen *et al*, 2010).

Since the 1970s, *Clostridium difficile* has been a leading cause of intestinal problems, ranging from mild diarrhoea to severe pseudomembranous colitis. Prior to this decade, poor health concerning the colon had been attributed to *S. aureus*. In 1974, frequent reports of diarrhoea following treatment with clindamycin, led to conclusion that the pathogen was flourishing with a depletion of competitive bacteria within its environment (Bartlett, 2008). In addition, stool samples of those affected gave a negative result when tested for *S. aureus*. In 1992, a clear distinction was made between *S. aureus*-related enterocolitis and *C. difficile*-related colitis. The danger of *C. difficile* in abundance is due to the production of two toxins, A and B. While both are found to be cytopathic toxins, toxin B is found to be a 1000 times more potent than toxin A (Greer and Wendel Jr, 2008).

The examples above demonstrate the consequences of allowing an infection to go undiagnosed and are why the installation of a widespread rapid diagnostic platform is of such high importance. These are diseases to which many are experiencing prolonged exposure, when a rapid diagnosis would make the situation avoidable. It is important that the infections described and others similar are contained and treated, as soon as possible and for that to happen, rapid diagnosis is essential. For this to be carried out effectively, diagnostic methods must be both easy to perform and also approachable for the patient. Any protocol must also be carried out at a cost which can be managed regarding the target population.

1.2 Diagnosis of infectious diseases

First and foremost, a diagnostic test is used to alert both clinician and patient of the presence or absence of a suspected infection. The positive or negative diagnosis of an infection, not only determines how the patient should be managed clinically and effectively, it can, in addition, necessitate the implementation of protocols for containment and reduce likelihood of further spreading, including the potential of contact tracing. It is critical that diagnostic tests are reliably accurate, whilst also being practical and affordable for the intended population. Furthermore, speed of diagnosis is critical in ensuring effective management and treatment (Reid *et al*, 1995). In some circumstances, diagnosis during the early onset of an infection can

prevent irreversible complications associated with long term exposure and, again, minimise the risk of further transmission. Due to a wide variety of potential diseases associated with only a small number of symptoms, an accurate diagnosis can specify treatment for the particular disease, whilst also avoiding the negative outcomes of incorrect treatment. The latter potentially carries the consequence of unnecessary exposure of the patient to medication and also unnecessary overuse of antibiotics, something which is becoming a greater concern. Certain diseases can often require screening of populations, as they can be asymptomatic. Epidemiological studies also necessitate similar screening programs (Banoo, 2010).

1.2.1 Traditional techniques for diagnosis of infectious diseases

There is a large variety of well established diagnostic tests available for the detection and identification of infectious organisms. This stion outlines the leading methodologies currently in use for the detection and diagnosis of infectious diseases focussing on bacterial-based infectious organisms. Bacterial infections will be the focus for the remainder of the report.

1.2.1.1 Culture

1.2.1.1.1 Blood

Blood culturing is commonly used when testing for possible bacteraemia or septicaemia. This occurs when an infection has spread from its origin into the bloodstream. While an early diagnosis is vitally important in the case of septicaemia, often a clinician will begin treatment with a generalised antibiotic before a positive result has been received, due to the potential early onset of serious disease. In the event of a positive diagnosis and identification of causative organism antibiotic treatment can then become more specialised.

Culture is often carried out in bottles containing specialised media consisting of nutrients and supplements required for bacterial growth. On reaching a certain threshold of growth, the organism can be detected by a biochemical signal or change in turbidity (Ford, 2010). These methods do, however, have certain limitations, such as a variation in the behaviour of different organisms, leading to different levels of response in the bottle. In addition, the sample must be left for several hs to settle

before turbidity related to the suspected organism can be distinguished from red blood cells.

More recently, several adaptations have been developed, in order to eliminate these problems. Radiometric methods incorporate ^{14}C radiolabelled glucose molecules which are converted to radiolabelled CO_2 by present bacteria (Hung, 2009). This CO_2 can be detected in the headspace of the bottle using a beta particle counter (Hawkley, 2005; Ford, 2010). Rate of bacterial growth can also be increased with agitation of the bottle. Radiometric methodologies have been further improved by detecting CO_2 by fluorescence or reflectance sensors incorporated in to the bottle (Figure 1.2). Light sensing methodologies are preferred as they bypass the use of radioisotopes.

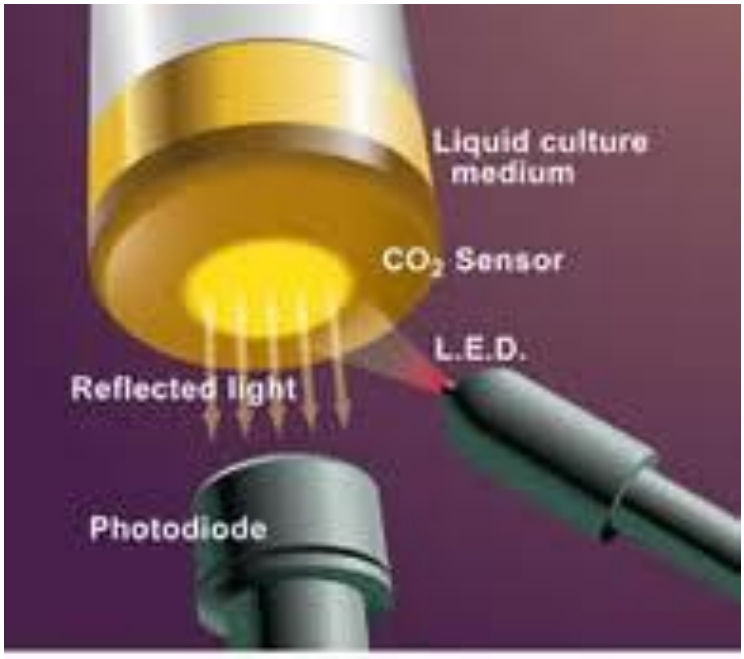

Figure 1.2: Image of commercial blood culture bottle.

Image shows a commercially available detection system for the analysis of CO_2 in blood cultures to determine the presence of bacteria (www.drdangslab.com, 2014).

1.2.1.1.2 Urine

For urine based diagnostics, a number of culture methodologies are being utilised. The Rant Shepherd method utilises a microtitre tray and infectious bacteria are counted using a microscope (Hung, 2009). This type of microscopy has been automated and commercialised by Yellow Iris Automated Urinalysis Workstation International Remote Imaging Systems, Chatsworth, California^{TM} to recognise a wide

range of particles in urine, including leukocytes and bacterial cells. Urine-based culturing aims to establish whether a significant number of infectious organisms are present. Generally 10 x 10^5 per ml are considered enough to give a positive result for a urinary tract infection (Hawkley, 2005, Ford, 2010).

The calibrated loop technique offers an alternative method which can be used to deliver urine to an agar plate in volumes ranging from 1µl to 10 µl (Cardoso, 1998). Colonies formed (see stion 1.4.1.5) can then be counted and adjusted to a millilitre through simple calculation. This does, however, limit the sensitivity of the technique to around 10 x 10^5 colony forming units (CFU) ml^{-1}.

For both blood and urine, culturing agars are available which are treated with substrates which react with bacteria present allowing for visual identification of any bacterial growth which occurs (Broekema, 2009). Cysteine lactose electrolyte deficient (CLED) is most frequently used and can be treated with an indicator for enhancement (Table 1). In addition compounds such as antibiotics can be added to agar, in order to determine antibiotic resistance.

Table 1-Colony morphology on CLED with and without Andrade indicator

Shows how a variety of bacterial targets can be identified by different colours in agar gel. Adapted from Ford (2010).

Organism	CLEDagar	CLED with Andrade indicator
Escherichia coli	Yellow, opaque colonies with a slightly deeper coloured centre	Bright pink, semi translucent colonies with a surrounding pink halo
Proteus mirabilis	Translucent blue colonies around 1 mm	Blue green translucent colonies
Klebsiella spp	Mucoid, variable colour, yellow to whitish blue	Grey green mucoid colonies
Enterococcus faecalis	Yellow colonies, 0.5 mm in Diameter	
Staphylococcus aureus	Deep yellow colonies about 0.75 mm diameter	Smooth, entire, opaque, bright golden yellow colonies
Coagulase negative staphylococci	Pale yellow or white colonies	Smooth, entire, opaque white colonies
Salmonella spp	Flat, blue colonies	N/A
Pseudomonas aeruginosa	Green colonies, matt surface and rough periphery	N/A

1.2.1.2. Nucleic acid-based detection

Although culture techniques for diagnosis of bacterial infections such as C. *trachomatis* have traditionally dominated the industry, the last two decades has witnessed the emergence of the nucleic acid amplification test (NAAT) (Ripa and Mardh, 1977, Barbeyrac, 1995, Van Dyck *et al*, 2001, Chernesky, 2005). Here, detection and identification of infectious organisms is achieved by isolating nucleic acids from clinical samples (Figure 1.3), based on its nucleotide sequence and then exponentially amplifying specific target sequences, using deoxyribonucleic acid (DNA) polymerase enzymes.

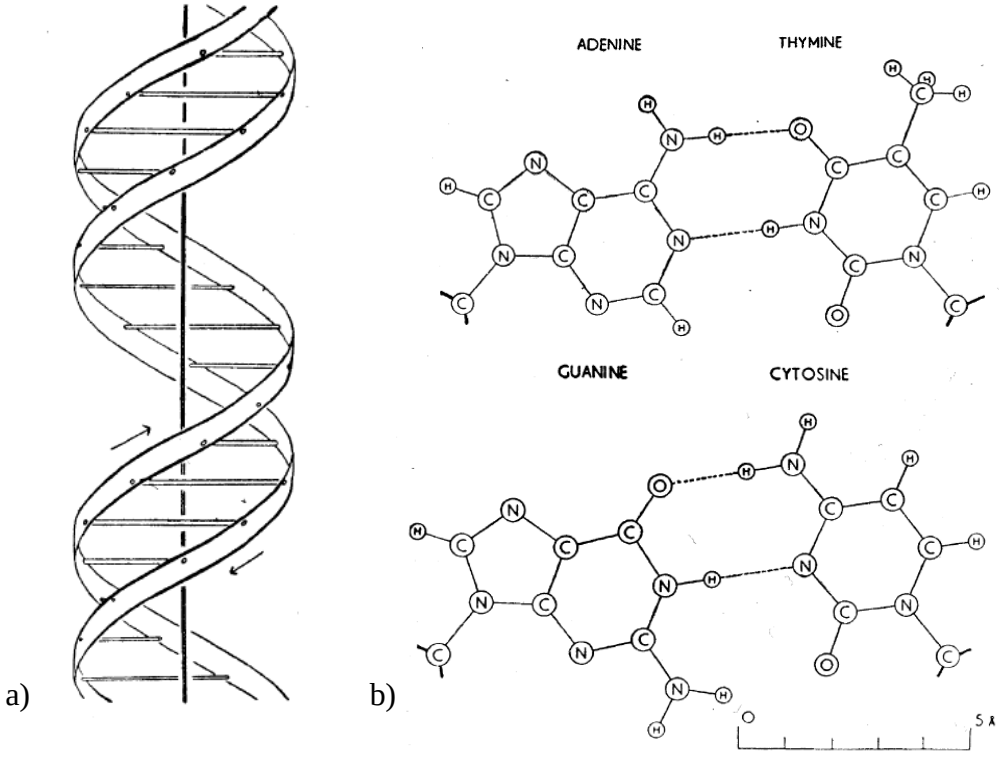

Figure 1.3: Illustration of DNA molecular structure.

a) Illustration of the DNA double helical structure and b) Illustration of base interactions (Watson, 1953).

This process is preceded by a purification step in which the nucleic acids are extracted from target bacterial cells and isolated from the biological matrix, which may contain components which will inhibit amplification. Nucleic acid amplification is followed by detection of specific target sequences which are selected to permit identification of

an infectious agent. This process is discussed further in stion 1.4. NAATs are generally favoured over culturing techniques, as they are a faster alternative, with the latter taking a number of days, while NAATs can be carried out in less than a day. The high sensitivity of this method in the detection of C. *trachomatis* and *N. gonorrhoea* has been documented heavily in the literature (Van Dyck *et al*, 2001, Wisniewski *et al* 2008). NAAT have also been well documented for detection of *S. aureus* and other resistant strains (Warsa, 1996; Matthews *et al*, 1997; Martineau *et al*, 2000). C*. difficile* diagnosis using NAAT has also been documented.

C. difficile is generally isolated from faecal samples and demands additional analysis, due to the existence of both toxigenic and nontoxigenic strains. Using culture techniques like those previously described, that are followed by additional analysis in order to confirm the presence of a toxigenic strain. (Delmee *et al*, 2005). As with other culture techniques, this can be very time consuming, encouraging use of NAAT as both preliminary tests and confirmation tools (Lemee *et al*, 2004).

1.2.1.3 Matrix assisted laser desorption ionisation- time of flight (MALDI-TOF) Mass Spectrometry

The ability to obtain 16s ribosomal protein profiles by MALDI-TOF mass spectrometry has assisted in the identification of bacterial, yeast and fungal agents from patient clinical samples. Spectral peaks providing information about the molecular mass of the organism can be compared to those of known reference strains. The technique has made identification possible in short experimental timescales (< 2 h) and is becoming increasingly common in clinical laboratories (Spanu *et al*, 2012; Martiny *et al*, 2013; Pulcrano *et al*, 2013), however, high cost of instrumentation and materials, means MALDI-TOF facilities are not widespread.

1.2.1.4 Lateral flow immunochromatography (LFI)

LFI approaches employ a paper strip (commonly made from nitrocellulose) containing probes to target proteins such as antigens or host antibodies which will recognise and bind to target proteins. A liquid sample is added to one end and capillary forces cause the sample to migrate down the strip, which gathers labelling reagents which are stored within the capillary, as it migrates. If the targets are present,

they will be captured and aggregate further along the strip, giving a visible indication of their presence. Commonly gold nanoparticles (GNP) are used as a visible reference. An illustrative example is shown in Figure 1.4. Leading commercial applications of this technology range from pregnancy to fertility and drug testing, however lateral flow tests have now been commercialised for detection of HIV, malaria and avian fluA (Posthuma-Trumpie *et al*, 2009; Zhang *et al*, 2009).

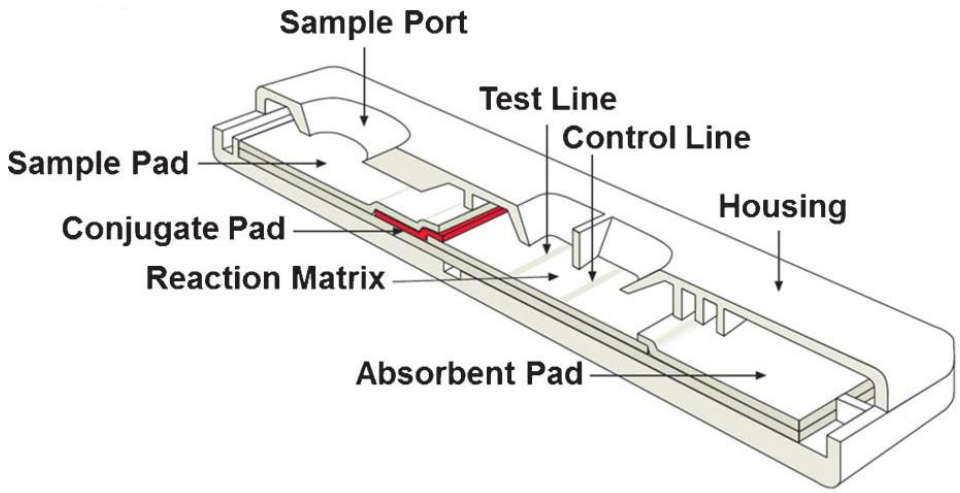

Figure 1.4: Illustration of a typical lateral flow test

Sample is added at the sample port and capillary forces cause it to migrate along the strip past the reaction matrix and the test line to allow identification. Image taken from Merck (2013).

In addition lateral flow tests have been used in conjunction with NAAT by introducing a test following with probes complementary to the target amplicons. The lateral flow test will give an indication as to whether amplification has been carried out successfully, thus giving positive or negative results. Mens *et al* (2008) demonstrated detection of parasitic infection, malaria using a system of this nature and developed the work further by integrating blood into the amplification process (Mens *et al*, 2012).

1.2.2 Standard methodologies for diagnosis of infectious disease

At present diagnostic methodologies used by the National Health Service are variable dependent on the target organism in question. Generally *C. trachomatis* is diagnosed initialling using microscopy and confirmed using NAAT methodologies (Mania-Pramanik, 2012). *N. gonorrhoea* is detected using a combination of microscopy and culture techniques, however NAAT is also used (Lai-King Ng, 2005). The presence of MRSA is generally achieved using agar plates and NAAT can also be used. MALDI-TOF methodologies are beginning to be used more frequently around the UK, however at present; cost is limiting the introduction of instrumentation to all clinical laboratories.

1.2.3 Point of care diagnostics

Point of care (POC) testing aims to transfer an entire diagnostic process to a format which can be easily implemented in the hospitals, general practitioner practices, clinics or even the community or home (Niemz *et al*, 2011) and in some circumstances be operated by the patient. An instrument of this nature should also be practical and affordable in the developing world (Dineva *et al*, 2007). Furthermore, an intrinsic goal of POC diagnostics should be a requirement for minimal user intervention. This in turn, allows staff/ patient to operate them with minimal training, whilst also reducing the potential for contamination. Concerning LFTs (discussed in stion 1.2.1.3), these have had a huge positive influence in areas of POC diagnostics and those reporting a union of NAAT and LFT techniques have been able to demonstrate sensitivities competitive with that of a laboratory-based NAAT. The nucleic acid lateral flow test does, however, not meet the one-step philosophy of a point of care system, as it requires additional human intervention and introduces potential for contamination.

By contrast, microfluidic/ lab-on-chip technologies have emerged in the last 25 years as a platform which offers to provide full automation and complete integration of all necessary steps within a single contained device. The NAAT, for example, which provides the user with the necessary sensitivities for detection, is a multi-step procedure. As a result, it is predominantly performed by skilled staff in centralized laboratories, with samples often requiring up to two weeks processing

time. This has led a large number of groups to attempt to transfer the NAAT process to a single microfluidic device or "lab-on-chip" (Siegrist *et al*, 2009). The complexity of the process and also the large number of applications associated with NAAT within a microfluidic format, has produced a wealth of literature, discussing individual steps, integration and sample characteristics. It is anticipated that microfluidic chip-based technologies will have a significant role in the future of bacterial infections, however, they are yet to be a dominant part of commercialised diagnostics.

1.3 Microfluidics

1.3.1 Fundamental principles

Microfluidics defines systems which operate using volumes at microlitre levels. The format received an initial surge of interest, due to the increasing demands from molecular biology. As described here, groundbreaking work in genetics required an increased throughput of genomic testing for both clinical and forensic applications. So while large-scale innovations, themselves, witnessed unprecedented levels of sensitivity, diagnostics was in need of faster and cheaper methodologies, which miniaturisation could provide. In addition to this, the growing fears of chemical and biological weaponry injected further interest in handheld devices equipped to detect such risks in the field at remote locations. Media friendly issues such as these provided the necessary impetus for many research groups to follow these new ideas with more confidence. Typical laboratory procedures, such as electrophoretic separation techniques and chromatography were being successfully downsized to a capillary format, demonstrating the potential for the miniaturisation of a wide range of long established techniques. Finally, the platform for the new technology was to be strongly re-enforced by recent advances in microelectronics which provided laboratories with highly suitable and economical fabrication methods (Whitesides, 2006; Ong *et al*, 2008).

First and foremost, in diagnostics, the miniaturised format offers the user a manageable and potentially portable device in which its contents can be kept contained, free from contamination. Such benefits in turn allow easy handling, packaging, distribution and importantly, the ability to operate *in situ*. POC devices

can also provide the user with a higher degree of automation, letting them bypass the sometimes laborious laboratory protocols which allow little margin for error. Furthermore, in the form of a self-contained disposable product, the potential 'one shot' use of a microfluidic device, recent advances in fabrication technology ensured that a proposed design can be mass reproduced on a huge scale. Manufacturing materials such as glass and polymers can be obtained cheaply, while reagent usage is also minimised, due to the smaller fluidic dimensions (Ong *et al*, 2008). As well as financial benefits, fluid dynamics on the micro-scale also provide useful qualities that are not evident otherwise.

Fundamentally, flow can be described as either laminar or turbulent. Laminar flow will pass through a channel uniformly, whereas turbulent flow will pass through a channel in a more disordered state. The former can be mathematically modelled and can therefore be monitored more closely (Ong *et al*, 2008). As described in stion 1.3.2, fabrication techniques and various synthesis routes can provide the user with complex, high surface area structures within a microfluidic channel, however the downsizing of basic channel dimensions alone can increase surface to volume ratios (S/V). Advantages of this include the increased influence of surface activity on the contents of the channel. The silica properties of a simple glass channel alone carry a negative charge which can be utilised for electrokinetic transport methodologies, while also being ready for binding to polar molecules. Further surface functionalisation steps, particularly silanisation techniques, can also provide a wider range of surface chemistries (Tian *et al*, 2000). Heat transfer within microfluidic devices is far more rapid compared to large-scale methods due to a reduced thermal mass. Processes dependant on precise temperature control, such as thermal cycling for PCR (see stion 1.3) benefit from this, by eliminating much of the ramping time associated with temperature change (Ong *et al*, 2008).

For fluid movement within a microfluidic device, traditional hydrodynamic pumping can be employed, allowing effective transport from one region of the device to the next, however more recently electrokinetic transport systems, such as electrophoresis and electroosmotic flow (EOF) (stion 1.5.4.2), have been explored.

Ultimately, microfluidics aims to take advantage of the physical benefits described above in order to improve on a growing number of large-scale analytical

processes. In addition to this, sub-processes can be integrated to steps that precede them and follow them, without the need for any human intervention.

1.3.2 Fabrication

Today, there is a diverse range of materials and fabrication methodologies for manufacturing microfluidic devices. The most well-investigated material, thus far, is glass. To fabricate devices from glass requires a combination of photolithography and wet etching (Figure 1.5). The chip substrate is layered with a metal cover before a photo resist is layered on to the metal into which the desired channel is patterned. Exposure of the photo resist enables the pattern to be etched into the metal to expose the glass substrate, which can then be etched away using a suitable etchant, such as hydrofluoric acid. On completion of channel etching the metal and photo resist protective layers are removed and a sond glass layer is thermally bonded to the base glass substrate which retains the etched channels and features. This is now a two layer microchip with enclosed channels. The advantage of glass is that it is optically transparent, thermally stable, highly resistant to organic solvents and well suited to surface functionalisation. It is also very applicable to electrophoretic and electroosmotic flow techniques, which is why capillary electropheresis (CE) applications are well documented on glass (stion 1.4.7). One disadvantage to glass is that fabrication costs are considered relatively expensive compared to chip fabrication materials which have been more recently introduced (McCreedy, 2000). Several years after glass-based microfluidics emerged, polymer-based devices were developed and these are today the most commonly used materials. Polymers used in fabrication of devices can be described in three main subsets; elastomers, thermoplasts, thermosets (Ren *et al*, 2012). Elastomers are made up of cross-linked chains, which are flexible under exerted pressure, but will return to an original shape. The most widely used elastomer and also most widely used material is polydimethylsiloxane (PDMS), which owes its popularity to its relatively low cost and ease of manufacture. PDMS chips are made from a liquid PDMS starting material and set in a pre-designed mould. The low surface tension allows highly complex designs (nm scale) to be imprinted on to the PDMS chip. Two key features of PDMS is that it is both biocompatible and gas permeable, making it highly applicable to biological

applications such as cell, screening, cell culture and biological assays (Kastrup *et al*, 2008). In addition, the capacity for precision fabrication of nanoscale channels within PDMS make it suitable for single cell analysis (Younan Xia *et al*, 1998)

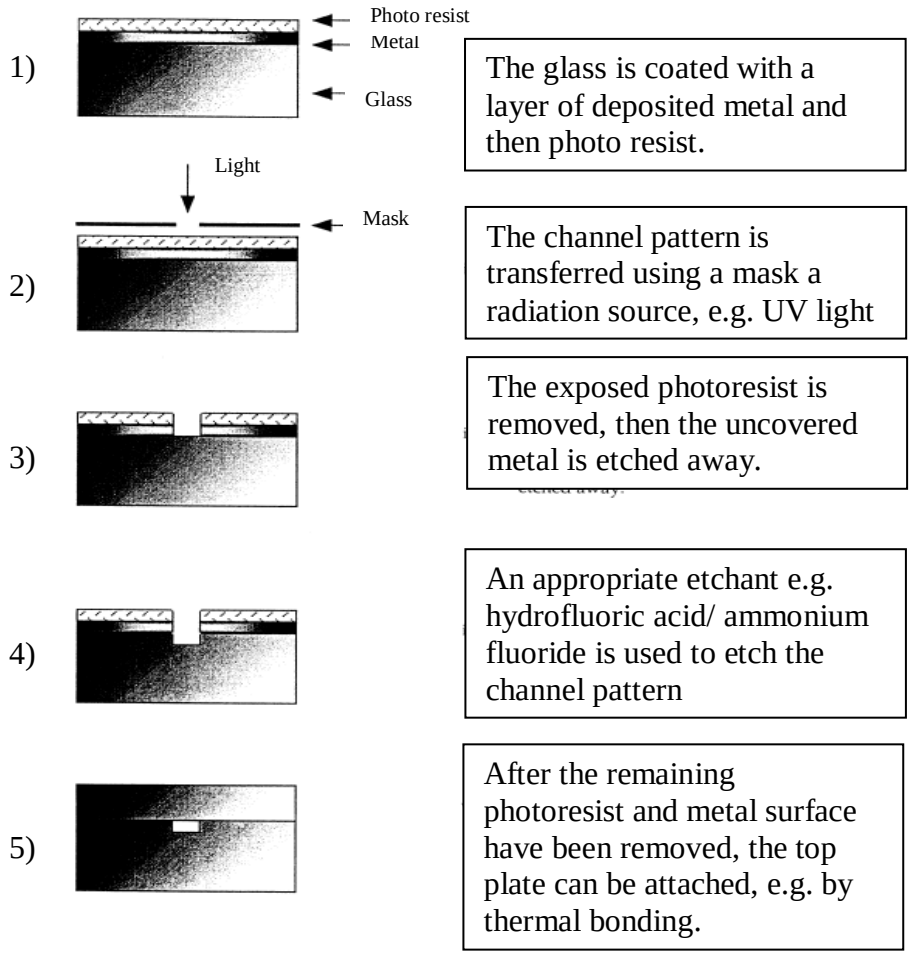

Figure 1.5: Schematic of glass-based chip device fabrication methodology.

The process uses a combination of standard lithography and wet etching techniques (McCreedy, 2000)

The high gas permeability, however, also contributes a disadvantage to PDMS applications, in that it is susceptible to water evaporation over prolonged experimental periods, altering reagent concentration within the chip. The methyl-rich surface is also prone to adsorption of biomaterials and hydrophobic compounds making it unsuitable for certain biological applications. It is also incompatible with many organic solvents.

Thermoplastics, such as poly(methylmethacrylate) and polycarbonate differ from elastomers, in that they are usually purchased as solid precursor materials and then moulded for use. They are more compatible with organic solvents than PDMS, however their rigidity makes them less applicable for biological applications, such as cell culturing.

Thermosets (e.g. polyimide), are malleable upon curing, but cannot be manipulated afterwards. Thermosets are optically transparent and resistant to most organic solvents. Although, there are reports of thermosets in microfluidic applications, the fabrication is relatively expensive, compared to that of elastomers and thermoplasts (Ren *et al* 2012), making their usage less common.

1.3.3 Microfluidics in diagnostics

The microfluidic technologies described in this stion demonstrate tantalising potential for greater applications in diagnostic, chemical synthesis and forensic applications. The literature has reported examples of miniaturised methodologies of the diagnostic techniques described in stion 1.2.1. Lateral flow tests are generally carried out on a microfluidic scale, using nitrocellulose paper. Microfluidic devices have been shown to accurately simulate the environments necessary for cell culture, (Ziolkowska *et al*, 2010). There is, however, little reported in terms of culture-based diagnostics, due to the lengthy timescales required for incubation. There are numerous reports of MALDI-TOF-based systems which have been coupled to microfluidic devices (Ro *et al*, 2006; Kuster *et al, 2013)*, however the process itself has not yet been transferred on-chip, likely due to mechanical complexity. NAATs have shown the most promise in a microfluidic format, with a wealth of literature being presented over the last 20 years. This is discussed in depth in stion 1.4.

Regarding any diagnostic process, microfluidic platforms must also face the challenges of connecting the macro or “real-world”- sample to that of the µl-scale of the microfluidic device or chip. The larger the sample, the greater the challenge. Much of the work reported focuses on the novelty achieved inside this microchip, however for commercialisation, the transferring of sample to chip must also be achievable in a simple and reproducible manner. The simplest form of interface described would be that of a sample well situated inside the chip, juxtaposed to

neighbouring channels (Lagally *et al*, 2001; Seong *et al*, 2003). A setup such as this is effective for a simple CE system for example. Integrated connection mechanisms have been reported in which desired sample entry ports are built in to the device during fabrication (Bings *et al*, 1999; Chen *et al, 2003*). Due to the complications introduced during fabrication, separate interconnecting mechanisms have been reported which can be connected to the chip post fabrication for sample input (Wooley *et al*, 1996; Gaertner *et al*, 2003). This also allows reuse of components in some cases. Finally, partitioning of sample or "amortisation" has been reported in which the sample is added in increments to allow the device to cope with receiving large sample volumes (Cheng *et al*, 2001).

Ultimately, no one interface is universally accepted for all applications and the issue must be addressed with the sample type in mind. As described in further detail in stion 1.4.1, the potential variation of sample must also be acknowledged.

1.4 Nucleic acid amplification testing

As described in stion 1.3.2, NAAT can be broken down in to four stages. These are sample collection/introduction, DNA extraction/purification, DNA amplification and finally, detection. The following few pages will describe these four stages, with reference to the roles in microfluidic systems.

1.4.1 Sample collection

The first step in analysis of a biological sample for diagnosis of infectious disease is to collect an appropriate sample from the individual/patient. Efficient sample collection is essential to ensure an accurate result upon analysis. First and foremost, a sample must be sourced from the correct location to increase the likelihood of a positive diagnosis if the infection is present and in addition, the sample must be free from contamination from the surrounding environment. The following are examples of biological samples which are used for analysis of infectious diseases (Ford, 2010)

1.4.1.1 Blood

For conventional diagnostic purposes, blood is taken intravenously. It is generally taken by trained personnel, in order to minimise the possibility of injury or infection. Pin prick devices can be operated with no formal training and are commonly used for measurement of diabetes markers. Blood cultures generally require 5-10 ml of blood for an adult, with the first 5 mL being discarded. Due to reduced volume, blood samples taken for molecular analysis, often require an anticoagulant, such as heparin, ethylenediaminetetracetic acid (EDTA) or sodium citrate for prevention of blood clotting (Murray *et al*, 2013; Ford, 2010).

1.4.1.2 Urine

For culturing, mid-stream urine is considered suitable, however first pass urine (first 5-10 mL) is considered necessary for reliable diagnosis of STIs such as *C. trachomatis.* As urine provides an ideal environment for many microorganisms to grow, samples are processed as quickly as possible to avoid misdiagnosis due to growth of contaminants. In the presence of an indwelling catheter, the urine is collected via a catheter bag. As with venepuncture, all instrumentation is cleaned thoroughly with alcohol or by autoclave sterilisation to avoid contamination. In certain circumstances, involving young children and babies, samples can be taken via collection bags and/ or pads (Hawkley, 2005).

1.4.1.3 Swab samples

Swabs are an absorbent material made primarily of cotton and are an effective tool in obtaining samples from superficial parts of the body susceptible to colonisation of various pathogens. Areas such as the nose, throat, ear, eye, penis, vagina, cervix and rectum are accessible to swabs and in addition, it is common to swab open wounds, particularly if there is pus present. Once swabs have been applied they are contained in a sample tube before analysis (Murray *et al*, 2013; Ford, 2010).

1.4.1.4 Other sample types

Alternative samples, such as faeces, hair, nails, skin scrapings, cerebrospinal fluid and vesicle fluid can all be obtained for detection of infectious organisms. In all cases, the

sample retrieval areas must be cleaned to ensure contaminants are not present around the sample region (Hawkley, 2005).

1.4.1.5 Target concentration during sample collection

In biological analysis, the emergence of microfluidic methodologies has had little influence on sample collection protocols. Unless a sample collection mechanism is able to be integrated to the device itself, this is likely to stay the same. It is, however, essential that possible concentration of a particular pathogen within the sample is well characterised, as sample volumes for analysis are to typically be drastically reduced for all processing on a microfluidic format. For diagnostic testing purposes, it is critical to determine what quantity of a clinical sample will be required to ensure efficient detection of the infectious agent. While human genomic DNA (hgDNA) concentration is of great interest in forensic applications, clinical diagnostics is more concerned with the nucleic acids of invasive organisms. However, it must be acknowledged that a background of human DNA will be present due to non-discrimination during DNA extraction procedures. The genetic material of viruses vary in length, between 5 and 50 Kilo-base pairs (Kbp), which are equivalent to 2 x 10^7 to 2 x 10^8 copies per ng. Bacteria, for example *C. trachomatis*, has genome size of around 140 Kbp, providing 7 x 10^5 copies per ng (Frutos *et al*, 1989). It is common practice to refer to cell concentrations of bacterial organisms as colony forming units (CFUs).

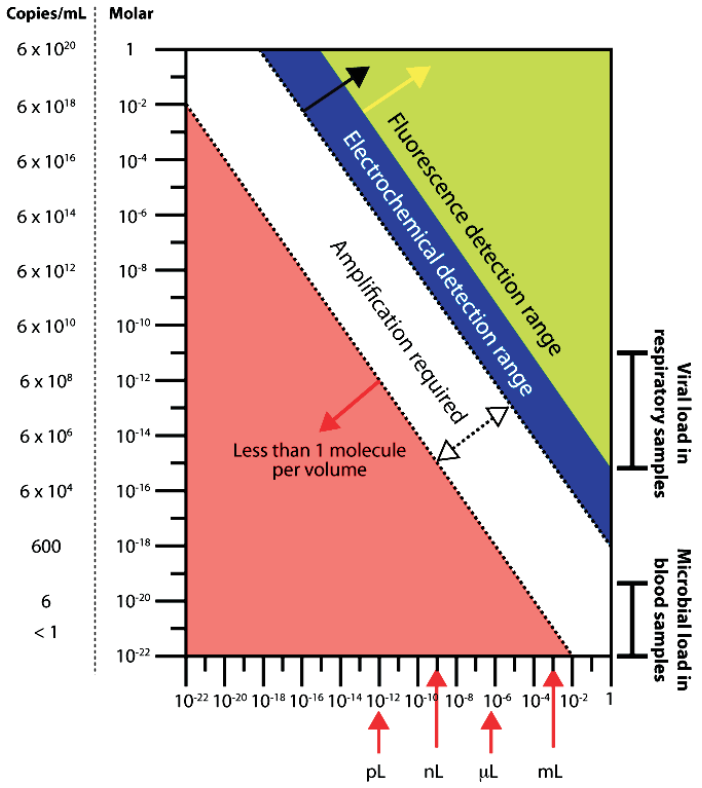

Figure 1.6: Graph illustrating required detection methodologies for varying target concentrations.

Shows the necessary volumes and target concentration for biological sample, in relation to current analytical methodologies. Taken from Siegrist *et al* (2009).

Figure 1.6 illustrates the requirements of a sample, with regards to any of the techniques used today. In clinical studies, Wathne *et al,* 1987 showed that of a group of patients diagnosed with *C. trachomatis*, 75% contained less than 10^4 CFUs/ml^{-1} in their urine sample provided. When referring to Figure 6, this level is within the region detectable by additional amplification, using samples of $>10^2$ µl. As a contrasting example, viral infection, HIV has been detected in much higher concentration, containing $>10^6$ copies of genomic DNA ml^{-1} in a blood sample. This would make it theoretically detectable in a nanolitre sample (Siegrist *et al,* 2009).

Another characteristic which must be considered in sampling is that described by Poisson, 1837. This describes the probability of finding a target analyte in a sample when considering the concentration of the population in random distribution. The

probability of having "s" targets in a sample with average target content is described in Equation 1.

Equation 1: Poisson's number

$$P(n,s) = \frac{(s^n)e^{-s}}{n!}$$

Where s is average target number per sample,

P is the probability the target will be within sample

n is sample number

To put this into perspective, an average of 1 target per sample, gives a 37% possibility of the sample being uninfected, despite the fact the larger sample is infected meaning that a greater sample size must be used to increase the likelihood of sample containing the target analyte. Although, NAAT generally process volumes which far exceed the necessary threshold, this is an important consideration when downsizing samples to a microfluidic format for detection of the target (Mariella, 2008).

While sample volume and target analyte concentration is highly variable when considering the wide variety of infectious agents, the numbers given by Poisson's equation provide some idea of the potential challenges associated with processing a biological sample.

1.4.2 DNA Purification

The isolation of nucleic acids from biological samples is an essential step in ensuring a sufficient quantity is made ready for the downstream amplification by PCR. PCR is highly susceptible to inhibition by a variety of substances. This purification step can serve to pre-concentrate DNA whilst also removing any of these endogenous PCR inhibitors. Inhibitors can vary, dependant on sample type. Blood for example, is rich in PCR inhibitors, such as haem, immunoglobulin G, haemin, bilirubin and bile salts, proteins and other biological components. For example, Al-Soud *et al*, 2000

demonstrated how it is the electrostatic interactions between immunoglobin G and the target DNA which prevent the *Taq* DNA polymerase from interacting with the DNA during the extension process of thermal cycling step. Concerning urine, however, it is urea which has also been shown to inhibit PCR. A short summary of PCR inhibitors associated with a variety of biological samples is shown in Table 2.

Table 2: Endogenous PCR inhibitors contained in biological samples. Adapted from Ford (2010).

Sample Type	Inhibitor
Blood	Haem, Immunoglobin G, haemin, bilrubin, bile salts
Urine	Urea
Saliva	Bacteria
Semen	Spermine, spermadine
Faeces	Bacteria
Hair	Melanin
Teeth	Ca 2+

1.4.3 Cell Lysis

Regarding bacterial targets, a lysis step is introduced to rupture or burst the target cell, in order to expose the nucleic acids for capture. There are a number of different lysis techniques which have been reported for both macro and microscale preparations. Chemical lysis techniques utilise chaotropic reagents such as guanidine thiocyanate and guanidine hydrochloride (Boom *et al*, 1990), and surfactants such as Triton X-100 or sodium dodecyl sulfate and reducing agents (Chen *et al*, 2006), such as dithiothreitol (DTT) (Bienvenue *et al*, 2006). Guanidine hydrochloride (GHCl) has been frequently reported in microfluidic applications from human cells (Bienvenue *et al*, 2006; Price *et al*, 2009; Reedy *et al*, 2010; Shaw *et al*, 2009), likely because it also contribute to DNA capture following lysis (see stion 1.3.4). Protinease K can also be used to aid lysis in bacterial cells and has been utilised in commercial kits (Qiagen, 2003). Gram positive bacterial cells can sometimes require additional treatment for

lysis, due to the more robust cell wall. Lysostaphin is an enzyme frequently used for lysis of staphylococcus species (Geary *et* al, 1986). Thermal lysis can be achieved with a two minute holding step at 94°C prior to PCR (Khandurina *et al*, 1999). It has been shown that by mixing cells and beads on a compact disc and applying centrifugal force, frictional forces with the beads causes the cells to lyse (Kim *et al*, 2004). Cell lysis can, alternatively, be forced using a microbeam laser to direct highly focused pulse (Quinto-Su *et al*, 2008). Modification of extracellular osmolarity can initiate hypoosmotic shock causing lysis as a result of excess swelling (Generelli *et al*, 2008). Ultrasonication uses sound energy to disrupt cellular membranes resulting in cell lysis. Electroporation is the generation of micropores by the application of an electric field. The increased porosity is irreversible at a high enough electric field causing the cells to lyse (Lu *et al*, 2005).

1.4.4 DNA capture

1.4.4.1 Large scale methods

Once the nucleic acids are in free solution, they need then to be isolated from all other cellular components in a rapid and reproducible manner. Several large-scale methodologies are well established. The chelex extraction method is a technique which is widely used. It is thought to work by protecting DNA from DNases during thermal lysis by isolating the necessary cofactor metal ion Mg^{2+} (Walsh *et al*, 1991). Phenol-chloroform extraction is another technique used to separate DNA from a biological matrix via a sondary aqueous phase (Sambrook, 2001). The phenol-chloroform method has been established for many years, however concerns over the toxicity of the reagents have prompted the development of alternative techniques (Price *et al*, 2009). A popular format was introduced with the emergence of DNA solid-phase extraction (SPE). Initially, already established liquid-liquid extraction chemistries were employed, reworking them in to a solid phase format using a silica-based network as the bulk substrate. Silica, however, was found to be conducive to DNA capture, due to its own chemical interactions with DNA. An example of a commercialised silica-based DNA SPE kit is that produced by Qiagen, UK. This operates by capture and release of DNA by passing the sample and reagents through a silica cartridge, using centrifugal forces (Qiagen, 2003). The ease and variety in

which silica materials could be incorporated in to smaller dimensions has meant that a plethora of silica-based DNA purification methods have been reported on a microfluidic format (Price *et al*, 2009). Furthermore, the physical advantages provided on the miniaturised format are conducive to what a SPE requires in terms of high surface area.

1.4.4.2 DNA-silica interactions

Fundamentally, the silica SPE of nucleic acids is achieved via hydrogen bonding between the bases of the DNA and the silanol groups of the silica (Figure 1.7), so an increased silica surface is necessary to provide a larger area for capture. This is a greater challenge dealing with the smaller volumes encountered within a microfluidic format. Four different types isolated, germinal, vicinal (bonded I and II) are shown (Nawrocki, 1997).

Chaotropic salts (CS) have been demonstrated to be highly influential on DNA binding to silica. When dissolved in solution, CS have a high affinity for H_2O molecules, which in the presence of a biological sample has a highly destructive effect on typical biological components, such as cells, proteins etc. The dehydration of the biological matter breaks any hydrogen bonds and other hydrophobic interactions, thus releasing DNA from the cell and providing it in free solution. The influence of the CS is further felt by the now exposed double stranded (ds) DNA. As the preferred conformation of the dsDNA duplex depends on interactions with H_2O molecules (approximately 0.6 g H_2O to 1 g DNA), the dehydration effects induced by the CS significantly reduces the amount of DNA-bound H_2O molecules. Thus, the dsDNA is now reconfigured from B-DNA to A-DNA, making it bind to the silica surface.

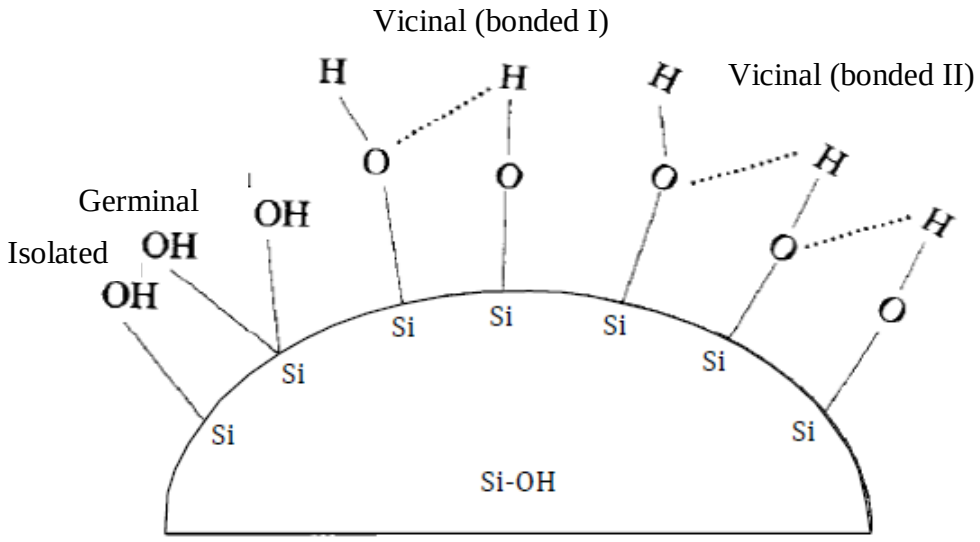

Figure 1.7: Schematic of silanol configurations on a silica surface.

It is at this stage the remaining matrix of biological debris and CS can be washed away using a non-polar solvent, such as ethanol, leaving the bound DNA behind. The reintroduction of H_2O in to the system rehydrates the DNA, releasing it from the silica surface and neatly eluting it in a purified state. The elegance of this simple process has made CS an essential part of silica-based DNA extraction and critically, the necessary dissociation effects are able to occur at a salt concentration which is non-destructive to the covalently bonded structure of the nucleic acids (Sawyer and Puckridge, 1973; Melzak *et al*, 1996).

Despite the widespread use of CS in DNA extraction methodologies, they do have some complications. Although optimum conditions are easily achieved for larger scale processes, the increased volume brought about by addition of the CS solution to the biological sample can also increase sample processing timescales, when implemented at microfluidic level. Following CS treatment, 9-fold increases in sample volume have been reported, which must all be transported through micro-scale channels (Shaw *et al*, 2009; Shaw *et al*, 2011). This has led groups to attempt to reduce processing volumes within the system and also attempt to incorporate a CS pre-treatment step of the silica in addition to adding the chaotrope directly to the sample (Wen *et al*, 2006; Reedy *et al*, 2010; Reedy *et al*, 2011; Kemp *et al*, 2012).

Due to the negative charge of both the DNA backbone and the silica surface there can exist an electrostatic repulsion between the two, which can hinder the potential for hydrogen bond interactions. The simple introduction of a low ionic strength buffer can serve to sufficiently protonate the silica surface and reduce the negative potential allowing the necessary hydrogen bonding to dominate. These effects were documented in detail by Tian *et al* (2000), who demonstrated how subtle changes of surface pH have a positive effect on DNA recoveries (Melzak *et al*, 1996).

1.4.4.3 Silica-based DNA extraction in a microfluidic format

The silica-based chemistries described above are generally found to be very robust and the literature is heavily populated with DNA-silica applications which have been adapted for the microfluidic format. Established large-scale commercial extraction kits, such as Qiagen, offer nucleic acid recoveries of 50%, by introducing the sample to a silica bed using centrifugal forces (Qiagen, 2003). Micro-scale silica beads have been integrated in to a microfluidic device by packing them in an extraction chamber (Wolfe *et al*, 2002). Although recoveries of ≈ 57% were achieved, the silica beads were disrupted easily by low back pressures and the process lacked reproducibility. As an alternative, silica beads have been stabilised with sol gel, providing DNA extraction efficiencies of 60-70%, although the results revealed similar complications (Kulinski *et al*, 2009). Finely etched, high surface area channels of silica pillars and posts have also been reported, however, complex fabrication steps have made mass production highly impractical (Wen *et al*, 2006).

A number of groups have reported the use of silica-coated paramagnetic beads in microfluidic devices, which operate like silica beads, but can be immobilised with the introduction of a magnetic field (Reedy *et al*, 2010). Hali *et al*, 2013 reported DNA purification from large volume urine samples (1 ml) using a bulbed transfer pipette filled with magnetic beads. The work held some potential for attachment to a microfluidic device for integration to downstream steps. This approach has been found to eliminate some of the issues associated with poor reproducibility regarding silica beads. In other work, Berry *et al* (2011) applied magnetic beads to a novel immiscible filtration assisted by surface tension (IFAST) system, in which the sample is introduced to a lysis buffer in the presence of magnetic silica particles allowing

binding to occur. Rather than a conventional wash step, however, the sample loading chamber is separated from an elution chamber by an immiscible phase (eg oil), which prevents contact of the two. Thus, by moving the magnetic beads from loading chamber to the elution chamber, any contaminants remain in the loading chamber while purified DNA can then be retrieved. Though, the IFAST system was carried out in less than one minute and offered a huge reduction in experimental timescale there are some mechanical complexities which would make a commercial device challenging (Sur *et al*, 2010).

As an alternative to silica beads, magnetic beads and prefabricated channels, a number of groups have reported chemically synthesised monolithic silica structures, providing a porous, high surface area for SPE. Photo-initiated silica monoliths have been developed in which a monomer-based solution can be positioned within the microfluidic device prior to subsequent polymerisation *in situ* by ultraviolet (UV) light. Work by Shaw *et al* (2009) demonstrated DNA extraction efficiencies of 58% using these monoliths. Photoinitiated monoliths have been to shown to possess pores in the region of 10 µm (Figure 1.8a).

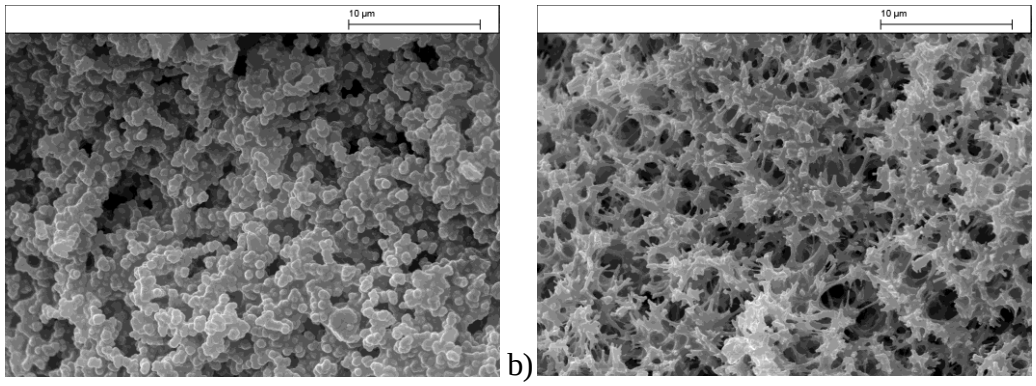

Figure 1.8: Scanning electron microscopy (SEM) images of silica monoliths

Images are a) Photo-initiated monolith, b) Potassium silica-based monolith. Images are a magnification of 10,000 x. While pore size is similar (≈5 µm), the images show structures are visibly different (Shaw *et al*, 2009).

Thermal curing of potassium silicate in formamide has been shown to generate an alternative porous structure, with pores averaging 1-5 µm (Figure 1.8b). Formamide is dispersed into potassium silicate at a 1:10 ratio, resulting in rapid hydrolysis (less than 5 min), followed by the formation of ammonium hydroxide. This transition from potassium hydroxide to the weaker base, lowers the pH from 11.8 to 10.8, driving

polymerisation of the silica (Kerker, 1976; Qu *et al*, 2003). This reaction scheme is shown in Equation 2.

Equation 2: Reaction of potassium hydroxide and formamide.

$$HCONH_2 + KOH + H_2O \rightarrow HCOOK + NH_4OH$$

The potassium silicate-based monoliths described here were synthesised *in situ* by deposition of the solution mixture into an extraction chamber or capillary. Curing at high temperatures ensures full dehydration of the silica and pore formation. Characterisation of potassium silicate-based monoliths for use as simple frits within microfluidic devices by Christenson *et al* (1998) showed that while surface area was maximised, such fine structures, led to high back pressures within the system. Shaw *et al* (2009) have demonstrated effective use of potassium silicate-based monoliths for extraction of DNA from biological samples, when assessing the influence of carrier RNA on DNA extraction performance (RNA has been shown to have high affinity for the sites on the silica surface, where DNA would normally bind irreversibly), achieving recoveries of 70% in ≈ 20 min (Sambrook, 2001).

An alternative approach to the production of porous silica monoliths (PSM) has employed silicon alkoxides under acidic conditions to produce porous structures when synthesised in the presence of polymers or other organic additives. The reaction scheme for this process is shown in equation 3 (Nakanishi, 1997).

Equation 3: Sol gel reaction scheme.

Reaction scheme for sol gelation of silicon alkoxide in acidic conditions

Hydrolysis: $$Si(OR)_4 + 4H_2O \rightarrow Si(OH) + ROH$$

Condensation: $$2(RO)_2SiOH \rightarrow (RO)_3Si - O - Si(OR)_3 + H_2O$$

$$(RO)_4Si + (RO)_3SiOH \rightarrow (RO)_3Si - O - Si(OR)_3 + ROH$$

R= methyl, ethyl……etc

Wu *et al* (2006) have demonstrated DNA extraction efficiencies of 70% from whole blood using tetramethyl orthosilicate (TMOS)-based structures inside a microchip *in*

situ. The porous materials described demonstrate a very stable, efficient and reproducible substrate for DNA extraction. They are an attractive alternative to silica beads, however at present all work has described *in situ* synthesis. Much like the silica bead format this would complicate mass production of a microfluidic device.

As a similar alternative to silica-based SPE, an aluminium oxide membrane has been shown to extract DNA utilising chemistries similar to that of silica-based system (i.e. hydrogen bonding) (Dames *et al*, 2006; Oblath *et al*, 2013)

1.4.4.4 Anion exchange-based DNA extraction

While the interaction between DNA and silica has spawned a variety of microfluidic formats for solid-phase DNA extraction, the introduction of organic solvents (eg ethanol) and CS to the extracted sample typically associated with these methods has been shown to inhibit PCR. This has led to the complications of multiple wash steps and in some cases, drying steps having been implemented in order to evaporate excess wash solvents prior to nucleic acid amplification (Chen *et al*, 2006, Baier *et al*, 2009). More recently several groups have used different surface chemistries to obviate this problem. Anion exchange resins present a desirable alternative to silica-based methodologies as CS and organic solvents can be eliminated by utilising surface chemistries which facilitate binding and elution of DNA to/from the solid-phase by simple pH manipulation. Nakagawa *et al* (2005) developed a microchip which integrated a silicon wafer coated with amino groups to allow DNA recoveries of up to 40% from whole blood by the capture and release of DNA at pH 7.5 and 10.6 respectively. This does however demonstrate the same fabrication issues associated with similar high surface area channels.

More recently, several groups have exploited the similar surface activity provided by the highly versatile biomaterial chitosan (α(1→4)-linked 2-amino-2-deoxy-β-D-glucopyranose). The bioactive polymer, synthesised from the partial deacetylation of naturally occurring chitin recovered from crab shell, possesses a variety of physical characteristics, such as high solubility, viscosity and biodegradability (Dutta *et al*, 2004). Importantly, the presence of reactive amino side groups makes chitosan an ideal solid-phase matrix for DNA extraction, as deprotonation and, hence DNA release, can occur at pH 9, leaving the DNA in a

suitable media for subsequent PCR. Furthermore, the ability to treat silica surfaces with chitosan directly has quickly inspired a number of microfluidic applications and several high performing methodologies have emerged. Cao *et al* (2006). integrated chitosan-coated silica beads (CCSB) into a microfluidic device providing DNA recoveries from whole blood as high as 75% in under 10 min. Reedy *et al* (2010) used a similar approach in conjunction with a preceding silica-based step, highlighting chitosan as an especially effective tool for DNA preconcentration, providing a 50-fold reduction in elution volume. Minimising the volume to be flowed downstream to an amplification step is highly beneficial in a microfluidic system. More recently, Parton *et al* (2012). successfully implemented electrokinetic fluid transport to a CCSB system and Reedy *et al* (2011) demonstrated pre-fabricated polymeric micro-posts treated with chitosan for DNA extraction within microfluidic systems. While the chitosan-based systems offer the chance to eliminate the organic wash phase, mechanically they present the same challenges as their silica counterparts, possibly explaining why a chitosan-based system has yet to be seen on the market. All DNA extraction methodologies and performance are summarised in Table 3.

Table 3: A select summary of silica-based DNA extraction methodologies

Extraction Method	DNA recovery efficiencies (%)	Issues/problems	Reference
Microfabricated structures	20-50	Costly and time consuming on fabrication	Wen *et al*, 2006
Silica beads	60-70	Unstable beads resulted in irreproducablity	Wolfe *et al*, 2002
Immobilised silica beads	60-70	High elution volumes	Kulinski *et al*, 2009
Potassium silicate-based monoliths	65-75	Manufacturing issues. High levels of chaotropic agent used.	Shaw *et al* 2009
Photo-intiated monoliths	<58	Manufacturing issues	Shaw *et al*, 2009
TMOS monoliths	50-60	Complex synthesis when *in situ*	Wu *et al*, 2006
Chitosan beads	60-70	Possible issues with stability	Cao *at al*, 2006
Chitosan coated prefabricated channels	50-60	Costly and time consuming on fabrication	Reedy *et al*, 2011

1.4.5 Quantification of nucleic acids

The processes described above are effective tools in nucleic acid extraction and purification, providing DNA in a concentrated and amplifiable state. Evaluation of these methods is often carried out using a rapid non-specific quantification step, which can provide information about extraction performance. Picogreen™ (2-(n-bis-(3-dimethylaminopropyl)-amino)-4-(2,3-dihydro-3-methyl-(benzo-1,3-thiazol-2-yl)-methylidene)-1-phenyl-quinolinium) is used most frequently for simple DNA quantification (Shaw *et al*, 2009; Reedy *et al*, 2010). Picogreen (PG) is an intercalating dye which adopts a fluorescence intensity close to that of fluoroscein

(1000-fold increase), only when bound to dsDNA. A detailed study from Singer *et al* (1997) demonstrated the high sensitivity and also the absence of any significant background over a range of concentrations, while in recent work, Dragan *et al* (2010) described the multiple interactions on PG/dsDNA binding, attributing intercalation to a contribution of both electrostatic and non-electrostatic interactions (Figure 1.9). In addition to PG, SYBR® green (N',N'-dimethyl-N-[4-[(E)-(3-methyl-1,3-benzothiazol-2-ylidene) methyl]-1-phenylquinolin-1-ium-2-yl]-N-propylpropane-1,3-diamine) is also used as a DNA quantification assay (Leggate *et al*, 2006).

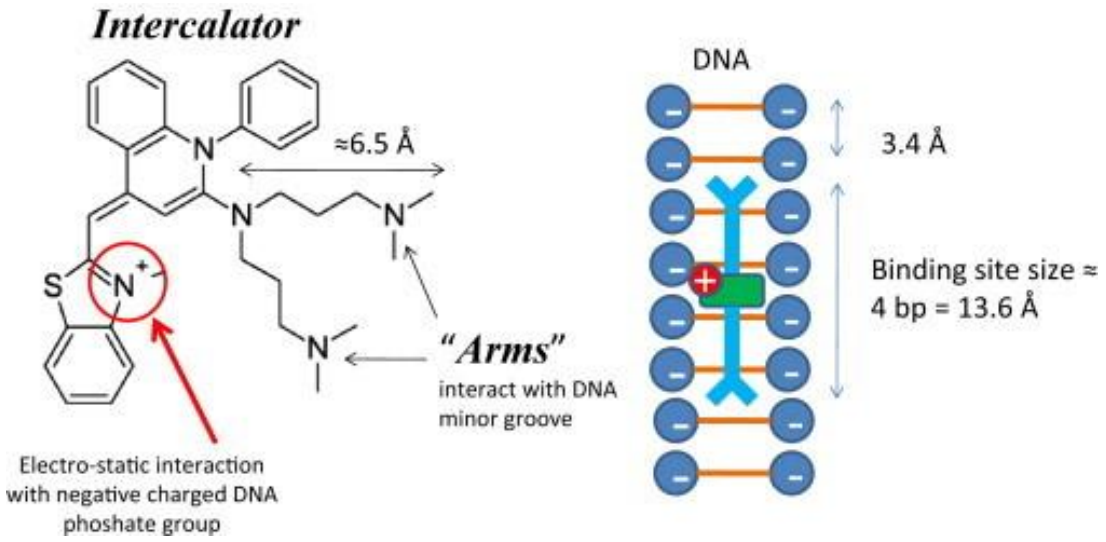

Figure 1.9: Characterisation of Intercalating Agent Picogreen™.

Image shows the chemical properties of Picogreen™ and interactions with dsDNA. Taken from Dragan *et al* (2010).

It is also possible to quantify DNA with UV spectrophotometry due to its absorption wavelength of 260 nm. In addition, this method can provide information about the purity of an eluted DNA sample, due to the absorption of contaminating proteins at 280 nm. This method does, however, lack sensitivity and it does not discriminate between DNA and other nucleic acids (Sambrook, 2001).

1.4.6 Nucleic acid amplification

1.4.6.1 Polymerase chain reaction

The purpose of amplification is to take trace levels of nucleic acid recovered from the extraction process and increase it exponentially, allowing the detection step to highlight as much target DNA as possible (Prakash *et al,* 2008). Conventionally, amplification is achieved by thermal cycling, utilising a thermally stable DNA polymerase to generate copies of DNA sequences. The process is as follows: dsDNA is first denatured in to single strands by heating to a temperature of ≈ 94^{o}C, by the breaking of its hydrogen bonds. Following this, temperatures are lowered to 55^{o}C-70^{o}C at which chosen sequence specific primers or oligonucleotides can anneal to the now exposed complementary bases of the single stranded DNA (ssDNA). Finally at 72^{o}C, a DNA polymerase enzyme (generally *Thermus aquaticus* or *'Taq'* polymerase enzyme, a globular protein) is the most frequently used enzyme for PCR) (Prakash *et al*, 2008) extends the primer sequence to synthesise the new complementary strand using deoxynucleotide triphosphate groups (dNTPs) to complete the structure. This thermal cycling is repeated (28-35 cycles is common) (Figure 1.10), generating an exponential growth of the target DNA (Green, 2012).

Thermal cycling for amplification of DNA on the macroscale is carried out in multiwell microtubes/ plates using commercial instruments. Such instruments are often fitted with a heated lid to avoid evaporation of the sample.

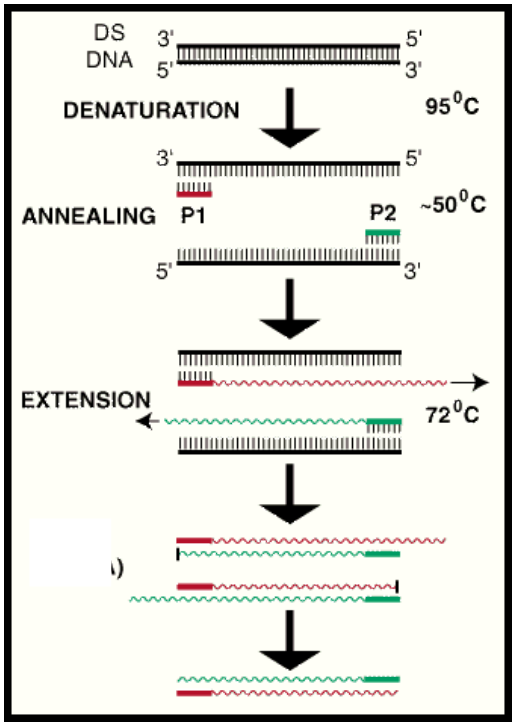

Figure 1.10: Schematic of PCR

Typical steps for the PCR process (CGDP, 2005). P1 and P2 are primer 1 and primer 2, respectively.

1.4.6.2 PCR on microfluidic devices

On the microfluidic level there have been reports of both static and dynamic PCR. The former carries out thermal cycling in bulk, as with off-chip methodologies, while more recently continuous flow PCR (Figure 1.11) applications have been developed, in which sample and reagents are transported through varying temperature zones in order to achieve the desired heating and cooling effect (Hashimoto *et al*, 2004). Chunsun *et al* (2006) reported a Polytetrafluoroethylene (PTFE) fabricated capillary, amplifying DNA in a total reaction volume of 25 µl in under 15 min. While this has complemented the microfluidic format, due to spatial benefits, the majority of microfluidic amplification systems that have been reported have been pre-dominantly bulk fluid heat cycling, possibly due to the added fabrication complexities of continuous flow (Northrup *et al;* 1998; Zhang and Ozdemir, 2009). Mahjoob *et al* (2008) reported rapid PCR on-chip based on the displacement of fluid at different temperatures. The fluidic heating chamber was composed of a porous polymer network for stable and rapid heat transfer.

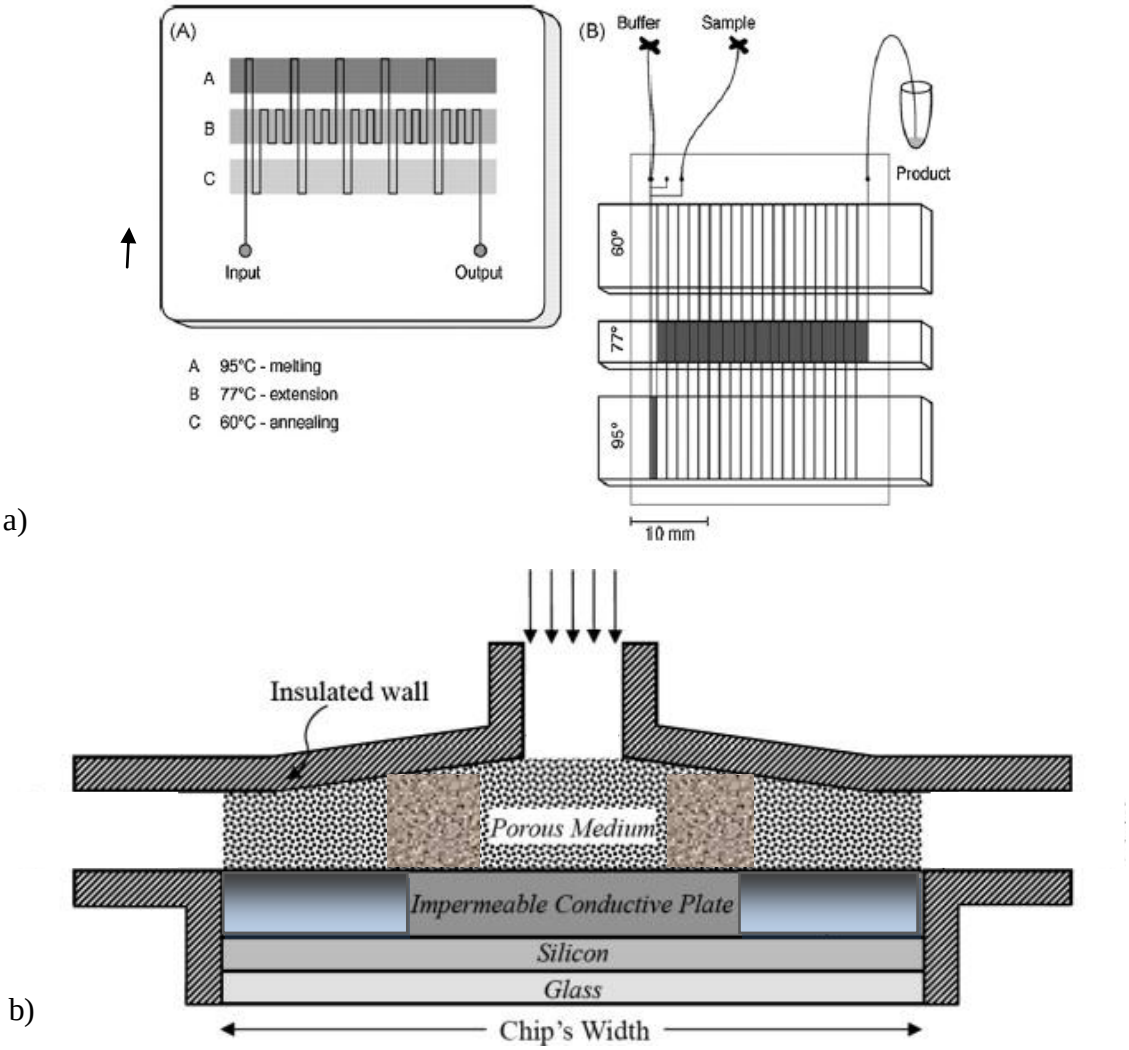

Figure 1.11: Microfluidic PCR Devices

a) Continuous flow PCR format microfluidic device. Sample is pumped into the device and passes through temperature zones allowing thermal cycling (Zhang and Ozdemir, 2009). b) PCR chamber aided by porous medium for thermal cycling. Porous medium allows greater heat transfer and quicker ramping rates (Mahjoob *et al*, 2008)

The literature reports a majority of on-chip PCR operations being carried out on volumes of 25 µl or less. Amplification using an increased reaction volume, however, provides the user with an increased likelihood of the target analyte being present and subsequent successful amplification. Unfortunately, increased sample volume, brings several disadvantages regarding thermal cycling, due to temperature gradients within the sample chamber. Higher thermal cycling timescales are required when heating and

cooling larger volumes, which increases the total processing timescale. Sample volumes of ≈ 10 µl and above often require dual heating elements to heat the PCR chamber from both sides (Northrup *et al*, 1998; Khandurina *et al*, 2000). This can be imagined as an adaptation of the common heated lid in conventional PCR machines. Qui *et al* (2010) have reported successful amplification on-chip from volumes as high as 100 µl, using a system of this nature. Off-chip, Orrling *et al* (2004) demonstrated successful uniform heating of a 15 ml reaction volume, using a microwave heating system.

1.4.6.3 Droplet-based PCR

Droplet-based PCR has been reported frequently in the literature over the last few years (Zhu *et al*, 2012). Microfluidic devices are engineered to produce water droplets in oil, as a continuous flow system, in which a PCR reaction can take place in each individual droplet. The method offers the chance to avoid adsorption of PCR reagents to device surfaces (see stion 1.4.6.8), uniform temperature and can process multiple reactions without the risk of cross contamination. Although, the system affords the user the potential to carry out even single cell analysis in an individual droplet (Schaerli *et al*, 2008; Tewhey *et al*, 2009), the fluidic process is dynamically complex and requires expertise to carry out.

1.4.6.4 Digital PCR

Digital microfluidics or "electrowetting" describes the manipulation of fluidic droplets, which are distributed on a surface connected to an array of electrodes allowing the droplets to be moved within a microfluidic device using electrostatic forces. This technique was utilised by Chang *et al* (2006) in order to mix PCR components before moving the complete reaction droplet to an area for thermal cycling. While attractive, the technology required for any digital microfluidic application is relatively complex.

1.4.6.5 Solid-phase PCR

Solid phase PCR is an attractive alternative to traditional PCR. Rather than target-probe reactions occurring in solution, oligonucleotide primers are covalently attached

to a solid surface by the 5′ end (Adessi *et al*, 2000). Upon thermal cycling the target will then attach to the bound probes and extension can take place. One strand of attached dsDNA will then be released back in to solution during the following denaturation step and the cycle is repeated. This type of amplification is called interfacial amplification. During the process, amplification can also occur with attached strands hybridising with neighbouring probes, which is known as surface amplification (Figure 1.12) (Kohsaka and Carson, 1994; Huber *et al*, 2001). Despite popularity in recent years solid phase PCR is not generally preferred over typical liquid phase PCR. This is most likely due to the complexity introduced regarding preparation of the surface with DNA probes.

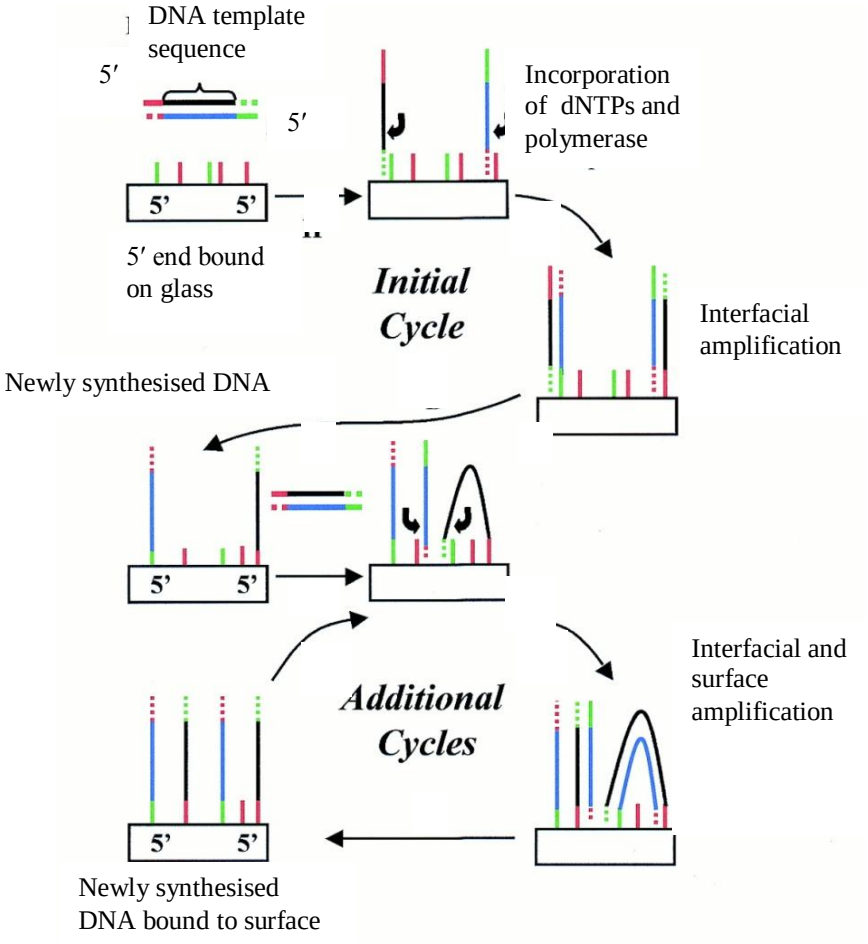

Figure 1.12: Solid phase PCR.

Outline of solid phase PCR process. Taken from Adessi *et al* (2000).

1.4.6.6 Isothermal amplification

Isothermal amplification methodologies have offered the possibility of bypassing the need for heat cycling by introducing a modified process containing an enzyme which denatures, anneals and extends at a single temperature. This can eliminate the requirement for complex thermal cycling mechanisms and also run on a lower power (Asiello and Baeumner, 2011). These are ideal features for a microfluidic POC format, providing the impetus for a surge of applications in recent years. Helicase-dependant amplification (HDA) has been used successfully to amplify viral and bacterial nucleic acids, such as HIV and *C. difficile*, respectively, while more recently microfluidic devices have implemented HDA for detection of *N. gonorrhoea* and *S. aureus* (Andresen *et al*, 2009). In this work, Andresen *et al* (2009) demonstrated on-chip amplification of multiple targets at temperatures of only 37^{o}C, highly desirable for POC systems. In this process the helicase enzyme will unwind dsDNA from either end, while the presence of a binding protein stabilises the single strands and allows primers to synthesise complementary strands separately. As with conventional PCR, the DNA is then extended by a polymerase enzyme (Figure 1.13). Other forms of amplification which bypass thermal cycling are strand displacement amplification (Burns *et al*, 1998), loop-mediated isothermal amplification (LAMP) (Hataoka *et al*, 2004), rolling circle amplification (Mahmoudian *et al*, 2008) all of which have been successfully introduced to the miniaturised format.

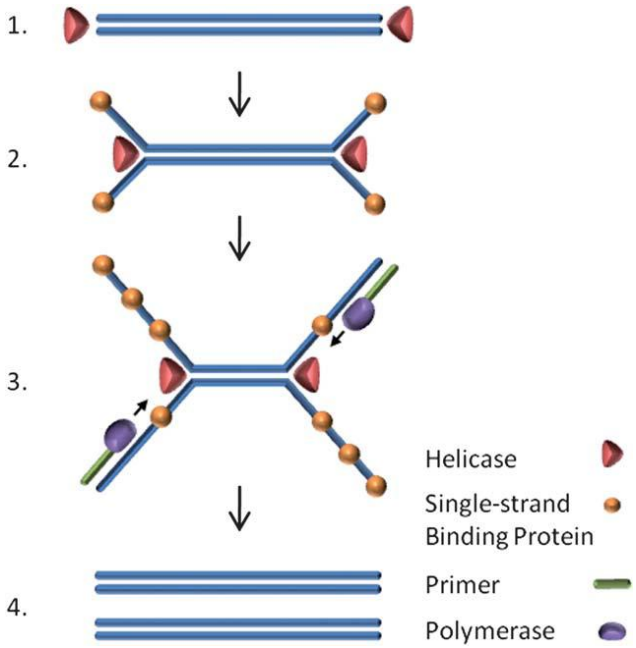

Figure 1.13: Isothermal helicase dependent amplification.

The dsDNA is unwound by the helicase enzyme, while stabilising proteins allow single strands to remain as such while selected sequence specific primers bind to the strand. Finally DNA polymerase completes the structure. Taken from Asiello and Baeumner (2011).

1.4.6.7 PCR amplification direct from unpurified sample

As described in the previous stion, high volume PCR tackles the issue of high DNA extraction elution volumes, however amplifying direct from the raw sample offers the opportunity to bypass the DNA purification step altogether. House *et al* (2010) explored and compared the detection of MRSA targets from purified samples, crudely prepared samples and boiled samples. Bu *et al* (2008) were able to amplify DNA directly from filter paper, by using an adjusted higher pH buffer in accordance with PCR performance. The work was based on that of Al-Soud *et al* (2000) (stion 1.3.2), in that immunoglobin G acts an inhibitor of PCR due to electrostatic interactions with the target DNA. The adjusted pH is effective as it reduces these interactions, suppressing inhibition of PCR. The work reported successful PCR from a 1 µl sample of blood. Similarly, Yang *et al* (2007) demonstrated the efficacy of an "AnyDirect" buffer in suppressing inhibition by components in whole blood, as well as inhibition from a range of anticoagulants, Misawa *et al* (2007) used a LAMP amplification

methodology to detect MRSA direct from blood cultures. Manage *et al* (2010) demonstrated successful use of a Phusion® hi-fidelity polymerase for direct amplification from blood on a microfluidic device. The Phusion® enzyme made by Thermo scientific™ is more resistant to the inhibitors contained in blood and can function without a purification step.

1.4.6.8 Real-time PCR

Real-time PCR or quantitative-PCR (q-PCR) is an amplification methodology which allows the user to quantify the target DNA in parallel with the amplification step. The process employs fluorescently tagged probes attached to an associated quencher, which are complementary to a sequence adjacent to the sequence targeted by the primer. During the extension step the *Taq* polymerase enzyme will build up the dsDNA and on reaching the fluorescent probe, will cause it to be released from the double-strand and move away from the quencher. These will then be detected in a higher amount throughout the amplification steps, as the product quantity is increased. An alternative method is to incorporate SYBRgreen in to the PCR mixture, which binds to double stranded DNA as it is produced.

On analysis of the fluorescence activity, the exponentially increasing signal will reach a specific threshold (crossing point) (Cp) before reaching a linear rate of amplification. Finally as the supply of fluorescent primers is exhausted, the rate of amplification, begins to decrease, known as the transition point (Tp), before finally reaching a plateau (plateau point) (Pp). This point can then be compared to that of an internal standard for quantification of the target. A typical real-time plot is shown in Figure 1.14. This method is a useful tool in diagnostics, allowing quantitative analysis of an infection organism (Zhang *et al*, 2006; Espy *et al*, 2006). Real-time PCR has been employed by several groups for microfluidic applications www.bd.com, 2014; Tsaloglou *et al*, 2011; Oblath *et al*, 2013; Cepheid®, 2014).

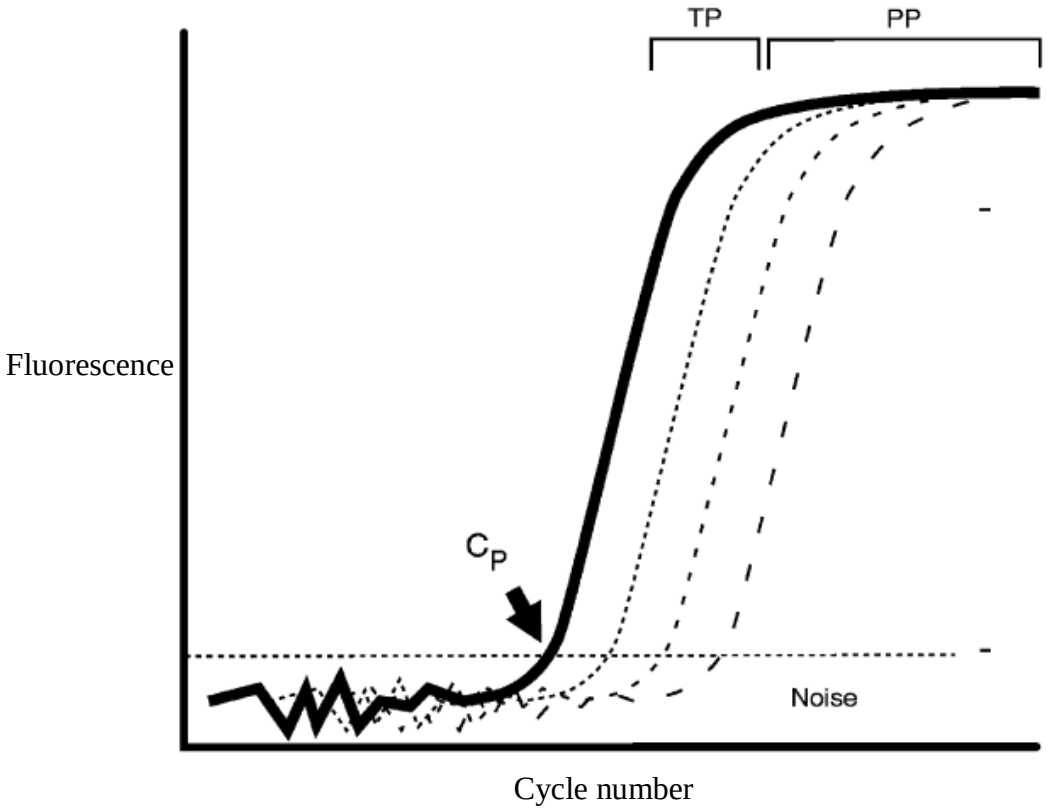

Figure 1.14: Typical real-time PCR graphical representation.

Plot shows the increase and plateau of fluorescence intensity. TP = Transition point, PP = plateau point, CP = crossing point. Taken from Espy *et al* (2006).

1.4.6.9 Thermal cycling techniques

Rapid thermal cycling of PCR samples and reagents in microfluidic systems has been achieved with several techniques. The Peltier effect is a popular way to control rapid heat cycling by coupling both p-type and n-type semiconductors. The two are able to transfer heat to and from a conductive material, eg ceramic, when connected to a DC voltage source. The heat from the ceramic is then transferred to the chip material and then the sample. An illustration of a Peltier system is shown in Figure 1.15. Peltier heating elements offer a high level of temperature precision, however, they can suffer from low heating ramp rates, due to large thermal mass. In addition, the Peltier material can often interfere with optical requirements of the microfluidic device, due to lack of transparency (Hansen, 1996; Lagally *et al,* 2000). Shaw *et al* (2010) demonstrated the use of a microwave heating system on a microfluidic device. This

provided reduced ramping rates and much shorter experimental timescales when using small (2 µl) volumes.

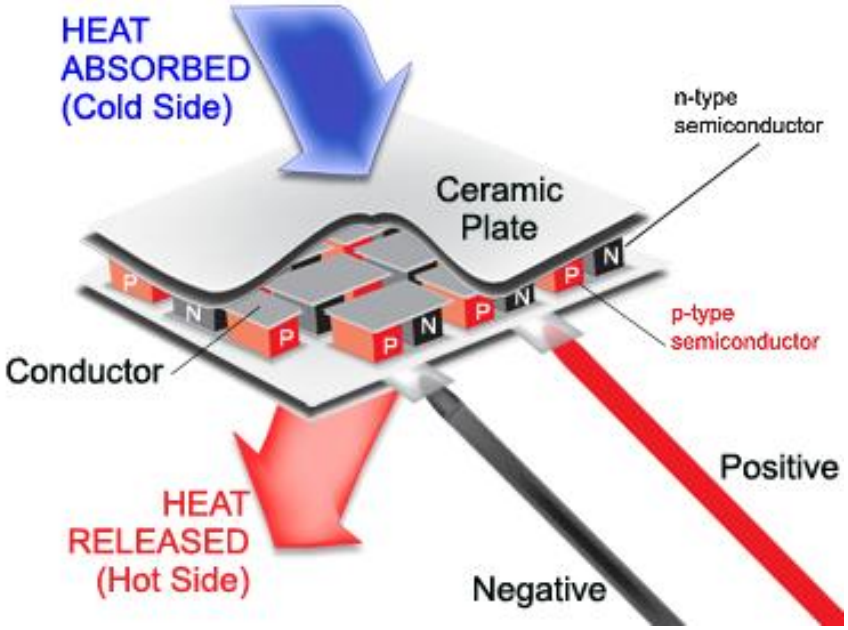

Figure 1.15: Schematic of a Peltier system.

Temperature is controlled by movement of electrons/holes from on side of the Peltier to the other by switching the charge applied. (Wavelengthelectronics, 2013)

1.4.6.10 Passivation techniques

As discussed in stion 1.3.2, many microfluidic devices have been fabricated in glass/silica. Since glass/silica is hydrophilic in nature and, due to the increased surface to volume ratio at the small scale (Ong *et al*, 2008), PCR in a microfluidic format can become inhibited by adsorption of essential components, particularly *Taq* DNA polymerase enzyme (Prakash *et al*, 2008) to the silica surface. To counteract this effect, groups have employed surface passivation techniques to minimise adsorption. These can be categorised as either static passivation or dynamic passivation (Oblath *et al*, 2013).

1.4.6.10.1 Static passivation

This involves the treatment of surfaces with non-inhibiting functional groups, in order to eliminate chemical interactions between inner surface of microfluidic device and PCR components. Silanising reagents are commonly used to functionalise silica

surfaces, in which functional groups are covalently bound to the silanol groups of the silica surface. Although the exact mechanism of silanisation of silica/ glass is not completely understood, Schlecht *et al* (2011) have proposed a model for how this occurs (Figure 1.16).

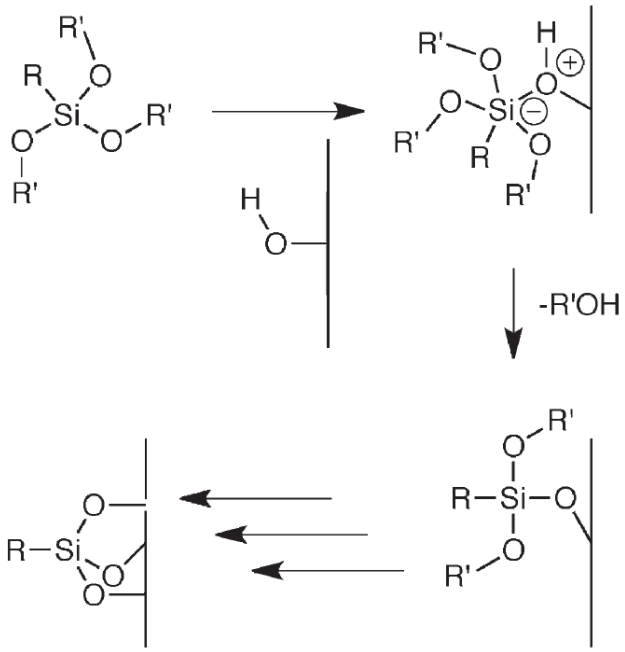

Figure 1.16: Mechanism for silanisation of glass/ silica.

Illustrates possible mechanism for silianisation of silica surfaces. A lone pair of the oxygen atom in silanol group attacks the silica atom of the silanising reagent resulting in covalently bound functional group (Schlecht and Maurer, 2011).

1.4.6.10.2 Dynamic passivation

In addition to surface treatments, dynamic passivation may also be necessary to lower adsorption of PCR components to the surface by adding competing compounds which block the sites which the *Taq* DNA polymerase enzyme would bind to. Addition of proteins, such as bovine serum albumin (BSA) has been shown to effectively reduce inhibition by adsorption to the surface (Garland *et al*, 2010*)*. Various other effective additives have been used similarly, including Tween-20, poly(ethylene glycol) (PEG), poly(vinylpyrrolidone) (PVP), poly(L-lysine) and poly(ethylene oxide) (Shaw, 2009). It is also common to add these reagents together to enhance the effect of inhibition of surface adsorption.

1.4.7 Separation and Detection of DNA

The final stage of the nucleic acid amplification test is the detection of the now amplified target DNA sequence. A number of methods have been employed to separate and/or detect products of amplification.

1.4.7.1 Traditional methods for detection of DNA fragments

1.4.7.1.1 Gel electrophoresis

Agarose gels provide a matrix for electrophoretic separation of DNA by size. Gel porosity can be customised to obtain a separation of a range of DNA sizes by varying the concentration of the gel. In addition, the fluorophore, ethidium bromide is used as an intercalating agent to permit visualisation of DNA (Green, 2012).

Once moulded the gel is injected with the sample(s), along side an appropriate size ladder of known fragments for reference. The gel is then submerged in an electrolyte-rich buffer and an electric current is applied at the cathodic end (negative) and positive at the anodic end. Due to the negative charge of the sugar-phosphate backbone, nucleic acid fragments will migrate electrophoretically toward the positively charged anode, the larger fragments more slowly. Finally, ethidium bromide staining of the gel can be used to highlight the areas of concentrated DNA which can be visualised under UV light. By comparing to the ladder, the size of the DNA fragment(s) can be established. It has also been reported that larger fragments tend to fluoresce more brightly due to higher binding capacity for the dye (Green, 2012). A typical gel is shown in Figure 1.17.

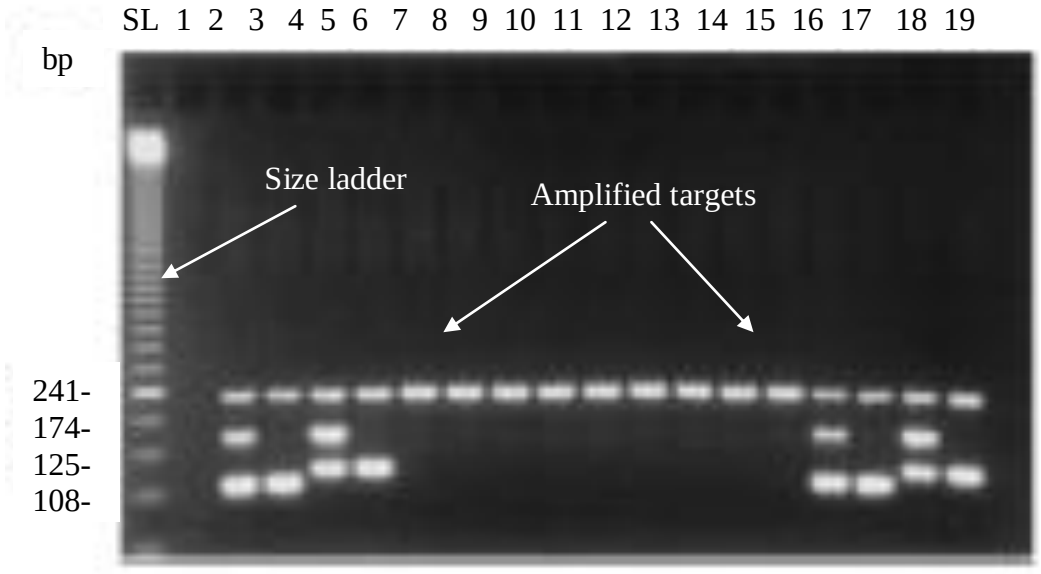

Figure 1.17: Typical agarose gel for analysis of DNA.

An agarose gel (2 %) on which DNA samples have been subjected to electrophoretic separation is shown. Lane farthest left shows size ladder of known fragment sizes. All other lanes contain amplified fragments which can be measured relative to the size ladder (Martineau *et al*, 2000).

1.4.7.1.2 Capillary electrophoresis

Like gel electrophoresis, CE techniques exploit the negative charge of the DNA to achieve separation and size analysis of DNA fragments. The glass capillary is commonly filled with an electrolyte buffer and it is connected between the anode and cathode. The sample is then introduced at the cathodic end. Due to electroosmotic flow (stion 1.4.8.2), all buffer and sample migrate towards the anode. It is also possible to use a gel or polymer, instead of a buffer within the capillary, which eliminates electroosmotic flow by suppressing the surface charge on the channel. This can vastly improve resolution of separation and sensitivity (Glynn *et al*, 1998).

The migration of DNA within a CE system can be described as the movement of a charged particle in relation to a stationary liquid. This can be modelled using equations 3 and 4. As shown with gel electrophoresis techniques (stion 1.4.7.1.1) the dependence of migration distance on the velocity of the analyte means electrophoresis techniques can be used in the separation of molecules of different size and charge. This allows DNA fragments of different length (bp) to be separated. However, while

large scale slab-gel techniques target sequences are related to a size ladder through visual analysis, CE techniques monitor the time in which the target is observed at a specific point. CE detection methodologies can include absorbance, fluorescence, electrochemical, and mass spectrometry, however, most often target DNA is fluorescently tagged, by using fluorescently labelled primers during the amplification step (Figure 1.18).

Note, as described in stion 1.4.6.7, real-time PCR techniques detect fluorescently labelled primers or "molecular beacons" in parallel with the amplification process, thus eradicating the requirement for post-amplification detection. However, this methodology does have limitations regarding detection of multiple targets, as the ability to distinguish between separate targets using real-time analysis is far more complex due to the overlap of multiple signals (Espy *et al*, 2006).

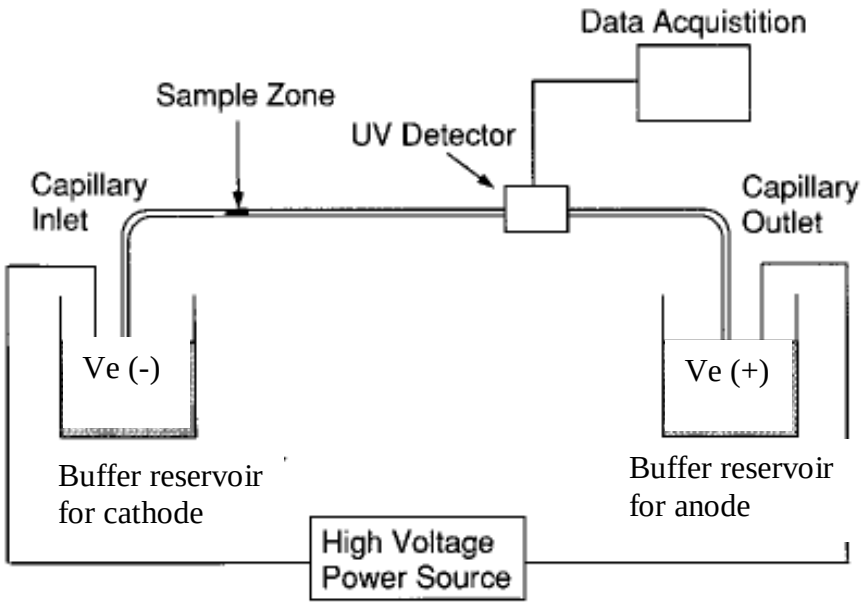

Figure 1.18: Schematic of a capillary electrophoresis system.

A voltage is applied to the anode and cathode and charged particles will move through the capillary and past the detection window. Adapted from Glynn *et al* (1998).

Equation 4: Electric force applied on particle.

$$\mathbf{F}el = ZeE$$

Where, **F***el is electric force, Ze, is charge on particle, and E is electric field*

This counter drag will then act upon this migration defined by the following equation

Equation 5: Drag on migrating particle.

$$F_{drag} = -6\pi\eta a u_{ep}$$

Where, $\mathbf{F}_{drag}$ is drag on migrating particle, α is radius of particle, η is viscosity and u_{ep} is velocity.

So total migration,

Equation 6: Total force applied on particle

$$F_{total} = F_{el} + F_{drag}$$

Where $\mathbf{F}_{tot}$ is total force applied in the particle.

(Bruus, 2008)

As described in stion 1.3.1, electrophoretic processes were some of the leading applications, driving the emergence of lab-on-chip technologies. For this reason, separation of DNA using electrophoresis has been documented extensively (Wooley and Mathies, 1994; Haab and Mathies, 1999; Kuschel *et al*, 2005). This has allowed groups to focus more closely on upstream steps in recent years, with the aim of potential integration to an electrophoretic separation/detection step. This also necessitates an environment in which the microfluidic device can be easily connected to external power supplies.

1.4.8 Fluid Manipulation

1.4.8.1 Sample introduction

Fluid manipulation and transportation is essential in microfluidic systems because it facilitates the movement of sample and reagents within a device. Sample introduction is most frequently carried out using simple micropipette placement of the sample or hydrodynamic pumping (Wu *et al*, 2006; Shaw *et al*, 2009; Reedy *et al*, 2010; Berry *et al*, 2011). Micropipetting will provide instant deposition of sample, while syringe pumping is able to introduce the sample at a predetermined and accurate flow rate and also provide the user with information about the volume dispensed. Liu *et al* (2014)

developed an automatic sample deposition device, which was controlled entirely by computer software.

1.4.8.2 Fluid manipulation on-chip

Once in the chip, fluid manipulation can become more challenging. Fluid can be moved electrokinetically using EOF. Like simple electrophoretic techniques, EOF is driven by an applied voltage. However, with respect to EOF, transport can be defined as the movement of liquid relative to a stationary charged surface (Bruus, 2008). Due to the layer of positively charged ions at the channel surface, known as the electric double layer, the application of a voltage across the channel causes the bulk flow to move towards the cathode. The movement of flow by EOF does display characteristic differences compared with hydrodynamic flow. This is shown in Figure 1.19.

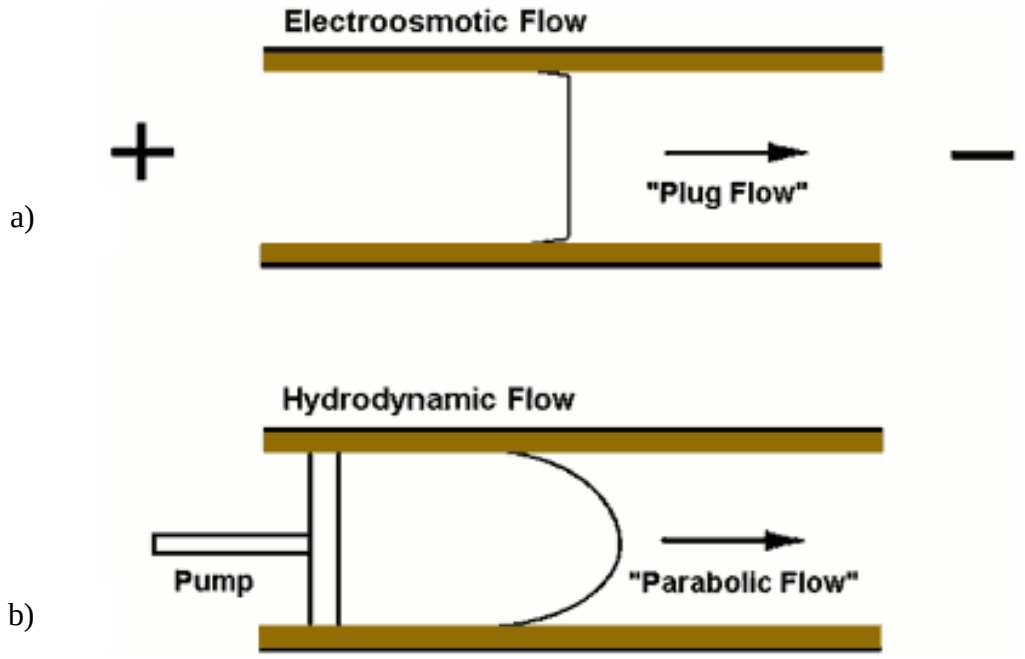

Figure 1.19: Flow velocity profiles of electroosmotic and hydrodynamic flow.

Schematic shows a comparison between the flow profiles of a) electroosmotic flow and b) hydrodynamic flow (Microtech, 2014).

EOF has allowed the user to transport liquid samples from one chamber to another within a microfluidic device. Notably, purified DNA samples can be introduced to a chamber of dried PCR reagents. Controlled EOF has been demonstrated by Parton *et*

al (2012) and Shaw *et al* (2011) in genetic applications. The incorporation of micropumps within a chip device can eliminate the need for external pumping mechanisms. Electroosmotic pumps (EOP) work by initiating EOF between two points on a chip within a greater flow system. The fluidic movement then pushes the neighbouring fluid in the desired direction. The flow can be reversed by simply reversing the voltage (Nge *et al,* 2013). For example, an electroosmotic pump has been successfully employed within a device, to pump fluid down a serpentine channel for DNA hybridization. Electrochemical pumps have also been reported in which electrolysis of water and the subsequent production of bubbles drives neighbouring fluid down the desired channel (Bohm *et al,* 1999). Traditional peristaltic pumps have been developed on a microfluidic scale by several groups (Skafte-Pedersen *et al,* 2009; Rhie and Higuchi, 2010; Nge *et al,* 2013*).*

1.4.9 Integrated microfluidic systems for DNA analysis

The microfluidic community within clinical diagniostics, above all, searches for a fully integrated, sample-to-answer device. As discussed, the complex NAAT multistep process (sample input, DNA extraction, amplification and detection) sets a huge challenge to achieve this. There have been many examples of partial integration, eg amplification/detection or extraction/amplification. The earliest published example of the integration of multiple steps in nucleic acid analysis was by Woolley *et al* (1996), in which integrated amplification and detection using CE was achieved. Lee *et al* (2003) reported integration of real-time PCR thermal cycling and electrochemical detection. Shaw *et al* (2009) integrated a PSM based extraction step to a PCR step on-chip using an EOF fluid transport mechanism, while Hagan *et al* (2011) also carried out extraction and amplification of RNA, using a combination of chitosan-based materials and reverse transcription-PCR (equivalent PCR for RNA amplification) (Shaw *et al,* 2011). Parton *et al* (2012) integrated DNA purification and amplification, using CCSB for DNA purification and electroosmotic flow was used for all sample/reagent movement.

Cepheid® have a commercial device which is marketed for the detection of *C. trachomatis* and *N. gonorrhoea* (Tabrizi *et al,* 2013; Valour *et al,* 2013), tuburculosis (Gous, *et al, 2013)* as well as other applications. The sample is received in a cartridge

and inserted into a device. The target cells of infectious organisms are lysed by ultrasonication and then DNA is captured by silica beads. Real-time PCR is then carried out, combining amplification and detection. A schematic is shown in Figure 1.20.

Handylab, inc have developed a sample-to-answer diagnostic device, which can detect *C. difficile*, MRSA and vancomycin-resistant *enterococcus*. This utilises a bench top instrument with a card pretreated with dried reagents and a fluidic system operated by a series of valves. The system employs a real-time PCR method to amplify target DNA (www.bd.com, 2014). Various sample-to-answer devices have been reported in the literature over the last decade. Easley *et al* (2006) reported a complete sample-to-answer device, which carried out purification, amplification and detection steps, using hydrodynamic pumping steps. Using this system anthtrax was detected in sub µl blood samples. Beyer *et al* (2009) achieved fully integrated analysis of blood samples ranging from 10-100 µl, to detect *Escherichia coli* K12 and *E. coli* O157 targets. The system incorporated magnetic beads for DNA purification and a micropump/valve system. Manage *et al* (2010) were able to integrate direct PCR amplification from blood with a fluorescence-based electrophoretic detection system. Targets (human platelet antigen (HPA1), fibroblast growth factor receptor 2 (FGFR2) and BK virus (BKV) were isolated and detected using the system, providing a full sample-to-answer device, bypassing DNA purification stages. Lui *et al* (2012) developed an integrated sample-to-answer device capable of detecting MRSA from samples containing 10^2 CFUs μl^{-1}, while in addition distinguishing between both live and dead organisms. The method operated as a typical NAAT, with the introduction of ethidium monozide pre PCR. Ethidium monozide penetrates dead MRSA bacterial cells, but not live ones and interacts with the DNA. In doing this it prevents the DNA from denaturing during PCR so only live MSRA would provide a positive result.

Despite an abundance of remarkable innovations by a number of groups there are still only a small number of commercially available sample-to-answer devices. Furthermore, those products on the market are systems comprised of intricate and complex steps, demanding a high cost. In the absence of an inexpensive option, the microfluidic research community continues to report novel and alternative systems and components, however the majority of the material still describes valves, nucleic acid extraction substrates and pumping mechanisms necessitating complex fabrication

and while often groundbreaking and innovative, do complicate the mass production of low cost, disposable devices (Chin *et al*, 2012). For a device to be easier to manufacture and thus lower in cost, it seems logical to simplify the system, rather than increase the complexity. Low cost would also make equipment and instrumentation more widely accessible, especially in the developing world. In addition, individual components are usually designed for a specialised application and are limited to a single sample volume and type.

Another important consideration is the way in which individual clinical sample types can vary in both viscosity and consistency dependent on composition, particularly, as it is the extreme deviations from a typical sample caused by a large infectious load, which will cause the device to fail (Siegrist *et al*, 2009). So while the real-world to chip interfaces themselves must be customised for the wide variety of clinical sample types (eg 1 ml urine sample or 10 µl blood sample), they must also be prepared for the variation observed within a single sample type. It would therefore be beneficial for a system to be adjustable to accommodate the variety of biological samples processed in diagnostics. This would make the use of a flexible device more widespread and encourage mass production of a simple operating instrument. The base instrument would serve as a platform and would possess an operating system for controlling all components within the chip. In addition, it would contain a heating element for DNA amplification, methodologies followed by a process for electrophoretic separation and detection of the markers of targeted organisms. The devices must then allow for incorporation of an appropriate interface for sample introduction and DNA purification steps, dependent on the sample type. As discussed, it is these interfaces which would require the most variation and if the system is then capable of accommodating the broad sample spectrum, then downstream steps should not require adjustment.

1.5 Aims

The literature reviewed thus far describes the many challenges encountered in the quest to develop effective "sample to answer" devices, for the diagnosis of infectious diseases. In this study, an investigation was carried out in to the development of a practical platform for the detection of infectious disease by nucleic acid amplification techniques for varying sample types. This required multiple and adjustable real-world to microfluidic device interfaces for the delivery of biological samples on to a microfluidic chip. Having discussed the large variety of microfluidic methodologies available for processing biological samples, it is evident that there is a need for establishment of a solid and reliable methodology for sample reception on chip, which is both simple to manufacture and implement. Ideally, this should be an adjustable process, to allow for the diversity of both sample volume and consistency. In other words, the manufacturing process should enable the user to create a 'fit for purpose' interface, dependant on sample type. In addition the interface should be able to receive the sample with as little pre-treatment and processing as possible.

The work presented follows the techniques of NAAT so described in the introduction. This technique has been demonstrated to be the most robust and sensitive mode of diagnosis, while also showing great potential for rapid processing. The interfaces were used in conjunction with a custom built, integrated genetic analyser (IGA) [JLS designs] in order to achieve a full sample-to-answer process. This device is described in detail in the materials and methods stion.

In order to evaluate and validate the microfluidic techniques developed here for clinical diagnostic applications, specific models of infectious samples were utilised in this study. Both MRSA and bacterial STIs, represent diseases which place significant burden on global healthcare resources and for which both treatment and prevention could be improved by the availability of simple and rapid POC diagnostic devices. Therefore, for the analysis of urine-based specimen types, STI causing organisms *C. trachomatis* and *N. Gonorrhoea* were employed as model targets, whilst for blood samples, MRSA was employed.

The project can be split in to the following main aims:

1) Development of a material for receiving a sample, which possesses both the structure and chemical surface for purifying nucleic acids. For urine-based analysis porous silica materials were selected because of high surface area and manufacturing benefits. In addition, the biopolymer, chitosan was explored as a possible material for DNA extraction.

2) An investigation in to the performance of interfacing of materials for DNA purification methodologies. This was carried out using well established silica-DNA chemistries using CS and a set of buffers of differing pH for chitosan-based DNA extractions

3) An investigation in to the incorporation of interfacing materials in to microfluidic devices. Glass was chosen as a material for potential in EOF operations and for good optical transparency. EOF would be highly beneficial for later integration to downstream steps. Good optical transparency is necessary for fluorescent detection which was intended for this system.

4) Investigation in to the integration of interfacing material to downstream steps such as PCR and detection by fluorescent techniques.

5) The development of an integratable electrophoretic detection system for amplified targets. An electrophoretic separation system was selected for simplicity and potential for multiplexing.

2 Materials and methods

The following chapter describes the materials and methods used throughout this research. Where more specific methodologies have been used, or where optimisation of methods has been conducted, details are given in the relevant chapters.

2.1 Preparation of materials

2.1.1 Preparation of Sol-gel based monoliths

Silica monoliths were synthesised using the method described by Fletcher *et al* (2011), based on the polymerisation of tetraethyl orthosilicate (TEOS) [Sigma Aldrich UK] in the presence of a water soluble polymer. 0.282g of polyethylene oxide (PEO) was dissolved in an aqueous solution of distilled water (0.291µl) and 1 M nitric acid (2.537µl) which were mixed in a 50 ml Falcon tube for 20 min on an ice bath. Once homogenous, 2.256 µl TEOS was added to the solution and stirred on ice for a further 30 min until a transparent solution was formed. The resulting solution was transferred to a 1 ml plastic tube (4.59mm internal diameter, 60 mm length) and sealed with PTFE tape, then dried at 40 ^{o}C for 3 days. Once dry, monolithic rods were removed from plastic tubes and washed for 24h in distilled water to remove excess nitric acid. Before further processing of the monoliths, the wash water was tested for neutrality with pH indicator paper. After washing, monoliths were placed in 1 M NH_4OH [Sigma Aldrich, UK] and heated under reflux at 80^{o}C. This was done in a silicon oil heater bath using a hot plate [Stuart®, UK]. Finally monoliths were removed from the solution and washed in distilled water before being dried. This was carried out incrementally, at 40 ^{o}C for 24 h, then 90 ^{o}C for 8 h to avoid cracking. Once dry, monoliths were calcinated at 550^{o}C to remove any remaining polymer. Following this the monoliths were ready for shaping for use.

Silica monoliths were also synthesised from TMOS [Sigma Aldrich UK] (2 ml), as described with TEOS. Using the same methodology, polymer, pluronic F127 [Sigma Aldrich UK] (0.432 g) was used rather than PEO. Polymerisation was catalysed by 0.02 M acetic acid (4 ml) rather than 1 M nitric acid.

2.1.2 Potassium silicate-based monoliths in capillaries

For preliminary analysis potassium silicate-based monoliths were formed in glass capillaries. 500 µl of potassium silicate (21% SiO_2 and 9% K_2O [VWR International, UK] was pipetted into a vial, and 50 µl of formamide [Alfa Aesar, UK] was added and mixed in to the potassium silicate. To ensure total dispersion, the formamide was added in two 25 µl doses and was allowed to homogenise gradually. On formation of a homogeneous solution one end of the capillary was submerged into the solution which was drawn into the capillary to a minimum depth of 10 mm via capillary forces. This process was carried out in < 5 min as rapid polymerisation results in a solution of high viscosity. Once the potassium silicate/formamide segment was in place within the capillary it was placed in an oven for 8 h (or overnight) at 90^{o}C for thermal curing. On removal, the monoliths were flushed with ethanol for 20 min at 5 µl min^{-1} to clear any unreacted material.

2.1.3 Chitosan coating of silica monolith

Monoliths were coated with chitosan (α (1→4)-linked 2-amino-2-deoxy-β-D-glucopyranose) [Sigma-Aldrich, UK], as described by Hinojosa Flores *et al* (2009). First, chitosan was dissolved to form a 1% w/v solution in 0.2 M acetic acid with manual shaking and ultrasonication in an ultrasonicator [SLS laboratories, UK]. Silica monolithic disks were immersed in the chitosan solution and heated to 60 °C in order to lower the viscosity of the chitosan solution and allow easy permeation of the monoliths. After 8 hs, monoliths were removed and washed sequentially with 0.02 M acetic acid and distilled H_2O three times, both at room temperature and then finally dried for 24 hs at 40 °C.

2.1.4 Fabrication of microfluidic devices

All microfluidic devices were fabricated in glass by Dr Steve Clark and Mr Mohammadmehdi Nasr Esfahani at the University of Hull. A combination of standard lithography and wet etching, together with milling techniques, were used (McCreedy, 2000). All mask designs were drawn using AutoCAD® and chip schematics were also drawn using Solidworks®. Masks [JD tools] were placed over glass substrate coated with photoresist and chromium and exposed to ultraviolet (UV) light for 1 min. The

exposed resist and chrome layer was removed using a 1:1 Microposit© Developer: H_2O solution [Chestech Ltd, UK] by submerging for 1 min, followed by removal of the chrome layer with Chrome Etch 18 Solution [Chestech Ltd, UK] by also submerging for 1 min. Hydrofluoric acid 1% / 5% ammonium fluoride solution was then used to etch the exposed glass. Etching was carried out at 65^{o}C to provide an isotropic etching at a rate of approximately 5 μm/min^{-1}. All remaining photoresist and chrome was removed with the solutions described previously. Entry ports were drilled in the top plate to a diameter of 1 mm for attachment of tubes for sample and reagent access using hydrodynamic pumping. Finally, top and bottom plates were bonded together at 595 °C for 3 hs.

2.1.5 Manufacture of gold nanoparticles

Gold nanoparticles (GNP) were manufactured using the Turkevich method (Turkevich *et al,* 1951). 250 ml of purified water was brought to boiling point in a conical flask. 1 ml of $HAu(III)Cl_4$ 1% [Sigma Aldrich, UK] was added followed by 5 ml 0.05 M sodium citrate [Sigma Aldrich, UK]. The mixture was stirred for 15 min. On reduction, gold aggregates produced GNP.

2.2 Structural analysis of silica structures

2.2.1 Scanning electron microscopy

SEM imaging was carried out by Mr Tony Sinclair, University of Hull. The monoliths produced were visualised using a Carl Zeiss EVO 60 scanning electron microscope [Carl Zeiss]. First, samples were mounted vertically on SEM stub using epoxy resin. The sample was then subjected to sputtering with gold/ palladium 82/18% V/V% [Agar Ltd, UK], in order to make the sample conductive. The samples were then irradiated with an electron beam (20 kV) to obtain SEM images.

2.2.2 Surface area and porosity analysis

Analysis of surface area and pore volume was carried out using a Surface Area and Porosity Analyzer [Micromeritics, Tristar]. All monoliths were weighed and placed in glass sample tubes, before being subjected to N_2 gas exposure. Measurements were

made using Brunauer–Emmett–Teller (BET) methods (Sing *et al*, 2008). The Tristar software was used to provide surface area measurements, porosity measurements and physisorption isotherms for analysis of pore characteristics. The following equations were used by the software to calculate surface area:

Equation 7: Relationship between volume of gas absorbed and partial pressure

$$\frac{1}{Va\left(\frac{P_0}{P}-1\right)}=\frac{C-1}{V_aC}\,x\,\frac{P}{P_0}+\frac{1}{V_mC}$$

Where Va is volume of gas adsorbed at standard temperature and pressure (STP) [273.15 K and atmospheric pressure (1.013 × 105 Pa)], in millilitres.

Vm is volume of gas adsorbed at STP to produce an apparent monolayer on the sample surface, in millilitres.

P is partial vapour pressure of adsorbate gas in equilibrium with the surface at 77.4 K (b.p. of liquid nitrogen), in pascals.

P_0 is saturated pressure of adsorbate gas, in pascals.

C is a dimensionless constant that is related to the enthalpy of adsorption of the adsorbate gas on the powder sample.

Equation 8: Total surface area

$$S_{total}=\frac{V_mN_a}{V}$$

Where N_a is Avogadro's number,

Vm is volume of gas adsorbed at STP to produce an apparent monolayer on the sample surface, in millilitres

V is volume occupied by 1 mole of the adsorbate gas at STP allowing for minor departures from the ideal, in ml.

S_{total} is total surface area (m^2)

Equation 9: Surface area per weight of structure.

$$Sbet=\frac{Stotal}{m}$$

Where S_{bet} is surface area ($m^2\ g^{-1}$)

Pore volume was calculated by the Tristar software using the following equation:

Equation 10: Volume of liquid on pores.

$$V_{liq} = \frac{P_a V_{ads} V_m}{RT}$$

Where, V_{liq} is volume of liquid N_2 in pores

V_{ads} is volume of gas adsorbed.

P_a is ambient pressure

R is gas constant (8.314)

T is ambient temperature

2.2.3 Back pressure measurements

The build up of pressure when pumping liquid through monolithic structures was measured, in order to establish the maximum tolerance of the structure to increased flow rates. Back pressures were measured using a device built in-house, adapted from a gas cylinder regulator [Engweld, UK].

2.2.4 Measurement of contact angles

All contact angles were measured using a Kruss contact angle measurement instrument [Kruss, UK]. For validation, a 5 µl droplet was placed on a glass slide coated with the same functional group as the surface to be analysed. The glass slide was then observed under a microscope with incorporated contact angle reference marker.

2.3 Collection of biological samples

2.3.1 Biological samples

Biological samples used in this project consisted of human saliva, blood and urine (all human). All samples were obtained from healthy volunteers at the University of Hull with full written consent and local approval. Urine was collected in sterile 100 ml plastic collection tubs and aliquoted into 1 ml quantities. The samples were stored at -20 ^{o}C and disposed of after 7 days. Blood samples were taken by a trained phlebotomist, providing in 1 ml quantities and storing at 4 ^{o}C for 7 days before

disposal. Anticoagulant, sodium citrate was also added. Saliva samples of approximately 5 ml were collected in 50 ml falcon tubes and used immediately. Bacterial genomic targets were obtained from Mrs Chris Murphy.

2.3.2 Artificial urine medium

An artificial urine medium (AUM) was used to simulate clinical samples in preliminary experiments (Kemp *et al*, 2012). The AUM is designed to simulate both the composition and pH of human urine. The composition of this is shown in Table 4.

Table 4: Composition of artificial urine medium.

List of components included in artificial urine medium, developed to simulate both composition and pH of a real urine matrix. Adapted from Brooks *et al* (1997).

Component	**Quantity (g)**	**Concentration (mmol 1^{-1})**
Peptone L37	1	Not given
Yeast Extract	0.005	Not given
Lactic Acid	0.1	1.1
Citric Acid	0.4	2
Sodium Bicarbonate	2.1	25
Urea	10	170
Uric Acid	0.07	0.4
Creatinine	0.8	7
Calcium chloride.$2H_2O$	0.37	2.5
Sodium Chloride	5.2	90
Iron II sulphate.$7H_2O$	0.0012	0.005
Magnesium sulphate.$7H_2O$	0.49	2
Sodium sulphate.$10H_2O$	3.2	10
Potassium dihydrogen phosphate	0.95	7
Di-potassium hydrogen phosphate	1.2	7
Ammonium chloride	1.3	25
Distilled water	Made to 11 g	

2.4 DNA extraction methodologies

2.4.1 Commercial spin column format DNA extraction

For DNA extraction experiments, a known concentration of human genomic DNA (hgDNA) was used to spike samples. hgDNA was purified from saliva samples using a QIAamp DNA Micro Kit [Qiagen, UK]. The kit offers a recovery of approximately 50% (Qiagen, 2003). The general procedure consisted of lysing cells within the sample using proteinase K and the lysis buffer provided. The sample was then passed through DNA extraction column using an EBA20 centrifuge [Hettich, Germany]. The centrifuge was then used to pass wash buffer through the column, before DNA was elute in the same way with elution buffer. The exact composition of reagents was not provided in the kit. All centrifuging was carried out at 5000 g.

2.4.2 Silica-based DNA extraction on-chip

All DNA extraction processes were performed using hydrodynamic pumping, allowing sample loading and recovery via entry and exit ports on the device. For studies of DNA extraction efficiencies, AUM (see stion 2.3.2) was spiked with human genomic DNA (hgDNA) (5 ng μl^{-1}) and mixed at a 1:9 ratio with a 5 M GuHCl in tris(hydroxymethyl)aminomethane (tris) / ethylenediaminetetraacetic acid (EDTA) buffer pH 6.7 solution [Sigma Aldrich, UK]. This total volume (50 µl) was then loaded onto the chip allowing binding of nucleic acids to the dual porous silica (DPS) monolith. 100% ethanol was then passed through the monolith to wash away contaminants before nucleic acids were eluted with water (process is discussed in further depth in stion 4.2). A series of 5 µl fractions were collected continuously from the outlet channel during the load, wash and elution stage and stored for further analysis at 5 ^{o}C (Shaw *et al,* 2009; Kashkary *et al,* 2012).

2.4.3 Chitosan-based DNA extraction

Preliminary DNA extraction efficiency experiments performed on chitosan-modified monoliths were carried out using AUM, loading the sample in 10 mM 2-(N-morpholino) ethanesulfonic acid (MES) buffer [Sigma Aldrich, UK] pH 5.05 at a 1:9 ratio, before flushing the monolith with MES buffer pH 5.05 to remove any unbound

contaminants. Finally, DNA was eluted using 10 mM tris(hydroxymethyl)aminomethane buffer with 50 mM KCl pH 9.

Subsequent evaluation of the system for extraction of DNA from human urine samples was performed by mixing with MES pH 5.05 at a 1:9 ratio and 150 µL total volume was loaded on to the monolith at 10 µL min-1. Subsequent steps were as described in 2.4.2.

2.4 DNA quantification

Quantification of DNA was carried out using a Quant-IT Picogreen® dsDNA Assay kit [Invitrogen, UK]. Picogreen® (PG) is a fluorescent molecule with an excitation maximum of 480 nm and emission at 520 nm (Dragan *et al*, 2010). 50 µl PG was diluted in 10 ml TE buffer. PG concentration was not provided. Throughout DNA extraction experiments 5 µl fractions were collected for quantification. This was achieved by depositing the fractions into a 96 well plate [Fisher scientific, UK] and adding 100 µl PG solution. Analysis of samples was carried out using a FLUOstar Optima Plate Reader [BMG Labtech, UK]. Figure 2.1 shows a typical sample layout for an extraction experiment. A calibration curve was generated by analysing 5 µl of a series of known DNA concentrations provided by the kit 10, 8, 6, 4, 2, 1, 0.5 ng μl^{-1} and a blank with the same 100 µl PG solution. A typical calibration curve generated by the BMG software is shown in Figure 2.2. Using this curve as a reference the unknown sample concentration could be established. For all experiments DNA extraction efficiency was determined as the total quantity of DNA eluted as a percentage of the quantity of DNA initially loaded onto the system.

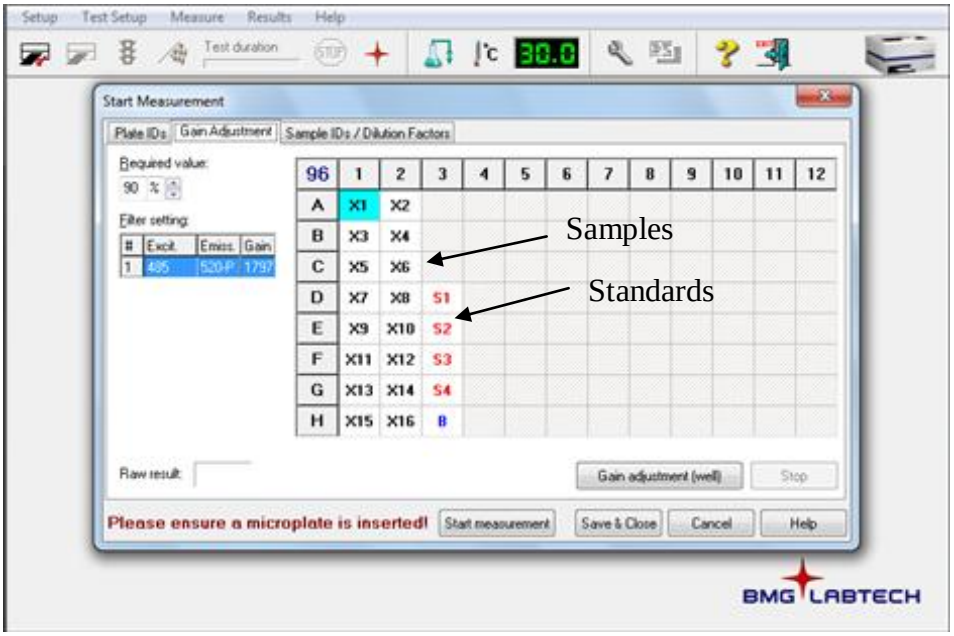

Figure 2.1: OPTIMA data analysis software.

A screen shot of OPTIMA Data analysis software [LABTECH]. The grid shows the layout of samples and reference standards. The grid indicates which wells are to be analysed by the instrument.

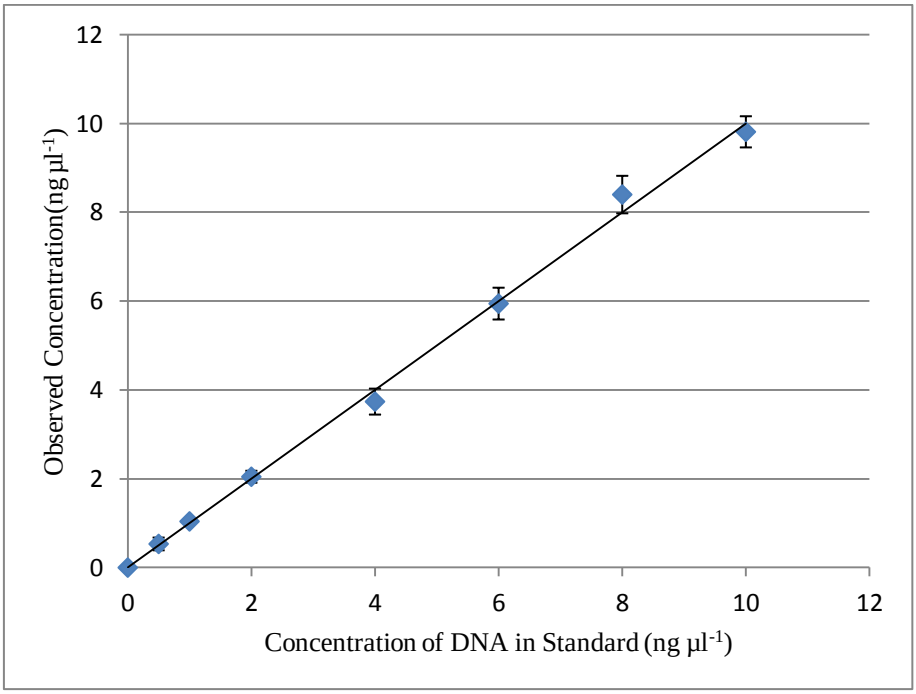

Figure 2.2: Picogreen® standard curve.

For quantification of DNA using PG assay, a typical calibration curve was generated for quantifying the DNA captured. The curve uses 8 concentrations (including a blank) as a reference for sample DNA quantity.

2.5 Amplification by polymerase chain reaction (PCR)

2.5.1 Commercial PCR kits used DNA amplification.

2.5.1.1 Standard PCR mixture.

Following the various DNA extraction procedures performed on the microfluidic device as described, the eluted DNA was subjected to conventional PCR amplification off-chip using a TC-312 thermal cycler [Techne, UK]. Samples of extracted DNA were added to a solution of: 2 units GoTaq® DNA polymerase [Promega, UK], GoTaq® buffer, 2 mM $MgCl_2$, 10 mg mL^{-1} bovine serum albumin [NEB Inc., UK], 200 µM deoxyribonucleotide triphosphates [Bioline, UK] and 0.1 µM each of forward and reverse oligonucleotide primers.

In addition, in some experiments, a commercial PCR MasterMix was used, comprising of the above components. 12.5 µl of the master mix was used with 5 µl H_2O and 2.5 µl selected primers and sample. Generalised conditions for thermal cycling were: 2 minute initial denaturation step at 95 °C followed by 30 s denaturation at 95 °C, 30 s annealing at 60 °C and 30 s extension at 72 °C for 35 cycles, with a final extension step of 7 min at 60 °C. Any deviation from these parameters will be described where relevant in the text.

2.5.1.2 Direct PCR amplification from blood.

For amplification of targets direct from blood without pre-treatment Phusion® direct blood kit [Thermoscientic, UK] was used. Samples of extracted DNA were added to 10 µl Phusion buffer, Phusion enzyme, 0.5 µM primer, 0.5 µM reverse primer, 1 µl blood and made up to 20 µL with dH_2O. Standard thermal cycling parameters were as follows: 3 min initial denaturation step at 98 °C, 1 s at 98 °C for 30 s and 60 °C and 30 s for 72 °C, then finally a 4 min final extension step at 72 °C. The TC-312 thermal cycler was also used here. Any devation from these general conditions is detailed in the relevant text. Following amplification samples were centrifuged to remove coagulated blood and the supernatant was retrieved for analysis.

2.5.2 Thermal cycling

A laboratory performing benchtop thermal cycler TC-312 [Techne, UK] was used to conduct PCR amplification to assess the quality of extract DNA and for validation of experiments to amplify DNA on-chip. PCR sample and reagents were prepared as described in stion 2.5.1. DNase/RNase free, thin wall polypropylene PCR tubes [Alpha Laboratories, UK] were used for carrying out reactions. The PCR instrument has a heated lid faculty (105 °C) which prevents evaporation of samples during thermal cycling. The thermal cycling parameters are described throughout the text in the subsequent chapters.

2.5.3 Oligonucleotide primers

Throughout this work, a series of primer sets were used for the PCR amplification of both bacterial and human genomic fragments. While primer sets targeting bacterial fragments were selected for each specific application, forensic primer sets [Eurofins MWG Operon, Germany]. were used throughout the developmental stages to optimise and validate the system. All primer sequences are shown in Table 5. Primer sequences comprising the size ladder were designed by Dr Kirsty Shaw, Manchester Metropolitan University.

Table 5: Oligonucleotide primer sequences.

Sequence of primer pairs (forward and reverse) for each target locus are shown. Primers were purchased from MWG Eurofin. Note, C. trachomatis and N. gonorrhoea primers are not disclosed for confidentiality reasons. Regarding size ladder, PCR products were generated from λ phage using a single forward primer and four reverse primers of different length.

Oligonucleotide Primer pair	Product size (bp)	Fluorescent label
Amelogenin (107/109 bp)	106 (male) or 106/112 (female)	
Forward: 5′ ACC TCA TCC TGG GCA CCC TGG 3′		FAM
Reverse: 3′ AGG CTT GAG GCC AAC CAT CAG 5′		
D21	*226*	
Forward: 5′ TGTATTAGTCAATGTTCTCCAGAGAC 3′		FAM
Reverse: 3′ ATATGTGAGTCAATTCCCCAAG 5′		
Chlamydia trachomatis, Neisseria gonorrheoa (Not disclosed)	*314, 204*	FAM (forward), ROX (Forward)
Staphyloccocus aureus	*107*	
Forward: 5′ AATCTTTGTCGGTACACGATATTCTTCACG 3′		FAM
Reverse: 3′ CGTAATGAGATTTCAGTAGATAATACAACA 5′		
MecA		
Forward: 5′ AAAATCGATGGTAAAGGTTGGC 3′		FAM
Reverse: 3′ AGTTCTGCAGTACCGGATTTGC 5′		
Size Ladder	*100, 200, 300, 400*	
Forward: 5′ GCGCTGTGGCTGATTTCGATAACC 3′		FAM
100 bp: 3′ AACGGCGTTTCGTGTCTCTGCCGGT 5′		
200 bp: 3′ TGGATACGTCTGAACTGGTC 5′		
300 bp: 3′ ACGGATGAAACTGCCGGTCAGGACA 5′		
400 bp: 3′ CCGCTCGCTGGGTGAA 5′		

2.5.4 Peltier heating systems

For thermal cycling procedures performed on microfluidic devices, a Peltier heating system [QuickOhm, Germany] was used. A T-type thermocouple [Omega, UK] was used to control and monitor temperature feedback and a convection heat sink was used to accelerate cooling. A Peltier thermal cycling heating system set-up was also incorporated in the portable integrated genetic analyser (stion 2.7). Thermal paste [RS Components Ltd., UK] was used to ensure efficient contact between Peltier and microfluidic devices. The Peltier system was controlled and monitored using a custom-written software [Labview]. A screenshot of this software is shown in Figure 2.3.

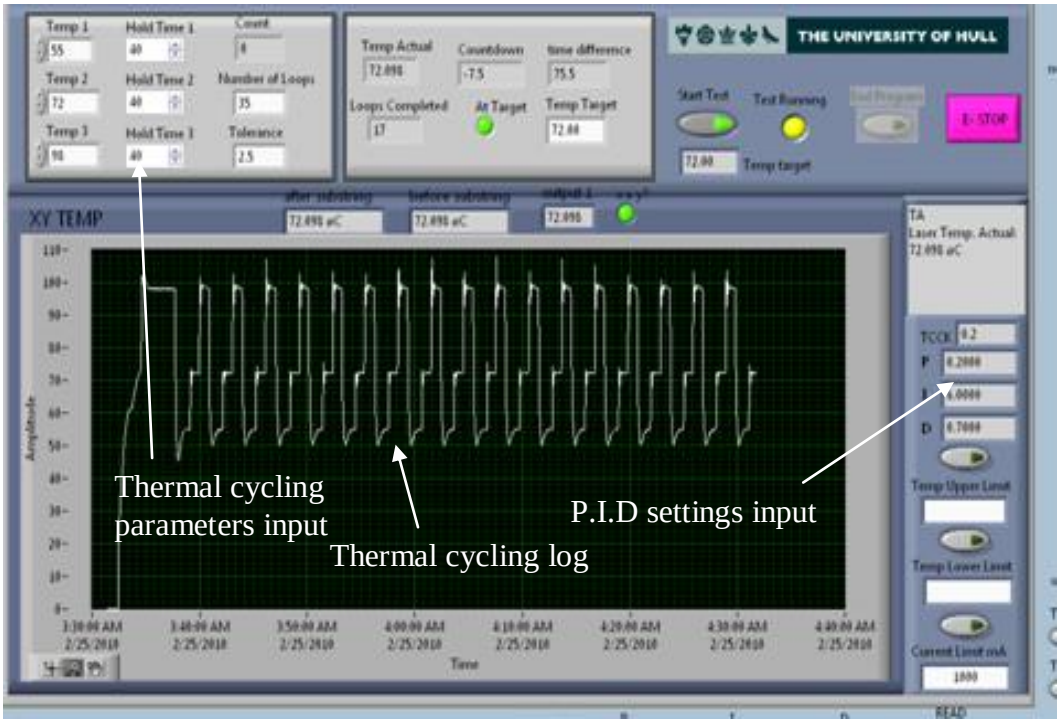

Figure 2.3: Peltier software display.

A representative screen shot of software [Labview™] to operate Peltier thermal cycling system. All thermal cycling parameters are input into designated stions prior to run.

2.5.5 Silianisation/surface treatment

For silanisation of surfaces, microfluidic devices were first dried overnight at 40^{o}C. Then, 145 µl trichloroperfluoroctyl [Sigma Aldrich, UK] was dissolved in 1 ml

isooctane [Sigma Aldrich, UK]. The solution was then flowed through the microfluidic chamber for 5 min at 20 µl min^{-1}. Following this, the chamber was then washed with isooctane, acetone and finally distilled H_2O. The device was then allowed to dry at 40^oC for 48 h.

2.6 Detection of PCR products

2.6.1 Analysis by agarose gel electrophoresis

Horizontal slab-gel electrophoresis was performed using 2 % (w/v) agarose gels, prepared by dissolving 3 g agarose [Bioline, UK] in 150 ml Tris, acetic acid, EDTA (TAE) buffer [Sigma-Aldrich, UK] with 1 drop of 0.5 µg/ml ethidium bromide [CLP, UK] added before allowing it to solidify in a 15 x 15 cm gel tray with comb inserted. Once cooled, the comb was removed, leaving sample wells and the gel was placed in a HU15 standard horizontal gel electrophoresis tank [Scie-Plas, UK] containing TAE buffer prior to sample loading. The sample loading solution consisted of 10 µl of PCR product with 2.5 µl of DNA loading buffer [Bioline, UK]. A 12.5 µl aliquot of DNA size standard, Hyperladder IV [Bioline, UK] was also added to one of the wells in the gel. Samples were subjected to 90 V for approximately 40 min until adequate separation was achieved. Gels were then visualised using a UV transilluminator [Syngene, UK]. Gel images were recorded using Genescan software [Syngene, UK].

2.6.2 Analysis by capillary electrophoresis

Amplified DNA samples were analysed using CE (3500 Genetic Analyzer, [Applied Biosystems, UK]. Samples (1 µL) were added to 12 µL of Hi-Di™ Formamide and 0.5 µL GeneScan™ 500 LIZ® Size Standard [Applied Biosystems, UK]. Prior to CE, samples were denatured at 95°C for 4 min, before being pipetted into a 96 well plate [MicroAmp, UK] for insertion in to instrument. The data was processed and analysed using genemapper software [Applied biosystems, UK].

2.7 Integrated genetic analyser

A custom-built integrated genetic analyser (IGA) [JLS Design Ltd] was employed to operate automatic processing of chip devices (Figure 2.4). The instrument was custom

designed at the University of Hull for integrating DNA extraction, amplification and detection processes on a single chip device to support complete genetic analysis (Shaw *et al*, 2011). The instrument was designed with a Peltier element and thermocouple incorporated for thermal cycling in PCR amplification. In addition a continuous wave 488 nm solid-state laser and avalanche photodiode detection (APD) system [Comar Optics, Canada] was fitted for detection of fluorescently tagged PCR products. A schematic of this detection system is shown in Figure 2.5. All movement within the device was carried out using an electrokinetic methodology. A range of power supplies 0-1kV, 0-4kV 0-7kV were present and were accessed though electrodes in the instrument lid, which make contact with carbon electrodes fitted in to the microfluidic device upon closing.

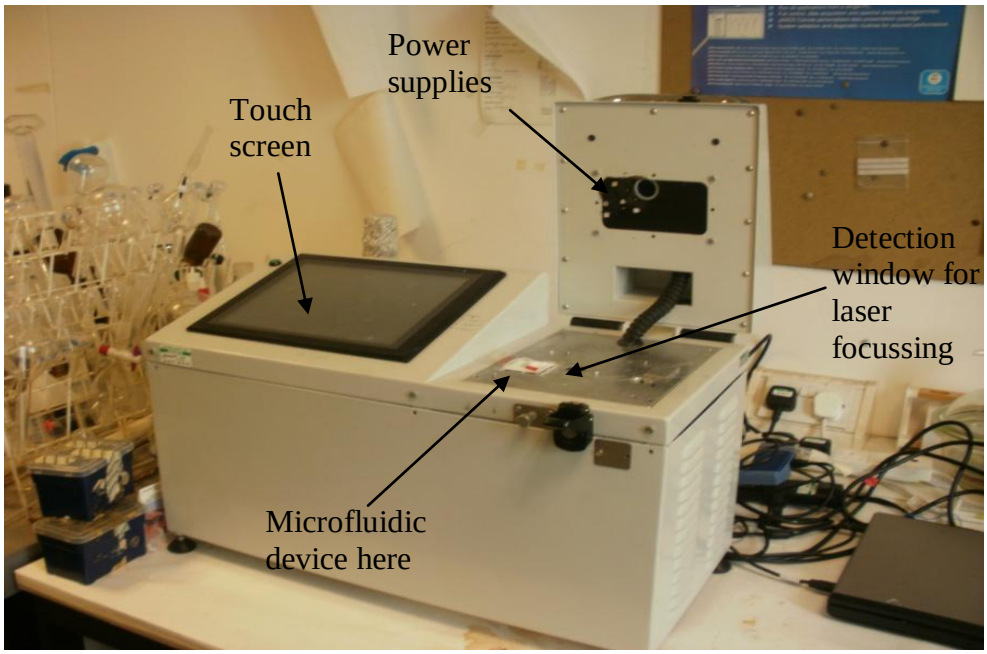

Figure 2.4: Image of integrated genetic analyser.

Power supplies (shown) inside the lid are attached to electrodes which make contact with electrodes in the microfluidic device. A detection window is located under the microfluidic device with a fitted laser beneath. A Peltier element is also fitted beneath the microfluidic device for thermal cycling. A touch screen user interface provides control of power supplies, laser and Peltier element. All operations were carried out using a touch screen control panel installed with control software [JLS design Ltd]. All fluorescence data is processed using K-LAB DNA data acquisition software.

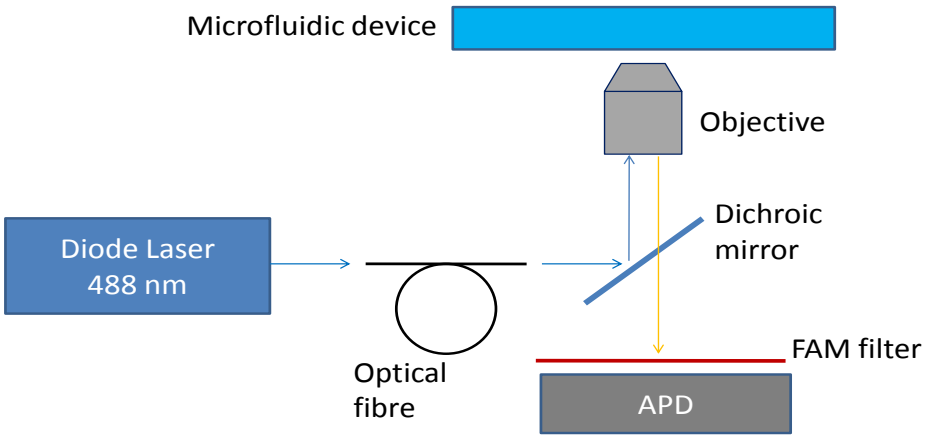

Figure 2.5: Schematic of integrated genetic analyser detection system.

Schematic showing the setup for avalanche photodiode detection system in the IGA.

2.8 Microfluidic integrated chip

2.8.1 Design and preparation

Chip (Figure 2.6) for performing PCR amplification and electrokinetic separation of DNA was prepared by injecting performance optimised polymer (POP7) in to all channels with a syringe. The chamber and electrode ports were filled with cathodic buffer. Carbon electrodes manufactured by Dr Peter Docker were then inserted in to electrode ports. Finally, the sample was added to the sample chamber for injection and analysis. Further information about injection is given in Chapter 5.

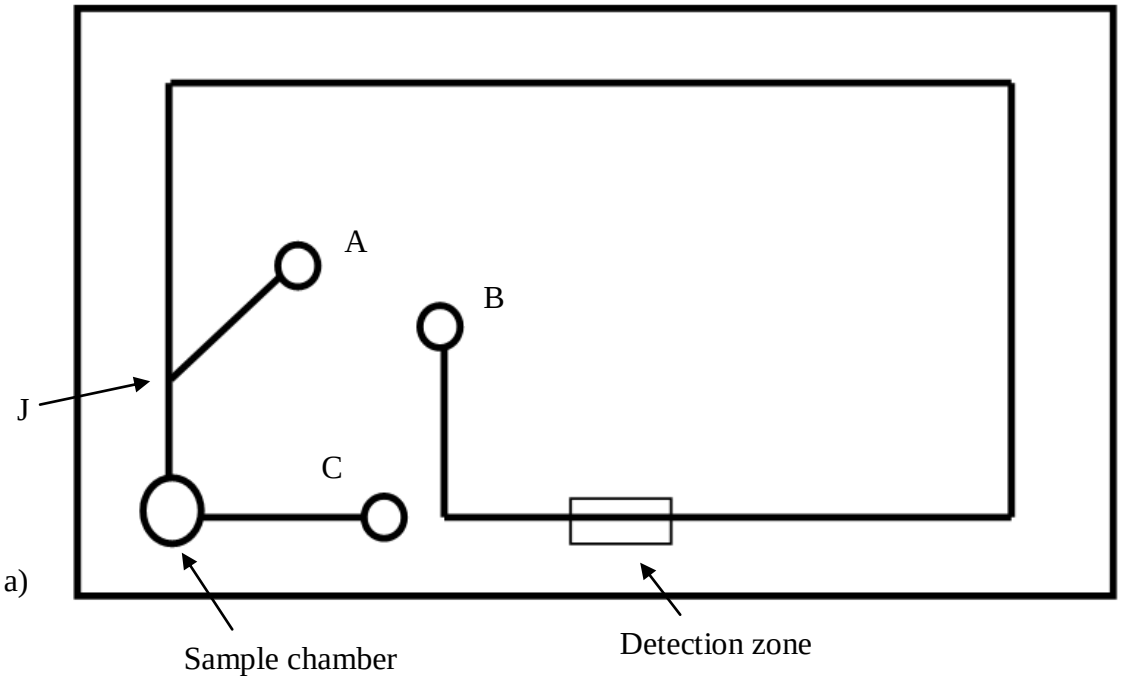

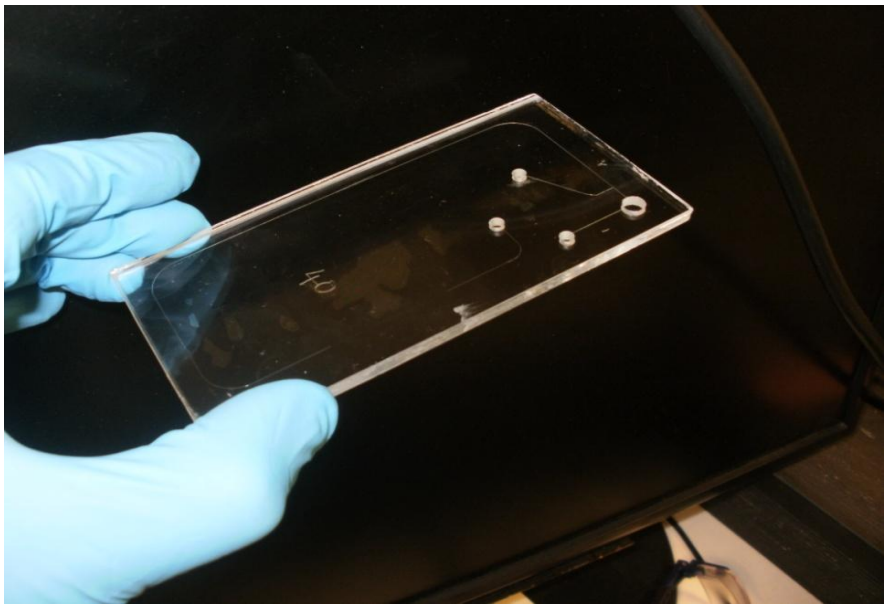

b)

Figure 2.6: Integrated microfluidic device for DNA analysis.

a) Schematic to show chip designed for IGA. A. B and C denote points for electrode contact. J is the junction used for generation of the DNA plug for separation. Detection zone shows where laser is focussed and DNA is detected. b) photograph of glass microfluidic device for use in IGA. All channels are 40 µm depth and 100 µm wide. Separation channel (measured as sample chamber to well C) comprises a volume of 0.712 µl.

2.8.2 Plug Injection

Using the power supplies within the IGA (Figure 2.6a), first 4000 V was applied between electrodes B (ve -) and C (ve +) to allow the sample to migrate through the channel. Then 1000 V was applied between A (ve-) and B (ve +) to cause DNA at junction (J) to move back in to sample chamber. This ensures a small plug of DNA held above junction J can be used for separation. Finally 7000 V was applied between A (ve-) and B (ve +) to separate and detect in the "detection zone". Throughout the separation phase the 1000 V applied between A and B was maintained. Standard timescales for stage 1 and 2 were 30 s and 600 s, respectively. Any deviation from this is described in the text.

3 Development, manufacture and structural analysis of materials for solid phase extraction of DNA

3.1 Introduction

This chapter describes the development and characterisation of materials for use as real-world to microfluidic device interfaces for NAAT. As discussed in stion 1.5, the interfaces were selected and developed to be adjustable, dependant on sample size and type. This would allow a wider range of applications to be carried out on a single platform. As an exemplary system, the work carried out in this and the following chapter aims to detect a multiplex of two STI targets from urine samples. A sample volume of 150 µl was selected as a more clinically relevant volume. This is significantly larger than samples processed in the work described in Table 3. As described in stion 1.1, STIs are a significant problem in the UK and are currently a serious threat in the developing world. Genomic targets *N. gonorrhoea* and *C. trachomatis* were used here as a model system. In addition, the interface, ideally, should be able to receive the biological sample in as unprocessed a state as possible.

The system could also be used as an interface for sample delivery for the detection of urinary tract infections, such as MRSA. While diagnosis of MRSA is generally performed from blood samples (Shin *et al,* 2010*),* including several reports of MRSA detection on microfluidic devices (Cooney *et al,* 2012), MRSA has also been found to be responsible for urinary tract infections. Notably, the elderly are often susceptible due to the repeated introduction of urinary catheters. Muder *et al* (2006) discussed in depth the significance of S. *aureus* isolation in urine samples and the correlation with an infection of the blood stream. Of 88 patients positively diagnosed with a urinary tract infection, 11% were found to have subsequent methicillin resistant staphylococcal bacteraemia. In addition to this, Anderson *et al* (2006) reported that 15.7% of patients were diagnosed with bacteraemia due to MRSA following an earlier diagnosis of an MRSA urinary tract infection (Baraboutis *et al,* 2010). Despite such coverage in the literature, the issue of MRSA detection in urine has been relatively unaddressed and a rapid diagnostic tool has not yet been proposed. Such a system would be a useful diagnostic option in clinical settings and homes for the elderly. Furthermore, an on-going screening program of patients/residents at risk for MRSA

infection would be relatively easy to put in place, as the non-invasive urine sample is preferable to a blood sample. The close link to sondary MRSA-based bacteraemia would also mean diagnosis could be made before progression of this stage occurs.

As described in stion 1.4.2, urea, a major constituent of urine, has been found to inhibit subsequent PCR analysis, requiring purification of the target DNA prior to amplification. Unlike inhibition associated with blood-based PCR (haem interferes with *Taq* polymerase), however, the extraction of DNA from urine serves with increased importance as a preconcentration step (Dineva *et al, 2007),* due to the larger sample volume and lower concentration of target DNA.

Silica is a well-characterised material which has been applied to SPE for DNA purification in numerous formats and was chosen for the development of the chip device delivery/extraction interfaces in this study. While there are several silica formats (e.g. silica beads, magnetic beads, fabricated channel) (stion 1.4.4.3) porous materials were chosen for their established and robust modes of synthesis and also their favourable mechanical features. DNA extraction efficiencies of 78 % and > 90% on porous materials have been reported by Shaw *et al* (2009) and Wu *et al* (2006), respectively, while bypassing issues of reproducibility associated with silica beads. Both methodologies did, however, necessitate *in situ* synthesis of monolithic materials. Recent work by Fletcher *et al* (2011) describes the development of PSM, which can be shaped in and retrieved from a mould for further treatment and manipulation. This work demonstrated the ability to manufacture silica monoliths with a variety of pore sizes within one structure by subsequent treatment with a basic solution. By way of dissolution/re-precipitation, the treatment is able to provide an increased structural integrity and full control over porosity. The ability to generate a distribution of micron-scale pores within a network of nano-scale pores is essential to ensure effective permeability, whilst maintaining a high surface area for chemical activity. As these monoliths could be adjusted in size and shape, they would be perfectly suited as an adjustable substrate, for multiple applications.

As described in stion 1.4.4.4, the introduction of chitosan to the silica system has been reported as an alternative DNA purification chemistry by anion exchange (Cao *et al,* 2006). The monoliths reported here were suitable for functionalisation with chitosan and an investigation into the efficiency of DNA extraction was carried out.

An investigation was carried out in to the performance of PSM which were designed to accommodate a large volume sample of variable and unpredictable consistency, whilst also maintaining a high surface area for capture of DNA. This was carried out by a simple SPE extraction methodology. For this reason surface area and pore characteristics were investigated, using BET techniques. In addition to this, the process of manufacture, including simplicity and scalability was evaluated. Finally, the monoliths were incorporated into microfluidic devices for integration to downstream steps in the NAAT process, so the feasibility for this was taken in to consideration when manufacturing the porous materials.

While this chapter will focus on the structural characteristics attributed to the materials investigated, Chapter 4 will describe all implementation and application of the materials for DNA extraction.

3.2 Materials and methods

3.2.1 Monolith synthesis

3.2.1.1 Silicon alkoxide-based monoliths

Silicon alkoxide-based monoliths were manufactured as described in stion 2.2.1. For preliminary experiments the rod-shaped monoliths were encased in heat shrink wrap (HSW) [Adtech polymer engineering Ltd] to generate airtight flow systems. This was achieved by placing the pre-formed monolith (length 5 mm, volume ≈ 62 mm^3) in HSW with a 5 mm length of glass tubing 3 mm outer diameter at either side. The complex was then subjected to heating at 330^oC. Following this, ethylene (tetrafluoroethylene) (ETFE) tubing was attached to glass tubing using epoxy resin and the complex was attached to a syringe. See Figure 3.1 for schematic of flow system.

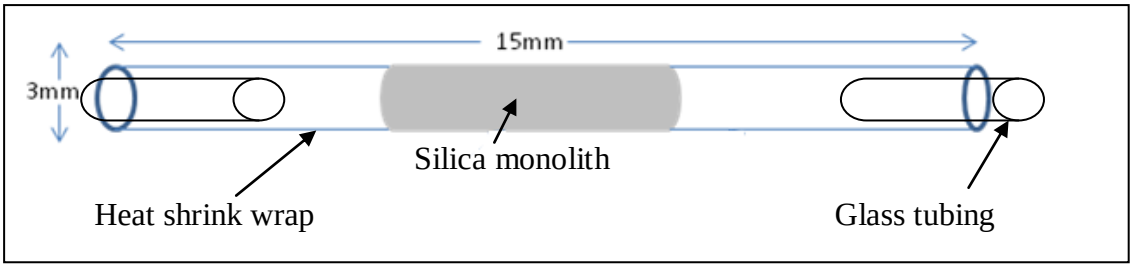

Figure 3.1: Silicon alkoxide-based monolithic flow system.

Schematic of silicon alkoxide-based monolith encased in heat shrink wrap with two lengths of glass tubing attached at either end. When shrunk the complex is an airtight flow system. A syringe pump can be attached at one end with ETFE tubing to permit hydrodynamic pumping through the system.

3.2.1.2 Potassium silicate-based monoliths

Potassium silicate-based monoliths were synthesised in capillaries for characterisation. This was carried out by mixing the components as described in stion 2.2.2 and drawing them in to the end of a glass capillary using capillary forces. The monolith within the capillary was 5 mm in length amounting to a monolith volume of ≈ 1.6 mm^3. See Figure 3.2 for schematic of flow system. In addition, potassium silicate-based monoliths were synthesised in plastic tubes (ID 4.59 mm) (Total monolith volume ≈ 62 mm^3).

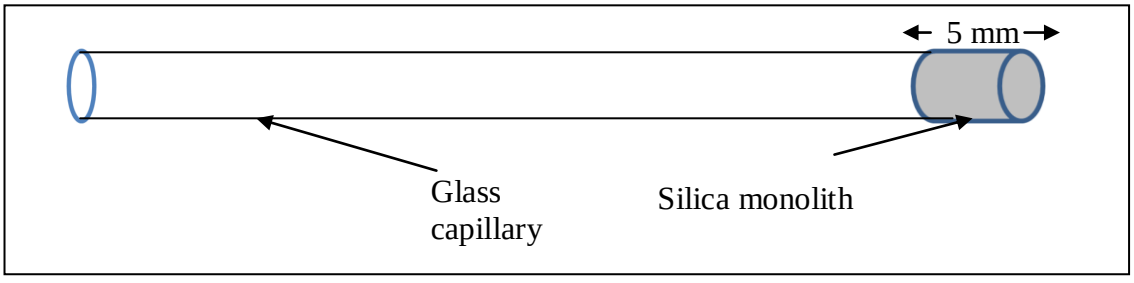

Figure 3.2: Potassium silicate-based monolithic flow system.

Schematic of potassium silicate-based monolith inside glass capillary. ETFE tubing is attached at one end to permit attachment to a syringe for hydrodynamic pumping of liquids through the system.

3.2.1.3 Chitosan-based materials

Chitosan/silica hybrids were synthesised by first dissolving 0.432 g pluronic F127 [Sigma Aldrich, UK] in 4 ml 0.02 acetic acid for 20 min, then mixing in 2 ml of a 1 % w/v chitosan solution in 0.2 M acetic acid. 2 ml TMOS was then added and stirred for 30 min. The resulting solution was then transferred to 2 ml syringes and sealed for gelation. The remaining steps were as described for silicon alkoxide monoliths (stion 2.2.1). In addition chitosan/silica hybrids were synthesised with potassium silicate and formamide by adding 1 % w/v chitosan solution in 0.2 M acetic acid to the potassium silicate/formamide mixture in a 1:10 ratio.

3.3 Results and Discussion

3.3.1 Manufacture and characterisation of silicon alkoxide-synthesised monoliths.

3.3.1.1 SEM analysis of monolith structures.

The silicon alkoxide precursors that were used in these studies were TEOS and TMOS. Synthesis and manufacture of these monoliths is described in stion 2.1.1. An initial visual evaluation of the structure of the TEOS-synthesised monolith was carried out. Importantly, the monoliths formed without cracking, which was an issue described as a major concern regarding the synthesis of porous materials regarding similar applications (Nakanishi, 1997). Following this, further analysis was carried out using SEM imaging. Figure 3.3a shows the structure at the centre of the monolith once all synthetic steps were complete. The image shows a uniform porous structure, in accordance with that reported in the literature (Fletcher *et al*, 2011). To observe the influence of the post-treatment with 1 M NH_4OH, the monolith was imaged without 1 M NH_4OH treatment (also imaged at centre of monolith), by drying immediately after removal from moulds (Figure 3.3b). A comparison of the images of the treated and untreated monoliths indicate a significant alteration of pore structure due to treatment with 1 M NH_4OH. Before treatment (Figure 3.3b) the structure is uniform, with pore sizes ranging between 10 and 40 µm, while post treatment (Figure 3.3a) images show a congelation of the finer structure within the monolith structure. The pore size of the monolith post-treatment lies within a smaller range of between 40 and 50 µm. In

agreement with the literature, the image demonstrates the effect of "Ostwald's ripening", in which smaller solids will dissolve and deposit on to larger solid and the latter will increase as a function of time by way of dissolution/ reprecipitation (Yao *et al*, 1992). This improves structural integrity at the expense of surface area (Nakanishi, 1997).

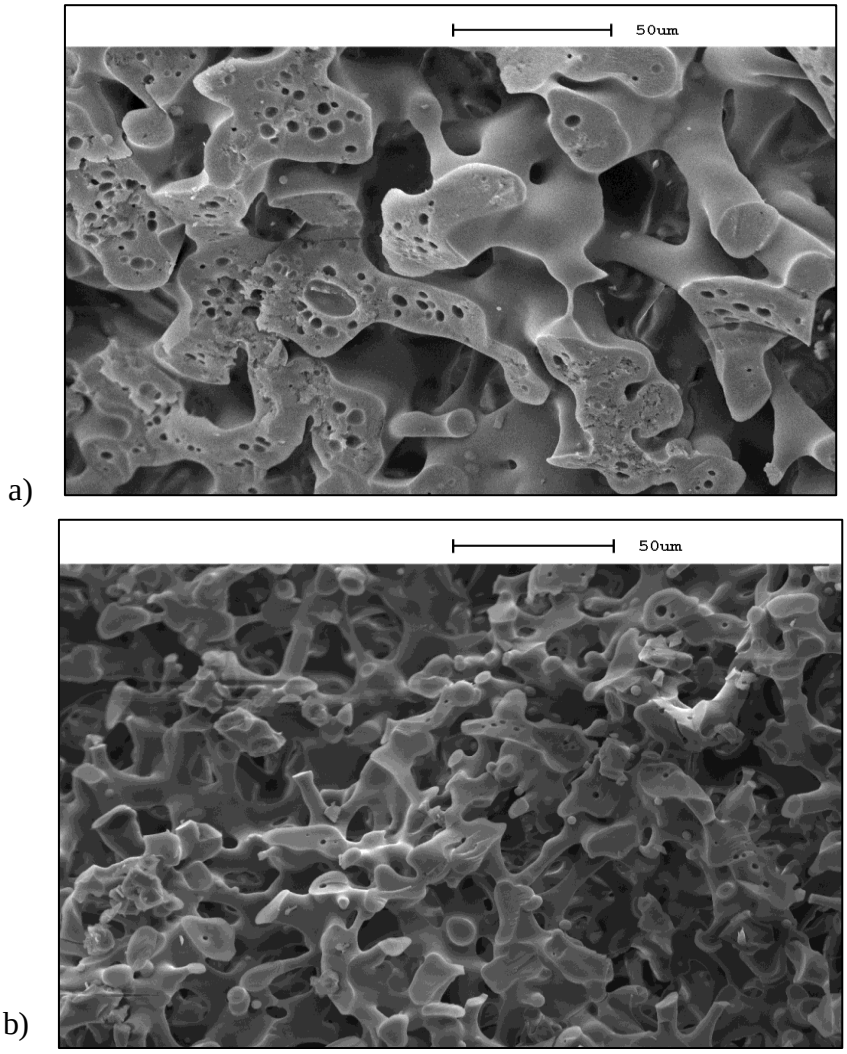

Figure 3.3: SEM images of TEOS-based monoliths.

SEMS images show a) TEOS monolith prepared with 1M NH_4OH treatment for 24 h and b) TEOS monolith prepared without treatment with NH_4OH. The larger features and pore sizes of (b) show evidence that dissolution/reprecipitation (Ostwald's ripening) has occurred. Images represent present typical structure. N = 3. Both images are magnified 2000x.

TMOS-based monoliths were then synthesised and analysed using SEM for comparison. The image shown in figure 3.4a are TMOS-based monoliths synthesised using an identical gelation procedure to that of the TEOS-based monoliths. Figure 3.4b is a further magnification of TMOS-based monolith, revealing a rough surface, contributing additional surface area to the structure.

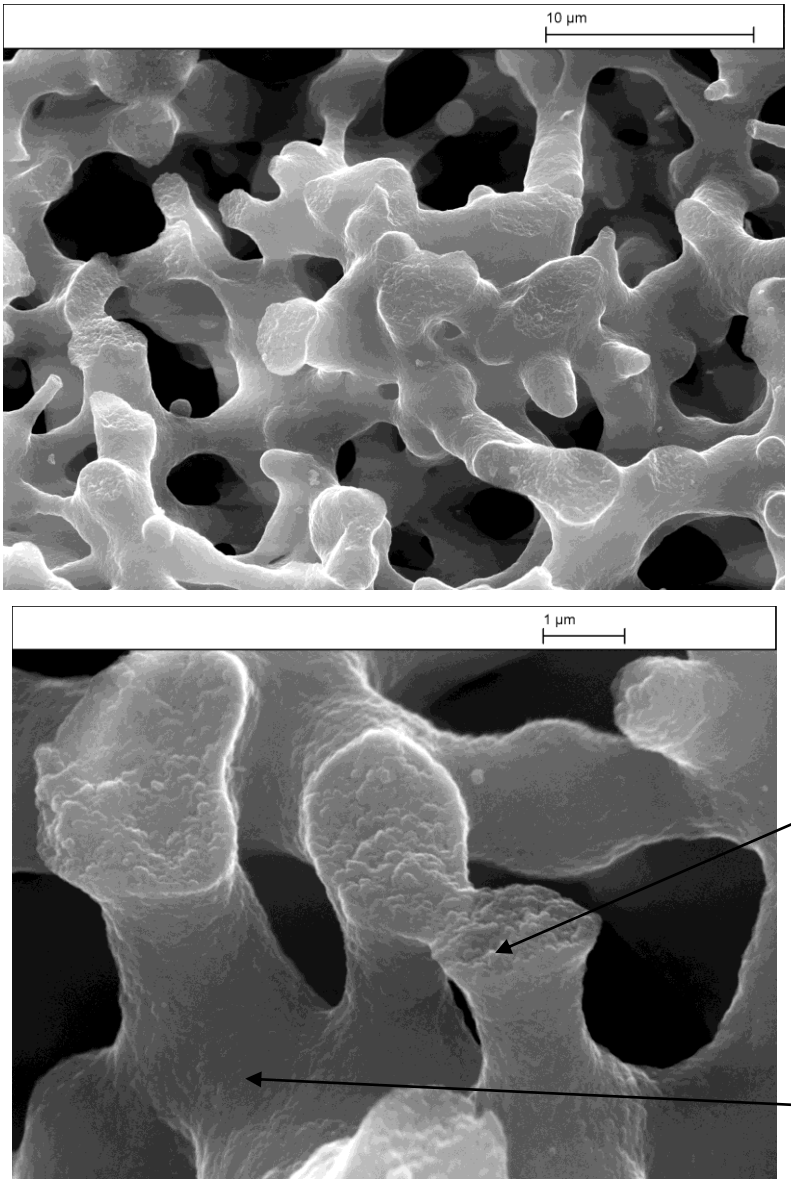

Figure 3.4: SEM images of TMOS-based monolith.

SEM images show a) TMOS monolith treated with 1 M NH_4OH for 24 h. Magnification 10,000x. Comparison shows a wider range of pores for the TMOS-based monolith ranging from 5 to 40 µm. b) Further magnification (20,000x) of TMOS monolith show rough surface, increasing potential surface area. Images represent present typical structure. N = 3

The resulting pore structure for the TMOS-based monolith provided a much finer structure with smaller pores ranging between 5 and 40 µm, much like the TEOS-based monolith untreated. It is postulated that despite the similarity in pore structure, the additional treatment of the TMOS-based monolith with 1M NH_4OH would comprise a greater structural integrity than that of the untreated TEOS-based monolith.

3.3.1.2 BET analysis

General pore classifications are summarised in Table 6. Generating a distribution of micron-scale pores within a network of nano-scale pores is essential to ensure effective permeability for sample movement, whilst maintaining a high surface area for extraction. BET surface measurement techniques were used to further characterise this porosity and also provide surface area measurements of TEOS and TMOS monoliths.

Table 6: Classification of pores.

Size range of micropore, mesopores and macropores. Data adapted from Sing *et al* (2008).

Pore size	Pore diameter range (nm)	Pore diameter range (µm)	Pore diameter* range (Å)
Micropores	< 2.0	< 0.002	< 20
Mesopores	2 – 50	0.002 – 0.05	20 – 500
Macropores	> 50	> 0.05	> 500

Due to the influence of 1 M NH_4OH treatment on pore structure it was postulated that an optimum surface area for DNA capture could be established by varying this treatment time. TMOS monoliths were, therefore, analysed following variations in 1 M NH_4OH treatment for 4, 8, 16, 32 and 48 h in order to understand further, the effects of treatment on the structure. The surface area ($m^2\ g^{-1}$) was found to gradually decrease with increasing length of treatment with 1 M NH_4OH (see Figure 3.5a). This is in agreement with work reported by Nakanishi (1997), as an increase in pore size

by dissolution/ re-precipitation would be at the expense of surface area. When not treated at all, the surface area was found to be negligible. It was postulated that the lack of surface area is due to much of the porous network having collapsed and having restricted flow throughout the structure. As the BET procedure depends on the distribution of N_2 throughout the network, the process would be hindered by this collapse.

While pore size is shown to increase on further treatment by SEM imaging (Figure 3.3), overall pore volume within the monolith ($cm^3\ g^{-1}$), was also found to decrease (see Figure 3.5b). This may be attributed to minimal pore closure. The uncontrolled nature of the dissolution/re-precipitation process at the micro-scale, results in the development of impermeable zones within the monolith. This would occur when areas within the silica monolith are structurally congealed in to a sealed pocket.

In addition physisorption isotherms were obtained, to identify the variety of pore characteristics generated within TMOS monoliths (TMOS 0-48 h 1 M NH_4OH treatment). On analysis of the adsorption and desorption of N_2 to the silica surface it was possible to establish the extent to which meso- and macro-pores were present, by monitoring the relative pressure (P/P_0) change within the presence of the sample (Sing *et al*, 2008). For example, in the event of adsorption/ desorption taking place on a structure with little or no pores, relative pressure change during desorption will be a direct reversal of that of the adsorption. This would be observed as a desorption curve superimposed on the adsorption curve. However, in the presence of meso-pores, the desorption process is hindered by the effect of capillary action, thus slowing down the release of N_2 from the porous network. This is visible in the isotherm with a shift in desorption curve.

a)

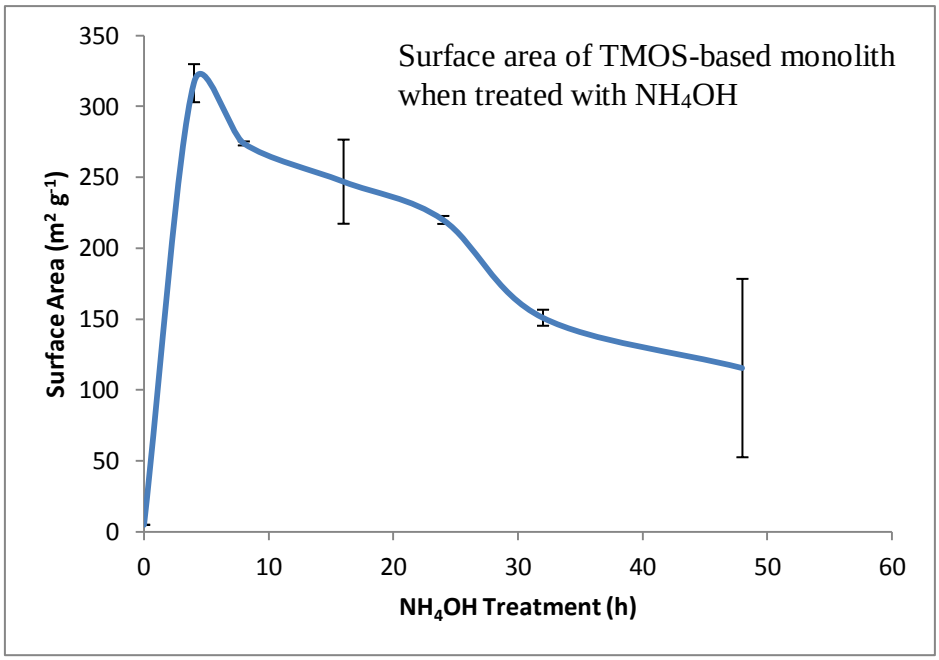

b)

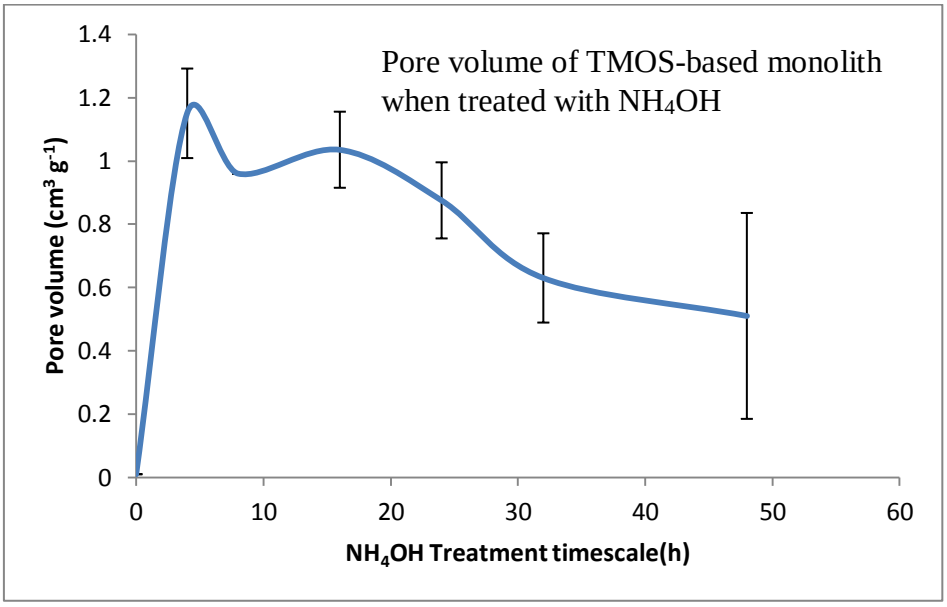

Figure 3.5: Influence of 1 M NH_4OH treatment on pore structure

Graphs shows the influence of 1 M NH_4OH treatment on (a) surface area (n=2) and (b) influence on overall pore volume within the monolith (n=2).

Meso-pores were evident for all TMOS monoliths treated for 4 h and above. Figure 3.6 is an isotherm for an untreated monolith and Figure 3.7 is a monolith treated for 24 h. The meso-pores are likely attributed to the rough surface demonstrated on the porous structure sub µm. (Figure 3.4b), providing and increased surface area.

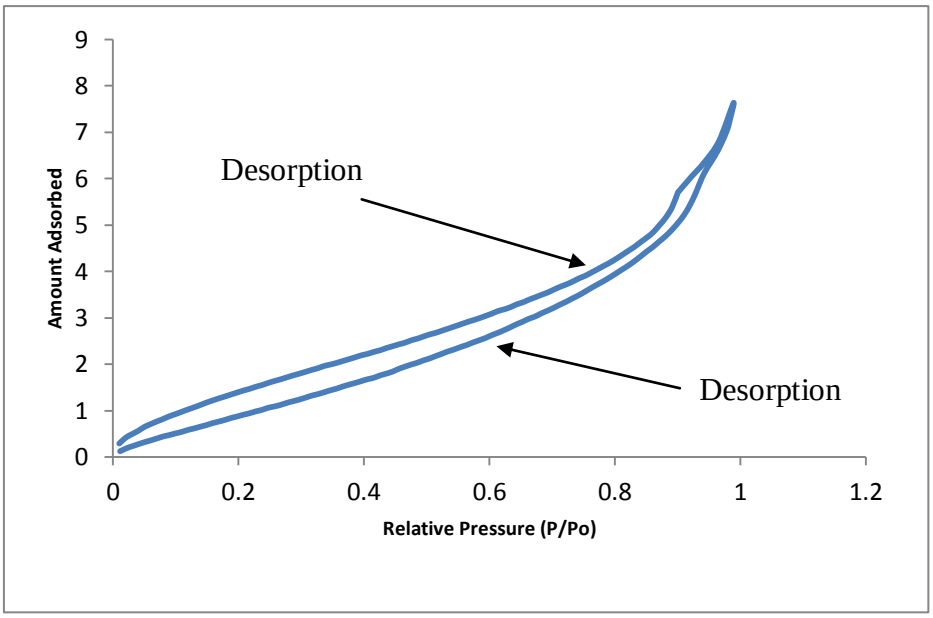

Figure 3.6: Physisorption isotherm for TMOS-based monolith untreated with 1 M NH_4OH.

Physisorption isotherms generated using BET N_2 adsorption analysis. Isotherm obtained with analysis of TMOS monolith without 1 M NH4OH treatment.

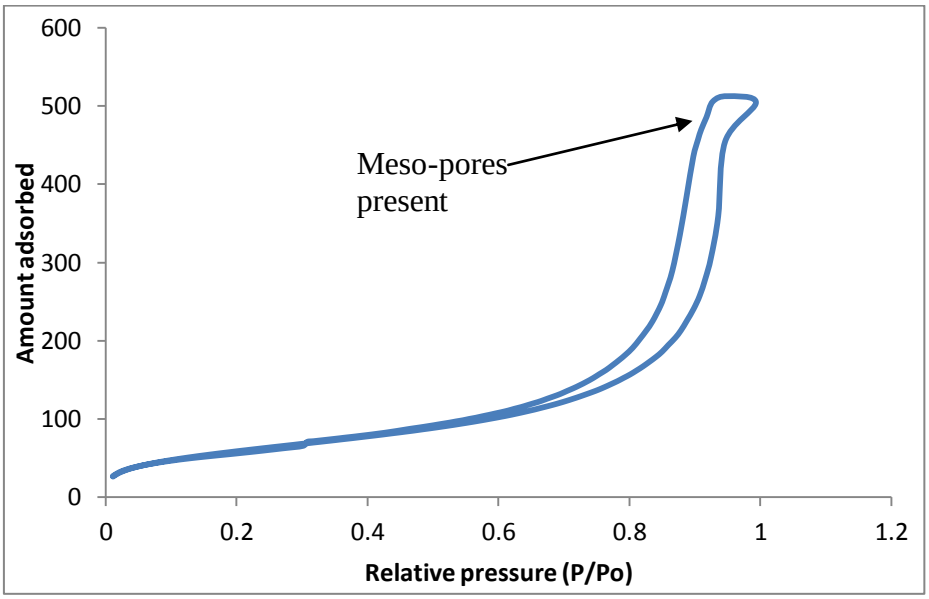

Figure 3.7: Physisorption isotherm for TMOS-based monolith treated for 24 h with 1 M NH_4OH.

Physisorption isotherms generated using BET N_2 adsorption analysis. TMOS monolith treated with 1 M NH_4OH for 24 h. Note, the shift in desorption peak is a result of capillary forces hindering release of N_2 gas from the structure, indicating the presence of meso-pores.

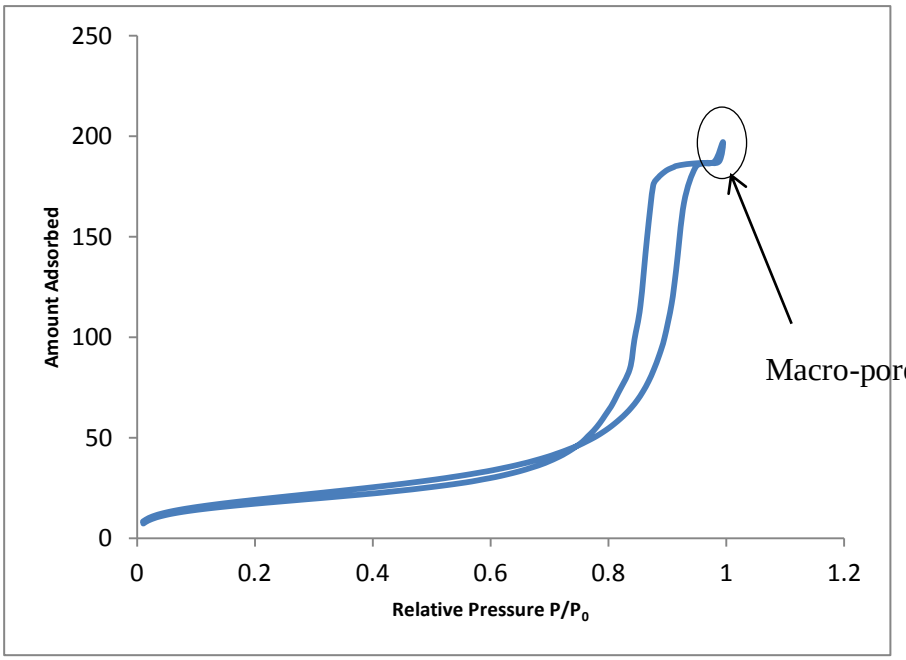

Figure 3.8: Physisorption isotherm for TMOS-based monolith treated for 48 h with 1 M NH_4OH.

Physisorption isotherm of TMOS treated with 1 M NH_4OH for 48 hs. Note the small increase in amount absorbed at P/P_o =1 is a result of a final rapid surge of N_2 gas absorbed indicating a high amount of macro-pores.

In the event of treatment beyond 24 hs, the isotherms show evidence of a high abundance of macropores within the monolith (Sing *et al*, 2008). Figure 3.8 shows how the final stages of adsorption display a rapid burst of adsorption which are a result of larger macro-pores assisting N_2 uptake.

3.3.1.3 Shrinkage of TMOS monolith upon drying

While shrinkage of the silica structure during the gelation step has been reported in detail (Fletcher *et al*, 2010), it was observed that varying levels of shrinkage occurred when drying the monoliths, dependant on length of 1 M NH_4OH treatment time. While this shrinkage does not compromise the structural integrity of the monolith, it was necessary to characterise shrinkage levels for design of integrated materials. Measurements of monolith diameter were taken before and after drying using a calliper. On analysis of both TEOS and TMOS monoliths prepared without treatment with 1 M NH_4OH, shrinkage was found to be approximately 33% and 22%,

respectively. However, when treated with 1 M NH_4OH, shrinkage was found to be less pronounced (see Figure 3.9) for both TEOS and TMOS structures.

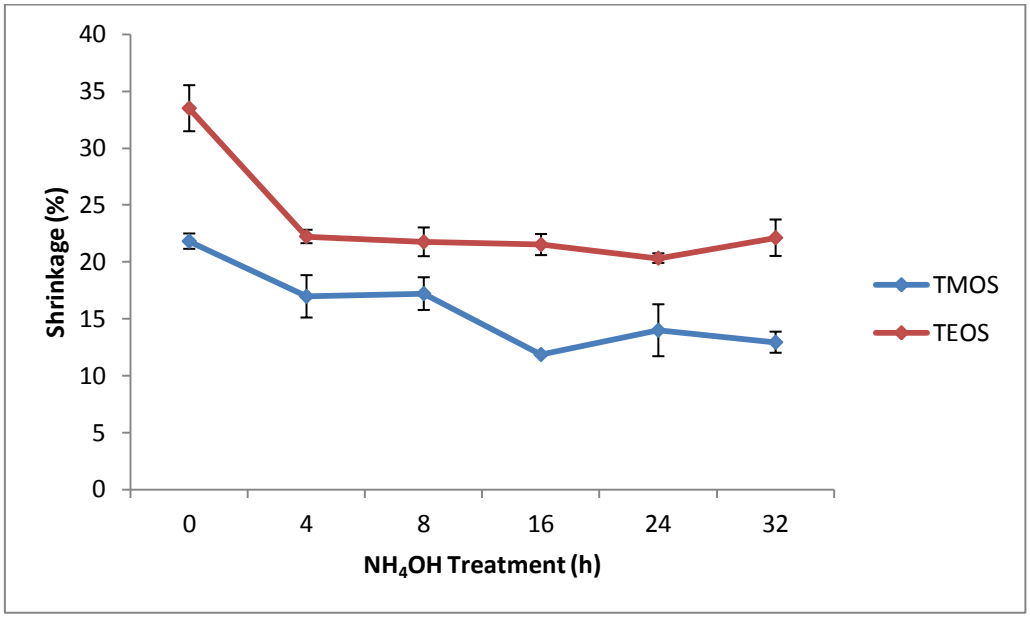

Figure 3.9: Graph of monolith shrinkage levels.

Graph to show the effects of 1 M NH_4OH treatment on the shrinkage behaviour of TEOS and TMOS-based monoliths (n = 3). Error bars show standard deviation. Both monolith types display a characteristic decrease in shrinkage with increased treatment time, however, TMOS-based monoliths shrink ≈ 10% less for all timescales.

This further enforces that the treatment of monoliths with 1 M NH_4OH provides a greater structural integrity, capable of withstanding subsequent contraction on drying. The increased shrinkage is also in agreement with the SEM images and negligible surface area as a result of structural collapse (stion 3.3.1.2). The lower shrinkage observed with the treated TMOS monoliths shows they are therefore able to retain the porous structure produced during synthesis and re-enforced during 1 M NH_4OH treatment, more efficiently than TEOS, providing an additional manufacturing benefit.

3.3.2 Potassium silicate-based monoliths

3.3.2.1 SEM analysis of monolithic structures

Following this potassium silicate-based monoliths were investigated as an alternative substrate for DNA extraction due to the different structural charactaristics and method for synthesis, as described in stion 1.4.4.3. Analysis of potassium silicate-based

monoliths by SEM revealed a structured characterised by sharp spike-like network of pores (Figure 3.10). This is characteristically different to the smoother and more rounded porous network observed with the TMOS/TEOS-based monoliths (Figures 3.4). On analysis, pores were observed to be in the range of 5 to 10 µm for potassium silicate-based monoliths, providing a more uniform pore size comparable with the smaller pores found in silicon alkoxide-based structures. The absence of larger pores would potentially inhibit flow through the monolith due to increased back pressures.

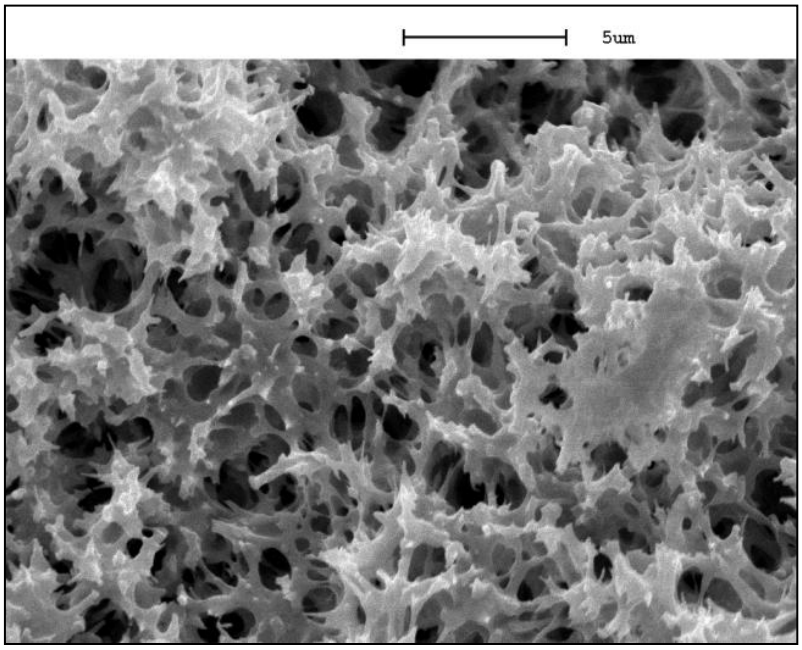

Figure 3.10: SEM image of potassium silicate-based monolith

Image (magnification x 5000) shows uniform porous structure with pores below 5 µm in diameter. Structure shows a characteristic spiky structure compared with silicon alkoxide-based monoliths. Images represent present typical structure. N = 3

3.3.2.2 BET analysis

In order to carry out BET analysis on the potassium silicate-based monolith, the capillary used for synthesis and containment was pre-weighed and the weight was taken away from the total weight post synthesis. BET analysis revealed that the potassium silicate-based monolith had a surface area of 157 ± 20 m^2 g^{-1} and a pore volume of 0.7 ± 0.1 cm^3 g^{-1}. The physisorption isotherm (Figure 3.12) emphasises the similarity of the adsorption and desorption peaks, implying meso-pores are in lower quantity and capillary forces were minimised. The vertical peak observed in the final

stages, is due to the location of the monolith within a glass capillary which is not completely filled. This behaves like one large macro-pore driving an equally rapid adsorption and desorption at higher pressures. The potassium silicate-based monoliths were treated with 1 M NH_4OH, as with silicon alkoxide-based monoliths (stion 3.3.1.1), however, the porous structure was found to be completely dissolved, implying a lack of stability when compared to those constructed from silicon alkoxides.

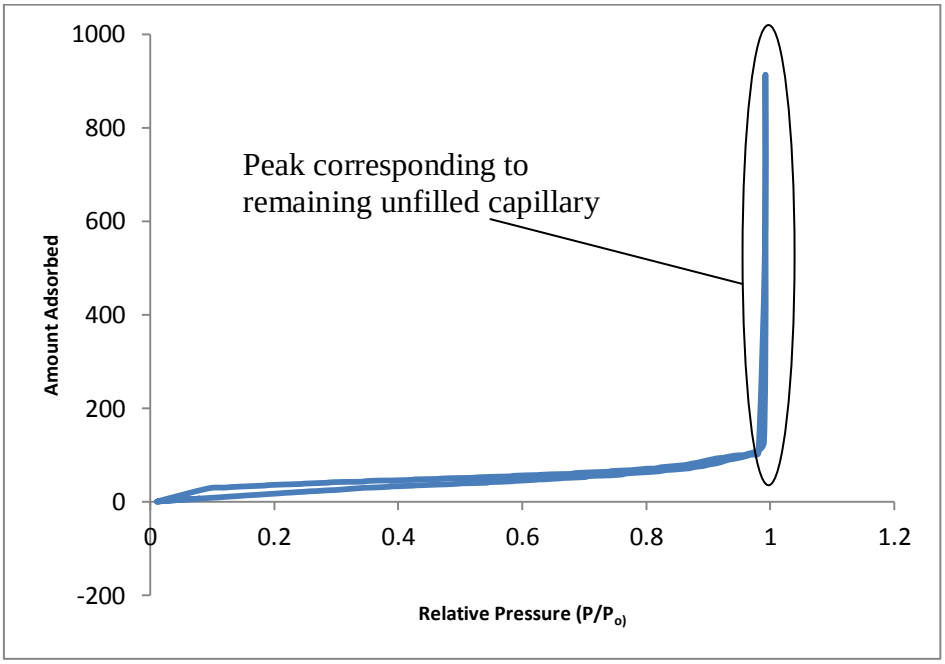

Figure 3.11: Physisorption isotherm for potassium silicate-based monolith.

Graph is physisorption isotherm of potassium monolith. Sharp increase near x = 1 is due to additional volume in capillary not containing monolith.

3.3.3 Alternative manufacturing methodologies for silica monoliths

Potassium silicate-based monoliths were also synthesised in plastic tubes (ID 4.59 mm) (stion 3.2.1.1) but were prone to severe cracking on curing, possibly related to over exposure to the atmosphere and rapid curing. It was hypothesised that the rigid network of pores provided by the TMOS-based monolith could be used as a framework to the potassium silicate-based monolith if the latter was cured inside a preformed TMOS-based structure. This would enable the synthesis of a larger network of potassium silicate-based monolith than previously reported. On mixing of the potassium silicate and formamide, the resulting mixture was injected in to a

TMOS-based monolith via syringe and ETFE tubing. Unfortunately, due to rapid kinetics of polymerisation, the solution was too viscous to penetrate the monolith. In a further attempt, the potassium silicate/formamide mixture was heated to 60^{o}C in order to lower the viscosity, thus allowing permeation of the TMOS-based monolith. However, this increased the reactivity between the potassium silicate and the formamide, making permeation very difficult to achieve. It was therefore decided this was not a practically viable approach for the synthesis of a silica-based monolith for DNA extraction.

3.3.4 Flow system back pressure

In order to further characterise the porous monolithic systems, both potassium silicate-based flow systems and TMOS-based flow systems were investigated to evaluate for build up of back pressure. Distilled H_2O was flowed, hydrodynamically, through the monoliths at 20 µl min^{-1}. It was found that the potassium silicate-based monolith had a measured back pressure of 25 psi after 10 min, 53 psi after 15 min and 90 psi after 20 min, before the seal with the syringe was breached at ≈ 95 psi. In comparison, TMOS-based monoliths showed back pressures of less than 10 psi throughout this time period. This would make TMOS-based structures more tolerant of higher flow rates during DNA extraction procedures

3.3.5 Chitosan functionalised silica-based monolith

3.3.5.1 SEM imaging

The introduction of chitosan to a silica surface has been utilised in a number of formats, in order to introduce alternative DNA extraction chemistries (stion 1.4.4.4). While porous materials have previously been modified with chitosan to the authors knowledge, they have not, as of yet, been utilised in DNA extraction (Hinojosa Flores et al, 2009). TMOS-based monoliths were coated with chitosan, as described in stion 2.2.3. It was not possible to visualise chitosan by SEM images (Figure 3.12) alone, as SEMs obtained were not distinguishable from the uncoated silica surfaces.

3.3.5.2 Colorimetric, infrared and BET analysis

As an alternative method of validation for surface coating and also analysis of chemical properties, GNPs (≈ 20 nm diameter, based on methodology provided by Turkevich, 1951) were used to identify, colorimetrically, the chitosan bound to silica (Cao *et al*, 2006). Negatively charged GNPs are found to mutually repel the negatively charged silanol groups of the silica surface, while the protonated form of the primary amine group found on the chitosan-coated surface would attract the GNPs and cause aggregation at the monolith surface. Silica monoliths either treated or untreated with chitosan were ground up with a spatula, and immersed in 4 ml colloidal gold. On mixing with pure silica, the solution remained pink while the mixture with chitosan-treated silica went clear and the silica turned a blue/purple, indicating an aggregation of colloidal gold (Figure 3.13).

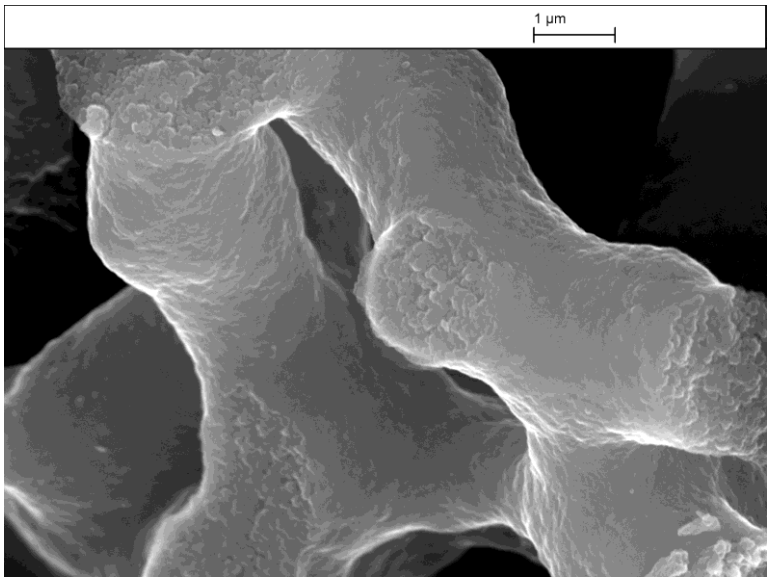

Figure 3.12: SEM image of chitosan-coated TMOS-based monolith.

Image does not clearly show chitosan compound when compared with TMOS-based monolith uncoated (Figure 3.4b). Magnification 20,000x. N=2.

The presence of chitosan bound to the silica surface was further validated with infrared (IR) analysis. Figure 3.15 shows IR absorption spectra of a bare silica monolith (a) and the chitosan compound in isolation (b) and in addition IR absorption spectra of chitosan-coated silica (Figure 3.15). The spectrum has peaks typical of silica network but also a small peak between 1640 and 1590 cm^{-1}. This illustrates the presence of a primary amine group within the silica structure (Lang and Morrow,

1994; Hinojosa Flores *et al*, 2009). Note, the observed peak is small in comparison to silica peaks, as the bulk structure is composed entirely of silica, whereas chitosan only forms a coated layer on the accessible surface.

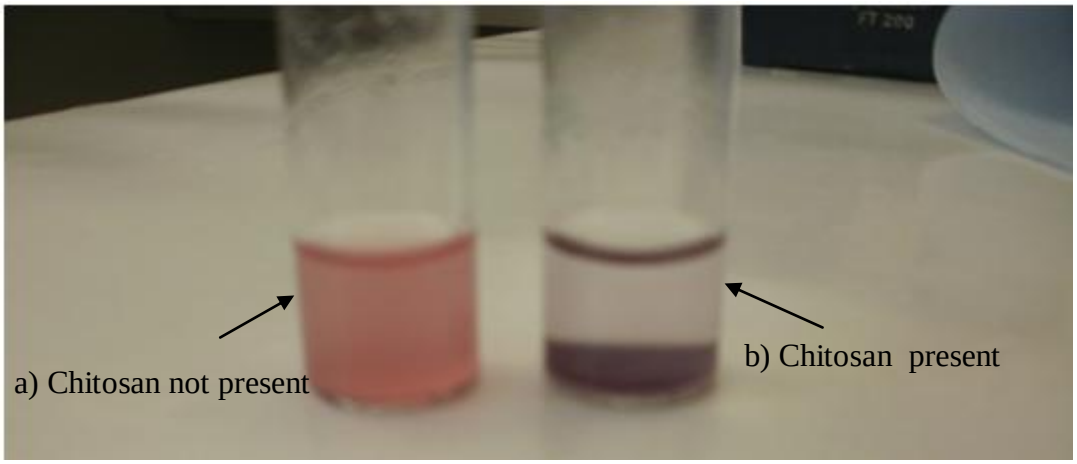

Figure 3.13: Colorimetric demonstration of chitosan coating.

Photograph shows two vials with crushed silica-based structures immersed in colloidal gold. a) Bare silica obtained from the crushing of TMOS-based monolith. Note, the solution has remained pink due to absence of interaction of gold nanoparticles with silica surface. b) Crushed chitosan coated TMOS-based monolith. Note, the solution has gone clear and GNP have aggregated around the silica due to interaction with chitosan coating.

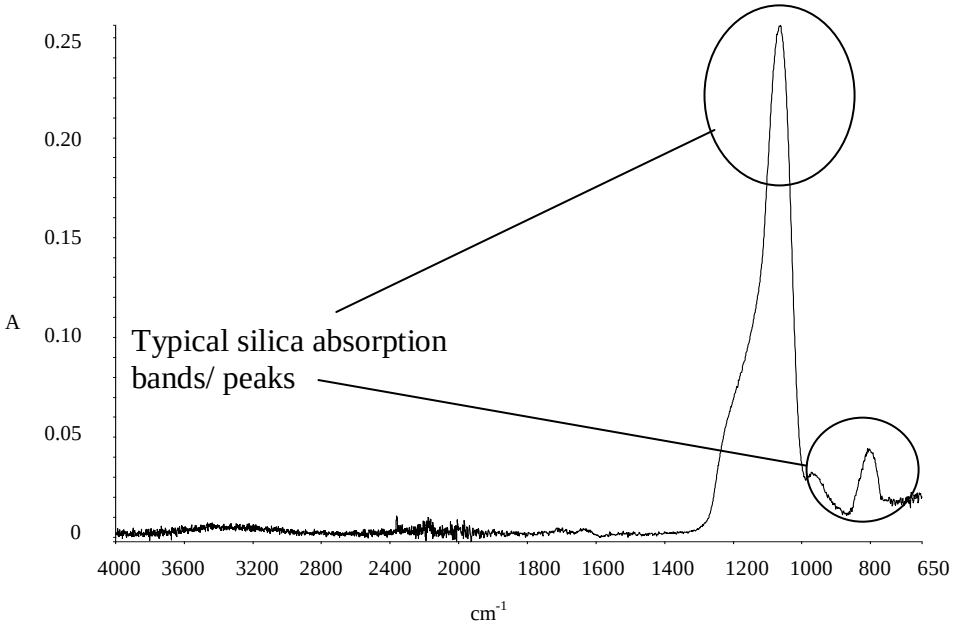

Figure 3.14: IR absorption of TMOS-based monolith.

IR absorption spectra. Spectra of bare silica monolith crushed. Spectra shows peaks at 1250-1000 cm^{-1} and 800 cm^{-1}, typical of a silica network.

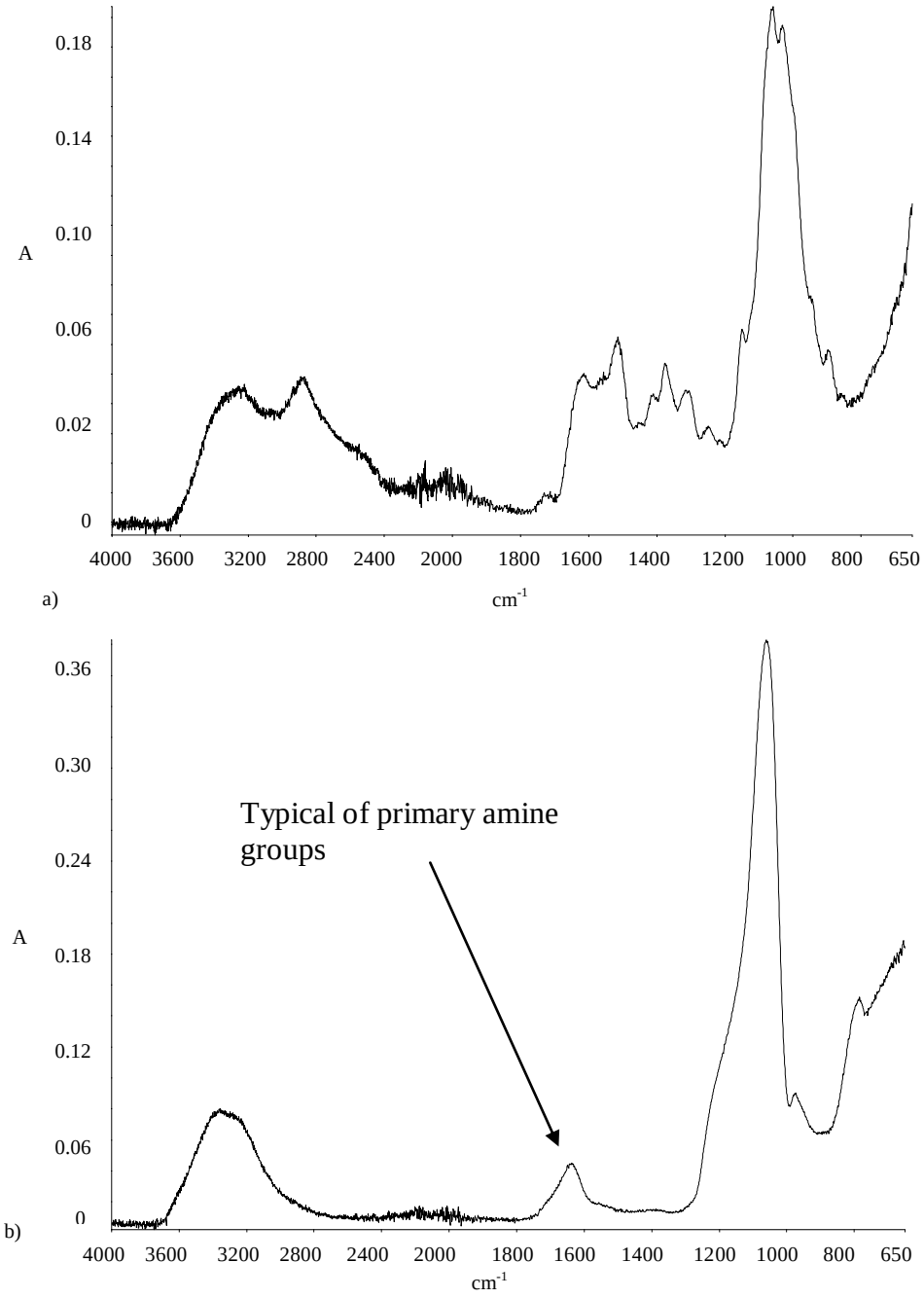

Figure 3.15: IR adsorption spectra of chitosan and chitosan-coated TMOS-based monolith.

a) IR absorption spectrum obtained of chitosan compound. This is typical fingerprint spectra for chitosan. b) IR absorption spectrum of TMOS-based monolith coated with chitosan. Typical silica absorption bands are present as in 3.14, however, a small peak observed between 1640 and 1590 cm^{-1} is highly characteristic of a primary amine group, indicating presence of chitosan (Hinojosa Flores *et al*, 2009).

Further BET analysis of silica coated with chitosan indicated that the surface area and pore volume were not shown to be significantly (< 10 %) affected by the presence of the chitosan, implying a thin layer across the surface of the silica structure had been achieved (see Table 7). This is further validated by the fact no significant alteration in the physical structure was observed by the SEM analysis.

3.3.5.3 Treatment of potassium silicate-based monoliths with chitosan

Treatment of potassium silicate-based monolith with chitosan was attempted by flowing chitosan (stion 2.1.3) through the structure. It was not possible, however, due to the structure being impermeable to the viscous solution. At flow rates of 1 µl min^{-1} solution monolith would block allowing no flow through, in agreement with Christensen *et al (*1998).

3.3.5.4 Silica/ chitosan hybrids

It was hypothesized that a continuous structure of chitosan and silica would be constructed rather than a thin coating of chitosan added post synthesis. This would simplify the manufacturing process if chitosan chemistries were to be utilised. TMOS/chitosan hybrid monoliths were synthesised using an adapted methodology to that of Lan *et al* (2010). The SEM images of these chitosan/TMOS hybrid structure are shown in Figure 3.16(a) revealing a similar porous structure, however, the addition of chitosan is clearly present as grain-like structures. The SEM does show the grain-like chitosan on the broken surfaces implying that chitosan has been distributed throughout the internal structure. This is in accordance with the particles synthesised by Lan *et al* (2010). Alternative chitosan/silica hybrids were also manufactured using the potassium silicate-based methodology with the input of additional chitosan (stion 2.1.2). Figure 3.16b shows the resulting structure in which chitosan was distributed heterogeneously within the silica structure, however the porous structure failed to form as it did for potassium silicate-based monoliths described in stion 3.3.2.

a)

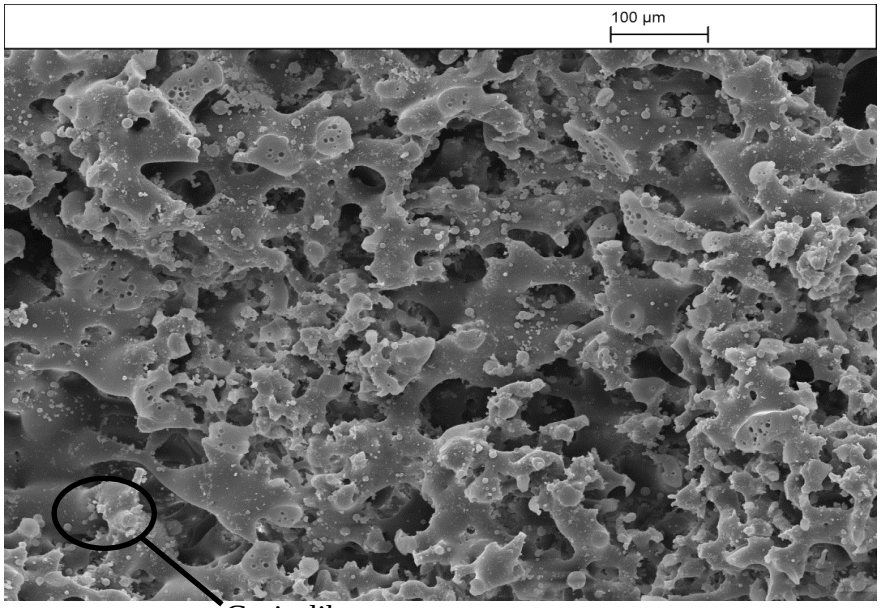

b)

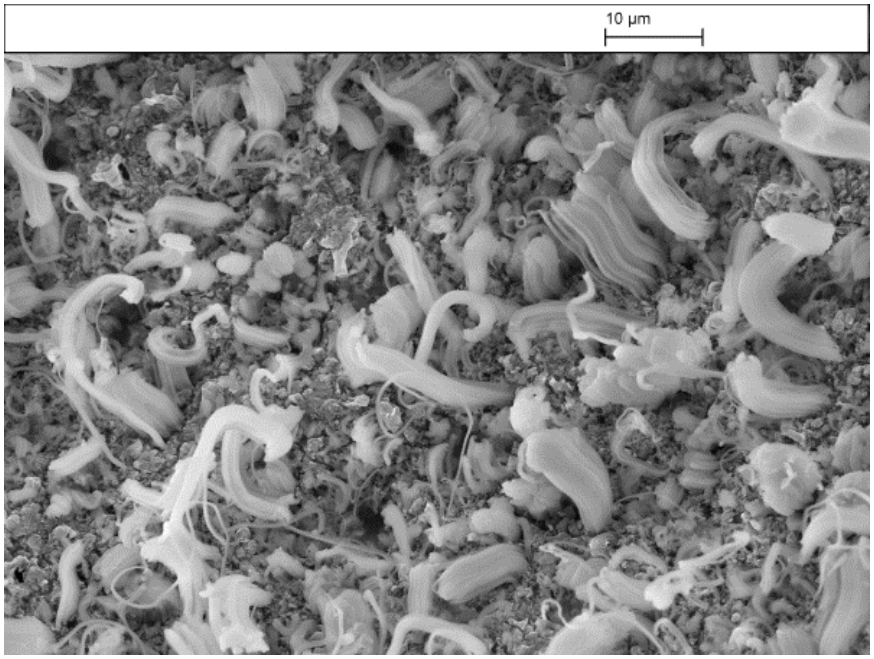

Figure 3.16: SEM images of chitosan/silica hybrids.

SEM images of a) SEM illustrates chitosan/TMOS hybrid. Magnification 250 x. b) SEM illustrates potassium silicate/chitosan hybrid. Magnification 10,000 x

3.4 Summary

In summary, five materials have been evaluated for potential use in SPE of nucleic acids in microfluidic devices. The structures investigated were potassium silicate-based monoliths, TEOS-synthesised monoliths, TMOS-synthesised monoliths and

TMOS coated with chitosan and silica/chitosan hybrids. While both silicon alkoxide- and potassium silicate-based studied display similar porous silica characteristics, notable distinctive features of each were observed; TMOS-based monoliths would not be able to be synthesised within a chip device due to shrinkage occurring on drying, which would lead to subsequent leakage of sample from the system, whereas potassium silicate-based monoliths, could be readily cured *in situ*. Regarding the latter, however, the structural integrity became compromised when synthesised at larger volumes with the monoliths showing evidence of cracking.

The surface area of the monolith types were evaluated. For silicon alkoxide-based monoliths, the surface area was further evaluated for varying the length of post-treatment with 1 M NH_4OH. All data is shown in Table 7. After comparing to porous structures described in the literature, surface areas were considered sufficient for use in DNA extraction methodologies (Zhang *et al*, 2006).

Table 7: Silica monolith structure characteristics.

Variation in surface area and pore volume before and after functionalisation with chitosan

Material/ substrate	**Surface area $m^2 g^{-1}$**	**Relative standard deviation of the mean (RSDM)**	**Pore volume $cm^3 g^{-1}$**	**RSDM**
Potassium silicate-based monolith	157	20	0.7	0.19
TMOS-based monolith (24 h NH_4OH treatment)	213	11	0.85	0.12
TEOS-based monolith(24 h NH_4OH treatment)	149	20	0.71	0.2
Chitosan-coated TMOS monolith	206	11.63	0.81	0.09

4 Implementation of porous silica materials into nucleic acid amplification testing

4.1 Introduction

This chapter describes an investigation into the DNA extraction performance of the porous materials detailed in the previous chapter. Following initial evaluation, a preferred structure was incorporated in to a microfluidic device for potential integration of downstream steps. As indicated in the previous chapter, the process under investigation at this stage was the isolation of DNA from STI microbes in urine samples. DNA extraction and purification is an essential step in providing DNA of a suitable quality and quantity for subsequent PCR amplification. As described in stion 1.4.4, a wide variety of DNA extraction techniques have been reported in the literature, with an increasing number being utilised at the microfluidic level. As the methodologies here were being investigated for use in the detection of STIs from urine, the interface was designed to accommodate clinically relevant sample volumes. A urine sample with a volume of ≥ 150 µl was used to validate the system with varying concentration of target bacterial DNA. The requirements of the real world-to sample interface can described as follows:
1) Ability to receive a sample from ”real-world” without pre-processing; 2) Provide suitable format for DNA extraction/ purification; 3) Permit recovery and retrieval of DNA of suitable and integrity for PCR amplification; 4) Provide a system that can be implemented in a chip device and easily manufactured.

Main aims

1) Investigate the performance of porous silica SPE materials characterised in Chapter 3 for DNA extraction purposes.

2) Incorporate porous silica monolith material in to a microfluidic device or “chip” and evaluate performance for DNA extraction.

3) Validation of the system for proposed clinical diagnostic applications using a model system: evaluation of performance for extraction of STI-causing bacteria genomic DNA from 150 µl human urine and subsequent PCR amplification.

4.2 Materials and Methods

4.2.1 Materials

The porous SPE flow systems utilised in this chapter have been described in chapter 3 (Figure 3.1 and 3.2). A photograph of the TMOS flow system set up is also shown in Figure 4.1.

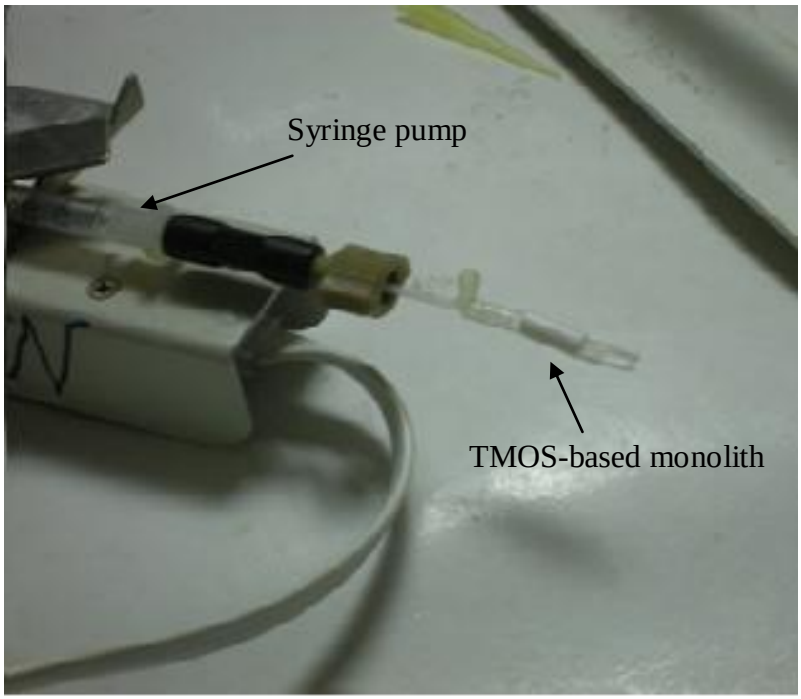

Figure 4.1: Monolithic flow system.

Photograph of TMOS monolith in heat-shrink wrap flow system. The flow system is set up with a syringe and syringe pump. All sample and reagents are pumped hydrodynamically through the monolith flow system with a syringe pump and effluent flow-through is collected at the outlet using a micropipette.

4.2.2 DNA extraction methodologies using porous materials

4.2.2.1 DNA extraction from artificial urine medium

For studies of DNA extraction efficiencies, an AUM (Brooks and Keevil, 1997) was spiked with human genomic DNA (hgDNA) (5 ng μl^{-1}) and mixed at a 1:9 ratio with a 5 M GuHCl in tris/EDTA buffer pH 6.7 solution. GuHCl is a CS which serves as a cell lysis agent and also denatures nucleic acids to enhance binding to the silica surface (Melzak *et al*, 1996). The total volume (50 µl) was then loaded onto the DNA extraction substrate to allow binding of nucleic acids to the silica monolith. 100% ethanol was then pumped through the monolith to wash away contaminants before nucleic acids were eluted with water. A series of fractions were collected from the continuous flow at the outlet during the elution stage. The double-stranded DNA (dsDNA) content of all elution fractions was then quantified using a Quant-iT™ PicoGreen® double stranded DNA Assay Kit [Invitrogen, UK] and analysed using a FLUOstar Optima Plate Reader [BMG Labtech, UK] (stion 2.7). For all experiments DNA extraction efficiency was determined as the total quantity of DNA eluted as a percentage of the quantity of DNA initially loaded onto the system.

Standard flow rates and sample collection for preliminary extraction experiments were adapted from Shaw *et al* (2009). Flow rates used were as follows:

1) Biological sample was loaded on to the porous silica solid phase at a 1:9 ratio with 5M GuHCl at 2.5 µl min^{-1} to enable capture of DNA

2) 100% ethanol was flowed through solid phase at 5 µl min^{-1} in order to wash away impurities (e.g. proteins, urea), before flushing with air to remove ethanol residue.

3) DNA was eluted from the monolith with dH_2O at 2.5 µl min^{-1}.

4) 5 µl fractions were collected from exit of flow system post-monolith throughout the experiment for perfomance analysis and quantification. A minimum of 5 fractions of wash solvent were collected prior to flushing with air, while elution fractions collected were a minimum of 20 consutive fractions. The number of elution fractions was later reduced accordingly, if the observed elution volume was found to be

significantly lower. All fractions were quantified using a Picogreen® quantification [Invitrogen] (stion 2.4). In addition, fractions were taken from experiments for validation by PCR amplification, when considered necessary. DNA extraction efficiency was calculated using the following equation:

Equation 11: DNA extraction efficiency calculation

$$DNA\ extraction\ efficiency = \frac{DNA\ eluted\ in\ elution\ phase\ (ng)}{DNA\ loaded\ on\ to\ system\ (ng)} X\ 100$$

Any deviation from these parameters during optimisation experiments are detailed with the relevant results.

4.2.2.2 DNA extraction from human urine samples

To demonstrate the application of these systems for the extraction of nucleic acids from high volume, clinically-relevant biological samples, human urine samples were collected from healthy volunteers, having first obtained appropriate ethical approval and donor consent (Departmental Ethical Committee Approved, University of Hull. GuHCl (0.072g) was then added directly to 150 µL of human urine in order to achieve a final concentration of 5 M, before loading onto the flow system/ monolith. Washing and elution steps were performed as previously described.

4.2.2.3 DNA extraction using chitosan-based porous material

Initial DNA extraction efficiency experiments performed on chitosan-modified monoliths were carried out using AUM, loading the sample in 10 mM 2-(N-morpholino) ethanesulfonic acid (MES) buffer pH 5.05 at a 1:9 v:v ratio, before flushing the monolith with MES buffer pH 5.05 to remove any unbound contaminants. Finally, DNA was eluted using 10 mM tris(hydroxymethyl) aminomethane buffer with 50 mM KCl pH 9. Subsequent evaluation of the system for extraction of DNA from human urine samples was performed by mixing with MES buffer pH 5.05 at a 1:9 v:v ratio and 150 µL total volume was loaded on to the monolith.

4.2.3 Validation by PCR

For all systems, PCR was carried out to ensure that DNA was of sufficient quality and quantity to permit amplification. This was achieved by taking 5 µl of elution volume and subjecting it to PCR amplification using specific primer pairs (stion 2.5.3) to the target of interest. Details of the PCR protocol are given in stion 2.5.1.1.

Thermal cycling parameters for amplification of *C. trachomatis and N. gonorrhoea* targets were as follows: An initial denaturation step at 94^{o}C for 300 s, followed by 5 cycles of denaturation at 94 ^{o}C for 180 s, annealing at 63 ^{o}C for 90 s and extension at 72 ^{o}C for 90 s. This was followed by 35 further cycles of denaturation at 94 ^{o}C for 30 s, annealing at 63 ^{o}C for 15 s and extension at 72 ^{o}C for 15 s.
Thermal cycling parameters for *Amelogenin* and *D21* forensic loci were as follows: an initial denaturation step at 95^{o}C for 180 s, followed by 35 cycles of denaturation at 95^{o}C for 30 s, annealing at 60^{o}C for 30 s and extension at 72^{o}C for 30 s and a final extension step at 72^{o}C for 240 s. Amplified DNA samples were subsequently analysed by CE (stion 2.6.2).

4.2.4 Silanisation of porous silica materials

All silanisation of materials was carried out as described in stion 2.5.4. Silianisation of porous monolith structures was carried out using an immersal technique. The monolith was immersed in the trichloroperfluoroctyl/isooctane mixture for 20 min before being immersed sequentially in isooctane, acetone and H_2O for 10 min each. The monoliths were then left to dry at 40^{o}C overnight.

4.3 Results and Discussion

4.3.1 TEOS/ TMOS Synthesised monolith

4.3.1.1 DNA extraction efficiency

Preliminary extractions were carried out using monoliths treated with 1 M NH_4OH for 24 hs. Samples used were AUM (5 µl) spiked with hgDNA. The monolith encased in HSW provided a good pathway for sample and reagent flow with negligible back

pressures (< 10 psi). On analysis of the DNA extraction profile, a clear peak was observed at the beginning of the elution phase, indicating presence of DNA, while nothing was observed prior to this during loading and washing stages, showing silica-DNA SPE chemistries were performing as described in the literature (Melzak *et al*, 1996). DNA extraction for TEOS based monoliths demonstrated efficiencies of 45 ± 3% (n=3). For TMOS synthesised monoliths the efficiency was found to be slightly higher 52 ± 5% (n=3). Example extraction profiles of TEOS and TMOS are shown in Figure 4.2 and 4.3 respectively. The profiles indicate the quantity of DNA in fractions collected during load, wash and elution steps. It is important to note that no DNA is present in fractions during the load step. This implies that all unrecovered DNA is being successfully captured on the silica matrix, but remains bound during elution, as opposed to passing through and failure to bind.

In accordance with the literature, inhibition of the subsequent PCR was observed, demonstrating that there were likely significant traces of ethanol present in the eluted DNA volume (Claveau *et al*, 2004). This effect was shown to be prevented by flushing the monolith with air and introducing an additional drying step (5 min) at 40 °C following the wash step. The drying process permits evaporation of the residual ethanol retained within the porous silica structure enabling downstream PCR amplification of extracted DNA to be carried out successfully. This is in agreement with the reported issues described by Baier *et al* (2009) and Chen *et al* (2010). Figure 4.4 is an electropherogram of the D21 forensic locus amplified from the hgDNA template, amplified from DNA extracted using a TEOS-based monolith.

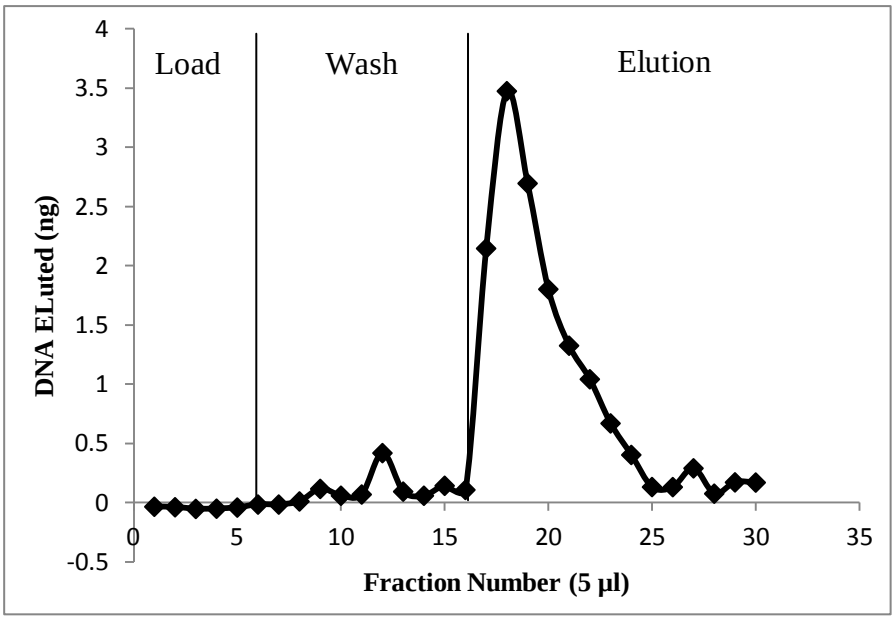

Figure 4.2: DNA extraction profile for TEOS-based monolith

Typical profile for TEOS based flow system. DNA is eluted at fraction 17-24 with > 50% of DNA eluted in first four elution fractions. There is no DNA is observed in the wash step indicating that the DNA remains bound until elution step. Extraction provided 48.3 % recovery of total DNA. N = 3

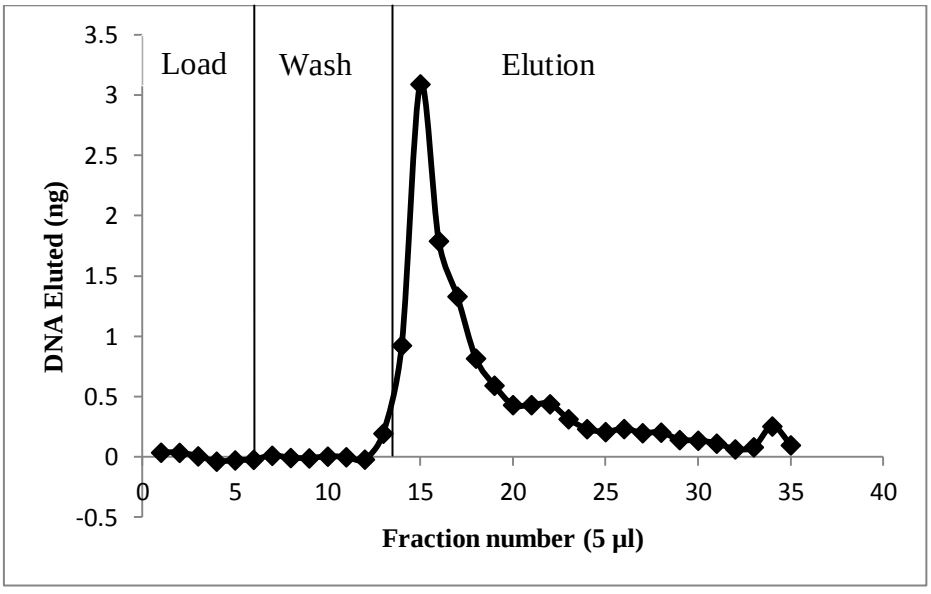

Figure 4.3: DNA extraction profile for TMOS-based monolith

TMOS based flow system. DNA is eluted at fraction 13-31. There is no DNA eluted in the load and wash step, indicating that DNA remains bound until elution step. Extraction provided 55 % recovery. N = 3 .

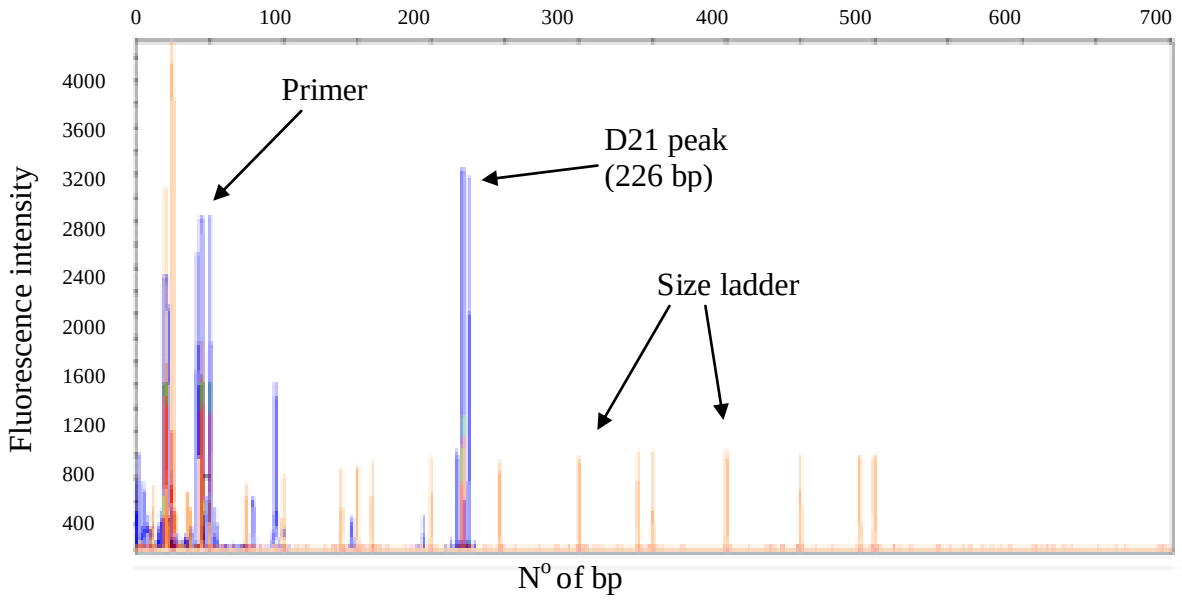

Figure 4.4: Electropherogram of amplified DNA when extracted from TEOS-based flow system.

Electropherogram of DNA extracted from TEOS-based flow system following amplification by PCR. The electropherogram shows peak at 226 bp indicating a successful amplification of D21 locus. N = 3

Based on the findings in stion 3.3.1, concerning porous silica surface area with regards to a variation of length of treatment with 1 M NH_4OH (Figure 3.5a), it was postulated that DNA recovery would be higher for monoliths treated with reduced timescales of treatment, as a result of increased surface area. The treatment timescale for monolith synthesis optimised by Fletcher *et al* (2011) was 24 h, which is what was used for experiments described in Figures 4.2 and 4.3. DNA extraction was further investigated for monoliths prepared using 1 M NH_4OH treatment times scales of 0, 4, 8, 16, 24, 32 and 48 hs for both TEOS and TMOS-based monoliths.

For TEOS-based monoliths it was found that optimum DNA recoveries of ≈ 49% were achieved following 16 h of treatment, while recoveries for higher and lower timescales showed a reduction in recovery. DNA recoveries were ≈ 30% and 20% for 4 h and 48 h treatment, respectively. TMOS monoliths showed a similar effect, however highest recoveries of ≈ 52% were observed for the 24 h treatment time, when compared to longer and shorter timescales (≈ 10-15%). The DNA recoveries when

using monolith which were not treated with 1 M NH_4OH were negligible, likely due to collapse of monolith on drying.

The surface area, however, described in Figure 3.4 for treatment ranging 0 h to 48 h demonstrates a lack of correlation with that of the DNA recovery. On analysis of the extraction profiles for the varying treatment timescales it was observed that DNA was not being eluted during load and wash steps. It is postulated that whilst the surface area for the monoliths treated for shorter timescales provided higher surface area (see Figure 3.5), the lower recoveries associated with treatment for shorter timescales can be attributed to a flow hindrance within certain parts of the monolith structure preventing sample and reagents accessing all parts of the monolith. This could be a result of poor structural integrity causing minor collapse in certain parts of the structure; this problem could potentially be overcome by increasing the length of 1 M NH_4OH treatment. The closed area within the monolith would also cause quantities of DNA to be trapped within the monolith with subsequent recovery not possible. In addition, a surface with reduced conditioning may have an abundance of micropores or small mesopores which would not facilitate DNA release. The reduction in DNA recovery when treating for timescales beyond 24 hs could be a result of the reduction in micro and meso-pore and increase in macro-pores, which could potentially be destructive to the structure for longer period of time causing pore closure (Sing *et al*, 2008). This is further enforced by the lower pore volume described in stion 3.3.2.1.

Based on the results presented thus far, TMOS-based monoliths treated for 24 h with 1 M NH_4OH were chosen for further development. Analysis in chapter 3 showed greater structural integrity, while in chapter 4, DNA extraction efficiencies were also shown to be slightly higher when using TMOS-based than when using TEOS-based monoliths.

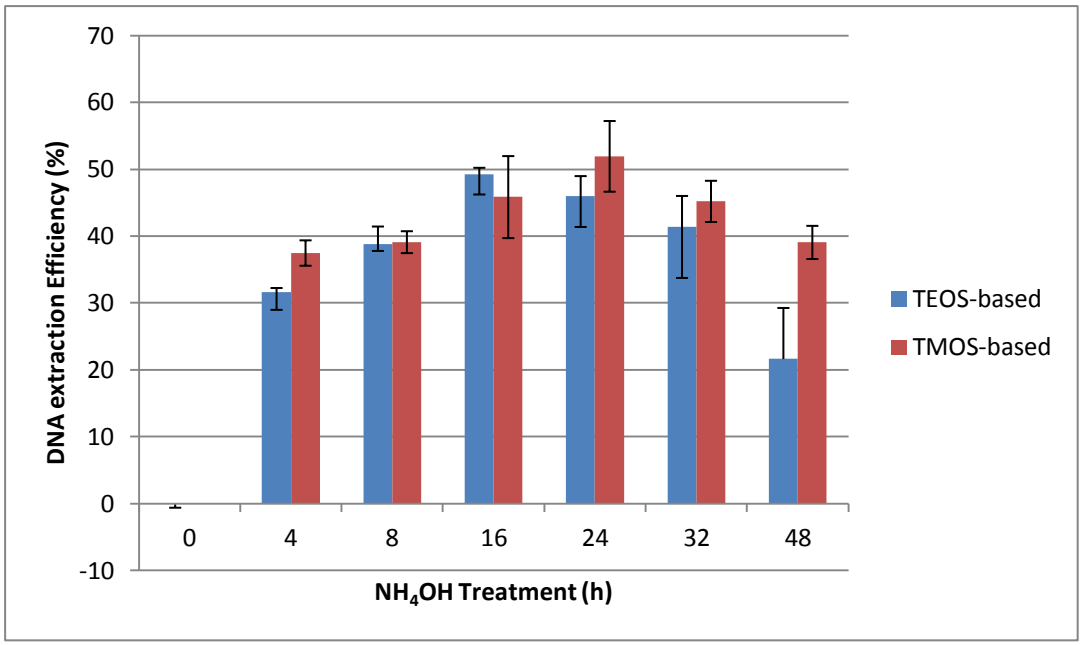

Figure 4.5: Influence of 1 M NH_4OH conditioning of monolith on DNA extraction efficiency.

Bar chart to show the influence of 1 M NH_4OH on DNA recovery (%) (N=3 for all experimental groups). For TEOS synthesised monoliths optimum recoveries of ≈ 49%, are achieved when treated for 16 h. For TMOS synthesised monoliths optimum recoveries of 52% were achieved when treating for 24 h.

4.3.1.2 Influence of surface treatment with TE buffer on DNA extraction efficiencies

As discussed in stion 1.4.4.2, the surface pH of silica can affect interactions with the negatively charged backbone of DNA. By treating with a TE buffer pH 6.7 prior to loading the sample, the negative charge of the silica surface can be decreased, thus reducing the repulsion of DNA and maximising the effects of hydrogen bonding. The influence of pretreatment of monolith with TE buffer at a pH 6.7 was investigated by pumping through the monolith at 5 µl min^{-1} for 0, 2 and 4 hs, however a significant change in DNA recovery was not observed over the timescales investigated (Figure 4.6). This could be due to the treatment with 1 M NH_4OH introducing OH^- groups to the surface prior to use, eliminating the effects of additional protonation. For this reason TMOS-based monoliths were not treated using TE buffer pH 6.7 for the remainder of the work.

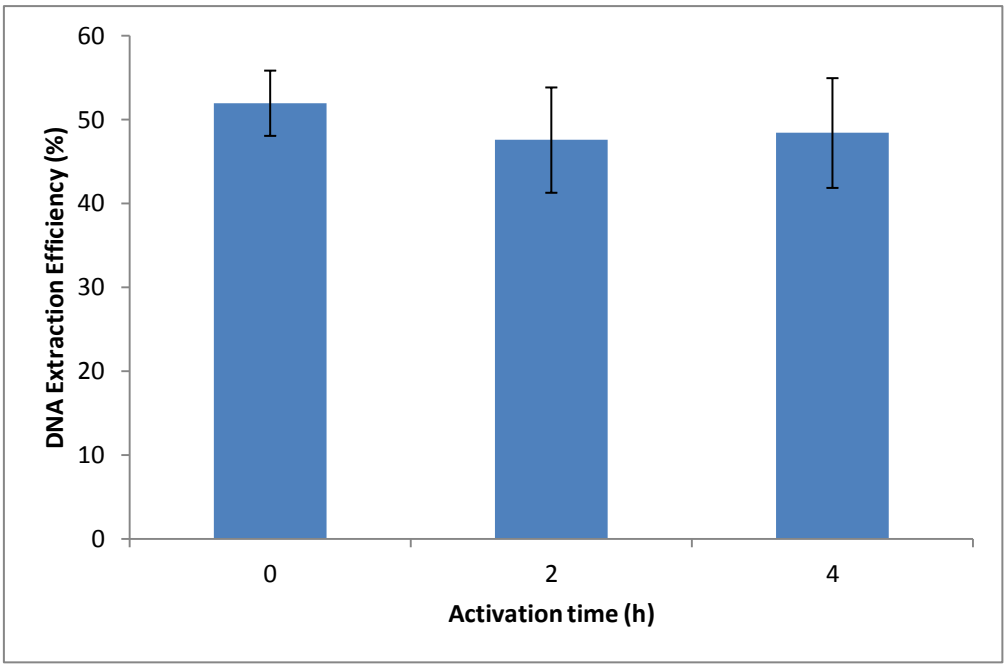

Figure 4.6: Influence of TE buffer treatment on DNA extraction efficiency.

Bar chart to show the influence of monolith treatment with TE buffer pH 6.7 on DNA extraction effiency. The treatment for 2 and 4 hs showed no affect on extraction efficiency when compared with no treatment (N = 3).

4.3.1.3 Rapid deposition of sample onto porous monolith

It was hypothesised that loading time could be made negligible without a significant decrease in DNA extraction efficiency by simply depositing the sample on to the monolith and allowing capillary forces to take it in. The sample could then be incubated in the monolith to allow DNA capture. DNA extraction efficiencies were obtained for this process which included a delay in the ethanol wash step in order to allow the DNA to diffuse sufficiently to the silica surface. This delay of the wash step was varied between 0, 10, 20, 40 and 120 min in order to establish optimum diffusion time. It was found that 10 min was the optimum time to delay the wash. Figure 4.7 shows the DNA recovered in both, the elution and that recovered in steps prior to elution for varying delay times. DNA recovered in elution step was ≈ 23% with no delay time, whereas the DNA recovered for a delay time of 10 min was ≈ 31%. Beyond this time scale the DNA recovery decreased. The DNA recovered in the wash step was an inverse of this, as would be expected, demonstrating an inability for the DNA to bind to the silica surface. It is postulated that the lower quantity of DNA

recovered when delay time is zero is due to insufficient time for diffusion and binding to occur, while the decrease in DNA recovered for longer timescales is due to possible inhibition of DNA-silica binding by the ethanol causing subsequent DNA to be found in the ethanol-wash fractions. This is different to that of the extractions by hydrodynamic pumping, in which all DNA was captured, but was not all eluted. Samples extracted using the optimum 10 min delay step were validated by PCR amplification of the D21 forensic locus and analysis by CE. This confirmed that the DNA extracted in this way was of sufficient quantity and quality for PCR amplification.

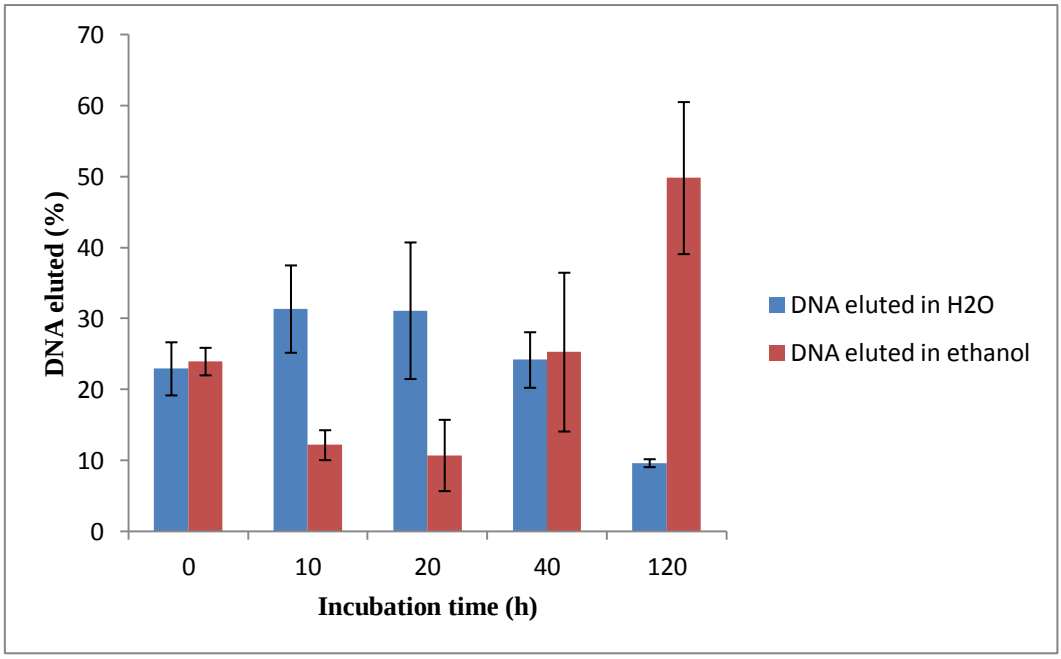

Figure 4.7: Influence of incubation time on DNA extraction efficiency.

Bar chart showing the influence of rapidly depositing and incubating the sample within the monolith, followed by prior to wash step. Optimum incubation time was found to be 10 min (≈ 32%) with a steady decrease in DNA recovery for longer timescales. This is further illustrated by the steady increase of DNA released during wash stage. For the maximum timescale 50 % of the DNA is released during the wash stage (N = 2).

While the elimination of the loading step would be beneficial for a rapid point-of-care diagnostic system, the reduction in DNA recovery, due to hindered binding, meant this approach was not further developed. It must also be noted that a loading step by rapid deposition would require a monolith customised to a size accommodating of the

sample volume, whereas a load by hydrodynamic pumping would not. While the monolith size was sufficient for loading of the sample volumes used during these experiments, clinically relevant sample volumes may necessarily be significantly larger as described later in the chapter, which would require much larger monolithic structures. On further evaluation, therefore, it is considered that a methodology such as this would be more applicable to an alternative application, requiring a smaller sample volume, such as analysis of a blood or saliva (< 10 µl) in forensic applications.

4.3.1.3 DNA-binding capacity

The capacity of the silica monolith was analysed by flowing a known quantity of DNA through the monolith and identifying the point at which the DNA no longer had sites to bind to. This could be achieved by generating a DNA binding capacity profile, in which DNA will bind to the monolith before beginning to pass through and eventually reaching a plateau, in which all DNA is passing through the monolith.. The DNA passing through the monolith could then be subtracted from the total amount loaded to give the amount of DNA bound. Studies of DNA-binding capacity of the TMOS monolith demonstrated a capacity of 4.70 ± 0.5 ng of DNA per mm^3 of monolith (n=2). Figure 4.8 shows a typical profile generated from a DNA binding capacity experiment. Initially, collected fractions 1-52 show no trace of DNA as it binds to the silica surface. On approaching full capacity, the effluent fractions begin to show an increase in DNA content due to its passing straight through monolith, before finally reaching a maximum (fractions 58-61) in which all DNA is passing through without binding. In order to obtain total value for DNA loaded onto the monolith, 5 M GuHCl was passed through the monolith following the DNA load, to ensure any unbound DNA was flushed through the monolith.

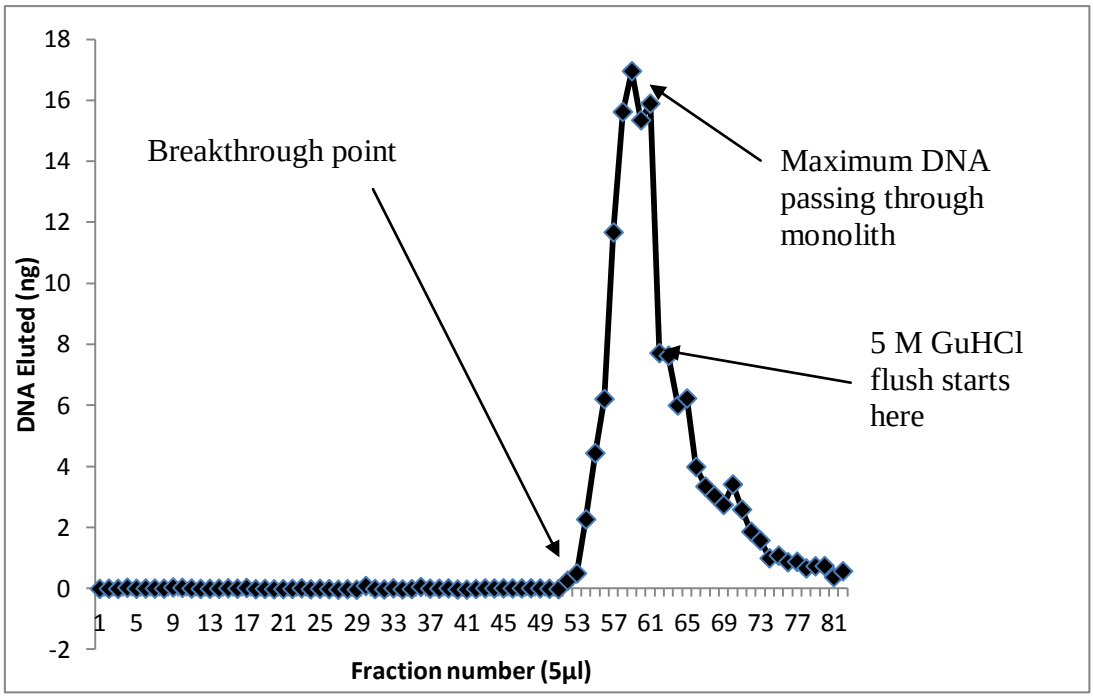

Figure 4.8: DNA capacity capture profile using TMOS-based monolith.

Plot to show DNA binding capacity of TMOS-based monolith. Monolith begins to pass through the monolith at fraction 53 and increased, then as all DNA begins to pass straight through monolith without binding, a steady concentration of DNA from fraction 58-61 is observed. Following this, 5 M GuHCl was flushed through to remove any unbound DNA. N = 2

4.3.1.4 Evaluation of real human urine samples

Preliminary extractions of DNA from human urine samples were performed primarily to assess the ability of the porous monolith to accommodate samples of varying viscosity and composition since considerable heterogeneity is observed between urine samples. The DNA extraction from human urine sample differed from the validation extractions performed using a model AUM system in that the CS was added as a solid powder rather than added as 5 M buffered solution (Kemp *et al*, 2012). More specifically, 0.075g GuHCl was added to 150 µl human urine sample, which maintained the chaotropic conditions at a 5 M concentration. No additional DNA was spiked into the urine. The direct addition of CS, rather than a CS-based solution meant the human urine was not diluted in any way, thus, the sample would have to permeate

the monolith in its state on release from the body. This would mean that the sample can be added with no processing other than the addition of CS.

When using the TMOS monolith, the sample was able to permeate through the monolith with no significant back pressure observed. On loading, some biological components were retained in the monolith (observed as yellow colouring), before being eluted in the ethanol wash step. Finally the elution fractions were analysed for hgDNA using Picogreen® kit. While hgDNA does not accurately represent the DNA of an infectious organism, it is, however, a suitable target for assessment of the capability of the monolith to process a real urine sample and support DNA extraction. Note, accurate DNA extraction efficiencies (%) could not be obtained for human urine due to the unknown quantity of host DNA, which was present in the sample. Of DNA extractions carried out from 3 different urine samples, each of the eluted samples were subjected to PCR and amplified successfully.

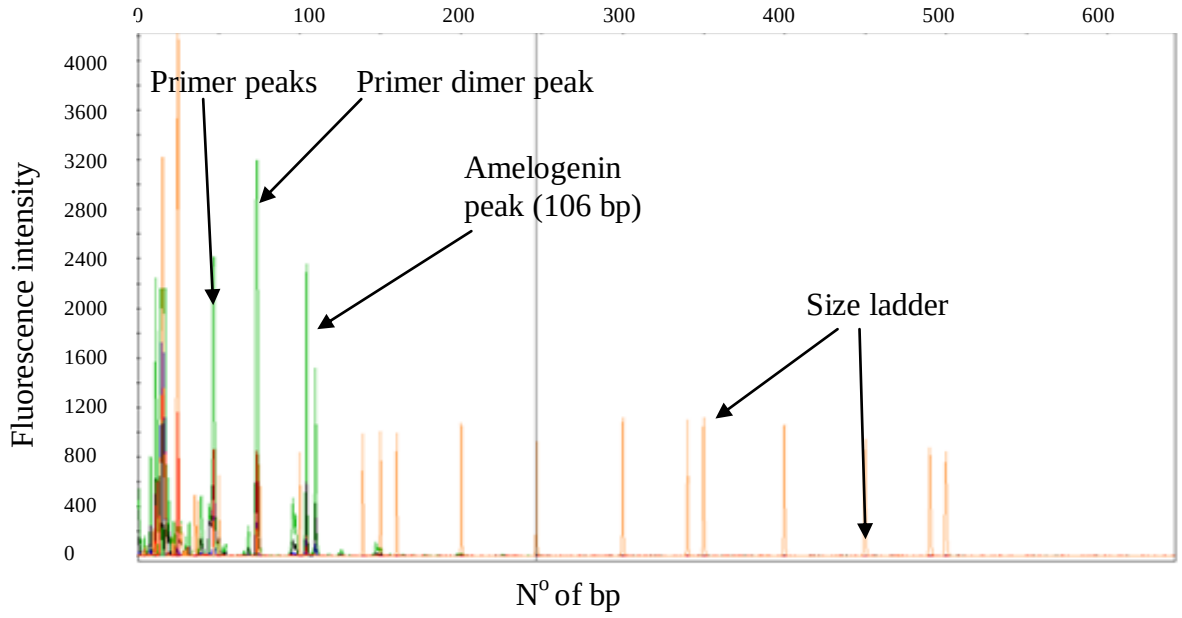

Figure 4.9: Electropherogram of amplified DNA extracted from human urine sample.

Electropherogram of DNA extracted from human urine subjected to PCR using primer pair to target the amelogenin locus, shows peak at 106 bp indicating successful amplification of the amelogenin locus.

Both the D21 locus and amelogenin gene (see Figure 4.9 for electropherogram of the latter) were shown to be successfully amplified, indicating that specific target sequences in the extracted DNA are intact and the eluted samples are of sufficient purity and integrity to support PCR amplification. This is a significant observation as urea within urine is known as a potential inhibitor of PCR and the successful amplification shows that any inhibitory components were removed. The hgDNA quantity extracted, however, varied widely providing quantities of DNA ranging from 5 to 27 ng (13 ± 10 ng) giving an indication of the varying DNA concentration of urine sample. This huge variation in the background host DNA content of human urine samples further enforces the necessity for the monolith to have a high capacity for DNA binding, as the silica will be taken up largely by a background of hgDNA, limiting the surface area for the binding of the target genomic DNA.

4.3.1.5 Reduction of experimental flow rates for DNA extraction

In order to reduce the sample processing time, the effect of varying the flow rate on DNA extraction efficiency was investigated, as it was considered necessary to maximise the flow rate without lowering the DNA recoveries significantly. Based on the experimental parameters described for AUM-based extractions (stion 4.2.2.1), the load timescale can be calculated from the volume (50 µl) and the flow rate, giving 20 min load time. As 5 wash fractions were collected, the entire wash phase was approximately 15 min and elution, based on 4 fraction elution volume was approximately 25 min, a total of ≈ 60 min. With the additional drying step this was ≈ 65 min.

To investigate the potential to reduce time taken for sample processing a series of experiments was conducted, varying the flow rates at 5, 10, 15 and 20 µl min^{-1}. DNA extraction efficiencies were measured for each flow rate and found to be unaffected at flow rates of 5 and 10 µl min^{-1} but a further increase to 15 µl min^{-1} produced a decrease in efficiency of ≈ 15 % (Figure 4.11). Finally at flow rates of 20 µl $min^{-1,}$ the average DNA extraction efficiency was below 10 %. Figure 4.10 shows comparison of profiles for 5, 10, 15 and 20. Unlike previous extractions, at flow rates of 15 and 20 µl min^{-1}, DNA was detected during the loading phase, implying it is passing straight through the monolith without binding. In addition the elution peaks

are spread over many more fractions (≈ 15). Data is summarised for all the flow rates used in Figure 4.11. From this, the optimal flow rate was identified as 10 µl min^{-1} due to the DNA extraction efficiencies still remaining competitive at this rate. The experiments described provide a reduction from ≈ 65 min to ≈ 20 min with drying step. When considering a 150 µl sample, this is a sample processing time of ≈ 35 min.

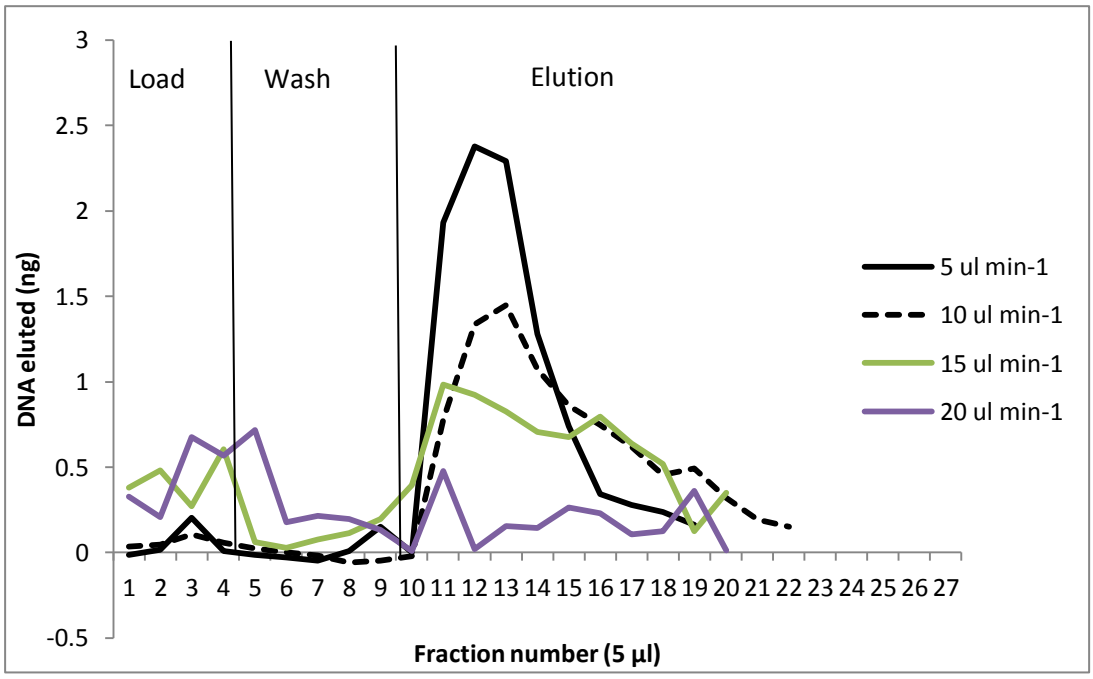

Figure 4.10: Influence of flow rate on DNA extraction profile.

Shows comparison of DNA extraction profiles using TMOS-based monolith at varying flow rates of 5, 10, 15 and 20 µl min^{-1}. The DNA content in elution fractions decreases as the flow rates are increased. In addition a larger quantity of DNA is observed in load and wash fraction when flow rates are increased to 15 and 20 µl min^{-1}, implying flow rates are too fast for total DNA binding.

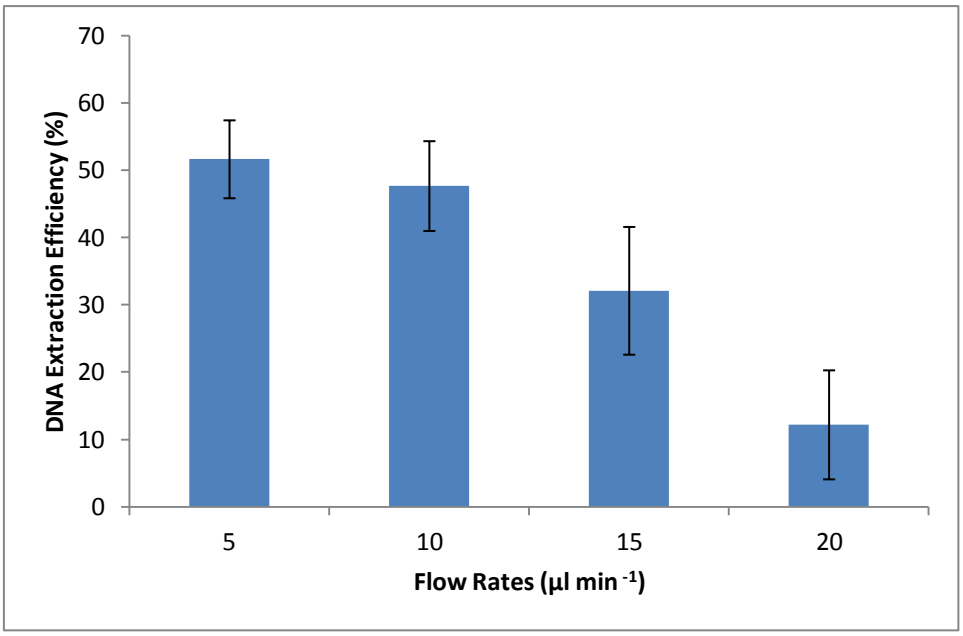

Figure 4.11: Influence of flow rate on DNA extraction efficiency.

Bar chart showing the influence of increasing flow rates for DNA extraction procedures. All flow rates are kept uniform throughout load, wash and elution steps. Flow rates of 5 µl min^{-1} and 10 µl min^{-1} (N = 3) show similar DNA extraction efficiencies to that of the experiments with flow rates described in stion 4.2.2.1, while further increase in flow rate shows a sharp decline in DNA recovery.

4.3.2 Potassium silicate-based monoliths

4.3.2.1 DNA extraction efficiency

The preliminary experiments performed on potassium silicate-based monoliths synthesised in capillaries (stion 3.2.1.2) using AUM spiked with hgDNA. The potassium silicate-based monolith demonstrated DNA extraction efficiences of 54 ± 9% (n=3). The loading, washing and elution fractions were found to be similar to that of silicon alkoxide-based monolith extractions. However, due to the smaller size of the capillary, the fractions collected here were of a lower volume (2 µl) so DNA is preconcentrated to a greater extent. As with silicon alkoxide-based monoliths, the pH of the silica surface was adjusted through treatment with TE buffer pH 6.7. Tian et al (2000) described in detail, the influence of optimum pH of the DNA-silica extractions, attributing the effects to increased hydrogen bonding interactions and reduced electrostatic repulsion. On varying the monolith treatment time using the TE

buffer of pH 6.7, it was shown to have a significant effect when carried out for 2 and 3 hs providing average DNA extraction efficiencies ≈ 75% (n=3)(Figure 4.12), with elution fractions containing ≈ 10 ng of DNA in a single 2 µl fraction (see Figure 4.13 for extraction profile comparison). Due to the absence of DNA in load and wash steps for all treatment times investigated it is presumed that the optimum surface pH of the silica monolith aids DNA release as opposed to DNA capture. Further increase in treatment time for 4 hs resulted in decreased DNA efficiencies of ≈ 45%, indicating saturation of the silica had occurred. It is postulated that continued treatment with TE buffer eventually hinders the interactions between the DNA and the surface by damage to the monolith structure. Notably, ethanol was not retained in the monolith and, unlike silicon alkoxide-based monolith extractions, a drying step was not necessary prior to amplification. Sample processing time using standard flow rates (stion 4.2.2.1) was approximately 40 min.

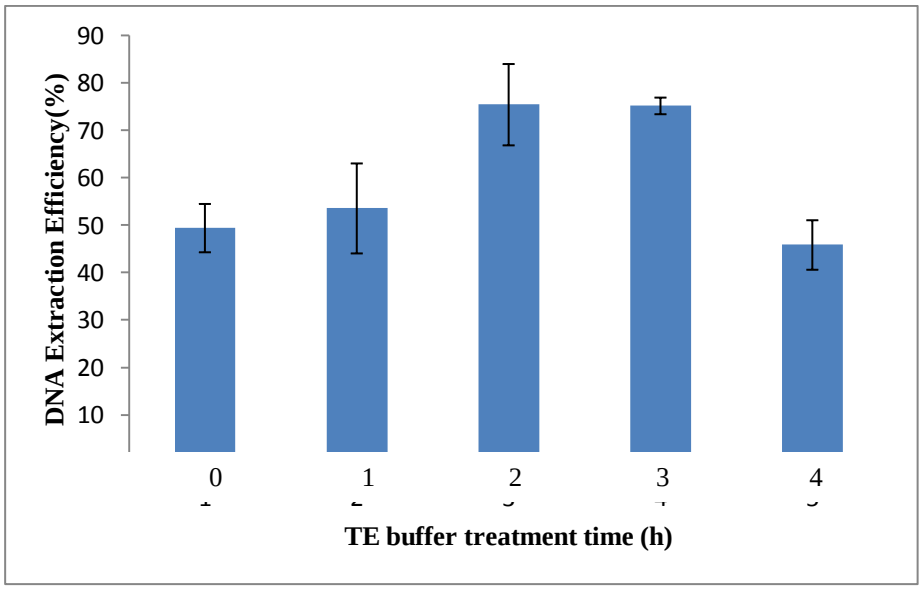

Figure 4.12: Influence of TE buffer treatment time on DNA extraction efficiency when using potassium silicate-based monoliths.

Bar chart to show the influence of treatment with TE buffer pH 6.7 (n=3). Optimum treatment time was in the region of 2 and 3 hs, providing optimum DNA extraction efficiencies of ≈ 75%. N = 3

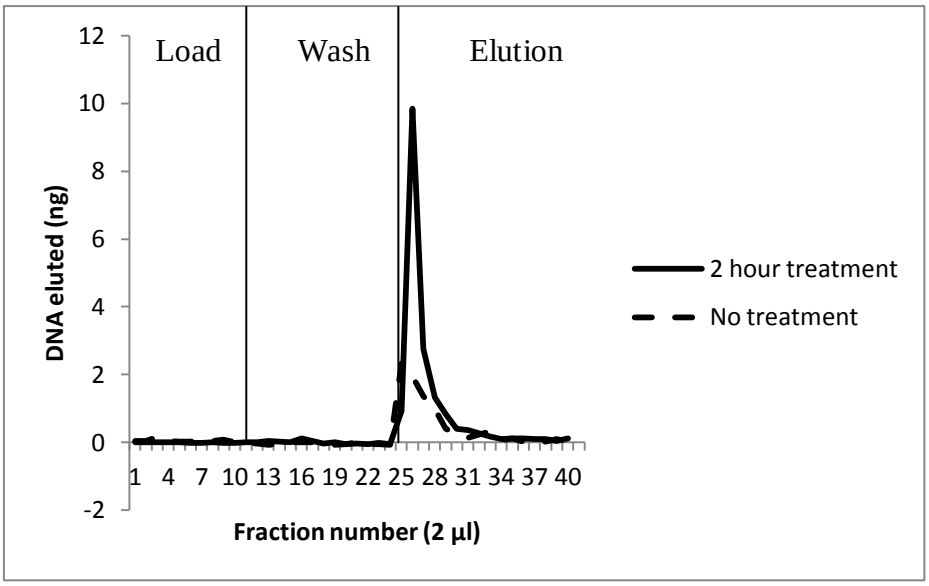

Figure 4.13: DNA extraction profile for potassium silicate-based monolith.

DNA extraction profile comparison for DNA extractions performed using potassium silicate-based monolith for no treatment and 2 h treatment with TE buffer pH 6.7. Experiment reveals DNA extraction efficiency of 51% and 82% extraction efficiency for no treatment and 2 h treatment, respectively. N = 3.

4.3.2.2 DNA binding capacity of potassium silicate-based monolith

A study in to the DNA binding capacity of potassium silicate-based monoliths was carried out, as with TMOS-based monolith (stion 4.3.1.3). The finer porous structure of the potassium silicate-based monolith showed a higher DNA capture per monolith volume (25.11 ± 0.20 ng of DNA per mm^3 of monolith) (n=2) compared to the TMOS-based monoliths (stion 4.3.1.3), which is understandable due to the increased surface area provided as described earlier (see Figure 4.14 for capacity profile). The TMOS monoliths used for DNA extraction, however, have a total volume of ≈ 62 mm^3, which would provide a DNA binding capacity of ≈ 304.6 ng of DNA per monolith, whereas the potassium silicate based monoliths have a total binding capacity of ≈ 40 ng of DNA. As indicated in stion 3.3.3, the volume (≈ 3 mm diameter) of the potassium silicate-based monoliths is limited in volume due to cracking. For this reason the higher surface area per volume cannot be exploited with larger monoliths resulting in a preference to use the less efficient TMOS-based

monoliths for DNA capture, due to there increased size and permeability. A comparison is shown in the bar chart in Figure 4.15.

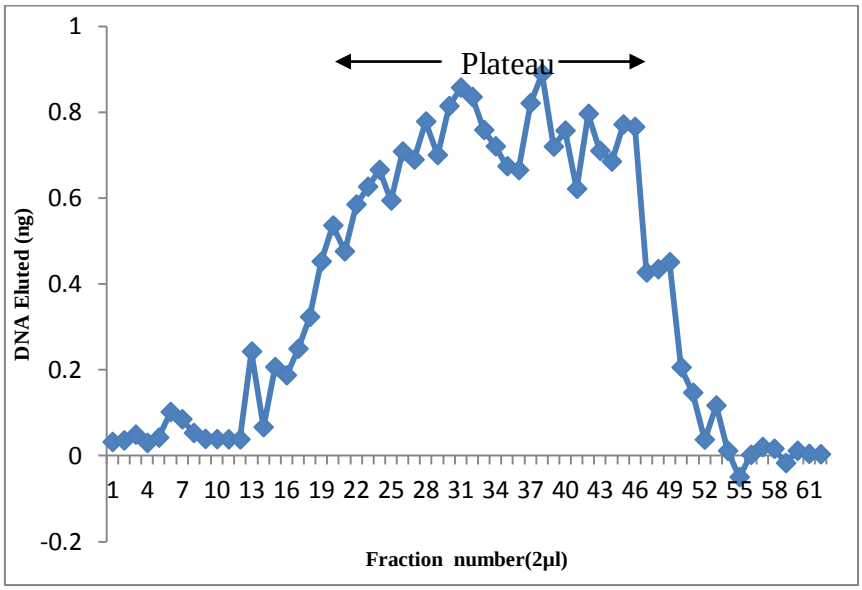

Figure 4.14: DNA capacity profile using potassium silicate-based monolith.

Profile illustrating the the capacity of potassium silicate-based monolith. DNA binds to the monolith from fractions 1-13, before breakthrough occurs at fraction 14 and plateaus at fraction 24. Total DNA bound to the monolith was ≈ 40 ng.

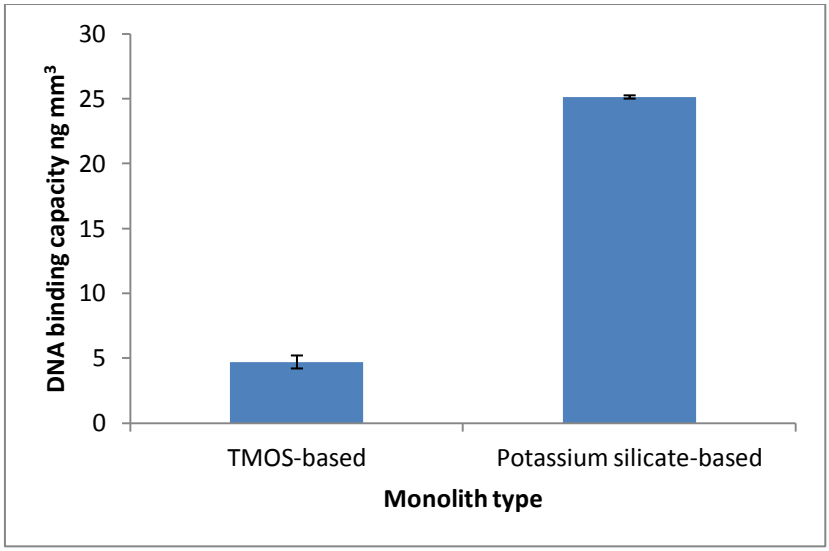

Figure 4.15: Binding capacities of TMOS-based and potassium silicate-based monolith DNA binding capacities.

Bar chart to show the comparison between DNA binding capacity of TMOS and potassium silicate-based monoliths (ng of DNA per mm^3 of monolith)(n=2).

4.3.2.3 Evaluation with human urine sample

The potassium silicate-monolith was then evaluated for processing of a human urine sample. On analysis with human urine, it was found that untreated urine samples were not able to permeate through potassium silicate-based monoliths and caused the system to frequently block. This is likely to be a result of the fine porous structure and absence of larger macropores to aid flow-through. This issue was not apparent with the AUM-based DNA extractions, however real urine specimens contain mucus and debris, which would increase sample viscosity and are likely responsible for the blockage. For this reason, despite the high extraction efficiencies demonstrated, potassium silicate-based monoliths alone were not considered suitable for the processing of 150 µl volume urine samples, and this system was not developed further. The issue could be, however, potentially addressed with the introduction of a pre-filtration system, e.g. syringe filter or tip engineered with a course filter to remove mucus/debris.

4.3.3 Incorporation of TMOS-based monoliths into a microfluidic device

4.3.3.1 Dual porous silica (DPS) solid-phase extraction system on-chip

On establishing a suitable material for processing and DNA extraction from the samples discussed, an investigation was then carried out into the incorporation of TMOS-based monoliths into a micofluidic device. Due to the flat dimensions of the microfluidic device or "chip", TMOS-based monoliths were selected to be further developed and to be incorporated as a monolithic disk rather than as a rod. To achieve this, TMOS monolith rods were produced using plastic tubes (ID 8.10 mm), as in stion 3.2.1.1 and sequentially cut into disk with a glass cutter. This also introduced an increased potential for mass production, which is necessary for a diagnostic device of this nature. Furthermore, the proposed design was considered to facilitate integration of DNA extraction and sample processing to downstream steps, such as PCR amplification and detection. This chip-device comprises a glass chip with an extraction chamber milled to accommodate a silica disk (Figure 4.16). The disk (7 mm in diameter and 2 mm thick) has a volume of ≈ 76 mm^3.

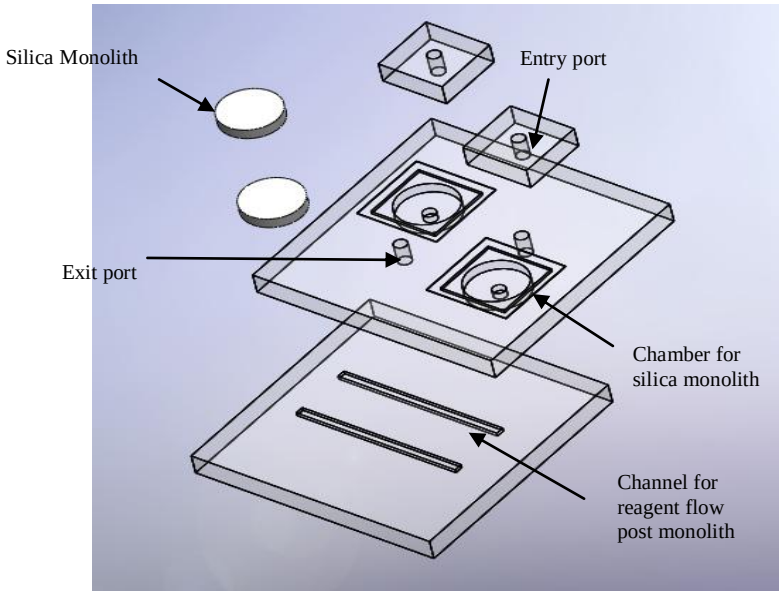

Figure 4.16: 3D representation of the DNA extraction microfluidic device.

Microfluidic devices were fabricated from 3 mm borosilicate glass by milling an extraction chamber to a depth of 2 mm and diameter 7.5 mm and with drilled exit ports in a top plate before bonding to a bottom plate containing a channel 500 µm wide and 100 µm deep, produced by photolithography and wet etching. Each device includes two separate identical chambers each incorporating a single PS disk (7 mm diameter, 2 mm length), permitting duplicate experiments in parallel on the same chip. All DNA extractions were performed using hydrodynamic pumping, allowing sample loading and recovery via entry and exit ports.

The monolith was then sealed into the chamber to provide an airtight pathway for DNA extraction methodologies. Sealing of the monolith disk in to the microfluidic device was based on the following rationale. While both monolith types (silicon alkoxide- and potassium silicate-based) studied displayed similar porous silica characteristics, notable distinctive features of each were observed; TMOS-based monoliths could not be synthesised within the chip device due to the shrinkage occurring on drying, which would lead to subsequent leakage of sample from the system, whereas potassium silicate-based monoliths, could be readily cured *in situ* without notable shrinkage. The potassium silicate-based monoliths, however, were found to be limited in terms of practical usage since they became compromised when synthesised at larger volumes with the monoliths being prone to cracking. For these reasons, incorporation of a silica monolith in to microfluidic device was achieved

using a novel approach whereby TMOS-based monolithic disks were synthesised and the disk was subsequently inserted post-fabrication into the microfluidic device, to provide a primary porous silica structure for SPE methodologies, whilst a sond potassium silicate–based layer was coated onto the perimeter of the disk to both reinforce the disk and seal it in place within the device (Figures 4.17 and 4.18).

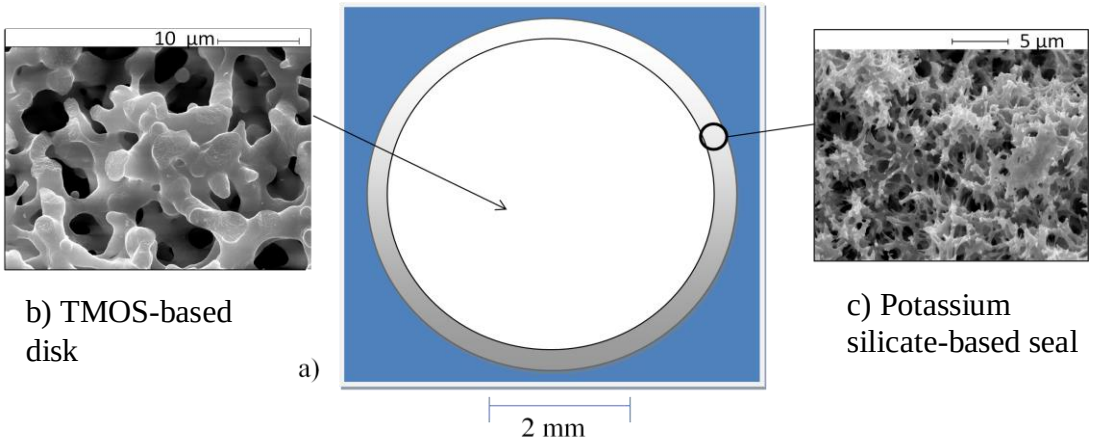

Figure 4.17: Dual-porous silica solid-phase extraction system

a) Schematic to illustrate the arrangement of the porous silica structures within the microfluidic device. Inserts show scanning electron micrographs revealing the structures of b) TMOS synthesised monolithic disk and c) potassium silicate synthesised peripheral seal layer.

On initial mixing, the potassium silicate solution was of a viscosity suitable for coating onto the perimeter of the disk without the porous structure of the disk being penetrated and also sealing the disk within the extraction chamber of the chip-device. On curing at 60 °C this created a seal composed entirely of PS between the monolithic disk and the microfluidic chamber wall, producing a DPS monolithic structure within the device.

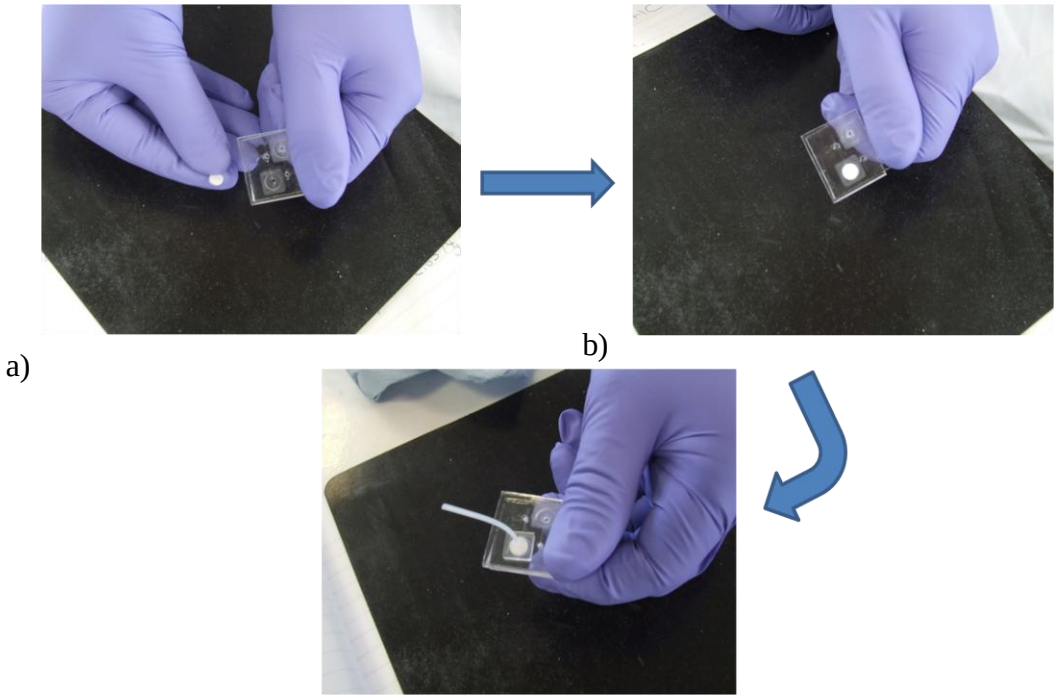

Figure 4.18: Schematic of disk insertion into the chip device.

Schematic shows how disks were inserted into the chip. a) Prefabricated disk prior to insertion. b) Disk placed inside extraction chamber. c) Chip sealed with glass plate using epoxy resin. A samples and reagents were subsequently loaded and pumped through the disk vertically, allowing DNA capture on the silica monolith by SPE.

Before carrying out DNA extraction on the DPS system, coloured food dye was used to first investigate whether permeation of fluid occurs entirely through the monolith, by flowing dye onto the device at 20 µL min^{-1} and observing the flow pathway. When the PS disk was used alone without a potassium silicate sealing layer then the dye was observed to flow around the outside of the disk showing some fluid was not passing through the main PS structure. When the PS disk was used in conjunction with the sondary potassium silicate layer, forming the DPS structure, however, this showed the establishment of an efficient seal between the PS disk and the extraction chamber wall, allowing the dye to fully permeate the PS monolithic disk structure whilst the perimeter was not breached and no leakage was observed around the edges. While all of the disk was observed to be permeated by the dye, the vertical passage focused on the centre of the disk which may result in small areas of dead volume near the edges, causing some loss of sample.

For DNA extraction experiments, all samples and reagents were loaded onto the chip and hydrodynamically pumped through the monolithic disk vertically via PTFE tubing (see Figure 4.18 for setup), allowing capture of the analyte DNA on the porous silica surface. Back pressures measured at flow rates of 10 μL min^{-1} were less than 10 psi for sample loading, washing and elution stages, demonstrating that the porous structure was sufficiently permeable to both sample and reagents. Using AUM spiked with hgDNA (≈ 25 ng) as a model sample, DNA extraction efficiencies of 44 ± 3% (n = 3) were obtained. This efficiency is lower than the TMOS-based flow systems (stion 4.3.1.1), possibly due to the likely dead volume thought to be occurring within the PS disk as described above. An extraction profile comparison is shown in Figure 4.19.

In addition to the slightly lower DNA extraction efficiency of the TMOS-based disk, when compared to the TMOS-based flow system, the DNA extraction profile illustrates a more distributed and less predictable elution volume, probably due to the shape of monolith within the device causing a less defined flow pathway to that of the TMOS-based flow system. The chip-based DPS disk system was evaluated for the extraction of nucleic acids of sufficient quantity and integrity for downstream applications by subjecting the DNA recovered to PCR amplification. As with flow system extractions, it was observed that if there were significant traces of ethanol present in the eluted DNA volume then inhibition of the subsequent PCR resulted (Claveau *et al*, 2004). It was shown that could be prevented by flushing the DPS structure with air using a syringe and including an additional drying step by placing the device in an oven for 5 min at 40 °C following the wash step. The drying process permits evaporation of the residual ethanol retained within the PS structure and by adopting this drying step, downstream PCR amplification of extracted DNA was carried out successfully.

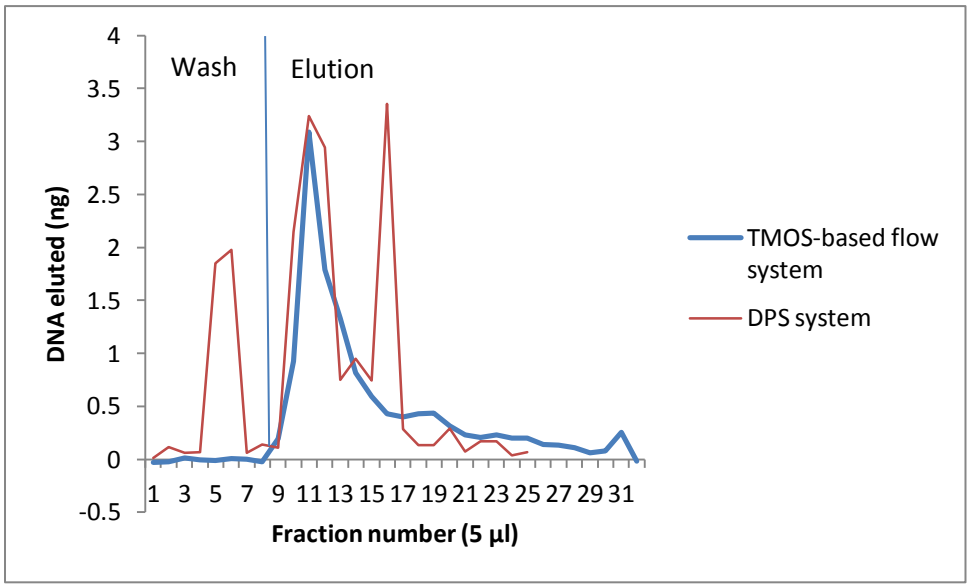

Figure 4.19: DNA extraction profiles for TMOS-based flow system and DPS system.

The elution phase for the TMOS-based flow system is a single well defined peak (fractions 11-13), however for the DPS the eluted DNA is spread over a larger number of fractions (11-17). In addition the DPS system shows some DNA was eluted in the wash step. N = 3.

When compared with other reported chip-based systems the DNA extraction efficiencies demonstrated here are lower. The bead-based systems reported (Wolfe *et al*, 2002, Kulinski *et al*, 2009), however, have reported lack of reproducibility during manufacturing, whereas such problems are not anticipated with the robust monolith synthesis and incorporation methodology proposed here. Those reporting prefabricated intricate channels have described increased manufacturing timescales, due to the intricacies of fabrication (Wen *et al*, 2006). This is also something which is not an issue with the DPS approach. Shaw *et al* (2009) reported a silica monolith on-chip using a potassium silicate-based methodology. While the work reported good DNA extraction efficiencies of > 60 %, the application discussed was for forensic analysis and dealt with smaller samples (> 5 µl) when compared to those used in the work described here. In this investigation, when using the potassium silicate-based monoliths for larger volume urine samples, they were found to block. This is something which has been addressed by the DPS system, which was able to process them reproducibly.

4.3.3.2 Dual-porous silica with chitosan

For the DPS system described, an alternative methodology was explored in order to shorten the sample processing times described thus far. As described in Stion 1.4.4.4, the introduction of the biopolymer chitosan to a silica-based extraction system, offers the opportunity to eliminate the drying step, bypassing the ethanol wash step and altering the surface chemistry to that of nucleic acid capture and release by pH shift. For this reason TMOS-based monolith disks were functionalised with chitosan, as described in stion 2.1.3. Due to the mode of production, the monolith disks were able to be functionalised with chitosan in batch by a simple immersion technique. In addition, the incorporation and sealing of the chitosan-coated disk within the microfluidic device was carried out at 60°C, which was not destructive to the chitosan compound. A comparison of potassium silicate-based monoliths cured at 90 ^{o}C and 60 ^{o}C to confirm that the monolithic seal could be cured at the lower temperature (Figure 4.20). SEM images show no evidence that the structure of the silica disk is affected by the lower curing temperature.

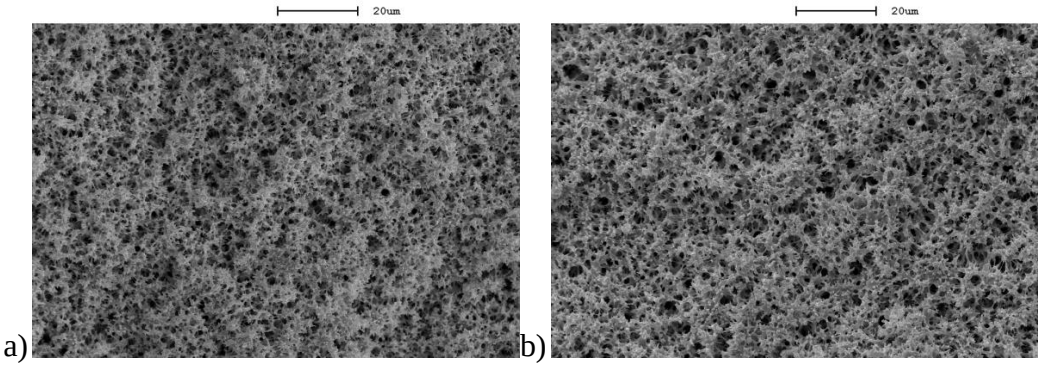

a) b)

Figure 4.20: SEM image of potassium silicate-based monolith formed using varying curing temperatures.

Images show structure cured in capillaries at a) 90^{o}C and b) 60 ^{o}C. Magnification 2000x. The difference in curing temperature showed to have no obvious affect on porous structure and size of pores.

Evaluation of DNA extraction performance of the chitosan-coated TMOS-based disks was conducted as in stion 2.4.3. The experiments carried out here provided average DNA recoveries of ≈ 40 ± 8 % (n=3), using buffer pH change of pH 5.05 to 9.1. This is slightly lower than both uncoated TMOS-based systems (stion 4.3.1.1 and 4.3.3.1),

however, the chitosan-coated TMOS-based disk extraction may be also affected by the issues of dead volume, which affected the uncoated TMOS-based disk extraction. The chitosan-coated DPS extraction efficiency is also slightly lower than chitosan-based DNA extraction systems reported in the literature. DNA extraction efficiencies between 60% and 70% have been reported by Cao *et al* (2006) and 50-70 % by Parton *et al* (2012) who used chitosan coated beads and Reedy *et al*, 2011, who used chitosan-coated prefabricated channels. However, monoliths offer a desirable alternative to a coated bead-based system, as beads have shown a lack of reproducibility, due to instability within the device, which is a problem the silica monolith can be used to alleviate. In addition prefabricated channels can be very time consuming and complex during the manufacturing process. Manufacture and incorporation of these monolith disks is something which has been shown to be simple and robust in comparison.

The extracted DNA was subsequently amplified by PCR to ascertain whether it is of sufficient quantity and quality for downstream analysis. As with uncoated TMOS-based DPS, DNA was distributed in more elution fractions than with that of the flow systems-based extractions, again likely due to dimensions within the device. In addition, some of the DNA was eluted in the wash phase (Figure 4.21). Despite this, the DNA in the elution fractions was able to be amplified without a drying step, which could not be achieved with a simple silica extraction (Figure 4.22). This was also achieved without a significant change in extraction efficiency. Whilst this holds some potential as a DNA extraction process, an additional complication associated with the chitosan-based extraction is that the sample must be diluted by MES pH 5.5 in order to achieve capture of target DNA.

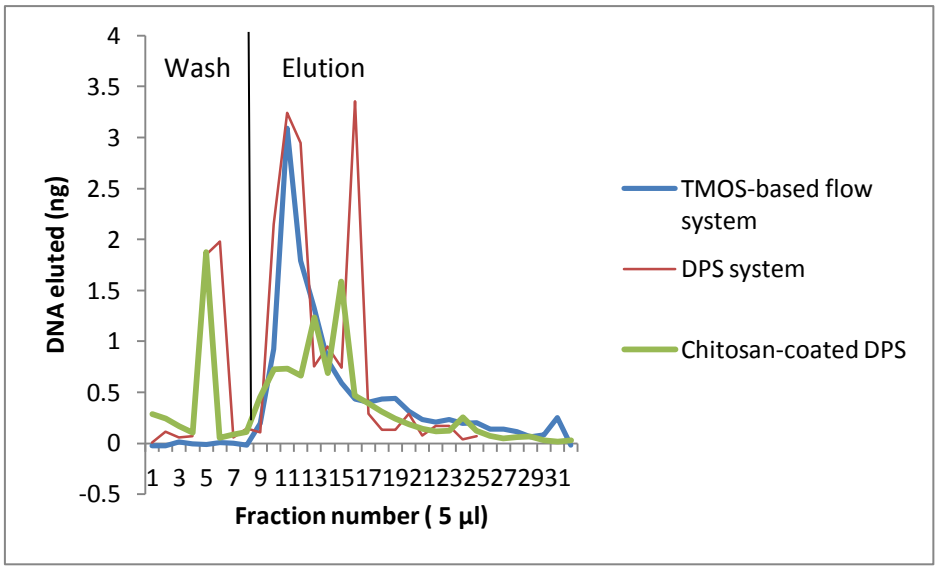

Figure 4.21: DNA extraction profile comparison for TMOS-based flow system, DPS and chitosan coated DPS.

The elution phase for the flow system is a single well defined peak, however for the DPS disk on-chip with and without chitosan, the eluted DNA is spread over a larger volume of eluent. N = 3 for all DNA extraction substrates.

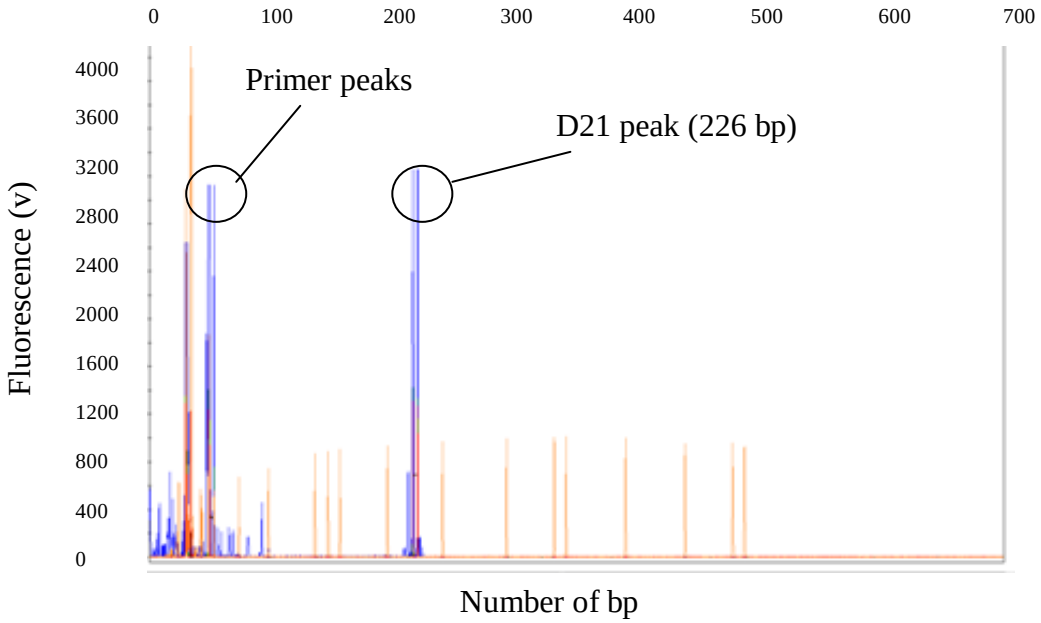

Figure 4.22: Electropherogram of amplified DNA extracted using chitosan-coated DPS.

Electropherogram of extracted DNA subjected to PCR amplification using D21 locus primer pair. The peak 226 bp is in agreement was that of the D21 locus implying target has been successfully amplified. N = 3

While, it was possible to add the CS directly to the sample (stion 4.3.2.3), it was not possible to transform the urine sample in to a chemically similar environment using a MES pH 5.5 buffer, so a high volume sample (eg 150 µl) would require 1.5 ml of the MES diluted sample to be pumped through the monolith, thus increasing the processing time significantly. For this reason the chitosan-based DPS was not ideally suited for samples of this volume.

One further observation made for the chitosan-based DPS was that flow through the monolith was variable throughout the experiment. While the buffers were able to permeate through the monolith sufficiently for a competitive extraction performance, flow became restricted as the experiment progressed. It has been reported in the literature that chitosan has pH dependant swelling properties in which low pH favours uptake of H_2O molecules (Rohindra *et al,* 2004). Such properties have been utilised in drug delivery systems and wound dressing, as well as other biomedical applications. With regard to the DNA extraction procedures described here, it is likely that that the chitosan will swell as the MES pH 5.5 is pumped through and due to the rigidity of the monolith, this could cause partial closure of the porous structure. This could possibly explain the high standard deviation observed (≈ 8%) for DNA extraction efficiencies.

4.3.4 Chitosan /silica hybrids

As described in the previous chapter, chitosan was introduced to both TMOS-based monolith and potassium silicate-based monoliths for an investigation in to chitosan /silica-based hybrid structure. The TMOS-based silica /chitosan hybrid monoliths were synthesised using a methodology adapted from Lan *et al* (2010). It was hypothesised that a continuous structure of chitosan and silica could be synthesised, eliminating the need for coating the silica monolith post synthesis. Chitosan/ TMOS based monoliths were synthesised as rods and cut into disks, then incorporated in to the microfuidic device as described previously (stion 4.3.3.1).

Using the DNA extraction methodologies described in stion 2.1.3, the DNA extraction efficiencies were 27 ± 8%. The SEM images in stion 3.3.5.4 showed that the chitosan was dispersed uniformly throughout the monolith, but was sharing surface area with bare silica. The silica surface would be chemically ineffective, when

changing the pH of the buffers during the extraction process accordingly and it was decided that TMOS-based/chitosan hybrid was not a suitable methodology due to relatively low extraction efficiencies when compared with the other systems described in this work and that described in the literature.

When potassium silicate-based monoliths were synthesised with chitosan, the monolith would form in the capillary as normal without noticeable cracking. The chitosan-based DNA extraction protocol was carried out and recoveries of 17 ± 3% were observed, which is significantly lower than other methods investigated and is likely due to an incomplete functional surface area. This is further supported by the SEMs shown in stion 3.4.4.1, which showed that the porous structure had not formed as it did without chitosan present.

4.3.5 Application of DPS system to the detection of STI-causing bacteria

4.3.5.1 Detection of *C. trachomatis*

Following evaluation of the various silica-based monolith systems and chitosan-based systems for solid-phase DNA extraction the potential of each was subsequently demonstrated for the detection of target STI nucleic acids. Consideration of the advantages and limitations of each system led to the decision to use the DPS disk format without a chitosan coating. This is due to the competitive DNA extraction efficiencies (≈ 44 %) and the potential to integrate the DPS to downstream steps within a chip format. Chitosan-coated TMOS-based disk would require a very high loading volume (10-fold increase) compared with the silica-based extraction, due to the addition of MES buffer to maintain pH 5.05 for DNA binding. The DPS system was then used to process a model system of 150 µl human urine, spiked with *C. trachomatis* genomic DNA using progressively decreasing concentrations. The preliminary sample analysed was 2 µl *C. trachomatis* genomic DNA (10 ng μl^{-1}) in 150 µl human urine. On subjecting elution volume fractions to PCR, *C. trachomatis* was amplified target sequence successfully. This was then repeated for decreasing concentrations to determine the sensitivity of the system with respect to identifying the lowest amount of target DNA which could be successfully extracted, PCR amplified and detected. 1.33×10^{-3} ng μl^{-1} failed to produce PCR products in 3 of 4 experiments, with one positive result. 1.33×10^{-4} ng μl^{-1} failed to produce any positive

detections in 3 experiments (see Table 8). An example electropherogram for amplified *C. trachomatis* is shown in Figure 4.23. The inconsistency is likely due to the large and unpredictable elution volumes making target DNA content more diluted against the high background of hgDNA. These data are shown in Table 8. In addition, it has been reported that on-chip amplification and detection methodologies have provided an improved sensitivity to that of conventional PCR methodologies (Kashkary *et al*, 2012). This may improve sensitivities for the DPS system.

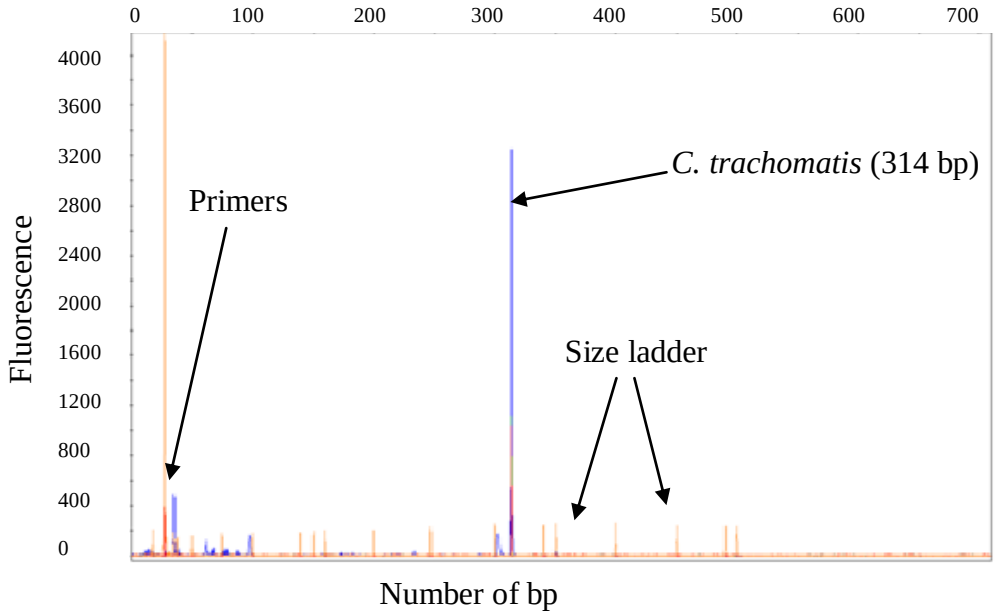

Figure 4.23: Electropherogram of amplified C. trachomatis target DNA

C. trachomatis DNA extracted from 150 µl human urine using the DPS system was subjected to PCR using *C. trachomatis* primer set. Peak at 314 bp corresponds to the expected product of amplification of *C. trachomatis* sequence, implying target DNA was extracted and successfully amplified.

Table 8: PCR amplification of C. trachomatis sequences from DNA extracted using DPS

Shows the concentrations at which a positive detection of *C. trachomatis* was possible by PCR amplification. √ denotes experiment undertaken. Negative control denotes 150 µl human urine sample with no target added. The equivalent copy number describes the amount of CFU corresponding to the total genomic DNA spiked into the sample.

Final concentration of *C. trachomatis* in 150 µl human urine	**Equivalent copy numbers in 150 µl urine sample**	**Amplicons detected**	**Amplicons not detected**
1.33×10^{-1} ng µl-^{1}	1.75×10^{7}	√	
1.33×10^{-2} ng μl^{-1}	1.75×10^{6}	√√√	
1.33×10^{-3} ng μl^{-1}	1.75×10^{5}	√	√√√
1.33×10^{-4} ng μl^{-1}	1.75×10^{4}		√√√
Negative control	N/A		√

4.3.5.2 Simultaneous detection of multiple targets

Often the presence of one STI in a patient increases likelihood of the presence of other STIs (Van Dyck *et al*, 2001). For this reason the DPS system was investigated for use in the capture and detection of multiple targets. DNA extraction procedures were carried out using 150 µl human urine samples containing *C. trachomatis* and *N. gonorrhoea* DNA targets (both 2 µl at 1 ng μl^{-1}) (see stion 2.4.2). The extracted DNA was subjected to PCR using both primers sets for amplification of *C. trachomatis* and *N. gonorrheoa*. Figure 4.24 shows PCR products corresponding to the predicted sizes of *C. trachomatis* and *N. gonorrheoa*, indicating that the targets were extracted detected and amplified successfully using this system.

The timescale of these DNA extractions performed on the microfluidic device was approximately 35 min, which is competitive for rapid DNA extraction directly from urine, compared with examples from the literature (Cao *et al*, 2006; Shaw *et al, 2009*). While the system did lack the sensitivity of other methodologies (Reedy *et al*, 2010; Berry *et al*, 2011), PCR conditions could be potentially further optimised. In addition the shape of the monolith could be narrowed in order to minimise elution volume and ethanol retention.

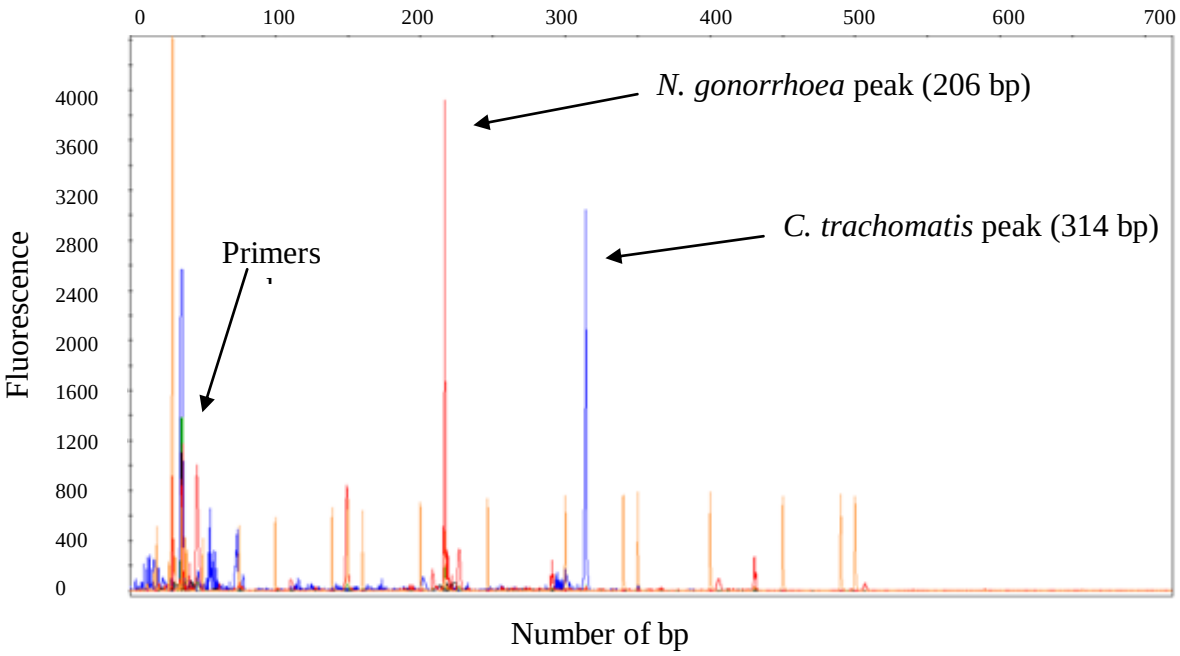

Figure 4.24: Multiplex detection of STIs using DPS system.

Electropherogram of amplified *N. gonorrhoea* and *C. trachomatis* targets which were subjected to PCR. Peaks at 206 bp and 314 bp correspond to expected target sequence sizes (Table 5) are indicative that both targets were successfully extracted and amplified. N = 3.

4.3.6 Direct PCR amplification on a silica monolith

The work thus far was based on conventional capture and elute DNA extraction techniques and it was shown that for the chip-based DPS system, much of the DNA was necessarily eluted in large volumes (>20 µl), which is undesirable for downstream processes within a microfluidic format and would require modification. The extraction profiles did, however, demonstrate that the capacity for DNA capture was very efficient and of high quantity (≈ 150 ng per monolith^{-1}). For this reason, it was proposed that rather than eluting DNA from the monolith for subsequent amplification, the DNA could be amplified within the monolith structure. This involved introducing reagents for PCR amplification on to the monolith while the DNA remained bound to the silica surface of the monolith, allowing the aqueous-based PCR mixture to elute the DNA on contact. It is, however, well documented in the literature that the silica acts as an inhibitor of PCR due to its hydrophilic

interactions with PCR components (Garland *et al*, 2010). Oblath *et al* (2013) showed that aluminium oxide Whatman® filter paper was able to function as a DNA capture substrate and also a well base for subsequent PCR amplification showing much less of an inhibition of the amplification step. They report that the PCR reagents release the DNA from the aluminium oxide paper into the well, permitting thermal cycling.

While the methodology described by Oblath *et al* (2013) performs PCR in contact with the aluminium oxide paper, it was postulated that the thicker silica monolith developed in this study could potentially perform similarly if the PCR conditions were optimised. For this reason the first step to eliminate PCR inhibition was to introduce the dynamic passivation component bovine serum albumin (BSA), in order to reduce adsorption of PCR components to the silica surface (stion 1.4.6.10.2). Initially, a PCR mastermix (stion 2.5.1.1) (25 µl) was mixed with a 2 µl sample of arbitrary target, *C. trachomatis* (≈ 10 ng μl^{-1}) and in addition 2µl BSA (10 mg mL^{-1}). The PCR mixture was deposited on to the monolith within the microfluidic device described in stion 4.3.3 and then covered with mineral oil to prevent evaporation, before being sealed as normal with epoxy resin. PCR thermal cycling was then carried out and the resulting mixture was collected by hydrodynamically pumping air though the monolith. If insufficient liquid (< 10 µl) was retrieved 20 µl of H_2O was passed through the monolith to retrieve any possible PCR product. 10 µl of retrieved mixture was then subjected to analysis by CE.

The PCR mixture failed to produce PCR products using this approach. Following this, the procedure was repeated using PCR amplification mixtures supplemented with increasing BSA additives of 4 µl, 6 µl and 10 µl (all 10 mg mL^{-1}), however, none were able to support successful amplification. As BSA is introduced primarily to competitively bind to the silica surface and prevent binding of the DNA polymerase enzyme, the possibility of eliminating inhibition by increasing *Taq* polymerase was investigated. *Taq* polymerase was increased 2x, 3x and 10x, however, none of the amplification reactions carried out provided PCR products.

Following this, the method of passivation was changed from dynamic to static, in which the surface is modified in order to stop surface adsorption. The functionalisation of the monolith surface in this way, however, would make it incompatible with DNA capture. It was therefore proposed that the monolith could be functionally compartmentalised, whereby and DNA could be captured within one

region and PCR carried out within another. For proof of principle, red and blue dye solutions were used to illustrate how the monolith could be functionalised within a specific region. This was achieved by hydrodynamically pumping each individual dye into the monolith at opposite ends and allowing to dry. An untreated region was left in between both treated regions. The resulting monolith is shown in Figure 4.25. For use in NAAT, for example, the blue or the red compartment would be silanised to permit PCR amplification while the central zone (colour-free) would remain untreated silica for DNA extraction. Captured DNA could then be moved from the extraction zone within the monolith to the amplification zone.

Monoliths were silanised as described in stion 4.2.5. Following this, the monolith was prepared in the chip-device as normal. When measuring the level of silanisation achieved using a glass slide it was found that the contact angle was ≈ 105^{o}. The literature has generally reported 110^{o} for elimination of PCR component absorption, so this was considered sufficient. It was found, however, that due to the strong hydrophobic interaction between the porous silica structure and the aqueous PCR mixture, the monolith was impermeable. When the monolith was prepared using a 1/10 concentration of silanising reagent, the effect was the same. This was therefore considered not a viable approach.

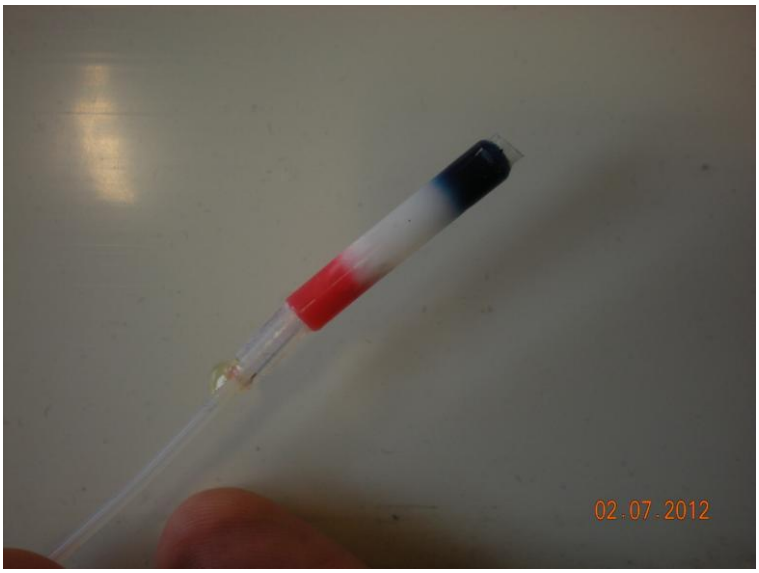

Figure 4.25: TMOS-based monolith treated with dye.

Image of TMOS-based monolith, which has been treated with blue dye at one end and red dye at the opposite end. The effect illustrates potential for compartmentalising the monolith for multiple functions.

In an attempt to simulate the environment of a conventional PCR reaction tube, the monolith flow system was used to accommodate the PCR mixture (25 µl) within the monolith and then sealed at each end with epoxy resin. The monolith was then immersed in mineral oil in a 200 µl PCR tube to allow heat conductance. The Eppendorf was placed in a Techne thermal cycler and thermal cycling was performed. The experiments describing a variation of BSA and *Taq* polymerase (stion 4.3.5) were then repeated in this format. When analysed by CE, all experiments had failed to produce PCR products, despite successful positive controls. Finally, denaturation, annealing and extension cycling times were increased to 60 s and 90 s, in order to ensure monolith was heated throughout, however analysis again revealed that no PCR products were formed. Following this, it was decided that PCR amplification directly within the monolith was not a viable option using the approaches explored here.

4.3.7 Elution of DNA from monolith by electrophoretic techniques

Following capture on the TMOS-based monolith, the DNA remains bound to the silica surface, however, in the presence of eluent the DNA becomes unbound. It was hypothesised that, if sufficient eluent was introduced to the monolith, an electrical voltage could be applied and it would cause the DNA to migrate out of the porous silica structure and could be transported into an adjacent chamber for PCR amplification. Using the IGA and microfluidic device (Figure 2.6) described in stions 2.7 and 2.8, the path between electrode A and B was used to investigate this possibility. As a proof of principle, first PCR-amplified products (1 µl at ≈12 ng μl^{-1}) of a *C. trachomatis* gene (314 bp) were deposited in the sample chamber in 50 µl cathodic buffer [Applied biosciences]. PCR amplified products were used for proof of principle, as the migration time would be less than that of a whole genome, due to reduced size. Channels between A and B were filled with POP7 polymer. Both chambers A and B were filled with cathodic buffer and carbon electrodes were inserted. A voltage of 1000V was applied between A(-ve) and B (+ve) for 10 min. Following this liquid was collected from both chambers A and B and analysed by CE, as described previously. In accordance with the migration of negatively charged DNA

towards a cathode, the liquid retrieved from well B was shown to contain the amplicons (Qiu *et al*, 2010).

Following this a stion cut from a TMOS-based monolith, diameter 3 mm and length 5mm, was immersed in the pre-amplified products (1 µl at ≈12 ng μl^{-1}) in 20 µl dH_2O. This monolith was then inserted into the sample chamber with cathodic buffer. 1000 V was then applied across the channel for 10 min. The liquid was then retrieved from both wells A and B well and analysed by CE. In this case, both wells showed no presence of the amplicon, meaning that either the DNA had failed to migrate out of the monolith or that migration was slower and the DNA was in a region of the channel joining both chambers. Considering this, the experiment was repeated for timescales of 20, 30, and 60 min, however none showed any evidence of amplicon migration out of the monolith. At this stage, it was decided not to pursue this approach further.

4.3.8 PCR in large volume chamber

The PCR volumes investigated thus far were 20 µl. In order to accommodate the large volumes of extracted DNA eluted off the monolith, it was hypothesised that using a PCR reaction of higher volume could allow for higher sample content (> 50 µl) and thus, increase the likelihood of successful amplification of target DNA. For this reason a PCR chamber of large volume (75 µl) developed was incorporated in to a microfluidic device (see Figure 4.27). While large volume PCR is not common, it has been reported in volumes as high as 100 µl off-chip (Qiu *et al*, 2010). The volume investigated here was 60 µl. The higher volume PCR reaction would also potentially eradicate the need for silanising of the glass chip, as surface to volume ratio is drastically reduced, compared with PCR chip-device reporting volumes < 10 µl (Zhang *et al*, 2006; Shaw *et al*, 2010). The larger chamber does, however, introduce larger temperature gradients, due to increased volume. For this reason it was necessary to thread a thermocouple in to the PCR reaction chamber and monitor the temperature in relation to the Peltier element to determine the actual temperature achieved within the PCR reaction mixture (Figure 4.27).

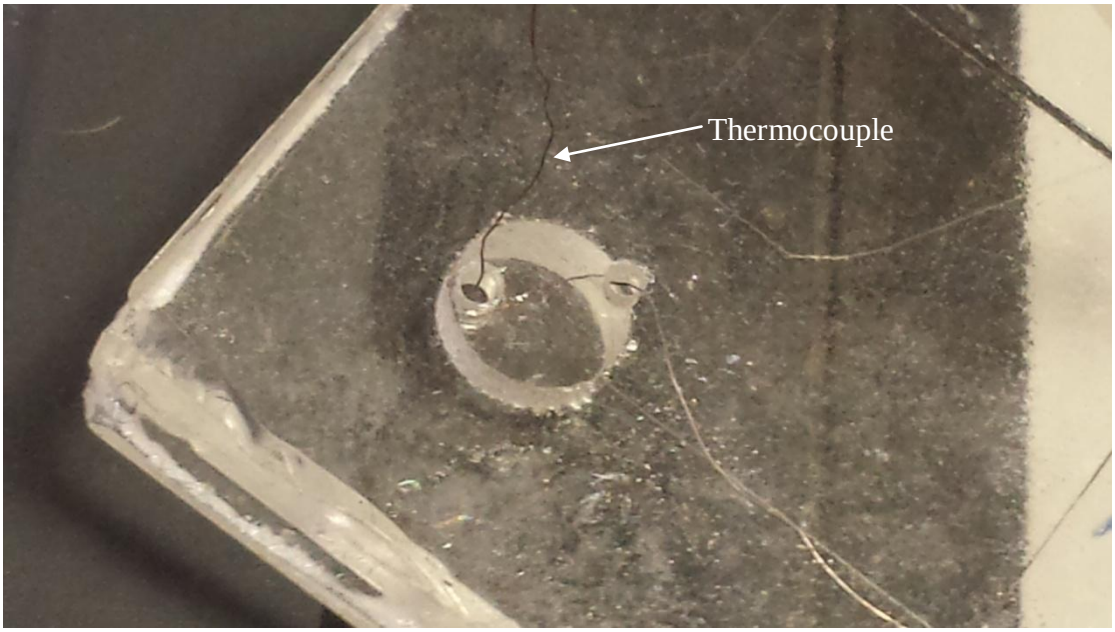

Figure 4.26: Large volume PCR chamber with thermocouple.

A K type thermocouple was inserted in to PCR chamber by threading through the inlet and outlet ports to monitor the temperatures achieved during thermal cycling procedures.

It has been reported in the literature that, due to loss of heat during transfer from the Peltier element to PCR chamber, it is necessary to establish the specific temperature within the chamber throughout thermal cycling. To ensure the required temperatures were achieved during thermal cycling, a thermocouple was threaded through the PCR chamber via inlet and outlet. The temperature was then monitored while the Peltier was cycled as normal. Solution within was the chamber was green GoTaq buffer (Promega) The necessary temperature of the Peltier element established were as follows:

Table 9: Conditions for Large volume PCR on-chip

The table shows the set temperature (^{o}C) required on the Peltier (Peltier element temp) in order to achieved the temperatures required for successful thermal cycling (Required temp) and also the time (s) in which the temperature must be held. A temperature of 106 ^{o}C was required for the denaturation step (11 ^{o}C higher), while annealing and extension temperatures were achieved with a 3^{o}C and 4^{o}C temperature difference, respectively.

	Required temp (^{o}C)	Peltier element temp (^{o}C)	Holding time (S)
Denaturation	95	106	60
Annealing	60	57	60
Extension	72	76	60

The measured temperatures achieved within the solution are shown in Figure 4.28. Using the temperature cycling data it was possible to extrapolate the necessary holding times for each temperature stage within the cycle.

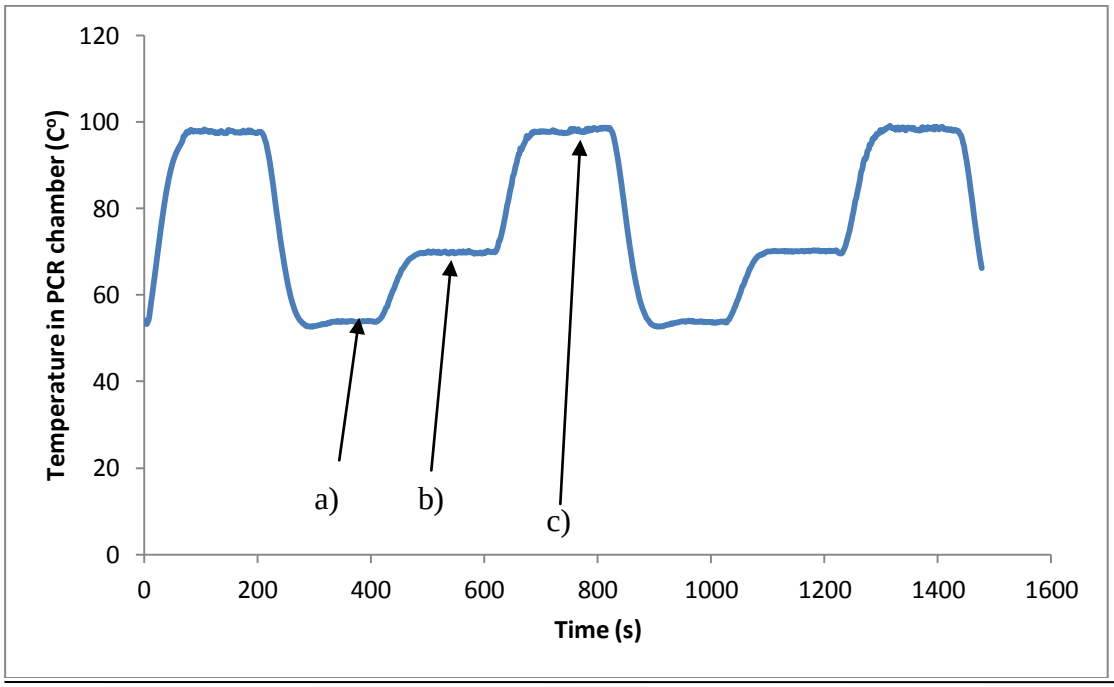

Figure 4.27: On-chip thermocouple temperature reading.

The graph shows a profile of temperatures achieved in the large volume PCR chamber, using Picolog Software [Pico technology, UK]. (a) denaturation, (b) annealing and (c) extension.

The chamber was silanised as described previously by filling the chamber for 5 min sequentially with silianisation and wash reagents (stion 2.5.5). The sample chamber was then filled with 60 µl PCR reaction mixture and sealed with optical adhesive tape and epoxy resin. In addition, all other chambers on the device were sealed with super glue [Loctite®, UK]. The PCR reaction mixture was then subjected to thermal cycling using the parameters established. It was, however, not possible to carry out analysis of the mixture following PCR amplification as it had undergone excessive evaporation throughout thermal cycling and the chamber became dried out. It is assumed that the larger volume of the PCR chamber resulted in higher pressures within the solution during thermal cycling causing the seal formed by the optical adhesive to be breached compromising the sealing of the chamber.

Following this, a sondary heating element was installed on to the upper side of the microfluidic device. While dual-heating systems such as this are installed primarily for thermal uniformity throughout the chamber, the sond heating element can also reduce evaporation effects, much like the heated lid in conventional PCR machines. The upper heating element was set to a constant 94 ºC and the PCR was repeated as before. However, while evaporation of the sample was reduced to ≈ 50%, on analysis by gel electrophoresis no PCR products were observed, suggesting that amplification had not been successful. It is suspected that the upper heating element would interfere with cooling phases due to the constant high temperature at 94^{o}C. It was decided that an upper Peltier heating element would be necessary to improve the system, which was not available at the time of study. While this approach was discontinued at this stage, it is, however, considered that this is worthy of future investigation.

4.4 Summary

In summary, a variety of porous silica monolith-based systems were characterised and evaluated for DNA extraction performance and, having considered the advantages and limitations of each, one was selected for the nucleic acid-based detection of STI causing organisms from urine. Investigations using potassium silicate-based monoliths showed that whilst they offered high recoveries of DNA (≈ 75% efficiency), the fine porous structure was susceptible to blocking with urine samples.

This problem could possibly be addressed by the introduction of a pre-filtration step prior to loading the sample on to the monolith. In addition the structure cracked when larger monoliths were produced. By contrast, monoliths synthesised from TMOS and TEOS were found not to crack and to also provide a more permeable porous structure and allow passage of sample and reagents without the issue of blocking, due to the larger sized pores aiding flow through. Both TEOS and TMOS-based monoliths gave a very similar DNA extraction performance, with recoveries in the region of 50 %. TMOS-based monoliths, however, were preferred due to slightly higher DNA recoveries and a more robust synthetic pathway. While the data obtained for altering 1 M NH_4OH treatment time of these monoliths, provided no improvement on the initial treatment time (24 h) in this circumstance, the influence of treatment on DNA recovery make it worthy of consideration for alternative silica-based SPE substrates. The TMOS-based monolith was shown to process a human urine sample, with pre-treatment consisting of only the addition of CS in solid form, demonstrating that the real-world interface could receive an unprocessed urine sample.

A microfluidic chip-device was designed to accommodate the TMOS-based monolith in the form of a disk (incorporated using a sondary porous silica seal), providing a DNA extraction efficiency of ≈ 44% recovery. The DPS system is, to the author's knowledge, the first reported amalgamation of two types of porous silica in one microfluidic device. The format did, however, prove to be less reproducible than in TMOS-based flow systems during elution phases, resulting in variable elution volumes. In addition, for all silicon alkoxide-based extractions the retention of ethanol on the monolith post-wash, was found to inhibit PCR and cause it to fail. This led to the introduction of a drying step post-ethanol wash which allowed all ethanol to be evaporated and PCR was carried out as normal. While the drying step proved effective in eliminating inhibition, the step introduced an extra stage to the methodology and further increased sample processing times (≈ 5 min). This is, however, a compromise made by others in the literature (Baier *et al*, 2009).

The use of chitosan-treated porous silica structures was also investigated for DNA extraction by anion exchange. As described in the previous chapter, potassium silicate-based monoliths were not able to be coated with chitosan due to blocking by the viscous solution, however, the TMOS-based monoliths were successfully treated with chitosan using both immersal coating and synthetic methodologies. Using a

chitosan-coated TMOS-based monolith the DPS system provided equally competitive recoveries of ≈ 40% when compared to the flow systems and in addition, extracted DNA was able to be subsequently PCR amplified, without a drying step, due to the elimination of the ethanol wash. Both potassium silicate- and TMOS-based monoliths treated with chitosan during synthesis, provided less competitive DNA recoveries of 17% and 27%, respectively. All TMOS-based systems were shown to successfully support extraction of DNA from human urine samples, yielding DNA of sufficient quantity and integrity to permit amplification of the D21 locus target sequence. Table 10 is a summary of all system performances.

Having demonstrated the capability of the chip-based DPS system for the extraction of DNA from urine samples, the system was then explored for the specific application of detecting STI-causing organisms from urine by DNA extraction, followed by PCR amplification of specific organism target sequences. The DPS extraction system supported DNA recovery and amplification of *C. trachomatis* target sequences (314 bp) from a 150 µl human urine sample (0.00133 ng μl^{-1}). Furthermore, the system was successfully demonstrated for performing multiplex extraction and PCR amplification of both *C. trachomatis* (314 bp) and *N. gonorrhoea* (206 bp) targets from 150 µl of human urine. Due to the lack of sufficient sensitivity, when compared with established procedures, and high elution volumes, the DPS using this methodology was not further developed for analysis of STIs. The sample processing time (≈ 35 min) was also considered too long for this application. The methodology could, however, potentially be improved by modification of the monolith dimensions and also optimisation of PCR amplification conditions.

Investigations to explore the potential for performing PCR amplification within the monolith showed it was not possible to overcome problems associated with adsorption of PCR components to silica surface. However in retrospect, if a further investigation were to be carried out, preliminary work measurements should be carried out to ensure sufficient temperature is reached throughout the entire monolith. One way to achive this would be to implant a thermocouple inside the monolith in order to monitor temperatures closely.

Investigation of the large volume PCR (≈ 60 µl) on a chip-device showed that despite sufficent temperatures being achieved within the PCR chamber during thermal cycling, it was not possible to contain fluid of that volume without breach of the seal

used in this approach. This is most likely a result of the high pressures associated with this higher volume. While it may be possible to contain liquid within the chamber with stronger sealants, such as a cover plate, the high pressure would be likely to perturb the adjacent polymer required for subsequent downstream separation and detection.

The author would like to note that while the DPS system would need further optimisation to be competitive for this particular application, the novel methodology for incorporation of the porous silica in to microfluidic device could be utilised for a much wider variety of applications, outside the scope of this work, such as drug extraction and water analysis.

Table 10: Summary of DNA extraction systems investigated

A comparison of the performance of all of the DNA extraction systems investigated in this study is presented, giving details of DNA extraction efficiencies, the DNA binding capacity, back pressures observed during sample loading, total time taken for DNA extraction and whether extracted DNA could be successfully amplified.

PS structure and sample type	**DNA Extraction Efficiency (n=3) (%)**	**Capacity (ng mg^{-1})**	**Back pressure(psi) (after ten min at 20 µl min^{-1})**	**Total time taken for sample processing (optimised flow rates)(min)**	**Extracted DNA successfully amplified Yes/No**
Potassium silicate-based monolith flow system	75	25	25	40	Yes
TMOS flow system	51	5	<10	20	Yes
TEOS flow system	48	Not measured	<10	20	Yes
DPS + artificial urine	44	Not measured	<10	<24	Yes
DPS/chitosan + artificial urine	41	Not measured	Not measured	<24	Yes
DPS + human urine (150 µl)	N/A	Not measured	Not measured	<35	Yes
Hybrid chitosan/TMOS-based disk	27	Not measured	Not measured	<20	No
Hybrid chitosan/ potassium silicate flow system	17	Not measured	Not measured	<20	No

5 Development of on-chip PCR amplification and detection methodologies: For use in the detection of Methicillin resistant *staphylococcus aureus* (MRSA)

5.1 Introduction

The work presented in this chapter describes the development of a custom-made fluorescence detection system designed and incorporated as part of an existing integrated genetic analyser (IGA) (previously developed for forensic DNA analysis) (stion 2.8)(Shaw *et al,* 2009). A detection system is required, as part of the NAAT process, for visualisation of fluorescence-labelled DNA fragments and accurate size analysis. There are many examples of real-time PCR within integrated diagnostic devices (www.bd.com, 2014; Oblath *et al,* 2013; Cepheid®, 2014), which offer the capability to combine amplification and detection steps. Other groups have shown that a simple CE-based detection system can be an effective alternative to real-time PCR when integrated to an upstream amplification step (Wooley *et al,* 1996; Easley *et al,* 2006; Manage *et al,* 2010*).* CE-based separation and detection is useful as a simple qualitative tool for visualisation of target amplicons and the necessary technology can be implemented with relative ease. The work here describes the application and optimisation of a detection system which utilises a combination of CE and avalanche photodiode/fluorescent techniques, using a fluorescent label (FAM) for both amplified sequences and size marker for added simplicity. Plug injections have been frequently reported on microfluidic devices as a means of introducing a small portion of the total sample to the separation channel difficult (Wooley and Mathies, 1994; Easley *et al*, 2006; Camilleri, 1997). Without doing so a continuous stream of target material will be withdrawn from the sample chamber and transported to the detector, making the generation of coherent spectra difficult. A plug injection methodology of this nature was considered appropriate for the system investigated here.

In addition, a simple on-chip PCR protocol was developed for amplification of bacterial genomic targets to be used in conjunction with the detection system. As described in stion 3.1, MRSA, as a urinary tract infection, was identified as an application which has been largely unaddressed to date. For this reason, a model system of *S. aureus* genomic DNA was used to permit detection of *S. aureus* and discrimination between MRSA and MSSA. The model was used to develop the

separation and detection system, with the ultimate intention to integrate this process to upstream sample processing and DNA extraction steps utilising the porous monolithic interfaces already described.

5.2 Materials and Methods

5.2.1 PCR reaction mix

PCR amplification was carried out using the PCR mastermix described in stion 2.5.1.1. All variations are described throughout the text where appropriate. As described in stion 1.1, the genome of MRSA contains the *mecA* gene, the product of which is responsible for the resistance of the organism to a variety of antibiotics. For this reason a primer pair (stion 2.5.3) was used for amplification of this gene (Martineau *et al*, 2000) yielding a product of 532 bp which is specific to MRSA. Thermal cycling parameters for amplification of the *mecA* gene sequence were as follows: Initial denaturation step of 95^{o}C for 180 s, denaturation, then followed by sequential 95 ^{o}C for 30 s, annealing at 55 ^{o}C for 30 s and extension, at 72 ^{o}C for 30 s for a total of 35 cycles and final extension step of 72 ^{o}C for 240 s. In addition, a primer pair (stion 2.5.3) was also selected to target a 107 bp sequence of the genome common to all *S. aureus* species (including both MRSA and MSSA). The amplified product was reported as 107 bp (Martineau *et al*, 2000). Thermal cycling parameters for amplification of this *S. aureus* sequence were as follows: An initial denaturation step of 95^{o}C for 180 s, then denaturation, 95 ^{o}C for 30 s, annealing at 60 ^{o}C for 30 s and extension at 72^{o}C for 30 s for a total of 35 cycles and a final extension step of 72 ^{o}C for 240 s. The two primer pairs were both used to describe various stages of development in this chapter.

5.2.2 PCR amplification on-chip

PCR was carried out using the chip device in Figure 5.1. The PCR mixture was injected in to the PCR chamber via the inlet port. Subsequently, all inlet/outlet ports were filled with mineral oil and sealed with optical adhesive tape and then epoxy resin.

In order to carry out amplification on the integrated chip device (see Figure 2.6), port A to PCR chamber was filled with PCR mixture. A 100 µm diameter hole in the top

layer of the PCR chamber allows the chamber to be filled without disturbance of neighbouring channels. All inlet and outlet ports were then covered with mineral oil and sealed with optical adhesive tape and then epoxy resin. The PCR chamber hole was also sealed with optical adhesive tape and epoxy resin. Using a Peltier heating element, the PCR chamber was then subjected to thermal cycling, as described in stion 2.5. Following this, the sealant was removed and all chambers were filled with cathodic buffer and carbon electrodes were inserted. The sample injection, separation and detection procedures were then performed as described (stion 2.8.2).

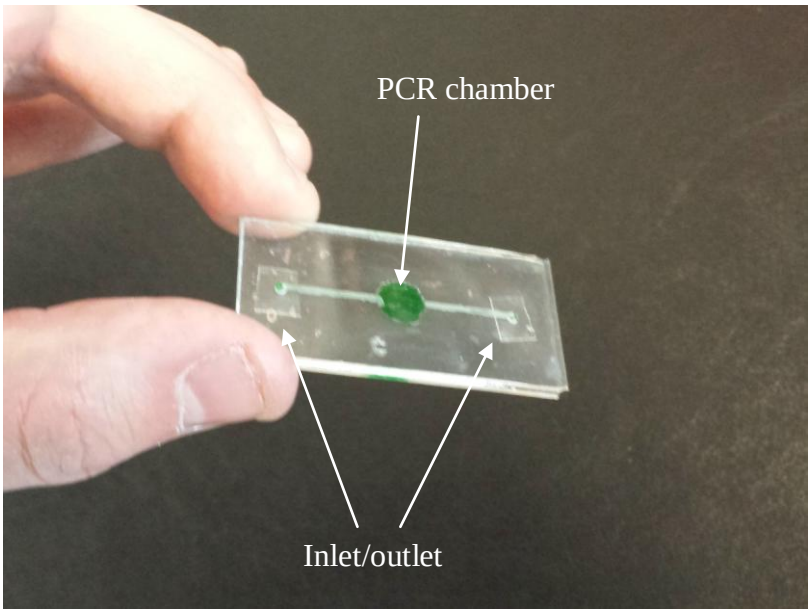

Figure 5.1: Microfluidic device for PCR.

Chamber and channels are 250 µm depth. The PCR amplification chamber comprises a volume of 12.5 µl. Inlet/outlet allow for injection and retrieval of sample. PCR chamber is highlighted here with green dye.

5.2.3 Detection on chip

For detection of PCR products using the IGA, the processes were carried out as described in stion 2.8.2. Sample volumes used for optimisation experiments were 2 µl pre-amplified PCR products in 50 µl cathodic buffer [Applied biosciences]. For size ladder experiments, 1 µl PCR products were used for all size markers plus 5 µl of target. All PCR products used were generated using PCR protocols described in stion 2.5.1.1 with ≈ 1 ng of template DNA. PCR products were fluorescently tagged by

incorporation of fluorescence labelled primers to permit detection. All further development of the IGA is described in the text.

5.3 Results and discussion

5.3.1 Conventional PCR amplification of *S. aureus* targets

This stion describes the work establishing a reliable and reproducible method for the amplification of *S. aureus* target sequences. Using the PCR mastermix described in stion 2.5.1.1, both *S. aureus* targets (*S. aureus* and *MecA)* generic were amplified using conventional bench top PCR amplification and detected by gel electrophoresis. Analysis by gel electrophoresis shows successfully amplified target sequences (Figure 5.2). Multiplex amplification of both targets was also achieved (Figure 5.3). The multiplex amplification demonstrated successful simultaneous amplification of both targets, however the amount of each product was lower than that of the single target amplifications, likely due to competition of the primer sets for MRSA genomic template of PCR reagents (see Figure 5.3, lane 3).

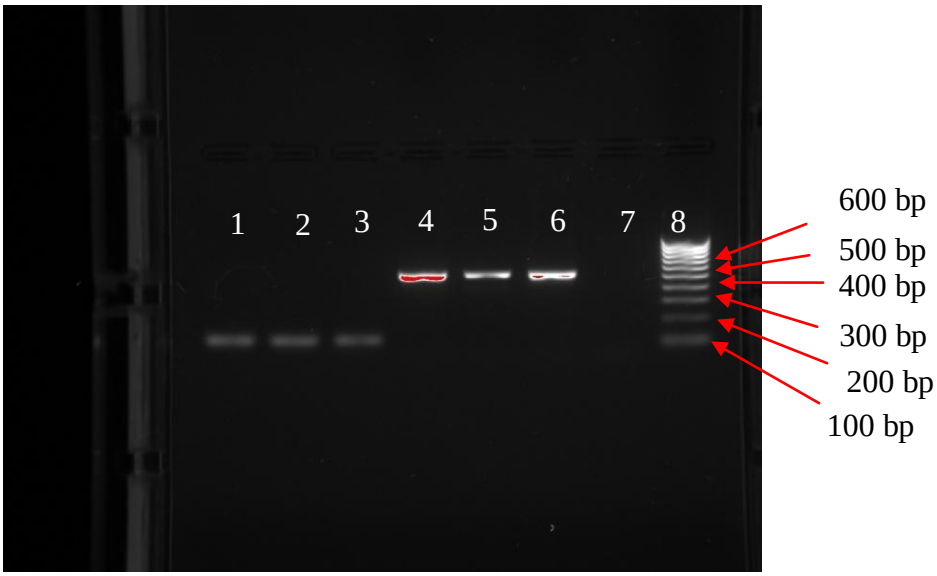

Figure 5.2: PCR amplified S. Aureus target DNA sequences

Image shows gel (2 % agarose) electrophoresis of amplified targets. Lane 1-3 shows products of 107 bp , approximately corresponding to expected length for *S. aureus* target sequence and lane 4-6 shows products of 532 bp, approximately corresponding to expected length for *mecA* target sequence. Seventh lane was a negative control and eighth was a hyp (IV) size ladder [Bioline, UK].

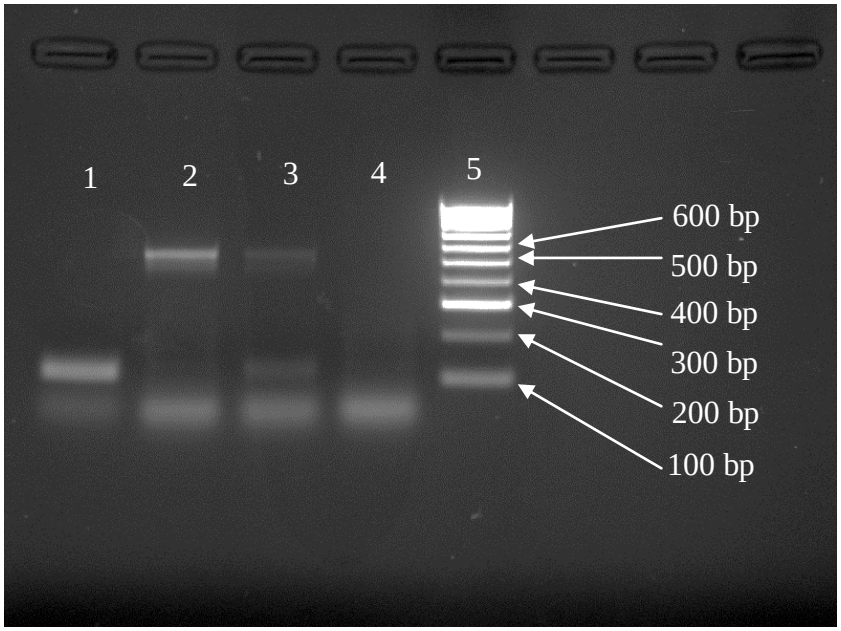

Figure 5.3: Multiplex PCR amplification of S. Aureus DNA sequences

Image shows PCR amplified *S. aureus* gel (2 % agarose) electrophoresis of amplified targets. Lane 1 shows product of 107 bp corresponding approximately to expected length for *S. aureus* target sequence and lane 2 shows product of 532 bp corresponding approximately to expected length for *mecA* target sequence. Lane 3 showed products of 107 bp and 532 bp corresponding to expected length for *S. aureus* target sequence and *mecA* target sequence. Fourth lane was a negative control and fifth was a hyp (IV) size ladder. N = 3.

The *mecA* primer pair (stion 2.5.1) were tested against a selection of genomic DNA targets of other sepsis-causing bacteria in order to demonstrate their specificity for MRSA. Using thermal cycling conditions described for amplification of the *mecA* target, amplification was carried out on purified genomic DNA from *Proteus mirabilis, E coli, Klebsiella pneumonia, methicillin susceptible S. aureus (MRSA)* and *Pseudomonas aeruginosa.*

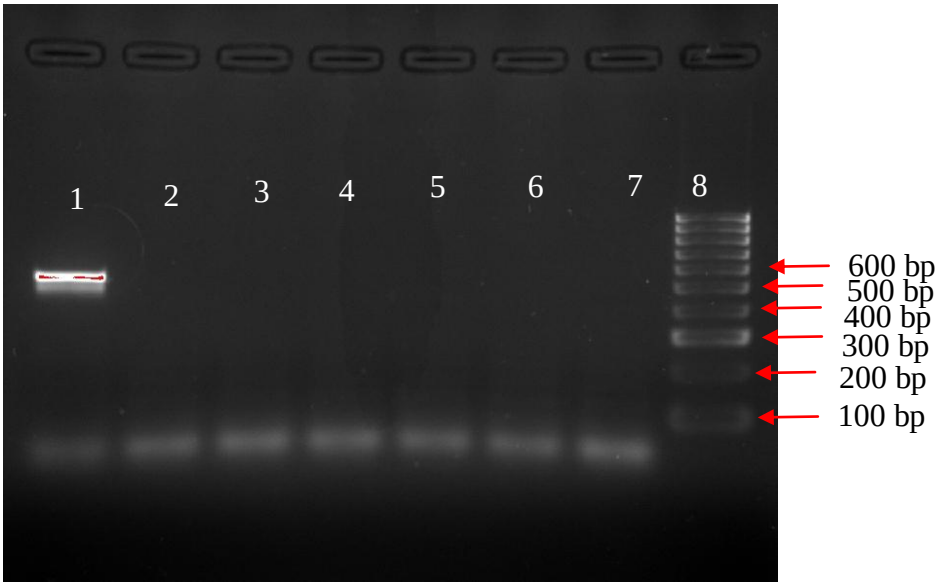

Figure 5.4: Validation of mecA primer pair specificity using gel electrophoresis

Gel (2 % agarose) to show the amplification of seven targets using *mecA* target primers. Lane 2 is *Proteus mirabilis,* Lane 3 is *E coli,* Lane 4 is *Klebsiella pneumonia,* Lane 5 is *methicillin susceptible S. aureus (MRSA)* and Lane 6 is *Pseudomonas aeruginosa* and Lane 7 is a negative control. The only target successfully amplified was that of MRSA.

In order to optimise PCR amplification conditions, further experiments were conducted whereby the primer concentration was reduced to establish whether the high concentration used previously was affecting amplification efficiency. Bands observed for 0.2 µM and 0.4 µM primer concentration were stronger than that of 0.6 µM and 0.8 µM suggesting stronger amplification had occurred. Consequently, all subsequent experimental work subsequently used 0.2 µM primer concentration of forward and reverse primers for PCR reactions.

Additionally, PCR optimisation experiments were conducted to identify the optimum concentration of $MgCl_2$. The initial $MgCl_2$ concentration of the PCR mastermix used was 3 mM. PCR reactions were setup containing $MgCl_2$ concentration of 3.2 mM, 3.4 mM, 3.8 mM, 4.2 mM and 4.6 mM and then PCR products were analysed by agarose gel electrophoresis (Figure 5.6). The result indicates that an increase in $MgCl_2$ concentration was not beneficial to the reaction. Therefore no additional $MgCl_2$ was added in subsequent experiments.

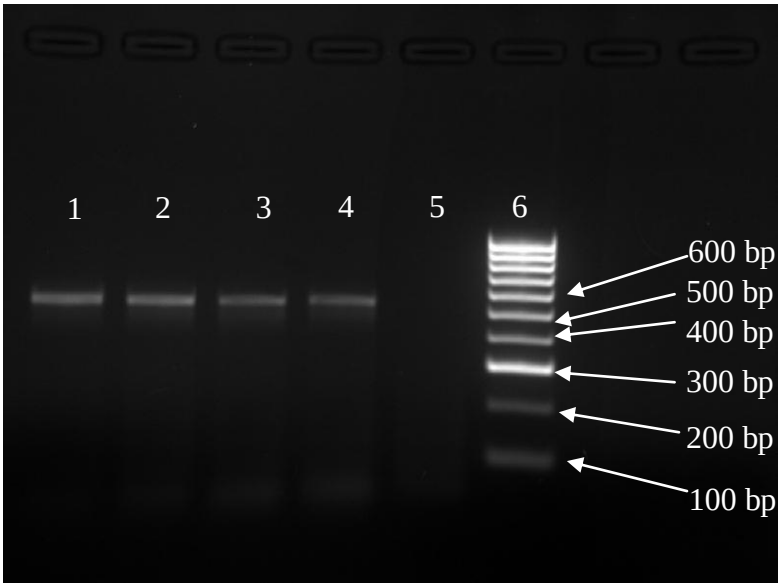

Figure 5.5: Gel showing the affect of primer concentration on PCR performance

Gel (2 % agarose) shows PCR products for varying primer concentration (µM). Lane 1, 0.2 µM, lane 2, 0.4 µM added, lane 3, 0.6 µM added, lane 4, 0.8 µM, lane 5 negative control. Lanes 1 and 2 shows a brighter band than that of 3 and 4, indicating that PCR product yield were higher using these conditions. N = 3

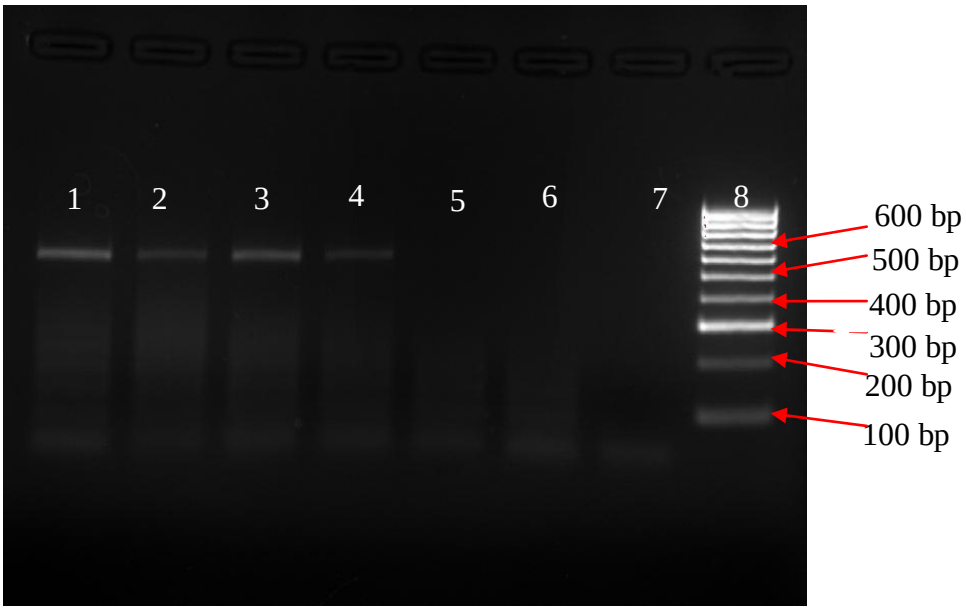

Figure 5.6: Gel showing the affect of MgCl2 concentration on PCR performance

Gel (2 % agarose) of PCR products of *mecA* gene with increasing $MgCl_2$ concentration. Lane 1, 3 mM, lane 2, 3.2 mM, lane 3, 3.4 mM, lane 4, 3.8, lane 5, 4.2 mM, lane 6, 4.6 mM and lane 7 is negative control. Bands show no increased PCR product yield from additional $MgCl_2$. N = 3.

5.3.2 PCR amplification on-chip

Having established a reliable and reproducible methodology for the amplification of MRSA-based targets using conventional bench top PCR, it was then attempted to develop this PCR method for amplification on a microfluidic chip-device. This was necessary to have a full integrated NAAT system. A schematic of the chip used is shown in Figure 5.1. The PCR reaction mixture used for the conventional bench top PCR procedure chip was transferred to the microfluidic device, using a reduced total volume of 12.5 µl. In addition, BSA was added to a concentration of 0.8 µg μl^{-1}, to avoid adsorption of PCR components to inner surfaces of the chip-device. PCR mixture (stion 2.5.1.1) with MRSA genomic DNA (≈ 5 ng) was injected in to the PCR chamber using a micropipette and inlet and outlet holes were first sealed with optical adhesive tape and then further sealed with epoxy resin to avoid evaporation of reagents from the chip-device during thermal cycling. It was predicted that there would be minor loss of heat transfer through the 1 ml thick chip, so samples were subjected to heating using modified thermal cycling conditions to take this into account: 3 minute initial denaturation step at 98 °C followed by 40 sonds denaturation at 98 °C, 40 sonds annealing at 55 °C and 40 sonds extension at 72 °C for 35 cycles, with a final extension step of 6 min at 60 °C. All of the temperatures were increased by 3^{o}C, based on previous work, regarding loss of heat on transfer (Shaw *et al*, 2011).

Products of the PCR amplification of the m*ecA* gene sequence on chip were analysed by gel electrophoresis (Figure 5.7). PCR amplification on-chip is shown to have performed as well as the PCR amplification using the conventional bench top PCR procedure. The simple chip-based system was therefore shown to be suitable for amplification using this approach and considered applicable for implementation to the integrated system.

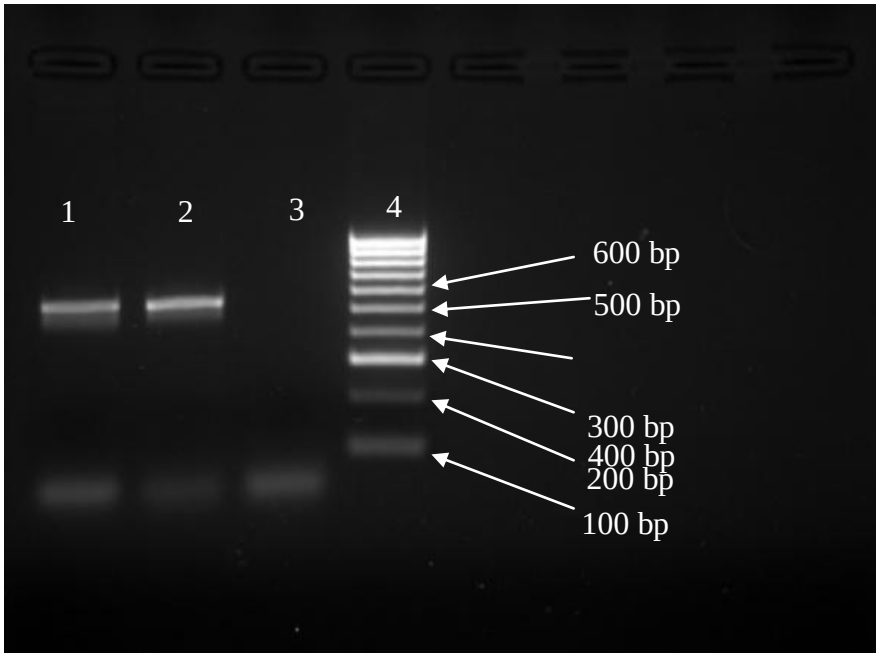

Figure 5.7: Detection of target amplified on-chip by gel electrophoresis

Gel (2 % agarose) showing PCR product of lane 1, amplified *mecA* gene (532 bp). lane 2 and 3 are positive and negative controls, respectively and lane 4 is hyp IV size ladder. N = 3.

5.3.3 Integrated genetic analyser

The targets discussed so far in this chapter were then used to develop and optimise the detection system provided by the IGA.

5.3.3.1 Alignment of laser

Before attempting detection of PCR products, it was necessary to ensure that the diode laser (488 nm) was correctly aligned to the CE channel over the detection zone (Figure 2.6). The laser was aligned using fluorescein to provide clear indication that fluorescent material could be seen by the detector. The fluoroscein was placed in the PCR sample chamber and 4000 V was applied between well B (-ve) and well C (+ve) causing the fluoroscein to migrate towards well C. Fluorescein was found to reach the detection window at ≈1500 s (Figure 5.8).

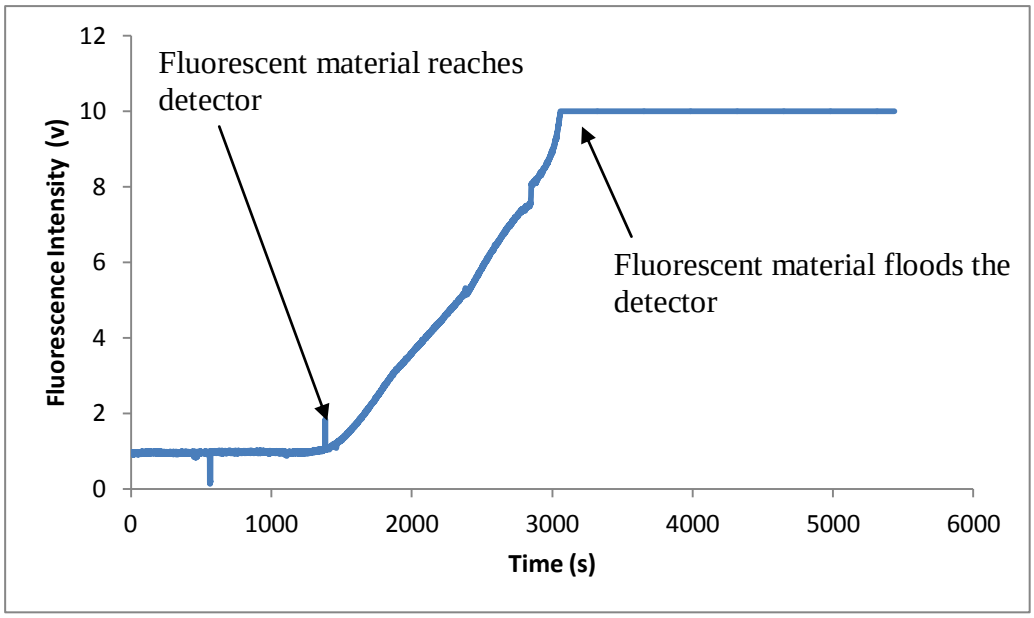

Figure 5.8: Detection of fluoroscein using IGA.

Shows an electropherogram obtained by moving fluorescein through the channel using the IGA. The fluorescein reached the detector at ≈ 1500 s showing the laser was correctly aligned. Sufficient fluorescein was used to saturate the channel and detector. In addition the graph demonstrates how the detector reaches it's maximum at 10 V. At this stage the system is flooded with fluorescein and plateaus.

5.3.3.2 Effect of bubbles of fluorescence detection

During these experiments it was observed that bubbles would emerge within the channels on the chip, possibly due to joule heating or bubbles introduced in the sample chambers and electrode ports. While the bubbles would generally occur at a stage in the experiment after the expected detection time for target DNA, it was important to characterise the effects of the presence of a bubble in the system, when seen by the detector. This would eliminate the possibility of bubbles being mistaken for fluorescent material. The plots shown in Figure 5.9a and b are examples of anomalies caused by bubbles observed during experiments. Both show a reduction in the measured fluorescence intensity of ≈ 0.15 V. On observation of these changes in the fluorescence output, the channel within the chip-device was viewed by eye. The presence of a bubble located by the detection window was consistent with this observation.

a)

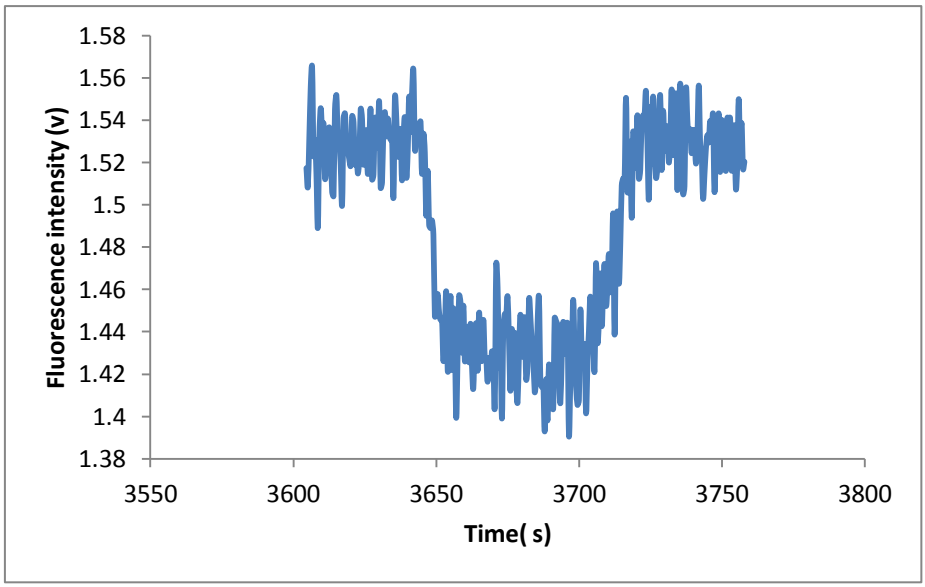

b)

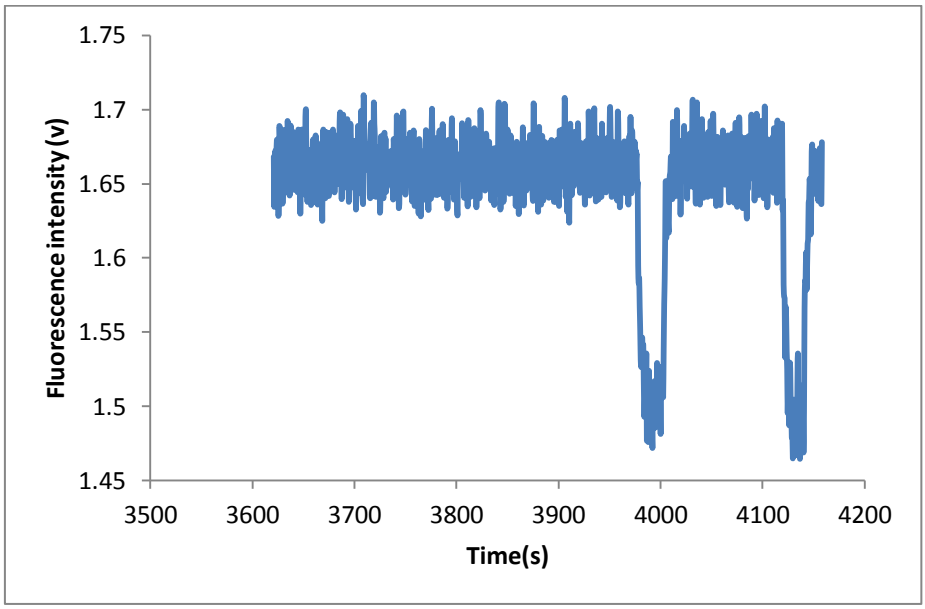

Figure 5.9: Effect of bubbles on fluorescence using the IGA.

Both a) and b) are electropherograms obtained from the IGA, which illustrate bubbles passing the detector. In the event that a bubble passes the detector a reduction of ≈ 0.15 V is observed until the bubble has passed.

5.3.3.3 PCR product detection on-chip

S. aureus and *mecA* amplicons, which had been previously amplified off-chip (stion 2.5.1) were used to further develop the detection procedure using the IGA. Analysis of the fluorescently labelled PCR products generated using conventional bench top techniques were analysed by conventional instrument [Applied Bioscience, UK]

revealing peaks corresponding to products of the expected sizes of 107 bp (*S. aureus*) and 532 bp (*mecA)* (Figure 5.10). Additionally, electropherograms of both samples, showed fluorescent matter was present in the size region of ≈ 0- 60 bp, which can be attributed to incorporated primers or primer dimers (Sambrook, 2001). The two electropherograms were used as references in order to compare data obtained from the IGA during the development of the detection system.

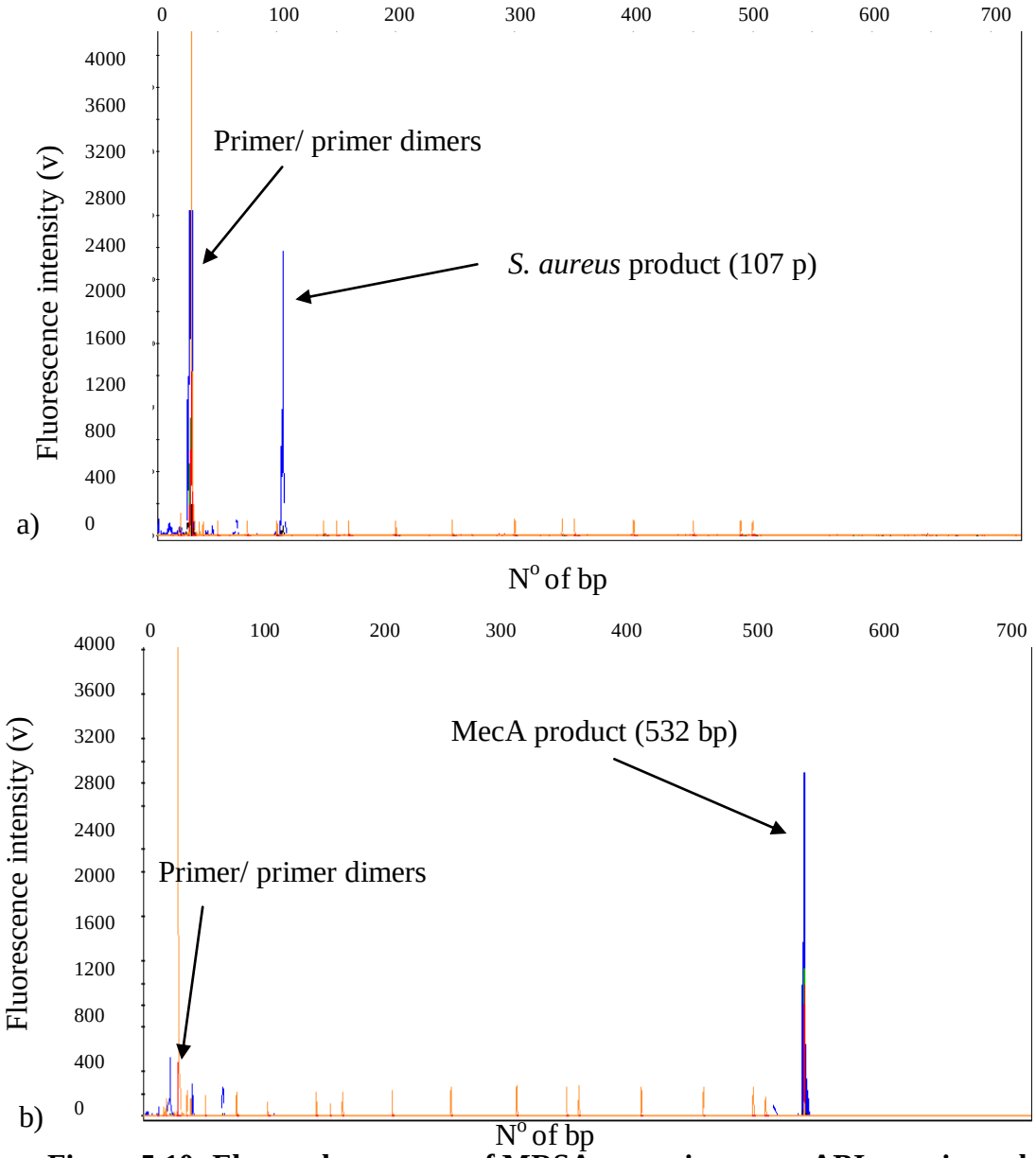

Figure 5.10: Electropherograms of MRSA genomic targets ABI genetic analyser.

Electropherograms obtained on the ABI genetic analyser [Applied biosciences] a) *S. aureus* amplicon (107 bp) and b) *mecA* amplicons (532 bp). Both electropherograms shows incorporated primers/ primer dimers in the size region between 0 and 60 bp.

5.3.3.3.1 Detection of *S. aureus* PCR product using IGA

Following this, to demonstrate the IGA was used to detect the MRSA-based target to demonstrate the potential for use in NAAT. Speed, resolution and reproducibility were consider in detail during this preliminary developmental stage. Based on the electropherograms of PCR products obtained from amplification of *S. aureus* and *mecA* sequences (Figure 5.10), it was expected that a fluorescent signal should be detected corresponding to both the primers/ primer dimers and the amplified target product. Following, sample input in to the sample chamber (2 µl pre-amplified *S. aureus* PCR products in 50 µl cathodic buffer), preliminary experiments were conducted using a simplified injection process in which 4000 V were applied between electrodes B(-ve) and C(+ve) for 6 min, followed immediately by 7000 V between electrodes A(-ve) and C(+ve) (see stion 2.8.2). Figure 5.11 shows an electropherogram generated during this process.

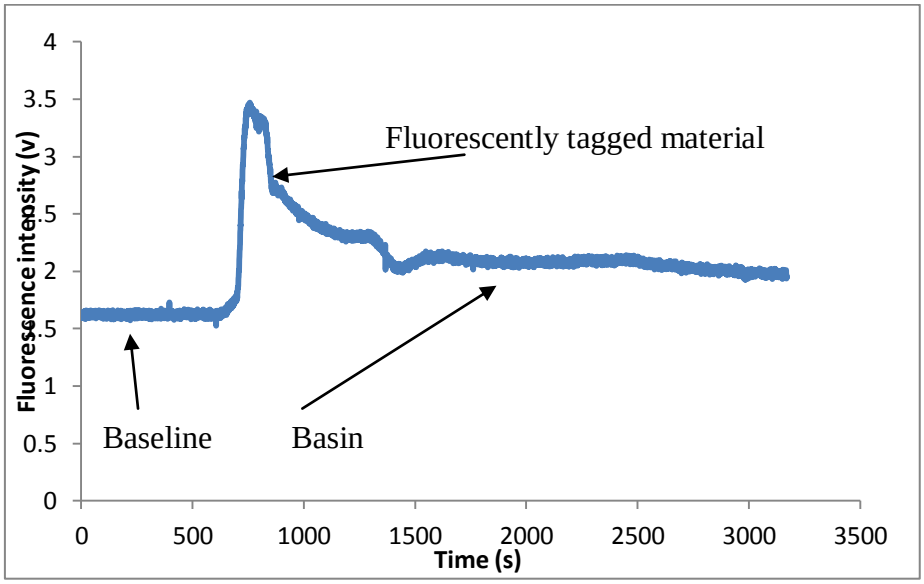

Figure 5.11: Detection of S. aureus PCR products (107 bp) when not using a pull back step

Electropherogram obtained on the IGA of *S. aureus* PCR reaction products. The signal observed demonstrates a sharp increase at ≈ 800 s and long tailing until 3000 + s. Tailing shows strong evidence of sample bleed from the sample chamber.

The electropherogram shows a baseline of ≈ 1.6 V. A strong increase in fluorescent signal is observed at ≈ 800 s followed by the peak tailing which basins at ≈ 0.5 V above the initial baseline. The nature of this peak tailing implies that material is

bleeding in into the separation channel from the sample chamber following the surge from the initial volume injected.

Following these initial experiments, an intermediate step was introduced in which the sample was eliminated from the sample chamber in order to isolate the plug within the channel and eradicate sample bleed from the chamber. As described in stion 2.8.2, this was achieved by applying a voltage (1000 V) for 10 min between electrodes A(ve-) and B(ve+) following initial injection step. Figure 5.12a shows electropherogram obtained when injecting the sample in this way for 3 min. A peak of fluorescence signal was observed at ≈ 800 s followed by tailing, however, the signal returned to the initial baseline, implying that material was no longer bleeding from the sample chamber. Following this the experiments were repeated, but with heating of the sample at 94ºC for 4 min in 50 µl formamide prior to loading, in order to denature and preserve the DNA sample in single strand form. It is reported that single stranded DNA provides better resolution than that of double stranded when separated using electrophoretic techniques (Sambrook, 2001). The electropherogram obtained is shown in figure 5.12b. The results observed showed a peak of fluorescence intensity at 800 s revealed a more complex profile, however it is not resolved in to two distinct signals.

a)

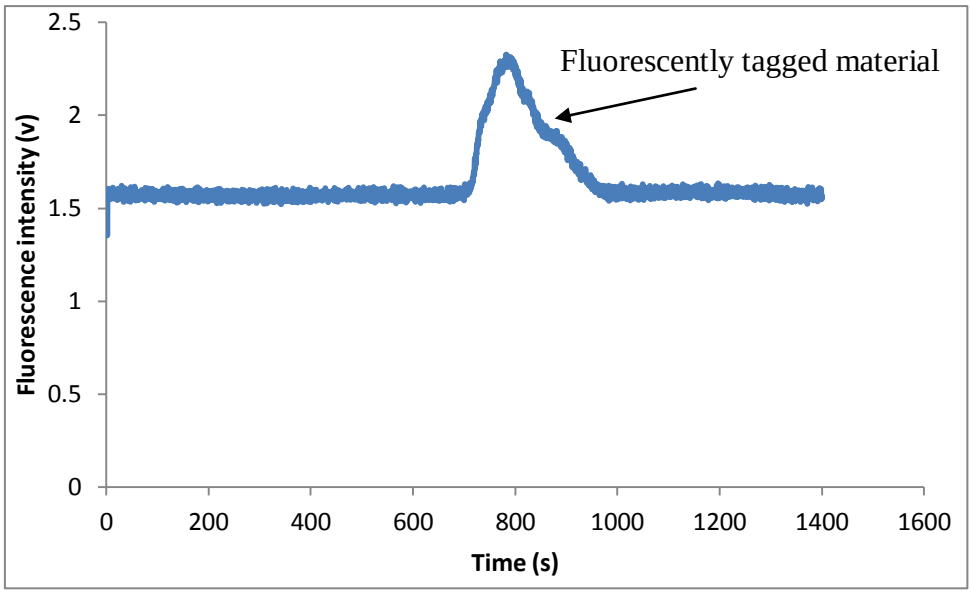

b)

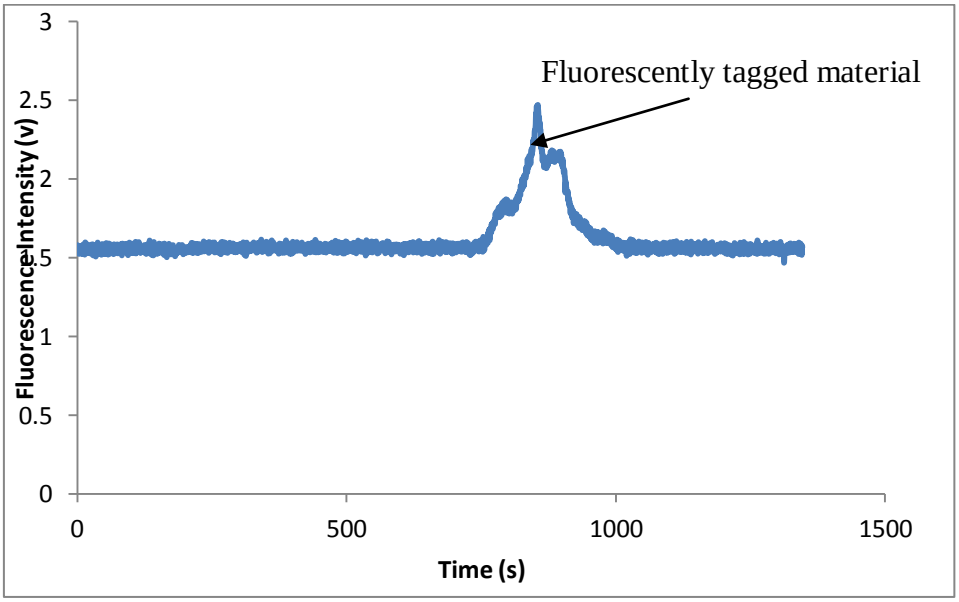

Figure 5.12: Detection of S. aureus PCR products by IGA when using pull back step.

Detection of *S. aureus* amplicons with a) double stranded DNA and b) single stranded DNA. The single stranded PCR products showed three distinct features within the peak, however, they were not resolved as individual peaks.

The length of the sample injection period was then further decreased to 90 s in an attempt to reduce the size of the plug. Using these conditions, an increased fluorescence signal was observed at 467 s and continued until 627 s. Significantly, two distinct peaks were observed, as would be expected for detection of the unincorporated primers and PCR products.

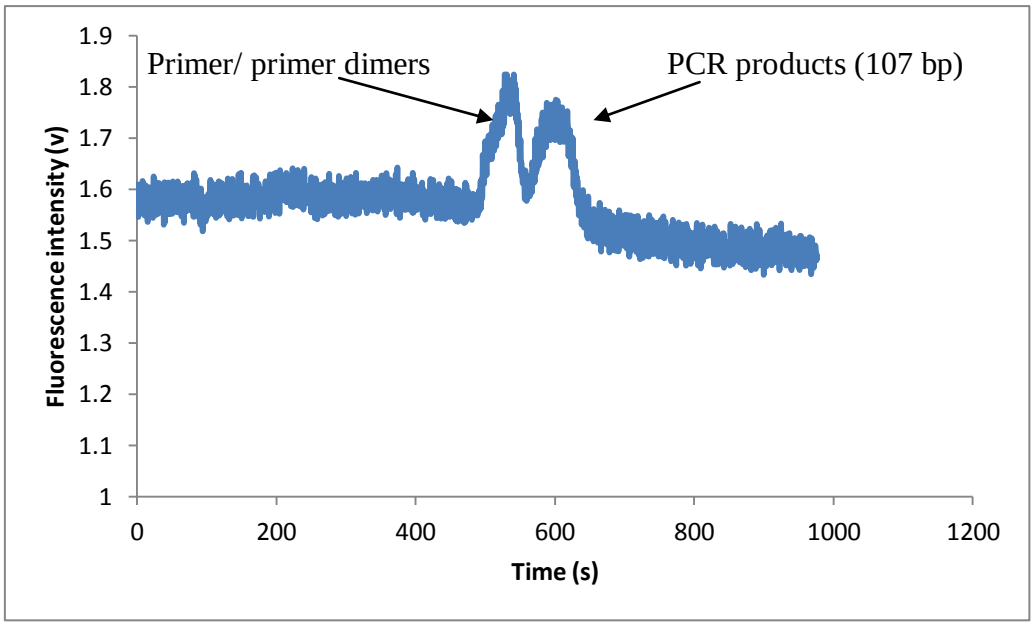

Figure 5.13: Detection of S. aureus PCR products (107 bp) using reduced injection timescale

Electropherogram obtained on the IGA for *S. aureus* PCR products using a 90 sond injection. Two distinct peaks are observed at 551 s and 581 s (Rs = 0.73).

Resolution of multiple peaks can be quantified mathematically (Equation 12). The value obtained or "resolution factor" is indicative of the level of separation and degree of certainty when identifying multiple components. The general value regarded as sufficient separation to identify to clearly defined peaks is > 2, however, the equation was used here to demonstrate the influence of parameters on the resolution of both primer / primer dimmers and target amplicon peak. Analysis of *S. aureus* PCR products at injection timescales of 360 s and 180 s provided only one peak, implying lack of separation. However, when injecting for 90 s, the resolution factor was found to be 0.73. This is below the threshold of 2, due to the minimal overlap present, meaning the peaks can be regarded as separate. Data is shown in Table 11.

For characterising the influence of parameters on positioning and resolution of target peaks the resolution equation was implemented, as described in Snyder *et al*, 1997.

Equation 12: Resolution factor

$$R_s = \frac{t_2 - t_1}{1.7\ x\ 0.5w_1 + 0.5w_2}$$

Where R_s is Resolution factor,

t_1 and t_2 are peak heights,

w_1 and w_2 are peak widths.

Table 11: Peak resolution of S. aureus PCR product using IGA

Shows the times in which an increase in fluorescent signal was observed when using different plug injection times. In addition, when injecting for 90 sonds two peaks were observed, in agreements with the primer area and PCR product (107 bp) . N = 3 for 90 s separation and N = 1 for all other separation timescales.

Plug injection time (s)	First peak observed (s)	Sond Peak observed (s)	Resolution factor	Separation achieved
360	860	-	-	No
180	845	-	-	No
90	508	572	0.73	Yes

5.3.3.3.2 Detection of *mecA* PCR product using IGA

Analysis of the *mecA* PCR products using the IGA was carried out following a similar approach to that in stion 5.3.6.3.1 for analysis of *S. aureus* PCR products. It was postulated that a longer injection time may be required to achieve optimal separation and detection of the *mecA* product, due to the expected increased migration time of this significantly larger product (532 bp). For this reason the initial injection time used in these experiments was 8 min. Using this injection time, two distinct peaks were observed with some overlap evident (Figure 5.14). While there is some overlap observed at ≈ 1200 s, there are undoubtedly two distinct fluorescence signal peaks, occurring at ≈ 900 s and ≈ 1300 s. The improved separation using this increased injection timescale is likely due to the larger amplicon size of the *mecA* product. The peak width observed was also very large, with the detected primer region spanning over ≈ 500 s. The resolution factor of the peaks observed was calculated as 1.93. As

with the *S. aureus* target, the process was then repeated, but the injection time was reduced to shorten the plug injection.

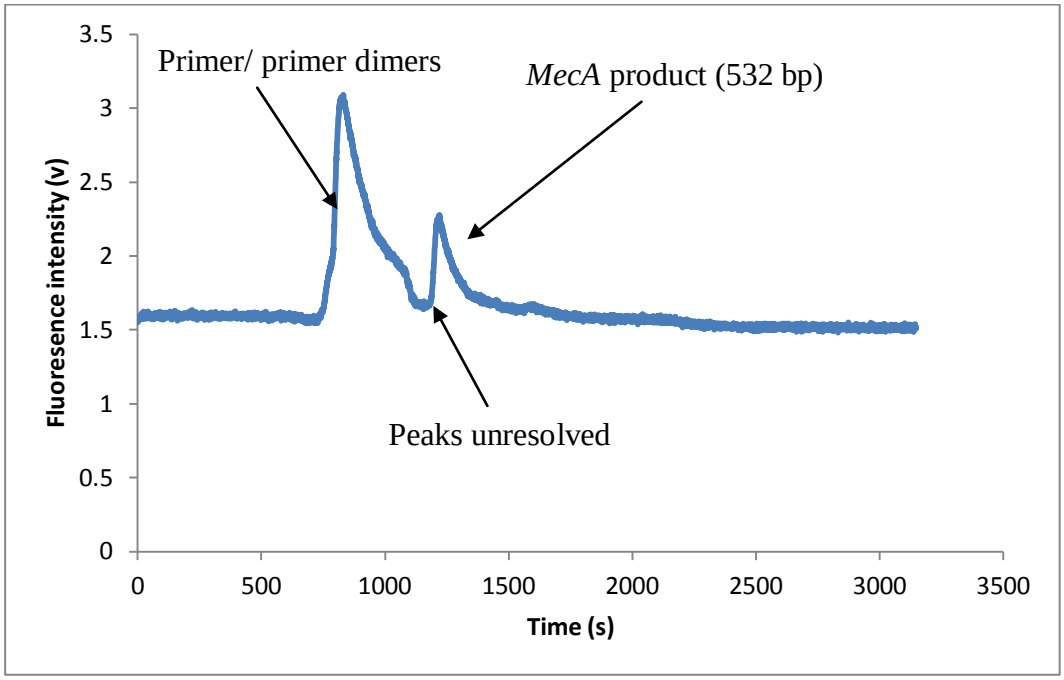

Figure 5.14: Detection of mecA PCR products using a 480 s injection

Electropherogram obtained on the IGA for *mecA* PCR products using a 480 sond injection. A peak is observed at ≈ 900 s, followed by a sond peak at 1300 s. The two peaks are slightly unresolved as signal does not fully return to the baseline. (Rs =1.93).

Further experiments were performed in which the injection time was reduced to 180 s, 90 s, 45 s or 30 s. When injected for 180 s there was still minimal overlap at ≈ 900 s (Figure 5.15), with a calculated resolution factor was 1.96. When the injection time was reduced to 90 s the overlap between peaks was eliminated with two clearly resolved peaks at ≈ 550 s and ≈ 950 s, giving a resolution factor of 2.52 (Figure 5.17). Further reduction of injection time to 45 s and then 30 s provided increased separation of the peaks (Figure 5.16 and 5.17). Resolution factors were 4.60 and 5.82, respectively. The gradual increase in resolution factor is indicative that the smaller plug provided by the decreased injection time provides a greater degree of separation. This data is summarised in Table 12. The total separation time was ≈ 25 min which is comparable to that of similar systems using DNA targets of a similar length (Easley *et al*, 2006; Oakley *et al*, 2009; Manage *et al*, 2010).

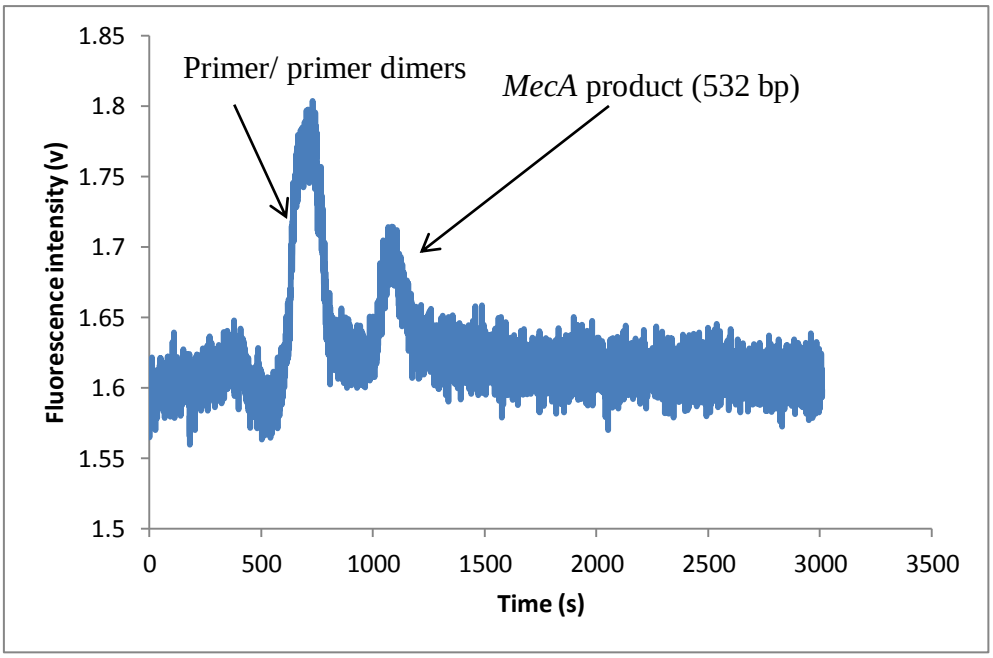

Figure 5.15: Detection of mecA PCR products using a 180 s injection

Electropherogram obtained on the IGA for *mecA* PCR products at 180 sond injection. A peak was observed at ≈ 700 s and a sond peak was observed at ≈ 1100 s. The two peaks overlapped at ≈ 900 s (Rs = 1.96).

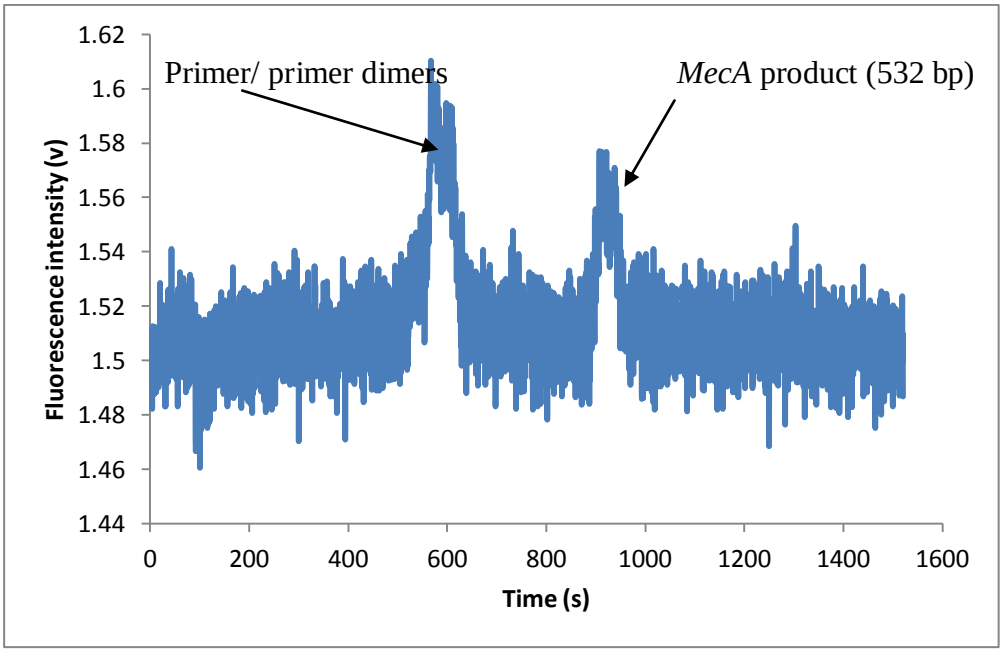

Figure 5.16: Detection of mecA PCR products using a 90 s injection

Electropherogram obtained on the IGA for *mecA* PCR products at 90 sond injection. A peak was observed at ≈ 590 s and a sond peak was observed at ≈ 900 s. There was no overlap of peaks observed (Rs = 2.52).

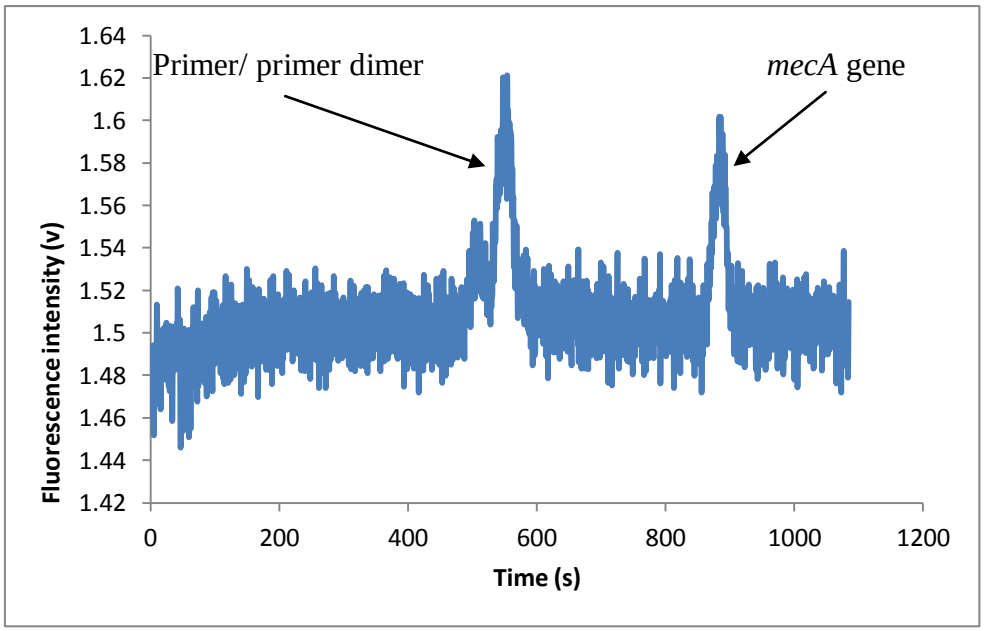

Figure 5.17: Detection of mecA PCR products using a 45 s injection time

Electropherogram obtained on the IGA for *mecA* PCR products at 45 sond injection. A peak was observed at ≈ 570 s and a sond peak was observed at ≈ 900 s. There was no overlap of peaks observed (Rs = 4.60).

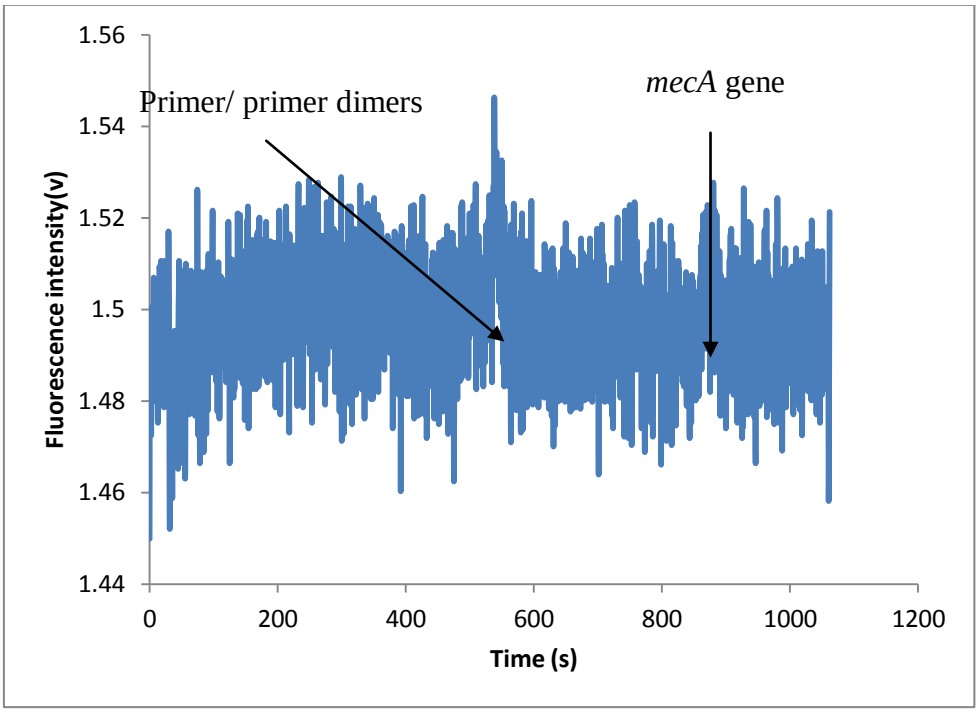

Figure 5.18: Detection of mecA PCR products using a 30 s injection time

Electropherogram obtained on the IGA for *mecA* PCR products at 30 sond injection. A peak was observed at ≈ 550 s and a sond peak was observed at ≈ 900 s. There was no overlap of peaks observed (Rs = 5.82). N = 3

Table 12: Peak resolution of mecA PCR product using IGA

Shows the timescale in which peaks were observed for electrophoretic detection of amplified *mecA* gene. N = 3 for 30 s separation, N = 1 for other separation timescales.

Separation timescale(s)	First peak observed (s)	Sond Peak observed (s)	Resolution factor	Separation achieved
480	810	1226	1.93	No
180	643	1072	1.96	No
90	571	927	2.52	Yes
45	560	873	4.60	Yes
30	543	860	5.82	Yes

Due to the smaller plug of DNA generated, the peak heights observed for the shortest injection times were significantly reduced. To overcome this issue, this was addressed by increasing the strength of the laser used from 1 mV to 3 mV, in an attempt to increase the signal response. Figure 5.19 shows an electropherogram obtained from analysis of *mecA* sequence PCR products when using a 30 sond injection time with laser strength of 3 mV. The electropherogram shows an increase of base line from ≈ 1.6 V to ≈ 4.25 V when compared to those observed using 1 mV (Figure 5.18). The peaks representing the primer/ primer dimers and *mecA* product corresponded to that of the electropherogram presented in Figure 5.19.

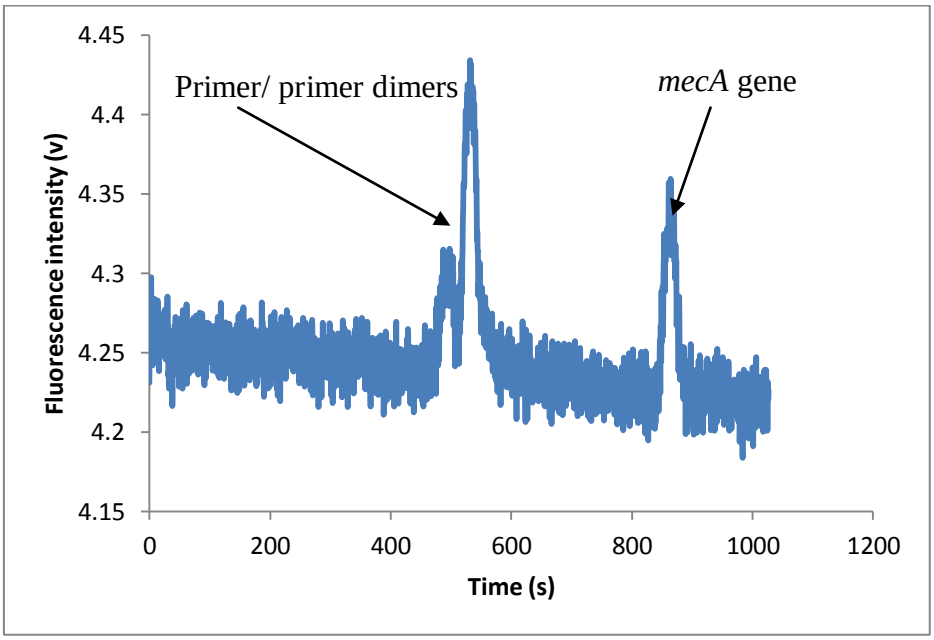

Figure 5.19: Detection of mecA amplicon using 3 mV laser strength Electropherogram obtained on the IGA for *mecA* PCR products at 30 sond injection with laser 3 mV. A peak was observed at ≈ 550 s and a sond peak was observed at ≈ 880 s. The baseline was ≈ 4.25 V.

Peaks were, however, of an increased height due to increased laser strength. When repeated with laser strength of 6 mV, the base line was increased to 8.10 V (Figure 20a). A combined electropherogram comparing fluorescence signal profiles obtained using laser strengths at 1, 3, and 6 mV are shown in Figure 5.20a and b, respectively.

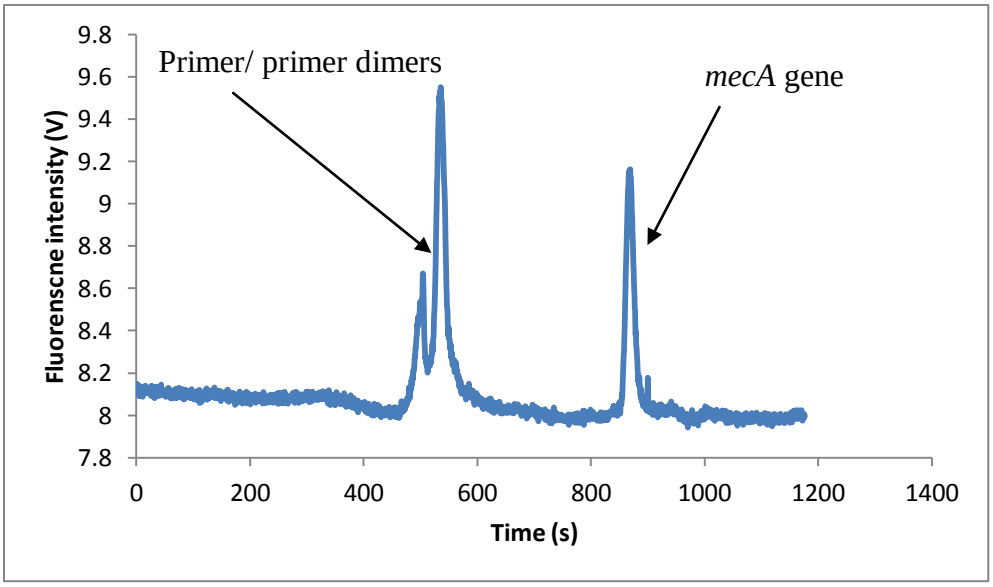

a)

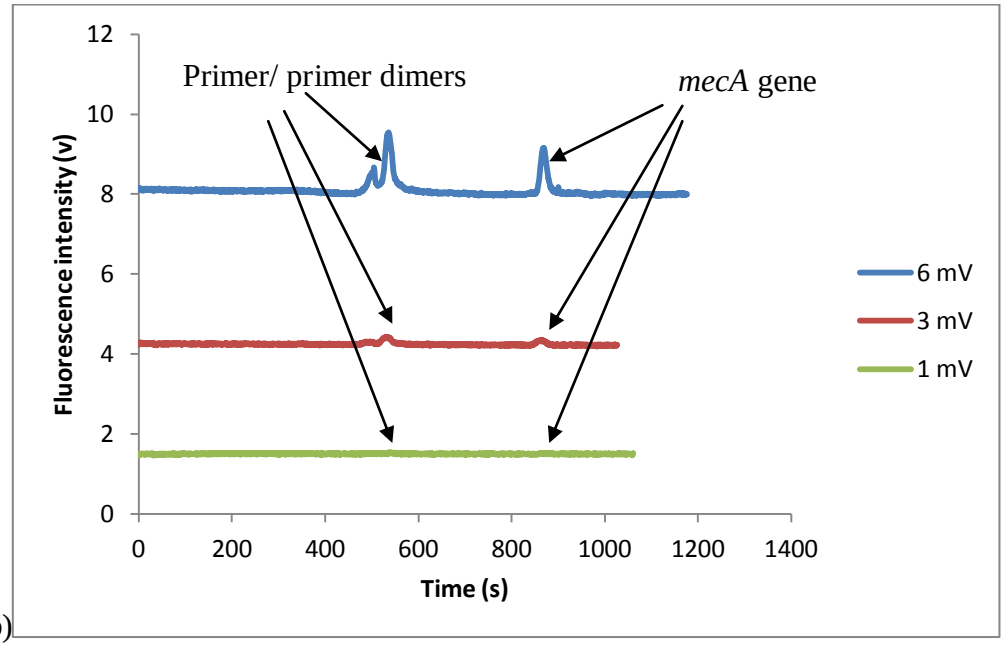

b)

Figure 5.20: Influence of laser strength on detected fluorescence signal.

Electropherograms obtained on the IGA for (a) *mecA* PCR products at 30 sond at 6 mV and (b) a composite electropherogram comparing fluorescence signal profiles obtained using laser at 1, 3 and 6 mV. The electropherogram generated using 6 mV laser strength produced a baseline of 8.10 V, compared with 1.70 V and 4.25 V for experiments obtained using 1 mV and 3 mV laser strength respectively.

5.3.3.4 Optimisation of CE separation voltage

A series of experiments was performed, whereby the separation voltage was reduced in order to assess the influence on the mobility of the DNA fragments. Figure 5.21 shows electropherograms for separation voltages at 7000 V, 5000 V and 3000 V. Reduction in the separation voltage used for CE revealed an increase in the time taken for targets to reach the IGA detection window. In addition, the time between observed peaks corresponding to primer and target amplicon increased as voltage is reduced. Detection times are shown in Table 13 and Figure 5.22 illustrating how the peaks become more spread apart with decreasing voltage. The result shows the potential for increasing resolution by decreasing voltage applied, however, this benefit is at a cost of an increased sample processing time.

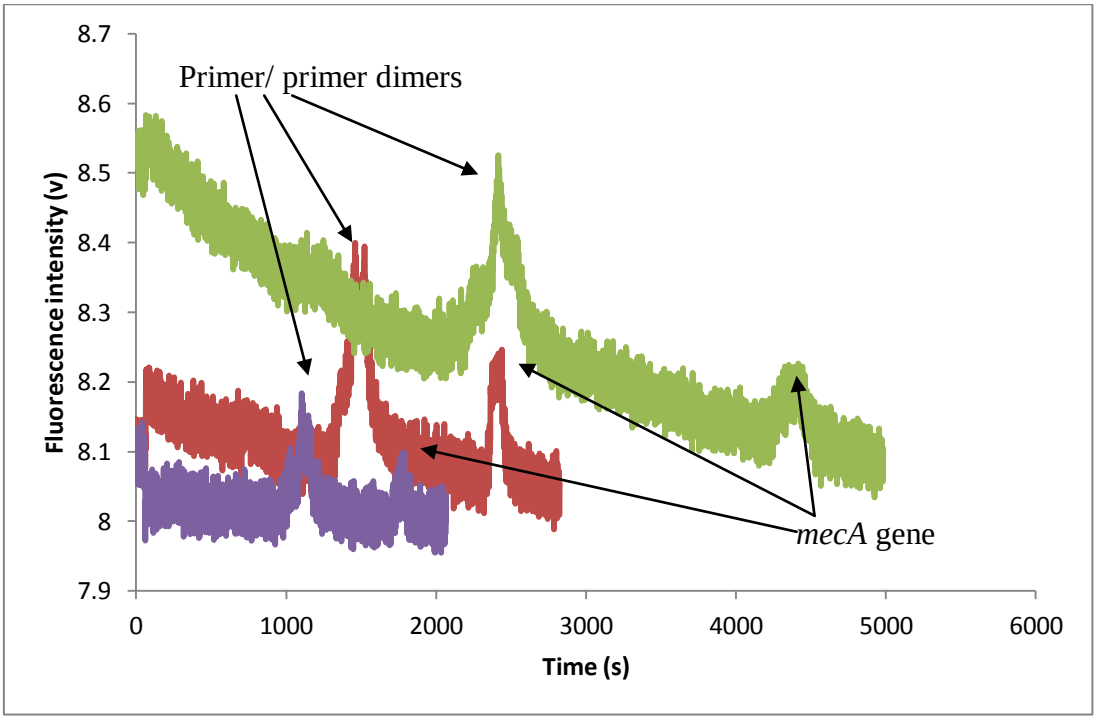

Figure 5.21: Influence of voltage on separation of DNA fragments.

Electropherograms obtained on the IGA for analysis of *mecA* PCR products (107 bp) using 30 sond injection at separation voltages of 3000 (green), 5000 (red) and 7000 (purple) V.

Table 13: Influence of voltage on separation of DNA fragments.

Shows the timescale in which peaks were observed for electrophoretic detection of amplified *mecA* gene PCR products when varying the separation voltage.

Separation voltage (v)	Peak observed (primer/ primer dimer) (s)	Peak observed (*mecA* PCR products) (s)	Time between peaks (s)	Total time (m)
3000	1195	2144	949	46
5000	721	1187	466	30
7000	540	857	317	25

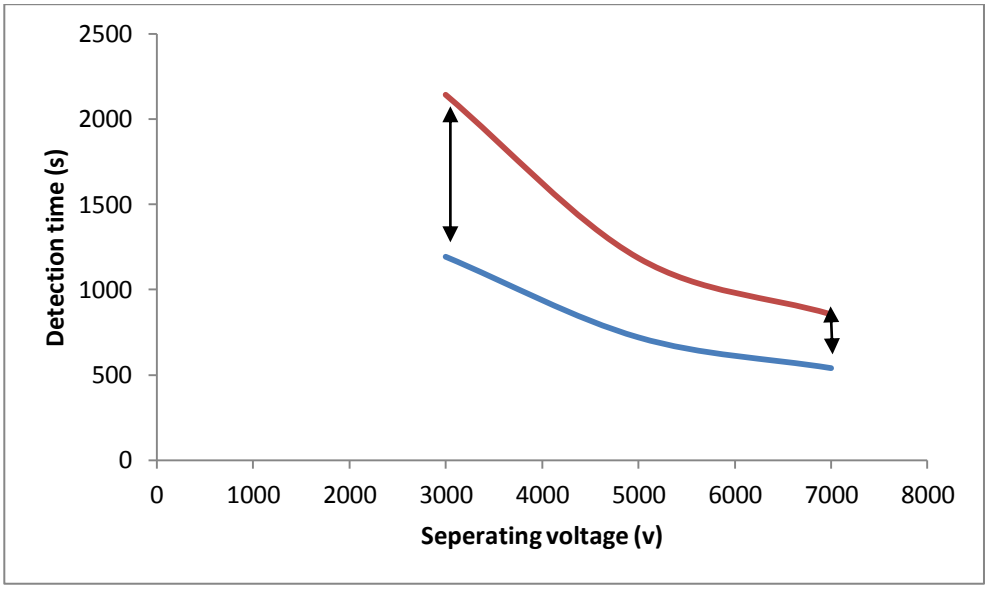

Figure 5.22: Relationship between separation voltage and separation time

Graph showing the influence of separation voltage on separation of DNA fragments. When separating at 3000 V peaks are ≈ 1000 s apart, while at 7000 V are ≈ 300 s apart. Red denotes mecA target and blue denotes primer/ primer dimers.

Based on optimum conditions (7000 V separation time, laser strength 8 mV), the IGA provided resolution comparable with highly regarded work of Wooley *et al* (1994) and Easley *et al* (2006). The IGA detection system demonstrated here does, however, provide the user with the additional benefits of the lid-based power supplies, which allow for space and easy access for further development. The IGA operating system also has the built in Peltier element on which the chip-device can be placed. Finally the touch screen control panel, provides the user with simple control and monitoring of operations.

5.3.3.5 Development of a size reference ladder for IGA

In order to permit calibration of the genetic analyser, a series of experiments were performed to evaluate the capability of the IGA to resolve multiple products using a custom-designed DNA size ladder. This would allow the size of DNA fragments to be defined by comparison to markers of relevant size, while also providing as an internal standard eradicating any potential variation in separation due to conditions, such as ambient temperature. To generate a custom-designed ladder, four primer pairs were designed to produce amplicons of 100, 200, 300 and 400 bp, when amplified from λ-phage DNA template (obtained from a Quant-IT Picogreen® dsDNA Assay kit). Primer sequences are detailed in stion 2.5.3. PCR amplification was carried out as described in stion 2.5.1, with denaturation, annealing and extension temperatures of 95, 66 and 72 ^{o}C, respectively. Figure 5.23 shows the four size markers amplified as a multiplex and analysed by conventional CE [Genetic analyser, Applied biosciences, UK]. The electopherogram reveals each marker has been successfully amplified with some background present. The resolution of size markers was considered sufficient for use in validation of the IGA detection system.

The amplified size markers were then subjected to electrophoretic separation and detection using the IGA detection system. The electropherogram is shown in Figure 5.24a. The electropherogram shows a series of peaks corresponding to the size ladder markers. While three markers are clearly defined, there was a region of high fluorescence intensity ranging between 600 and 700 s. It was postulated that the peak corresponding to the unincorporated primers was not completely resolved from the 100 bp marker giving overlapping peaks for primers and 100 bp marker, although this was not verified experimentally. This issue could, however, possibly be ameliorated by a pre-cleanup step to remove smaller fragments, such as primers and primer dimers.

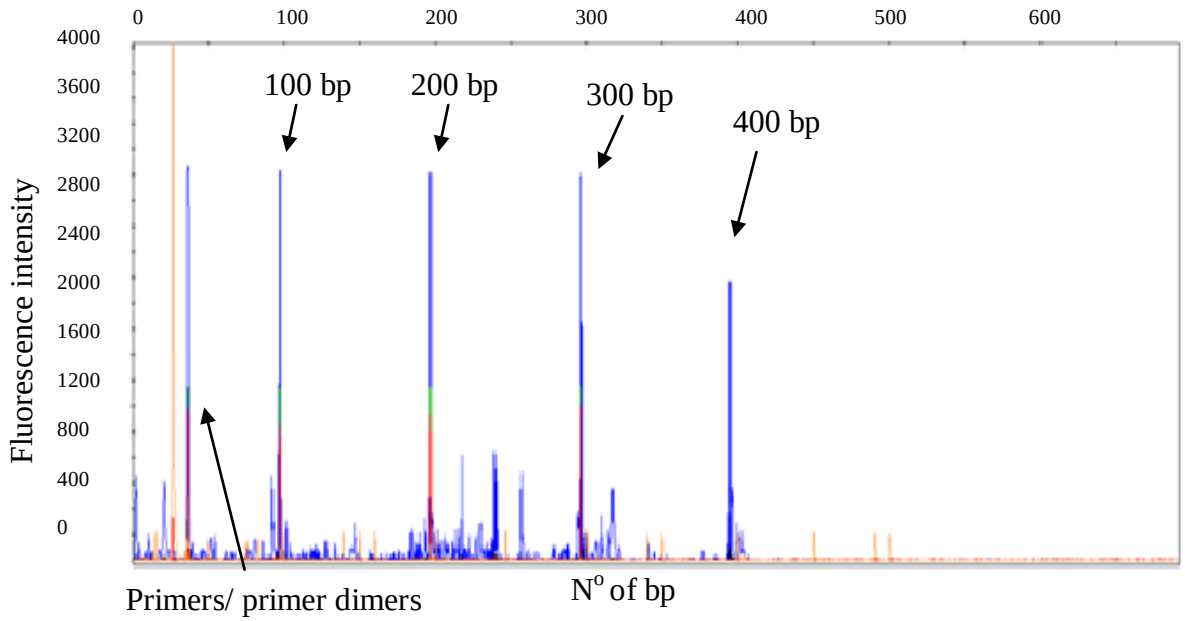

Figure 5.23: Electropherogram of size ladder reference markers

Electropherogram of a custom designed size ladder developed for use on the genetic analyser. Peaks correspond to 100 bp, 200 bp, 300 bp and 400 bp, products amplified in a multiplex PCR reaction. Note, primer dimers and unincorporated primers can be seen in the size region of 0-60 bp.

The four peaks were calibrated in order to evaluate the linearity of the size ladder points giving an R^2 of 0.9984. This is shown in Figure 5.24b. For separation of DNA molecules on a gel matrix there is a linear relationship between distance of migration of DNA and the logarithm of DNA length, causing larger fragments to require increasing migration timescales. However, the total migration timescale of the size ladder presented here is small enough that this relationship is not observed and the ladder is linear.

A further CE separation and detection was then performed on-chip using the IGA with the size marker ladder in addition to the *mecA* gene product. The electropherogram (Figure 5.25) shows the identical series of peaks with additional peak corresponding to the *mecA* target of 532 bp. These experiments were subsequently repeated at laser strength 6 mV. Figure 5.26a show the electropherograms for the four size markers and Figure 5.26b shows the same with the amplified *mecA* gene included.

a)

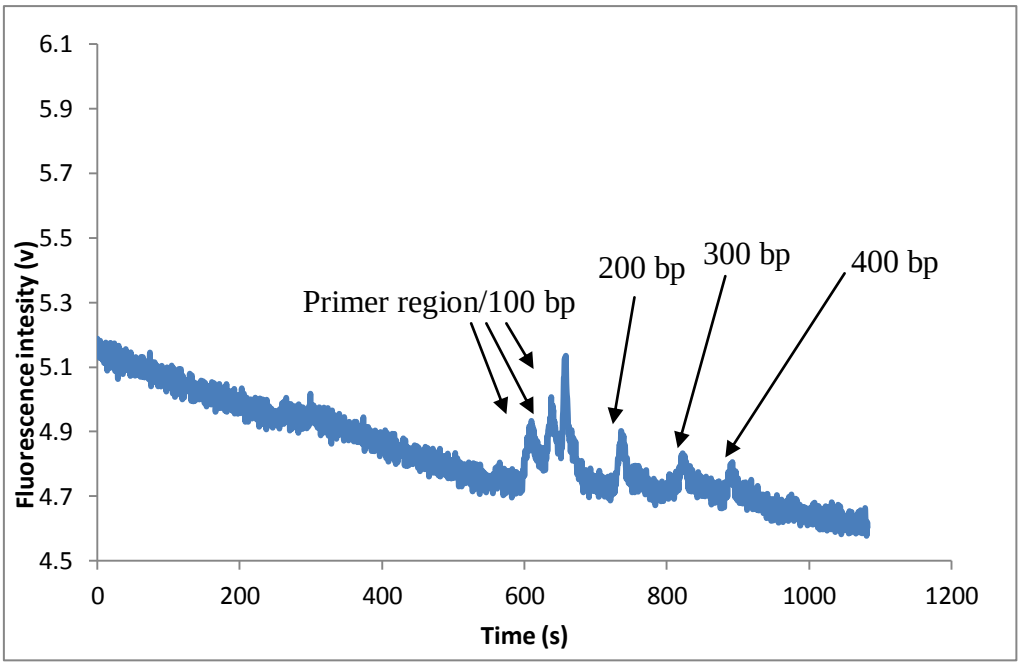

b)

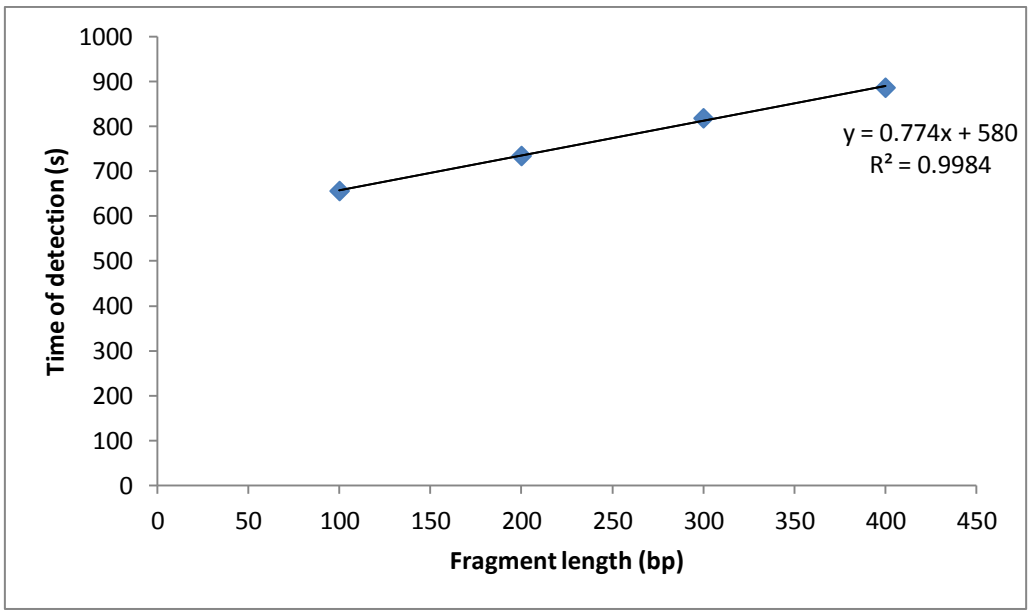

Figure 5.24: Separation of size ladder markers using the IGA

a) Electropherogram obtained on the IGA for size ladder products. Laser strength used was 6 mV. The electropherogram shows four distinct increases in fluorescence at 675, 750, 825, 900 and a region of fluorescence increase between 600 and 700. N = 3 b) The four points plotted as a graph, time of signal (s) against length of fragment (bp). The graph has an R^2 value of 0.9984, indicating a linear trend for the peaks in relation to the length of fragments.

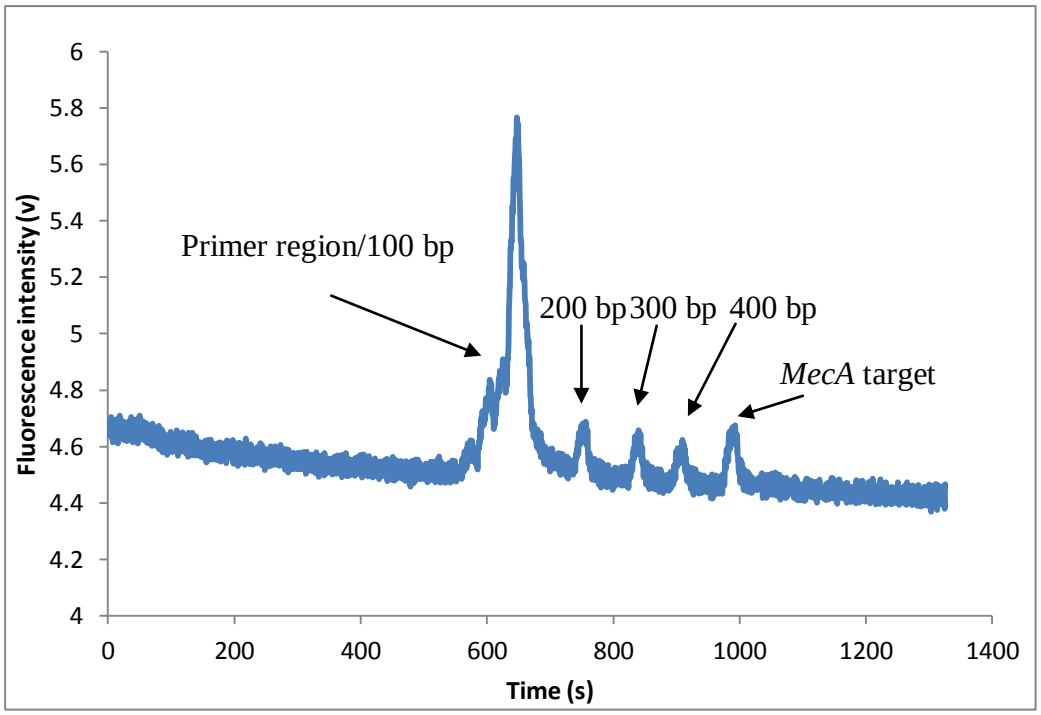

Figure 5.25: Four mark size ladder with mecA PCR product (as analysed on the IGA).

Electropherogram obtained on the IGA for size ladder products with additional *mecA* target (532 bp). Electropherogram was obtained using a 30 sond injection time. Laser strength 3 mV and separation voltage was 7000 V. N = 3.

The detection of *mecA* target in conjunction with the size ladder provided a reproducible signal in timescales of approximately 25 min, comparable with that of other groups (Fu and Lin, 2004; Wooley *et al*, 1996; Manage *et al*, 2010). The IGA detection system is performs at a standard to be suitable for use in point of care. diagnostic applications.

a)

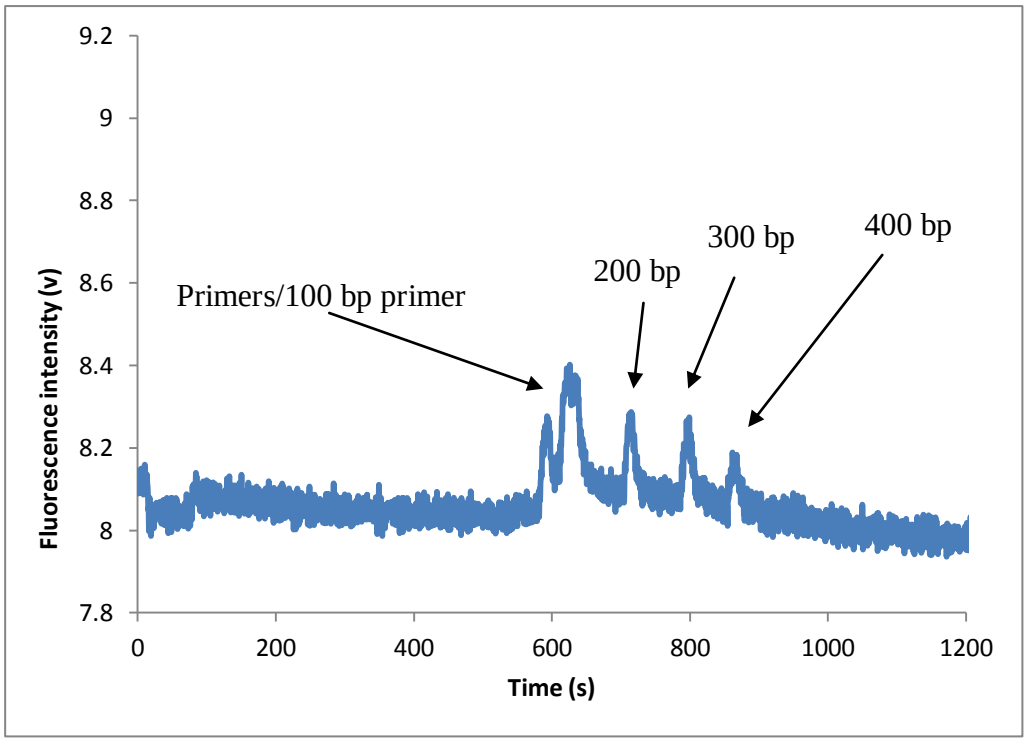

b)

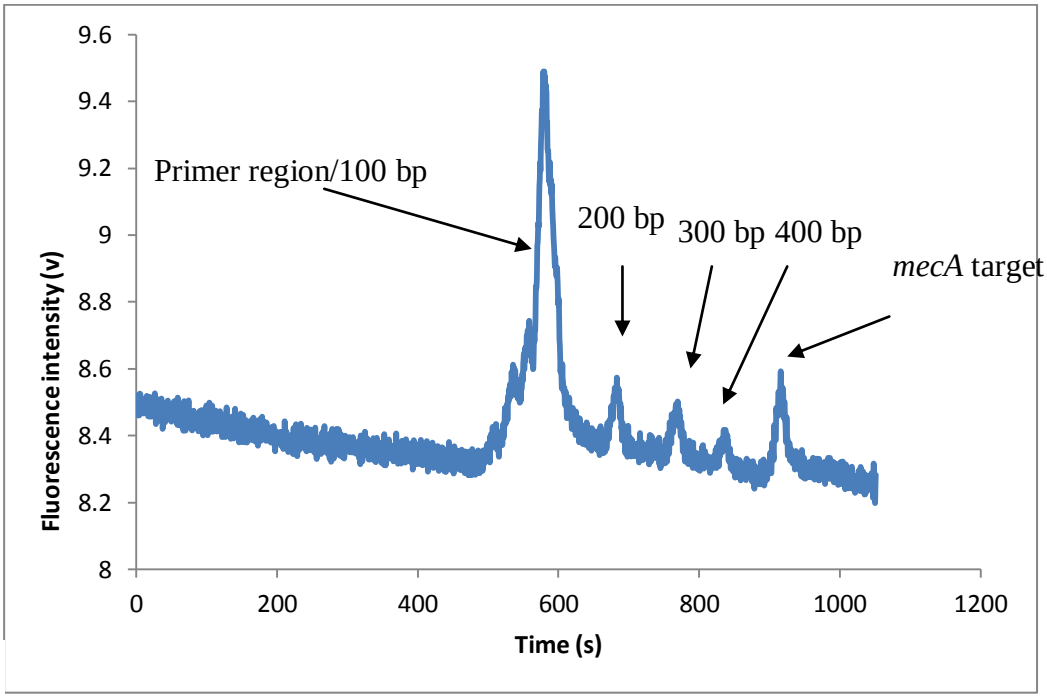

Figure 5.26: Four mark size ladder analysed with IGA (increased laser power)

a) Electropherogram obtained on the IGA for size ladder products b) Electropherogram obtained on the IGA for size ladder products with additional *mecA* target (532 bp). Both electropherograms were obtained using a 30 sond injection time with laser power of 6 mV. N = 3 for both experiments.

5.3.3.6 Integration of amplification and detection on-chip

An investigation was carried out to determine the potential for integration of PCR amplification and fluorescence-based detection of *mecA*. Integrating these two steps would eliminate the requirement for user-intervention between these stages and minimise the risk of contamination. Integration would also reduce the sample analysis time, as the transfer step would be automated within the chip. The successful PCR amplification (stion 5.3.2) was transferred to an identical chamber in the integrated chip. The chamber was then thermally cycled using a using a Peltier heating element and subsequently, the CE separation and detection of the amplified products were performed on the chip-device as described in stion 5.3.3.3.2. It was observed that several bubbles had formed within the POP7 filled channel local to the Peltier element during thermal cycling. Despite this, the injection, separation and detection process was able to run, implying the electrophoretic circuit was not broken. It is assumed that the POP7 remains thinly coated on the channel wall to allow electrophoretic movement of components. The electropherogram obtained, however, did not show fluorescent data comparable with that of detection data observed for the mecA detection throughout this chapter. It is postulated at this stage that due to the difference in size when compared to the chip used in stion 5.3.2, the larger chip contributed to some thermal loss. This would therefore require further optimisation of thermal cycling parameters.

5.4 Summary

The aim of the work in this chapter was to develop an on-chip amplification and detection system for detection and identification of an MRSA genomic target. An additional aim was to integrate the two steps on a single chip-device.

Successful PCR amplification of an MRSA genomic target was carried out on chip in a chamber of ≈ 12.5 µl. This chamber volume was able to be transferred to the integrated chip for potential integration to up and downstream steps.

Development of the detection system incorporated in to the IGA was able to reproducibly detect both generic *S. aureus* target and *mecA* target. This was then then detected with reference to a size ladder of four molecular weight markers. The size ladder could be visualised reproducibly, however the lowest marker (100 bp) was not

able to be resolved from fluorescent signal from the unreacted primers. This issue, however, could be potentially removed using a PCR cleanup methodology.

The system showed potential for integration of the PCR amplification, separation and detection steps, as the sample was thermally cycled and analysed on the IGA without any leakage or breakages in current during electrophoresis. The thermal cycling parameters will however require further optimisation as electropherogram did not show evidence that successful amplification was achieved in to the integrated chip-device.

The work described in this chapter holds potential for the application of detecting MRSA from urine, if integrated to a DNA extraction process, such as the monolith-based system described in Chapter 4. It is also important to state that the system demonstrated here could be used in other genetics-based applications, such as forensic DNA analysis.

6. Direct PCR amplification of bacterial targets from unprocessed blood samples

6.1. Introduction

As described in stion 3.1, bacteruria is commonly preceded by bacteraemia or *vice versa*, thus, there are clear benefits to a method for simple and rapid diagnosis of MRSA from blood to use in conjunction with a urine-based system. Such a system could be used to screen patients diagnosed with one form of MRSA infection for that of another. This would be highly beneficial to the patient to avoid prolonged exposure and could also provide the clinician with a rapid means of detecting MRSA from contrasting sample types. Due to the reported inhibition of PCR in the presence of the blood component haem, a DNA purification step is normally essential in NAAT for amplification of target sequences from blood samples (Ford, 2010). However, there have been a number of reports in the literature describing methodologies for amplification direct from blood samples, (see stion 1.4.6.6), in which a purification step is bypassed.

The aim of the work in this chapter was to establish a methodology for PCR amplification of target DNA sequences from unprocessed blood samples on a microfluidic chip device to be used for the detection of MRSA in low volume quantities of blood. This could then be incorporated in to the IGA platform described and be analysed using the electrophoretic separation/ detection system. This would provide a full sample-to-answer process which could be used for rapid detection of MRSA, without the demand for high volume blood samples from the patient. This would be far less invasive for the patient. In addition, this makes population screening far more achievable. The ability to amplify the target direct from the blood sample also means any processing step off or on chip is eliminated, meaning the sample can be added directly. As described in stion 1.3.3, Manage *et al* (2012) demonstrated amplification and integration on-chip using a Phusion® blood direct kit. The Phusion® kit works with a specialised enzyme which is able to withstand inhibition by known inhibitor, haem. While Manage *et al* (2010) used a valve-based pumping mechanism, the simplicity of the IGA would bypass the need for a complex pumping mechanism.

In addition, a dual-purpose chip is proposed in which both urine and blood can be tested for the presence of MRSA infection.

6.2. Materials and methods

6.2.1 PCR direct from blood off-chip

The use of the Phusion® blood direct kit (Thermoscientific, UK) has been described in stion 2.5.1.2. Human blood samples of varying volume were spiked with purified MRSA genomic DNA in order to observe the influence of blood concentration on PCR performance. All specific volumes and concentrations are detailed in the appropriate results stion.

6.2.2. PCR Direct from blood On-chip

Using the microfluidic device shown in Figure 5.1, PCR amplification from blood samples was carried out on-chip using the Peltier heating system described in stion 2.5.3. The parameters for thermal cycling used were an initial denaturation step of 98^{o}C for 180 s, followed by repeated steps of denaturation at 98^{o}C for 40 s, annealing at 55^{o}C for 40 s and extension at 72^{o}C for 40 s for a total of 35 cycles and a final extension step of 72 ^{o}C for 240 s. The reaction mixture was then cooled to 10^{o}C to preserve the sample.

6.3. Results and discussion

6.3.1. Preliminary experiments

The first aim was to establish working conditions for the amplification of the *mecA* genomic target from whole blood. Initial experiments carried out off-chip from a PCR mixture (total volume 20 µl) containing ≈ 5 ng MRSA gDNA showed successful amplification of PCR products were formed using the Phusion® blood direct kit. Following this, the same quantity of target DNA was amplified using increasing volumes of blood per reaction (H_2O content decreased accordingly to maintain final total concentration volume 20 µl) (stion 2.5.1.2)). Samples were amplified containing blood volumes of 1, 2, 3, 4, 6 and 8 µl and amplified products were analysed by agarose gel electrophoresis (Figure 6.1). Successful PCR amplification of the MRSA

target sequence was achieved for all reactions containing blood volumes up to 6 µl. No amplified products were observed when blood volume content was 8 µl. Whereas, the Phusion® blood direct kit reports efficient PCR with up to 40 % blood tolerance, the tolerance reported here is 30 %. It is unclear whether this is due to the high concentration of haem causing the PCR to fail, as the PCR process drops completely below detection at this concentration. Alternatively, it is also possible that the Phusion® enzyme is not able to migrate through the PCR mixture with enough celerity, due to the increased viscosity associated with high blood concentration.

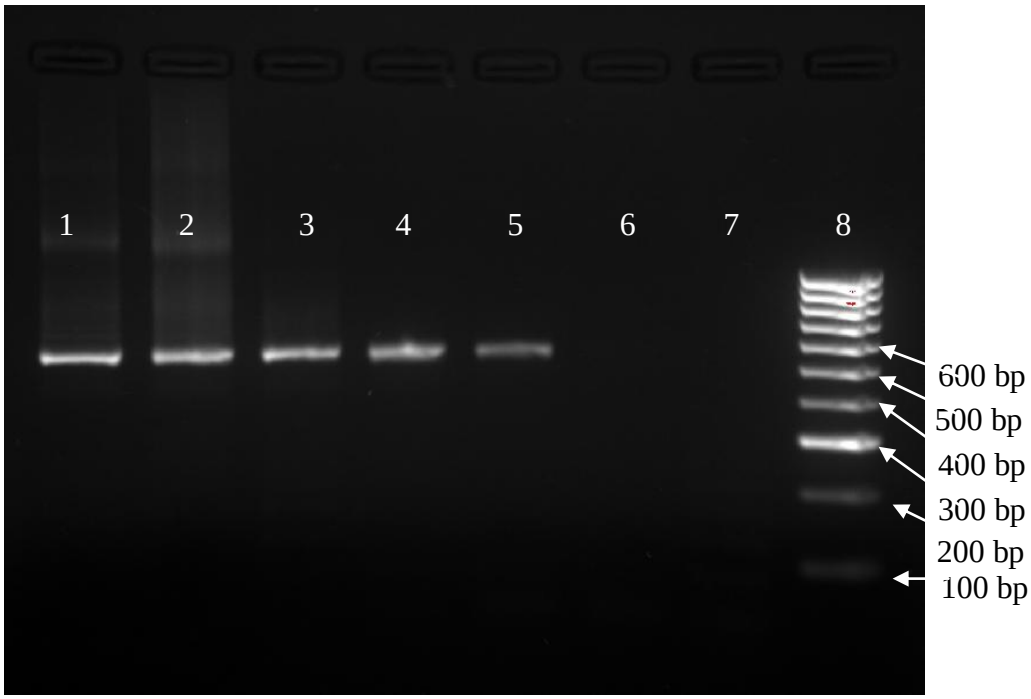

Figure 6.1: Effect of increasing blood volume on Direct PCR amplification

Gel of Phusion® direct amplification of *mecA* gene from MRSA (≈ 5 ng) genomic target. Lane 1 is 1 µl, lane 2 is 2 µl, lane 3 is 3 µl, lane 4 is 4 µl, lane 5 is 6 µl, lane 6 is 8 µl and lane 7 is negative control. Finally lane 8 is the Hyp IV size ladder (Bioline, UK). PCR products were not formed when 8 µl blood was used. N = 2.

Following this the concentration of MRSA genomic target within the sample was reduced in order to establish the effect of doing this. When decreasing the concentration of MRSA genomic target, 10-fold, the PCR was shown to work at the blood volume 1-6 µl. Figure 6.2 is an gel for blood volumes 1-6 µl. Significantly, there is no visible influence of blood volume on fluorescence signal. The slight variation could be attributed to some heterogeneity within the blood sample. The

result shows the potential for reducing target concentration and, thus, increasing the sensitivity of the system.

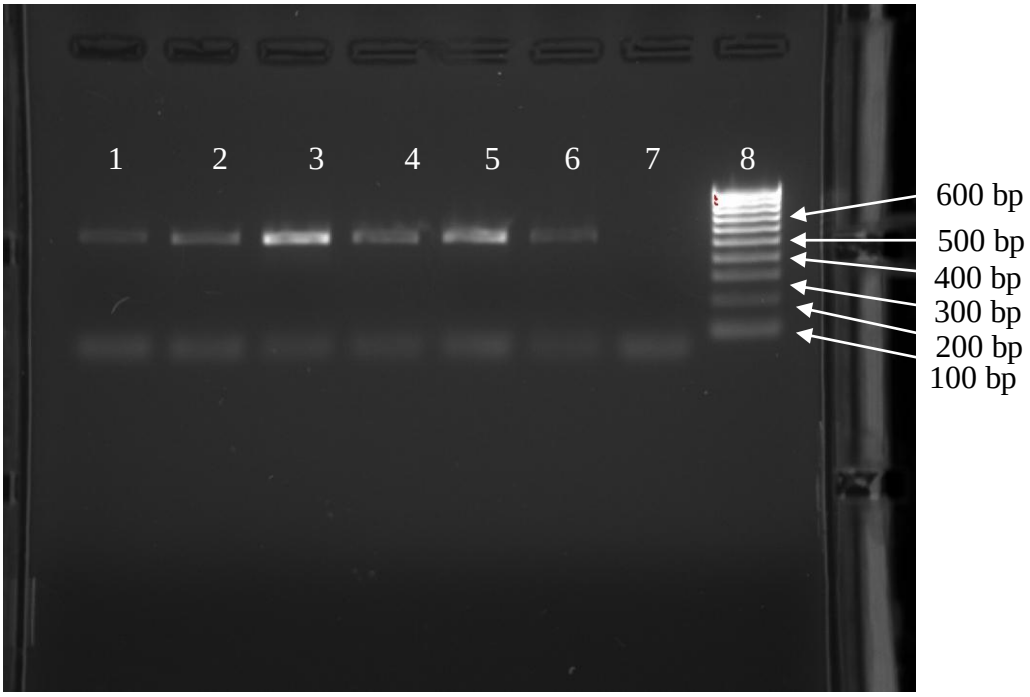

Figure 6.2: Decrease in *mecA* target concentration (DNA, 0.5 ng)

Gel of Phusion® direct amplification of *mecA* gene from MRSA (≈ 0.5 ng) genomic target. Lane 1-6 show increasing blood volume of 1-6 µl. Lane 7 is negative control. Finally lane 8 is Hyp IV size ladder . N = 3.

6.3.2. Analysis of Direct PCR using IGA Detection System

Using PCR products generated off-chip from a typical Phusion® direct amplification (stion 2.5.1.2) (5 ng genomic DNA (MRSA) in 6 µl human blood) the IGA detection system was used for detection of amplification products (separation voltage was 7000 V, injection time was 30 s and laser 3 mV. The electropherogram (Figure 6.3) was comparable with that obtained in stion 5.3.6. Clear signals were observed for both primer/primer dimers and *mecA* product, showing that DNA products amplified by this process were compatible with detection and analysis using the IGA and that the Phusion® amplification process has no detrimental effect or influence on the fluorescent label used to tag the oligonucleotide primers used.

Following this, the same process was carried out, bypassing the supernatant retrieval step to give complete deposition of the thermally cycled sample in to the

sample well, also containing buffer (50 µl) giving a total volume of 70 µl. When carrying out the injection for CE separation and detection, the injection time scale was increased to 180 s in order to ensure the target DNA had time to migrate from the uncentrifuged PCR mixture and in to the surrounding buffer. Separation and detection was performed using conditions described in stion 5.3.3.2 and an electropherogram was obtained (Figure 6.4). While no DNA size marker ladder was incorporated for size comparison/estimation during this process, there were two distinct signal peaks observed, which were characteristic of the primers/ primer dimers and *mecA* amplification product (532 bp) comparable to that of a typical separation with 180 s injection (Figure 5.16). The results obtained shows that for separation and detection on the chip-device, the amplified DNA is able to be transported from the PCR mixture containing blood, electrophoretically, without the need to partition the supernatant.

This method offers a similar approach to that of Manage e*t al*, 2010, but simplifies this process, as their work reported the requirement to flush the amplified sample through with a buffer prior to detection. The absence of a size marker in this experiment was due to the unknown migration timescales of the target amplicon from the blood mass not being known at the onset. To incorporate a size marker, this would have to be taken in to consideration, as the size marker would not be electrophoretically migrating from the same blood mass, but from the surrounding buffer. A DNA size ladder could be incorporated in to the PCR mixture pre-amplification, however, further studies must be carried out to ensure the ladder doesn't interfere with the amplification of target sequences. Alternatively, a modified alternative chip design could be produced with an additional chamber introduced for moving the PCR products to prior to electrophoresis. In this way, the amplified PCR products could be transported from the thermal amplification chamber to a sond chamber in which the size marker was already present to permit mixing prior to electrophoretic separation and detection.

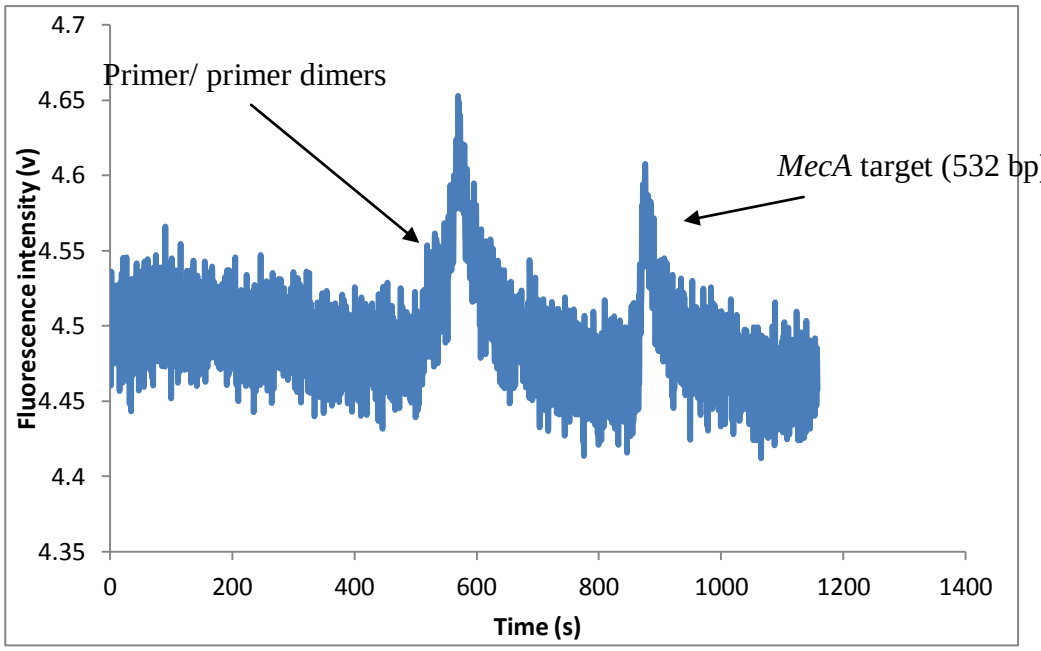

Figure 6.3: Detection of Phusion® direct amplified *mecA* product from PCR amplified off-chip.

IGA electropherogram illustrates detection of *mecA* gene target sequence (expected product 532 bp) amplified using Phusion® direct blood kit. Sample analysed was centrifuged and supernatant collected as with off-chip experiments. N = 2.

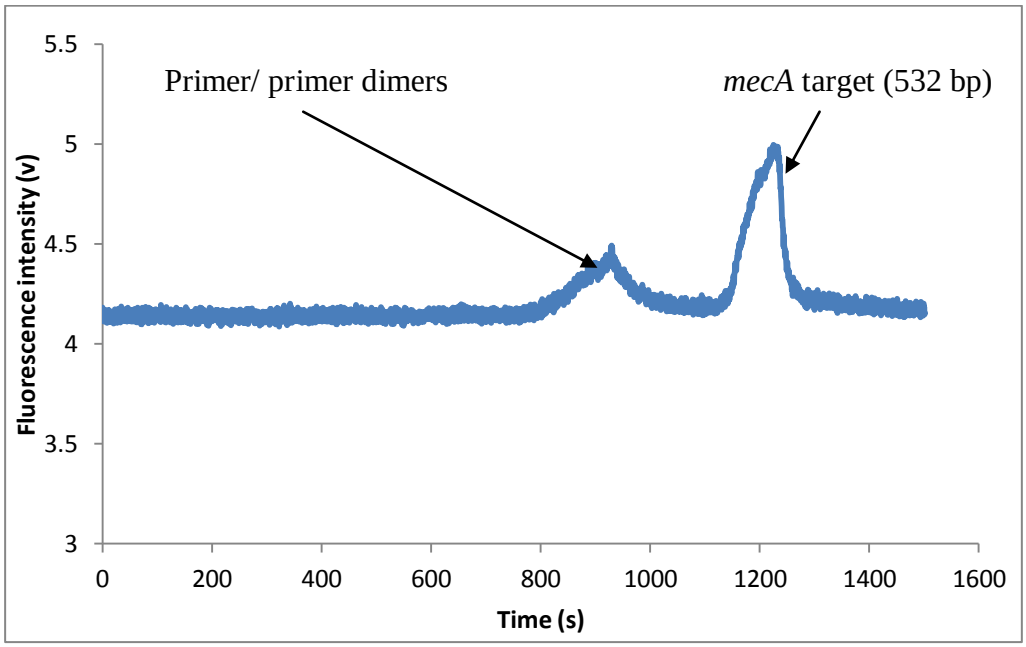

Figure 6.4: Detection of *mecA* PCR products direct from blood mass.

IGA electropherogram of Phusion® PCR product when bypassing the centrifuge step, requiring electrophoretic migration of the DNA from the blood mass. Result shows clear fluorescent signal for both primer (900 s) and PCR product (1200 s). N = 2.

6.3.3 Direct PCR amplification from blood carried out on-chip

The Phusion® Direct blood amplification process was then attempted within a glass microfluidic device in order to demonstrate that direct PCR amplification from blood can be carried out on a chip-device. The proof of principle experiment was carried out using a Phusion® Direct PCR reaction mixture prepared as described in stion with 1 µl human blood and ≈ 5 ng purified MRSA genomic DNA target. The PCR mixture was transferred to the microfluidic chip device and no significant back pressure was evident during loading of the sample, demonstrating that the mixture was of a viscosity compatible with the chip-device. Each of the wells on the chip were then filled with mineral oil and the chip was sealed with optical adhesive tape and epoxy resin. Thermal cycling was then conducted as described in 2.5.1. Photographs were taken of the chip-device before and after thermal cycling. The photographs (Figure 6.5) show the sample has undergone some coagulation due to the high temperatures in the reaction chamber. Following thermal cycling of the sample, the optical adhesive and epoxy resin seal was not breached, demonstrating that the seal can withstand the increased pressures within the amplification chamber when thermal cycling. The chamber shows evidence of coagulating from the high temperatures. When recovering the sample from the chip with a micropipette for detection with the IGA detection system, there were difficulties retrieving the whole sample due to sample components adhering to the chamber sides. It was, however, possible to retrieve sufficient volume (≈ 8 µl) for subsequent analysis using the IGA. It is important to clarify that this would not be an issue if the PCR reaction were to be directly integrated to a detection step since the entire sample would not have to be transferred out of the chip for subsequent analysis by electrophoresis.

a)

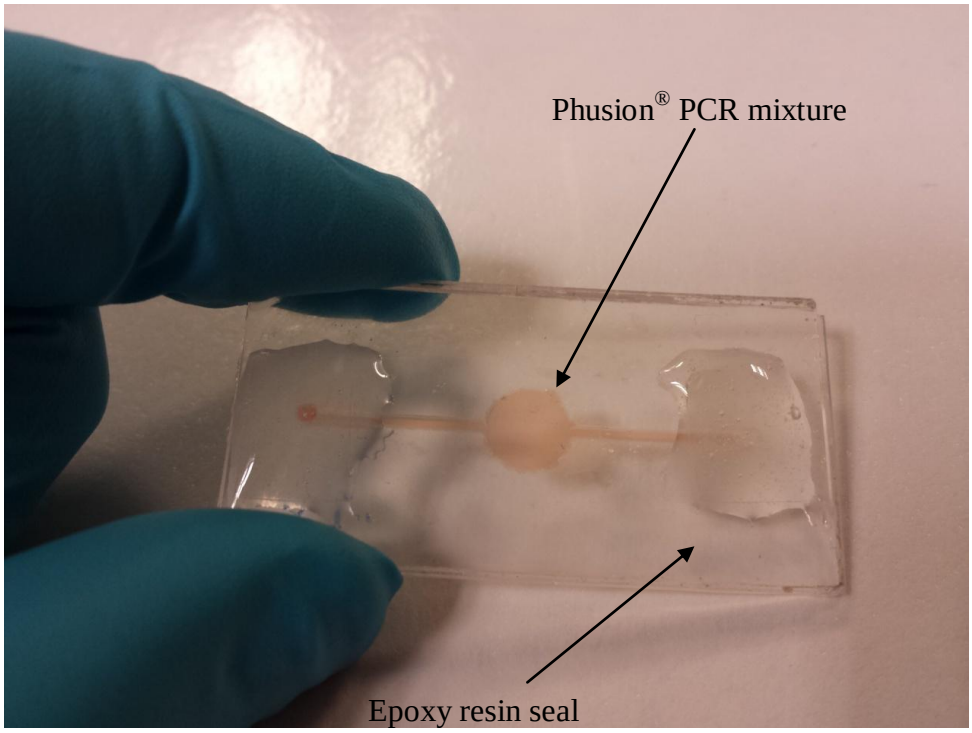

b)

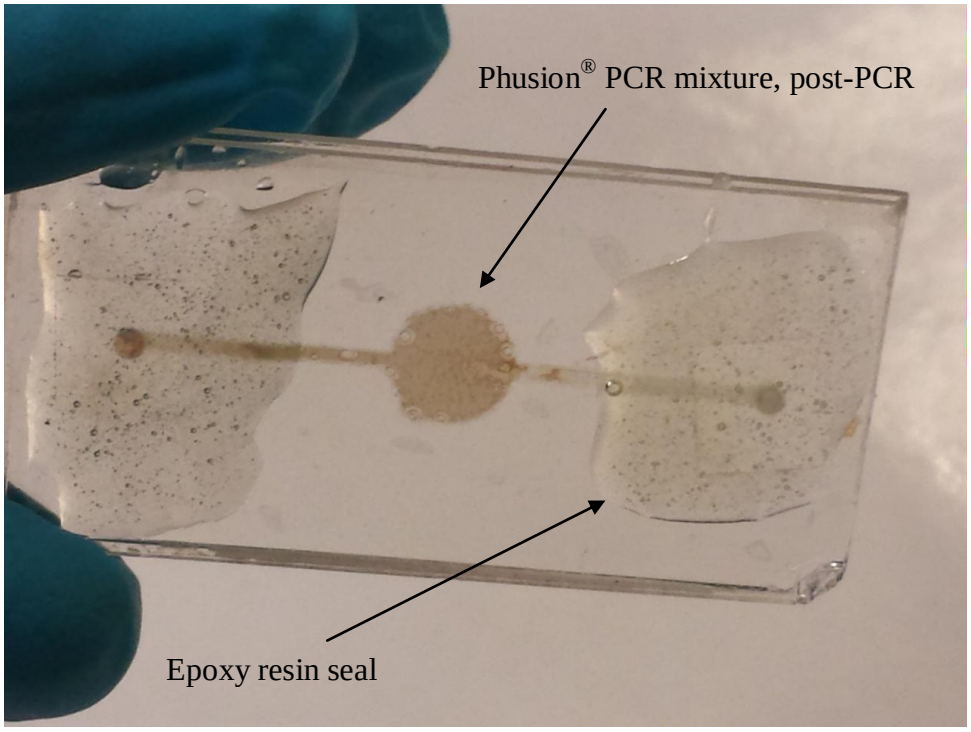

Figure 6.5: Direct PCR amplification from blood on microfluidic device.

a) Photograph showing the microfluidic device with Phusion® PCR mixture prepared containing 1 µl of human blood prior to thermal cycling. b) shows the same chip following thermal cycling. Both entry and exit are sealed with optical adhesive and epoxy resin. The post-PCR mixture is visibly coagulated by thermal cycling.

When the PCR amplified sample retrieved from the microfluidic device was analysed using the IGA detection system, using conditions as described in stion 5.3.3.3.2, a fluorescent signal peak was observed corresponding to the *mecA* gene sequence PCR product (Figure 6.6). This result demonstrated that an unprocessed human blood sample could be added to a chip and that amplification was possible. This was repeated incorporating the custom-designed DNA molecular weight marker ladder (stion 5.3.3.5) showing the *mecA* target to be present along side the four size markers (Figure 6.7). The series of experiments demonstrated amplification, CE separation and detection all successfully carried out, although it is acknowledged that for proof of principle that this had to be performed on two separate chip-devices since these processes have not yet been integrated on to a single device. As described in the previous chapter, the full integration of steps will require further optimisation of thermal cycling parameters on the integrated chip. The whole process was carried out in less than 2 hs (≈ 90 min PCR and ≈ 25 min detection), making it a desirable option for POC diagnostics.

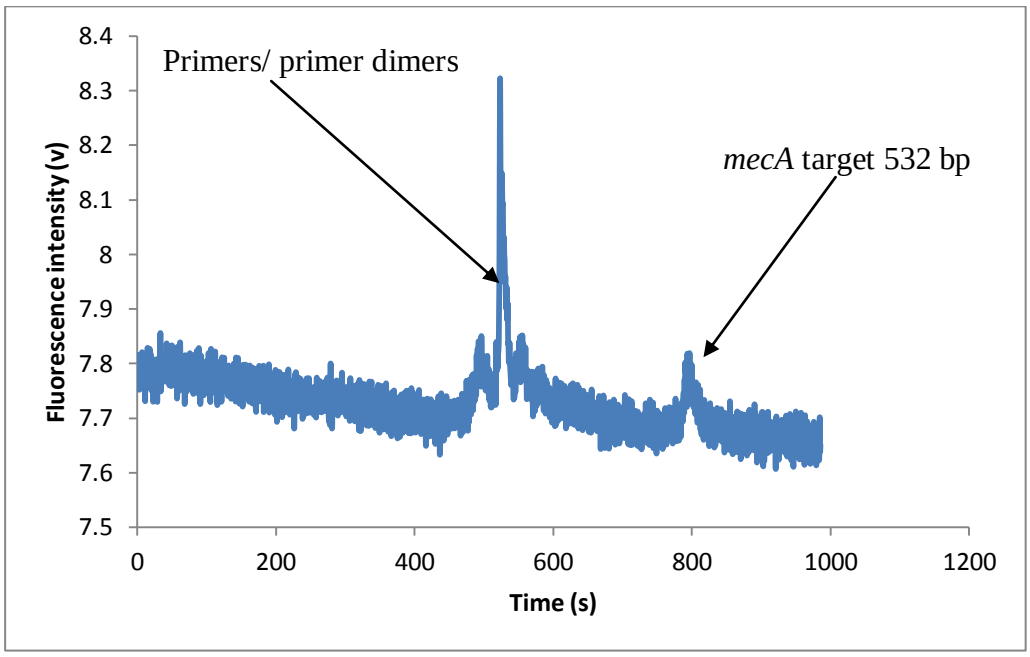

Figure 6.6: Detection of mecA product amplified direct from blood on chip.

Electropherogram showing separation and detection of products from the Phusion® Direct blood amplification of *mecA* target sequence carried out on-chip. Laser strength used of 6 mV. Peaks indicating the presence of *mecA* target are comparable with that in stion 6.3.2. N = 2.

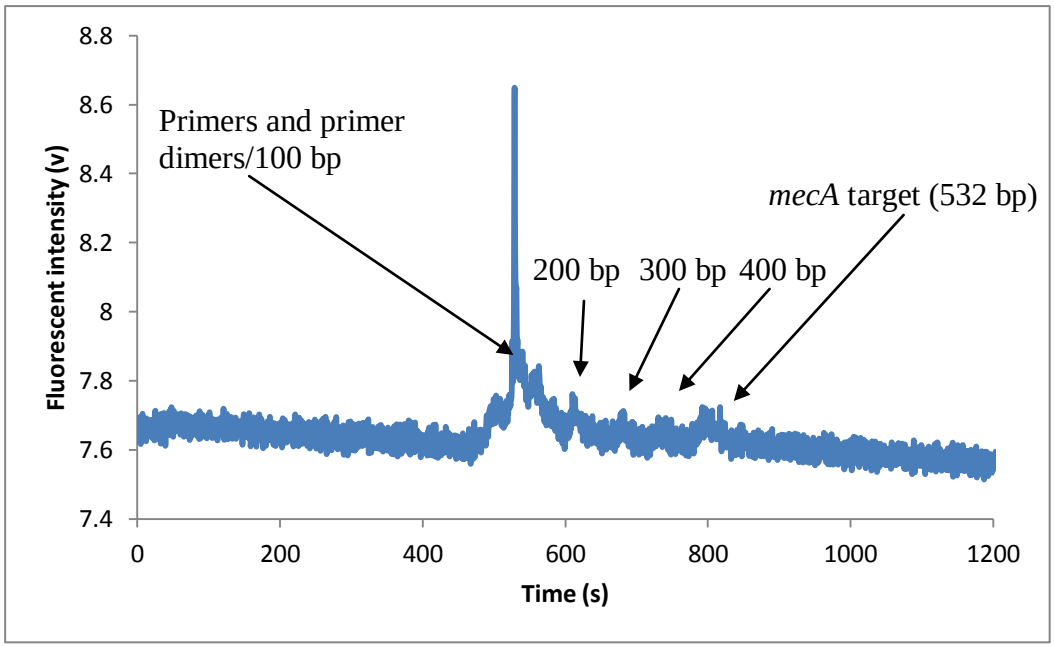

Figure 6.7: Detection of mecA product amplified direct from blood on chip.

Electropherogram showing separation and detection of products from the Phusion® Direct blood amplification of *mecA* target sequence carried out on-chip with size markers included (100 bp, 200 bp, 300 bp and 400 bp). Laser strength was 6 mV. N = 2.

Following this, the same protocol was carried out on-chip, using 6 µl human blood in the PCR reaction order to demonstrate that the chip could process the maximum blood content which had been demonstrated off-chip. This PCR sample was successfully injected in to the microfluidic device and thermal cycling was conducted, however, on attempting retrieval, the post-PCR reaction mixture was not able to be readily withdrawn from the microchip. This was due to the higher concentration of blood causing excessive coagulation leading to the mixture adhering to the inside of this chip. As a result, no analysis could be carried out. As already described in this stion, the development of a fully integrated system would obviate this problem, as the sample would already be in position for analysis by electrophoresis.

The process outlined in this chapter has successfully demonstrated multiple components for sample-to-answer analysis for the detection of genomic target sequences from infectious organisms in very small volumes of blood (≤ 6 µl). While, the proof of principle data presented here does not demonstrate the sensitivity of the system, it does demonstrate the successful transfer of the blood-based PCR mixture to

the microfluidic device developed throughout this work. For an extensive investigation of the sensitivity of the direct PCR amplification from blood process demonstrated here using model systems with MRSA targets, real-time quantitative PCR would be appropriate. This would allow you to establish limit of detection for the system, regarding the infectious load.

It will also be necessary to introduce whole organisms to the sample, rather than purified DNA, to ensure sufficient lysis is taking place prior to amplification. There is a short review of the cell lysis methods which have been reported on-chip (stion 1.4.3), however commercially, a leading methodology for lysis of bacterial cells is the use of ultrasonication (Cepheid®, 2014).

6.4. Summary

In summary, the Phusion® blood direct kit, which supports PCR amplification from blood samples was used to successfully amplify the *mecA* genomic target from sample concentration down to 0.5 ng. When adjusted to the maximum blood processed (6 µl) this is 0.083 ng μl^{-1}. The failure to successfully amplify PCR products from a sample with a higher volume of blood was attributed to either haem-inhibition of the enzyme or viscosity of the mixture. A real-time PCR methodology would be required to accurately establish the sensitivity of the system, however efficient PCR performance maintained for a range of blood volumes (1 µl – 6 µl in 20 µl). In addition, it is assumed that it will be possible to increase the total blood volume by upscaling the PCR amplification mixture in its entirety. This would, however, require a larger PCR chamber for on-chip experiments, which introduces additional complications (stion 1.4.6.2). The Phusion® direct PCR amplified product was also successfully analysed on the IGA detection system, showing compatibility for integration. This includes both centrifuged DNA sample and also electrophoretic migration of the DNA directly from within the post-PCR blood mass. This development is a huge advantage for integrating to a detection step, post PCR, as it would not necessitate a separation step (i.e. centrifugation or similar processing step).

The Phusion® blood direct PCR amplification process was successfully transferred to a microfluidic device and the PCR products were detected using the IGA detection system. The result demonstrated the direct transfer of an unprocessed blood sample to a chip device. Prior to the experiment, it was considered that the

presence of blood may hinder movement of PCR components during thermal cycling, thus inhibiting the process. The presence of amplified product does, however, mean this system has potential for direct integration on to the IGA, which would provide a complete sample-to-answer device.

7 Conclusions

The work here reports the development of a microfluidic platform for nucleic acid-based detection and analysis of infectious agents from biological samples. The two model systems that were used were STIs (*C. trachomatis* and *N. gonorrhoea*) and also methicillin resistant *S. aureus,* due to their relevance as global healthcare issues. The work supported the concept of a microfluidic platform which could be modified to accommodate a variety of samples types, without requiring prior processing. The study focussed mainly on the introduction of the sample to the microfluidic device and extraction of DNA, however PCR amplification on chip and detection by CE were also investigated. The IGA used in conjunction with a variety of real world-to-chip interfaces offered a very attractive, simple and low cost alternative to the more mechanically intricate technology described in the literature. The system, in its entirety remains a prototype, however, the following are key innovations within the work:

The series of DNA extraction methodologies that were developed held significant advantages over methodologies previously reported. They were shown to allow scalable manufacture with relative ease. The TMOS-based monolith was also shown to efficiently process human urine samples without sample pre-treatment, indicating that these would be highly compatible for use with clinical samples. The DPS system provided a novel and attractive way of incorporating porous materials in to a microfluidic device using a sondary porous silica seal. The methodology would be welcome in a clinical setting as well as many other SPE-based applications, such as drug extraction or water analysis. Furthermore, to the author's knowledge, it is the first reported juxtaposition of two types of porous silica in any microfluidic application. This is a technical innovation which could be further adapted and could inspire others to utilise the amalgamation of similar porous materials. Furthermore, the ease of functionalisation of the DPS, as shown with chitosan, also shows large potential for alternative applications outside the scope of this work.

Regarding the observed influence of NH_4OH on DNA extraction efficiency of the developed monoliths, it was postulated that the silica surface was conditioned in some way, thus facilitating efficient DNA release, although the mechanism through

which this occurs has not yet been investigated. To the author's knowledge, this has not been previously reported and should be a consideration for future development of similar silica structures, such as other porous materials and also silica beads.

The current investigation exploring the development of a methodology permitting the amplification of MRSA targets direct from human blood samples on a chip device showed great promise for further development. What was particularly attractive about this methodology was the ability to perform the thermal cycling on chip and also electrophoretically migrate DNA from the blood mass following thermal cycling. This was achieved despite significant congealing of the sample during heating. The ability to analyse blood samples of this volume in this way with little complexity is a suitable addition which complements the porous monolith-based interfaces already described. In union, they demonstrate how it is possible to tackle the problem of transferring very different sample types to a chip, while adhering to the same philosophy regarding cost and manufacture.

Finally, the custom-built IGA demonstrated robust detection of target sequences and appropriate size ladder with competitive resolution achieved. PCR amplification of MRSA genomic targets was also possible on-chip, however full integration within a single chip device was not achieved, possibly due to thermal loss, when using the larger integrated microfluidic device investigated. This can be potentially addressed with further optimisation of thermal cycling parameters. Due to the ease of chip manoeuvre provided by the IGA, the system would be highly applicable for integration to a variety of sample interfaces, including those discussed here. Therefore the IGA is highly promising for further development into the processing of clinical sampling.

During the period of completion of this work, several commercial products utilising NAAT approaches have become well established in point of care clinical diagnostics (Cepheid, 2014, Chin *et al*, 2012, www.bd.com, 2014). Cepheid®, 2014, for example, who are arguably responsible for the most notable of these innovations, developed a sample analyser (Cepheid GeneXpert system), which has been tested for a large number of applications for the detection of infections (stion 1.4.9) with very strong results. The cost of these instruments is high, however, due to the complexity of the individual components in the system. This makes the mass production of an instrument for clinics, hospitals and especially the developing world, more of a

challenge. The simplicity of the work presented here, however, provides potential for mass production at a comparatively much lower cost.

8 Further work

The work reported here has demonstrated the potential of DNA extraction on-chip from an unprocessed sample for use in clinical diagnostics. It is proposed that the systems described could be further developed and improved for a variety of additional applications. A number of potential avenues for future work are reviewed here.

While the TMOS-based monoliths were shown to be easily manufacturable and provide competitive DNA capture efficiency, there are still some challenges remaining to further develop and implement the system. Firstly, it is possible that the introduction of carrier RNA to the loading sample could provide higher DNA extraction efficiency (Shaw *et al*, 2009; Sambrook, 2001). Carrier RNA has been found to have a greater affinity for the areas of silica which fail to release bound DNA. By introducing this to the sample load, the RNA competitively binds to those regions allowing for target DNA to be released in a higher proportion, increasing the DNA extraction efficiency.

The main issue with the TMOS-monolith extraction was associated with the eluted DNA volume; this was a combination of high volume (> 20 µl) and also traces of ethanol in the eluted sample. Both of these contributed to unreliable amplification post-extraction. Regarding the ethanol contamination in the eluted DNA, while, certain groups have used centrifugal force to eliminate ethanol thoroughly from porous materials, this is impractical for the proposed chip-based format. It would, however, be feasible to vigorously flush the monolith with hot air in order to eliminate ethanol. Regarding the high elution volume, the TMOS monolith was manufactured in the chosen dimensions in order to receive a sample of high volume in a flat microchip. It may be possible to reduce the dimensions and narrow the monolith, in order to narrow the flow and concentrate the elution volumes. It is important to note that narrowing the flow pathway will reduce the area for binding if the chip depth is kept the same, meaning it may be necessary to deepen the DPS chamber inside the chip.

An alternative methodology for reducing the DNA elution volume would be to incorporate a potassium silicate-based monolith, post-TMOS monolith as a sondary DNA concentration step. Based on the elution profiles of the potassium silicate monoliths (stion 4.3.2), this would offer the chance to reduce the entire elution

volume to less than 5 µl. This would also eliminate problems with ethanol carryover, without the need for a drying step. It is acknowledged this may introduce complexity to the chip, however, the work here has shown that both monoliths are very low cost and simple to incorporate into a single device.

To fully demonstrate the system for the proposed application of isolation and detection of infectious bacterial organisms, it will be necessary to carry out DNA extractions using clinical samples containing these organisms. The chaotrope GuHCl was selected for use in DNA methodologies due to the ability to aid DNA binding to silica and for function as a cell lysis agent, however this is yet to be tested on the intact bacterial targets (Kemp *et al*, 2012). It is therefore necessary to begin to introduce whole organisms when an improved extraction protocol is introduced. In the event that a chemical lysis step is not sufficient for extraction of DNA from bacterial targets an alternative method will be introduced. Cepheid®, 2014 utilised an ultrasonic disruption step for lysis of bacteria targets (e.g. *S. aureus*), which would be entirely feasible as an additional step for this system.

The CE separation and detection system was shown to reliably detect DNA fragments with reference to a DNA size ladder. In addition, the amplification procedure was successfully carried out on-chip. The inability to integrate the two was attributed to thermal loss on the larger microchip. The next step here is to optimise the thermal cycling parameters to account for this thermal loss. This can be done by repeating experiments with adjusted parameters or it can optimised by insertion of a thermocouple, as shown in stion 5.3.4. Following integration of amplification and detection, integration to extraction methodologies can be investigated. The most likely chance of success for this would be to incorporate the PCR reagents into the device by freeze drying them in to the chamber.

Regarding the CE detection system alone; the system described in Chapter 5 was a demonstration of a positive and negative result against a four point size marker. While system provided excellent reproducibility and competitive sensitivity, further work must be carried out in order to maximise the potential of the system. Firstly this includes an improvement of resolution. As shown in stion 5.3.6.3.1, denaturing the DNA into single strands improves resolution, however it was not explored in depth with this system. In addition, lowering voltages (stion 5.2.6.4), can offer a greater spread, which can also be investigated further when considering resolution. Finally,

an investigation in to the sensitivities of the system can be explored in depth, including the possibility of data smoothing.

The work using the Phusion® blood direct kit, established a working amplification protocol on-chip. Due to difficulties in retrieving the sample from the chip post-amplification, experimentation using increased levels of blood was not able to be explored in depth, however, if integrated directly to the detection step described in Chapter 5, then it is likely this problem will be eliminated. The next step in this part of the integrated procedure, therefore, parallels that of the standard PCR protocol and, once optimal thermal cycling parameters are established, then the amplification reaction can be attempted with a higher content of blood. The system can then be tested thoroughly for sensitivity using the IGA. As with the DNA extraction protocol, whole target organisms could then also be introduced to the reactions.

A possible application for the collective work described in this thesis would be the development of a chip-device which utilises both the silica monolith-based DNA extraction system and the PCR amplification direct from blood system for a dual-purpose sample analysis chip. As described in stion 5.1, pathogens such as MRSA are known to invade and be isolated from all areas of the body. As a result, an infection of one part of the body (eg urinary tract) can be followed by the emergence of another (eg blood). Although no chip has been formally designed, it is proposed that this would be achievable using the IGA and one single microfluidic device. Due to the spacious platform and robust injection and detection system, it would be possible to run an integrated analysis using the chip as described with a similar configuration fabricated on a 180^{o} rotation of the device. A schematic of this concept device is outlined in the schematic drawn in Figure 8.1. For samples of larger volume, such as urine, requiring a pre-concentration step, the DPS system could be utilised, but for small blood samples, a direct PCR amplification step could be used. It would be essential that all electrode ports were aligned correctly and also that the separation channel be correctly aligned with both the laser (for excitation of fluorescent products) and with the two detection windows. For example the IGA could be applied to a urine sample to test for MRSA and then, the chip could be rotated and a blood analysis could be done. This could be also utilised for other sample combinations, eg blood/saliva, urine/saliva, faeces/blood etc and in addition, repeat experiments of the same sample type. As a further alternative, outside the scope of this work, the DPS

could be used for drug extraction from urine specimens to monitor for substances of abuse in conjunction with the PCR amplification direct from blood could be used for confirmation of identity of the sample provider. Such a device would be ideal for rapid sample processing at major sports events. Finally, a versatile system, such as this, also has the potential to deal with a variety of infectious organisms, such as viruses, fungi and parasites.

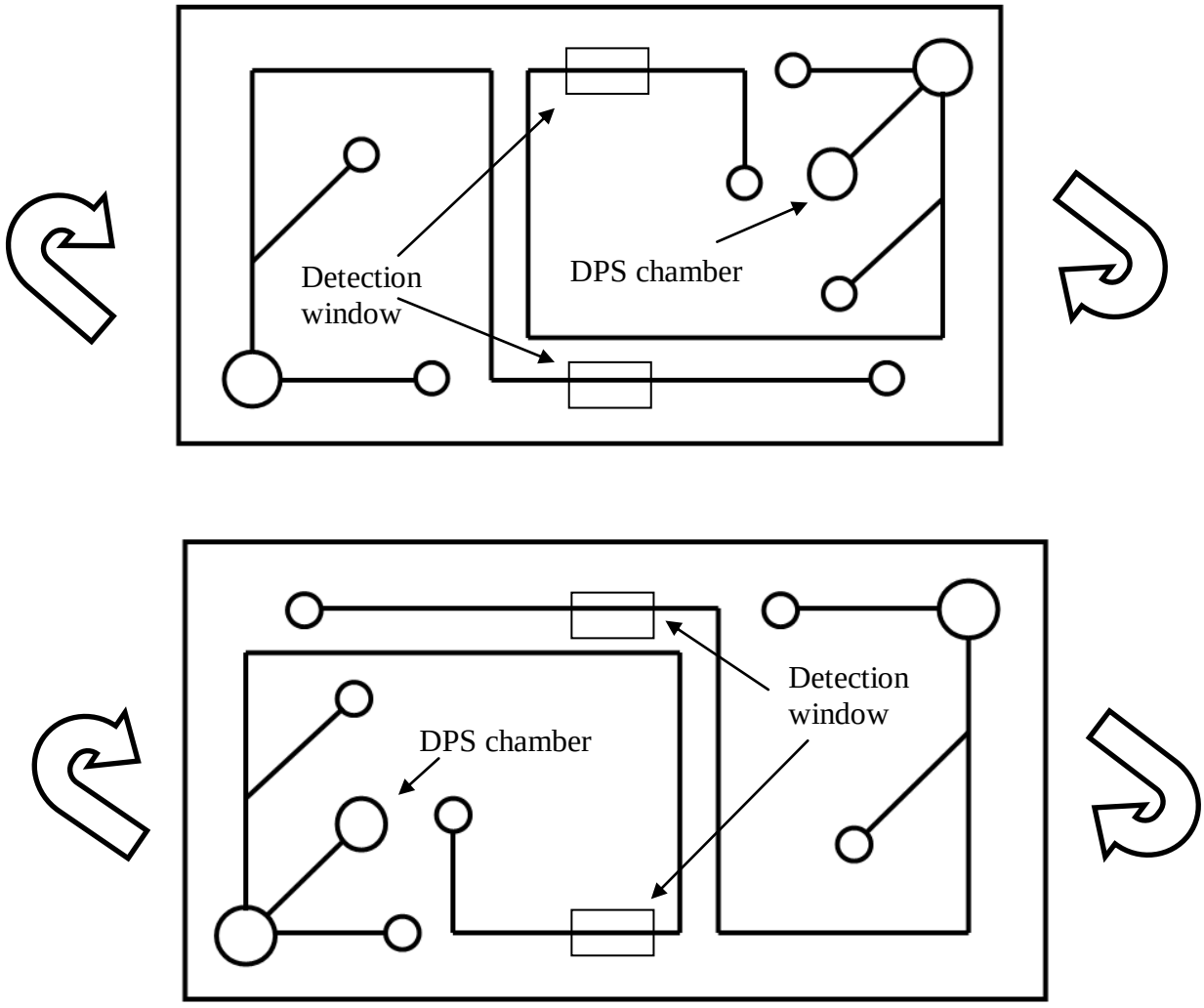

Figure 8.1: A schematic of the proposed chip for dual-sample experiments.

Injection area and detection windows are positioned so that a 180^{o} spin of the device would position it for a sond experiment. (a) and (b) are rotations of the same chip device. One experiment is designed with a chamber for incorporation of the DPS system. Note, channel configurations differ for two experiments in order to fit them on to a single device.

The device proposed incorporates a number of ideas reported in this work. The DPS required for SPE was developed and evaluated in Chapters 3 and 4. The plug injection-based detection system developed using the IGA was described in Chapter 5 and the PCR amplification direct from blood was described in Chapter 6. In addition, it is important to note that the unique design of the IGA, in which the power supplies are brought to the chip-device on the underside of the instrument lid is what makes this concept a realistic possibility.

It is the author's opinion that the platform and features described here form the basis of a very promising diagnostic instrument. If further developed, the benefits offered by the system would be welcome in any clinical setting and the cost and simplicity of manufacture, which were key considerations throughout the project, make it particularly suited for use in the developing world.

9 List of publications and presentations

Publications

1. Integrated DNA extraction and amplification using electrokinetic pumping in a microfluidic device.

J. Parton, C. Birch, C. Kemp, S. J. Haswell, N. Pamme, K. J. Shaw, Anal. Methods, 2012, 4, 96-100; DOI: 10.1039/C1AY05552F

2. Direct processing of clinically relevant large volume samples for the detection of sexually transmitted infectious agents from urine on microfluidic device.

C. Kemp, C. Birch, K. J. Shaw, G. J. Nixon, P. T. Docker, J. Greenman, J. F. Huggett, S. J. Haswell, C. A. Foy, C. E. Dyer, Anal. Methods, 2012, 4, 2141-4; DOI: 10.1039/C2AY25075F

3. **Microsystems for personalised biomolecular diagnostics.**

K. J. Shaw, C. Birch, E. Hughes, A. Jakes, J. Greenman, S. J. Haswell, Engineering in Life Sciences, 2011, 2, 121-32; DOI: 10.1002/elsc.201000175

4. **The influence of ammonium hydroxide-based Ostwalds ripening on the DNA extraction performance of porous silica monoliths**

C. Birch, S. J. Haswell, C. E. Dyer, Porous materials, 2014 (Currently in preparation)

5. Development of a real-world to microfluidic chip interface for the extraction of nucleic acids from urine, based on a dual porous silica monolithic structure

C. Birch, M. N. Esfahani, K. J. Shaw, C. Kemp, S. J. Haswell, C. E. Dyer, 2014, Analytical methods (Currently in preparation)

6. The Detection of MRSA from two different sample types using a single microfluidic device on a fully integrated genetic analyser.

C. Birch, , G. Benazzi, K. J. Shaw, C. Kemp, S. J. Haswell, C. E. Dyer, 2014, Analytical methods (Currently in preparation)

Presentations

Development of a real world-to-chip interface for the extraction of nucleic acids from urine, using a dual porous silica monolithic structure.

7th International Conference on Microtechnologies in Medicine and Biology (MMB 2013), California, April, 2013. (Oral)

Direct processing of clinically relevant large volume samples for the detection of sexually transmitted infectious agents from urine on a microfluidic device.

14th International Conference on Miniaturised Systems for Chemistry and Life Sciences (µTAS 2010), Groningen, The Netherlands, October, 2010. (Poster)

A simple, scalable system for DNA extraction of nucleic acids on a microfluidic device using a porous monolithic disk.

Analytical research forum, Manchester, UK, 2011. (Poster)

10 References

Adessi, C., Matton, G., Ayala, G., Turcatti, G., Mermod, J., Mayer, P and Kawashima, E. (2000) Solid phase DNA amplification: characterisation of primer attachment and amplification mechanisms. *Nucleic Acids Research* **28**(20)

Al-Soud, W. A., Jönsson, L. J. and Rådström, P. (2000) Identification and Characterization of Immunoglobulin G in Blood as a Major Inhibitor of Diagnostic PCR. *Journal of Clinical Microbiology* **38**(1): 345-350.

Anderson, D. J., Kaye, K. S., and Sexton, D. J. (2006) Methicillin-Resistant Staphylococcus aureus Bacteremia after Isolation from Urine. *Clinical Infectious Diseases* **42**(10): 1504-1505.

Andresen, D., v. Nickisch-Rosenegk, M. and Bier, F. F. (2009) Helicase-dependent amplification: use in OnChip amplification and potential for point-of-care diagnostics. *Expert Review of Molecular Diagnostics* **9**(7): 645-650.

Asiello, P. J. and Baeumner, A. J., (2011) Miniaturized isothermal nucleic acid amplification, a review. *Lab on a Chip* **11**(8): 1420-1430.

Baier, T., Hansen-Hagge, T. E., Gransee, R., Crombe, A., Schmahl, S., Paulus, C., Drese, K. S., Keegan, H., Martin, C., O'Leary, J. J., Furuberg, L., Solli, L., Gronn, P., Falang, I. M., Karlgard, A., Gulliksen, A. and Karlsen, F. (2009) Hands-free sample preparation platform for nucleic acid analysis. *Lab on a Chip* **9**(23): 3399-3405.

Banoo, S. (2010). Evaluation of diagnostic tests for infectious diseases: general principles. *Nature reviews.*

Baraboutis, I. G., Tsagalou, E. P., Lepinski, J. L. Papakonstantinou, I., Papastamopoulos, V., Skoutelis, A. T. and Johnson, S. (2010) Primary Staphylococcus aureus urinary tract infection: the role of undetected hematogenous seeding of the urinary tract. *European Journal of Clinical Microbiology & Infectious Diseases* **29**(9): 1095-1101.

de Barbeyrac, B. (1995) Detection of Chlamydia trachomatis by ligase chain reaction compared with polymerase chain reaction and cell culture in urogenital specimens. *Genitourin Med* **71**(6): 382-386.

Baron, E. J. and Tenover, F. C. (2012) Methicillin-resistant Staphylococcus aureus diagnostics: state of the art. *Expert Opinion on Medical Diagnostics* **6**(6): 585-592.

Bartlett, J. G. (2008) Historical Perspectives on Studies of Clostridium difficile and C. difficile Infection. *Clinical Infectious Diseases* **46**(Supplement 1): S4-S11.

Berry, S. M., Alarid, E. T and Beebe, D, J. (2011) One-step purification of nucleic acid for gene expression analysis via Immiscible Filtration Assisted by Surface Tension (IFAST). *Lab on a Chip* **11**(10): 1747-1753.

Beyor, N., L. Yi, L., Seo, T. S. and Mathies, R. A. (2009) Integrated Capture, Concentration, Polymerase Chain Reaction, and Capillary Electrophoretic Analysis of Pathogens on a Chip. *Analytical Chemistry* **81**(9): 3523-3528.

Bienvenue, J., Duncalf, N., Marchiarullo, D., Ferrance, J. P., Landers, J. P. (2006). Microchip-Based Cell Lysis and DNA Extraction from Sperm Cells for Application to Forensic Analysis. *Journal of forensic sciences* **51**(2): 266-273.

Bings, N. H., Wang, C., Skinner, C. D. Colyer, C. L. Thibault, P. and Harrison, D. J. (1999) Microfluidic Devices Connected to Fused-Silica Capillaries with Minimal Dead Volume. *Analytical Chemistry* **71**(15): 3292-3296.

Blackmore, T. (2000) When is a UTI really an STI?. *Royal New Zealand College of general practitioners* **27**(5).

Böhm, S., Olthuis, W. and Bergveld, P. (1999) An integrated micromachined electrochemical pump and dosing system. *Biomed. Microdevices* **1**(2): 121-130.

Boom, R., Sol, C. J., Salimans, M. M., Jansen, C. L., Wertheim-van Dillen, P. M. and van der Noordaa, J. (1990). Rapid and simple method for purification of nucleic acids. *Journal of Clinical Microbiology* **28**(3): 495-503.

Broekema, N. M., Van, T. T. and Warshauer, D. M, (2009) Comparison of Cefoxitin and Oxacillin Disk Diffusion Methods for Detection of *mecA*-Mediated Resistance in *Staphylococcus aureus* in a Large-Scale Study. *j. clin. microbiol*, **47**(1) 217-219

Brooks, T. and Keevil, C. W. (1997) A simple artificial urine for the growth of urinary pathogens. *Letters in Applied Microbiology* **24**(3): 203-206.

Bruus, H. (2008) Theoretical Microfluidics.

Bu, Y., Huang, H. and Zhou, G. (2008) Direct polymerase chain reaction (PCR) from human whole blood and filter-paper-dried blood by using a PCR buffer with a higher pH. *Analytical Biochemistry* **375**(2): 370-372.

Burns, M. A., Johnson, B. N., Brahmasandra, S. N., Handique, K. Webster, J. R. Krishnan, M., Sammarco, T. S., Man, P. M., Jones, D., Heldsinger, D., Mastrangelo, C. H. and Burke, D. T. (1998) An Integrated Nanoliter DNA Analysis Device. *Science* **282**(5388): 484-487.

Camilleri, P. (1997) Capillary Electrophoresis: Theory and Practice, Sond Edition

Cao, W., Easley, C. J., Ferrance, J. P., Landers, J. P. (2006) Chitosan as a polymer for pH-induced DNA capture in a totally aqueous system. *Analytical Chemistry* **78**(20): 7222-7228.

Cardoso, C. L. (1998) Simplified Technique for Detection of Significant Bacteriuria by Microscopic Examination of Urine. *J. Clin. Microbiol* **36**(3): 820-823.

Cepheid®. (2014) Cepheid.com, Accessed January 2014.

CGDP. (2005). Accessed January 2014.

Chang, Y. H., Lee, G. B., Huang, F., Chen, Y.Y. and Lin, J. L. (2006) Integrated polymerase chain reaction chips utilizing digital microfluidics. *Biomedical Microdevices* **8**(3): 215-225.

Chatterjee, O. M. (2013) Improved understanding of factors driving methicillin-resistant Staphylococcus aureus epidemic waves. *Clinial epidemiology* **5**(1): 205-217.

Chen, D., Mauk, M., Qiu, X., Liu, C., Kim, J., Ramprasad, S., Ongagna, S., Abrams, W., Malamud, D., Corstjens, P. A. M. and Bau, H
(2010) An integrated, self-contained microfluidic cassette for isolation, amplification, and detection of nucleic acids. *Biomedical Microdevices* **12**(4): 705-719.

Chen, H., Acharya, D., Gajraj, A. and Meiners, J. (2003) Robust Interconnects and Packaging for Microfluidic Elastomeric Chips. *Analytical Chemistry* **75**(19): 5287-5291.

Chen, X., D. Cui, Liu, C. and Cai, H. (2006) Microfluidic Biochip for Blood Cell Lysis. *Chinese Journal of Analytical Chemistry* **34**(11): 1656-1660.

Cheng, S. B., C. D. Skinner, Taylor, J., Attiya, S., Lee, W. E., Picelli, G. and Harrison, D. J. (2001) Development of a Multichannel Microfluidic Analysis System Employing Affinity Capillary Electrophoresis for Immunoassay. *Analytical Chemistry* **73**(7): 1472-1479.

Chernesky, M. A. (2005) The laboratory diagnosis of Chlamydia trachomatis infections. *J. Infect. Dis. Med. Microbiol.* **16**(1): 39-44.

Chin, C. D., Linder. V. and Sia, S. K. (2012) Commercialization of microfluidic point-of-care diagnostic devices. *Lab on a Chip* **12**(12): 2118-2134.

Chunsun, Z., Jinliang, X, Wang, J. and Wang, H. (2006) Continuous-flow polymerase chain reaction microfluidics based on polytetrafluoethylene capillary. *Chinese Journal of Analytical Chemistry* **34**(8): 1197-1203.

Claveau , S., Sasseville, M. and Beauregard, M.S. (2004) Alcohol-mediated error-prone PCR. *DNA Cell Biol* **23**(11): 789-795.

Cooney, C., Sipes, D., Thakore, N., Holmberg, R. and Belgrader, P. (2012) A plastic, disposable microfluidic flow cell for coupled on-chip PCR and microarray detection of infectious agents. *Biomed microdevices* **14**(1): 45-53.

Christensen, D., Johnson, P. S. W. P, McCreedy, T. and Skelton, V.G. and Wilson, N. (1998) The fabrication of micro-porous silica structures for micro-reactor technology. *Analytical Communications* **35**(10): 341-343.

Dames, S., L. K. Bromley, Herrmann, M., Elgort, M., Erali, M., Smith, R. and Voelkerding, K. V. (2006) A Single-Tube Nucleic Acid Extraction, Amplification, and Detection Method Using Aluminum Oxide. *The Journal of Molecular Diagnostics* **8**(1): 16-21.

Delmée, M., J. Van Broeck, Simon, A., Janssens, M. and Avesani, V. (2005) Laboratory diagnosis of Clostridium difficile-associated diarrhoea: a plea for culture. *Journal of Medical Microbiology* **54**(2): 187-191.

Dineva, M. A., L. Mahilum-Tapay, L.and Lourdes
Lee, H. (2007) Sample preparation: a challenge in the development of point-of-care nucleic acidbased assays for resource-limited settings. *Analyst* **132**(12): 1193-1199.

Dragan, A. I., J. R. Casas-Finet, Bishop, E. S., Strouse, R. J., Schenerman, M. A. and Geddes, C. D. (2010) Characterization of PicoGreen Interaction with dsDNA and the Origin of Its Fluorescence Enhancement upon Binding. *Biophysical journal* **99**(9): 3010-3019.

Dutta, P. K., Dutta. J. and Tripathi, V. S. (2004) Chitin and chitosan: Chemistry, properties and applications. *Journal of Scientific & Industrial Research* **63**(1): 20-31.

Easley, C. J., Karlinsey, J. M. Bienvenue, J. M., Legendre, L. A., Roper, M. G. Feldman, S. H., Hughes, M. A., Hewlett, E. L. Merkel, T. J., Ferrance, J. P. and Landers, J. P. (2006) A fully integrated microfluidic genetic analysis system with sample-in–answer-out capability. *Proceedings of the National Academy of Sciences* **103**(51): 19272-19277.

Easley, C. J., Karlinsey, J. M. and Landers. J. P. (2006) On-chip pressure injection for integration of infrared-mediated DNA amplification with electrophoretic separation. *Lab on a Chip* **6**(5): 601-610.

Espy, M. J., Uhl, J. R., Sloan, L. M., Buckwalter, S. P., Jones, M. F., Vetter, E. A., Yao, J. D. C., Wengenack, N. L., Rosenblatt, J. E., Cockerill, F. R. and Smith, T. F. (2006) Real-Time PCR in Clinical Microbiology: Applications for Routine Laboratory Testing. *Clinical Microbiology Reviews* **19**(1): 165-256.

Fletcher, P. D. I., Haswell, S. J., He, P., Kelly, S. M. and Mansfield, A. (2011) Permeability of silica monoliths containing micro- and nano-pores. *Journal of Porous Materials* **18**(4): 501-508.

Fonkwo. P. N. (2008) Pricing infectious disease. *EMBO reports* **9**(1): 46-74.

Ford, M. (2010) Medical microbiology.

Frutos, R., Pages, M., Bellis, M., Roizes, G. and Bergoin, M. (1989) Pulsed-field gel electrophoresis determination of the genome size of obligate intracellular bacteria belonging to the genera Chlamydia, Rickettsiella, and Porochlamydia. *Journal of bacteriology* **171**(8): 4511-4513.

Fu, L.-M. and Lin, C.-H. (2004) High-resolution DNA separation in microcapillary electrophoresis chips utilizing double-L injection techniques. *Electrophoresis* **25**(21-22): 3652-3659.

Gaertner, C., Becker, H., Anton, B., O'Neill, A. P. and Roetting, O. (2003) Polymer based microfluidic devices: examples for fluidic interfaces and standardization concepts. *Microfluidics, BioMEMS, and Medical Microsystems.*

Garland, S., Baker. A. Phillott, A. D.and Skerratt, L. F. (2010). BSA reduces inhibition in a TaqMan assay for the detection of Batrachochytrium dendrobatidis. *Diseases of Aquatic Organisms* **92**(2-3): 113-116.

Geary, C. and Steven, M (1986) Rapid lysostaphin test to differentiate Staphylococcus and Micrococcus species. *J Clin Microbiol* **23**(6): 1044–1045.

Generelli, S., Jacquemart, R., de Rooij, N. F. Jolicoeur, M., Koudelka-Hep, M and Guenat, O. T. (2008) Potentiometric platform for the quantification of cellular potassium efflux. *Lab on a Chip* **8**(7): 1210-1215.

Glynn, J. R., Belongia, B. M., Arnold, R. G., Ogden, K. L. and Baygents, J. C. et al. (1998). Capillary Electrophoresis Measurements of Electrophoretic Mobility for Colloidal Particles of Biological Interest. *Applied and Environmental Microbiology* **64**(7): 2572-2577.

Gous, N., B. Cunningham, et al. (2013). "Performance Monitoring of Mycobacterium tuberculosis Dried Culture Spots for Use with the GeneXpert System within a National Program in South Africa." Journal of Clinical Microbiology **51**(12): 4018-4021.

Green, M. R. (2012). Molecular cloning, 4th Edition.

Greer, L. and Wendel Jr, G. D. (2008) Rapid Diagnostic Methods in Sexually Transmitted Infections. *Infectious Disease Clinics of North America* **22**(4): 601-617.

Haab, B. B. and Mathies, R. A. (1999) Single-Molecule Detection of DNA Separations in Microfabricated Capillary Electrophoresis Chips Employing Focused Molecular Streams. *Analytical Chemistry* **71**(22): 5137-5145.

Hagan, K. A., Reedy, C. R., Uchimoto, M. L. Basu, D., Engel, D. A. and Landers, J. P. (2011). An integrated, valveless system for microfluidic purification and reverse

transcription-PCR amplification of RNA for detection of infectious agents. *Lab on a Chip* **11**(5): 957-961.

Hali, B., Russ, P. K., Wright, D. W. and Haselton, F. R. (2013) A Magnetic Bead-Based Method for Concentrating DNA from Human Urine for Downstream Detection. *PLoS ONE* **8**(7)

Hansen, N. (1996) Application of bismuth-telluride thermoelectrics in driving DNA amplification and sequencing reactions. *Thermoelectrics* 256-258.

Hashimoto, M., Chen, P. -C., Mitchell, M. W., Nikitopoulos, D. E., Soper, S. A. Murphy, M. C. (2004) Rapid PCR in a continuous flow device. *Lab on a Chip* **4**(6): 638-645.

Hataoka, Y., Zhang, L Mori, Y., Tomita, N., Notomi, T. and Baba, Y. (2004) Analysis of Specific Gene by Integration of Isothermal Amplification and Electrophoresis on Poly(methyl methacrylate). *Microchips. Analytical Chemistry* **76**(13): 3689-3693.

Hawkley, L. (2005). Medical Bacteriology.

Hinojosa Flores, N. I., Flores Ramirez, N., Espino Valencia, J.,
Vasquez Garcia, S. R. Luna-Barcenas, G. and Garcia-Gonzalez, L. (2009) Adsorption of Chitosan into SiO(2) Monoliths Materials: Physical and Chemical Properties. *Macromolecular Symposia* **283-84**: 191-198.

House, D. L., Chon, C. H., Creech, C. B., Skaar, E. P. and Li, D. (2010). Miniature on-chip detection of unpurified methicillin-resistant Staphylococcus aureus (MRSA) DNA using real-time PCR. *Journal of Biotechnology* **146**(3): 93-99.

Huang, F.-C., Liao, C. -S and Lee, G. (2006). An integrated microfluidic chip for DNA/RNA amplification, electrophoresis separation and on-line optical detection. *Electrophoresis* **27**(16): 3297-3305.

Huber, M., Losert, D., Hiller, R., Harwanegg, C,. Mueller, M. W. and Schmidt, W. M. (2001) Detection of Single Base Alterations in Genomic DNA by Solid Phase Polymerase Chain Reaction on Oligonucleotide Microarrays. *Analytical Biochemistry* ***299****(1): 24-30.*

Hung, E.C., Shing, T.K., Chim, S.S., Yeung, P.C., Chan, R. W., Chik, K. W., Lee V., Tsui, N.B., Li, C.K., Wong, C.S., Chiu, R.W. and Lo, Y. M. (2009) Presence of Donor-Derived DNA and Cells in the Urine of Sex-Mismatched Hematopoietic
Stem Cell Transplant Recipients: Implication for the Transrenal Hypothesis. *Clin chem* **55**(4): 715-722.

Joy, D., Feng, A. X., Mu, J., Furuya, T., Chotivanich, K., Krettli, A., U. Ho, M., Wang, A., White, N. J., Suh, E., Beerli, P and Su, X. (2003) Early Origin and Recent Expansion of Plasmodium falciparum. *Science* **300**(5617): 318-321.

Kashkary, L., Kemp, C., Shaw, K. J. Greenway, G. M. and Haswell, S. J. (2012). Improved DNA extraction efficiency from low level cell numbers using a silica monolith based micro fluidic device. *Analytica Chimica Acta* **750**(0): 127-131.

Kastrup, C. J., M. K. Runyon, Lucchetta, E. M., Price, J. M. and Ismagilov, R. F. (2008) Using Chemistry and Microfluidics To Understand the Spatial Dynamics of Complex Biological Networks. *Accounts of Chemical Research* **41**(4): 549-558.

Kemp, C., Birch, C., Shaw, K. J., Nixon, G. J., Docker, P. T., Greenman, J., Huggett, J. F. Haswell, S. J. Foy, C. A. and Dyer, C. E. (2012) Direct processing of clinically relevant large volume samples for the detection of sexually transmitted infectious agents from urine on a microfluidic device. *Analytical Methods* **4**(7): 2141-2144.

Kerker.M. (1976) Colloid and Interface Science V3: Adsorption, Catalysis, Solid, Volume 3.

Khandurina, J., Jacobson, S. C., Waters, L. C. Foote, R. S. and Ramsey, J. M. (1999) Microfabricated Porous Membrane Structure for Sample Concentration and Electrophoretic Analysis. *Analytical Chemistry* **71**(9): 1815-1819.

Khandurina, J., McKnight, T. E., Jacobson, S. C., Waters, L. C., Foote, R. S., Ramsey, J. M. (2000) Integrated System for Rapid PCR-Based DNA Analysis in Microfluidic Devices. *Analytical Chemistry* **72**(13): 2995-3000.

Kim, J., Hee Jang, S., Jia, G., Zoval, J. V., Da Silva, N. A. and Madou, M. J. (2004). Cell lysis on a microfluidic CD (compact disc). *Lab on a Chip* **4**(5): 516-522.

Kohsaka, H. and Carson, D. A. (1994). Solid-Phase polymerase chain reaction. *Journal of Clinical Laboratory Analysis* **8**(6): 452-455.

Kulinski, M. D., Mahalanabis, M., Gillers, S., Zhang, J. Y., Singh, S. and Klapperich, C. M. (2009) Sample preparation module for bacterial lysis and isolation of DNA from human urine. *Biomedical Microdevices* **11**(3): 671-678.

Kuschel, M., Buhlmann, C., Preckel, T. (2005) High-Throughput Protein and DNA Analysis Based on Microfluidic On-Chip Electrophoresis. *Journal of the Association for Laboratory Automation* **10**(5): 319-326.

Küster, S. K., Fagerer, S. R., Verboket, P. E., Eyer, K., Jefimovs, K. Zenobi, R. and Dittrich, P. S. (2013). Interfacing Droplet Microfluidics with Matrix-Assisted Laser Desorption/Ionization Mass Spectrometry: Label-Free Content Analysis of Single Droplets. *Analytical Chemistry* **85**(3): 1285-1289.

Lagally, E. T. Emrich, C. A. and Mathies, R. A. (2001). Fully integrated PCR-capillary electrophoresis microsystem for DNA analysis. *Lab on a Chip* **1**(2): 102-107.

Lagally, E. T., Simpson, P. C and Mathies, R. A. (2000). Monolithic integrated microfluidic DNA amplification and capillary electrophoresis analysis system. *Sensors and Actuators B: Chemical* **63**(3): 138-146.

Lai-King N. and Martin. I. E. (2005) The laboratory diagnosis of Neisseria gonorrhoeae. *J Infect Dis Med Microbiol* **16**(1): 15-25.

Lang, S. J. and Morrow. B. A. (1994) Infrared spectra of chlorinated silica. *The Journal of Physical Chemistry* **98**(50): 13314-13318.

Lee, T. M.-H., Carles, M. C. and Hsing, I. M. (2003). Microfabricated PCR-electrochemical device for simultaneous DNA amplification and detection. *Lab on a Chip* **3**(2): 100-105.

Leggate, J., Allain, R., Isaac, L. and Blais, B. W. (2006). Microplate fluorescence assay for the quantification of double stranded DNA using SYBR Green I dye *Biotechnol lett* **28**: 1587-1594.

Lemee, L., Dhalluin, A., Testelin, S., Mattrat, M., Maillard, K., Lemeland, J., Pons, J. (2004). Multiplex PCR Targeting tpi (Triose Phosphate Isomerase), tcdA (Toxin A), and tcdB (Toxin B) Genes for Toxigenic Culture of Clostridium difficile. *Journal of Clinical Microbiology* **42**(12): 5710-5714.

Lewis, M. (1998). Thorns on the rose.

Lim, D. and Strynadka, N (2002). Structural basis for the bold beta lactam resistance of PBP2a from methicillin-resistant Staphylococcus aureus. *Nat struct biol* **9**(11): 870-876.

Liu, K., N.-G. Zhang, Wang, S. and Deng, Y. and (2014) An automatic microfluidic sample transfer and introduction system. *Microfluidics and Nanofluidics* **16**(1-2): 101-108.

Liu, Y.-H.,Wang C. -H., Wu, J and Lee, G. (2012) Rapid detection of live methicillin-resistant Staphylococcus aureus by using an integrated microfluidic system capable of ethidium monoazide pre-treatment and molecular diagnosis. *Biomicrofluidics* **6**(3)

Lu, H., Schmidt, M. A. and Jensen, K. F. (2005). A microfluidic electroporation device for cell lysis. *Lab on a Chip* **5**(1): 23-29.

Mahjoob, S., Vafai K., Beer, N. R. (2008). Rapid microfluidic thermal cycler for polymerase chain reaction nucleic acid amplification. *International Journal of Heat and Mass Transfer* **51**(9–10): 2109-2122.

Mahmoudian, L., Kaji, N., Tokeshi, M., Nilsson, M. and Baba, Y. (2008) Rolling Circle Amplification and Circle-to-circle Amplification of a Specific Gene Integrated with Electrophoretic Analysis on a Single Chip. *Analytical Chemistry* **80**(7): 2483-2490.

Manage, D., Y. Morrissey, Stickel, A. J., Lauzon, J., Atrazhev, A., Acker, J. P. and Pilarski, L. M. (2011). On-chip PCR amplification of genomic and viral templates in unprocessed whole blood. *Microfluidics and Nanofluidics* **10**(3): 697-702.

Mania-Pramanik, J. (2012). Current Chlamydia trachomatis Infection, A Major Cause of Infertility. *j reprod infertil* **13**(4): 204-210.

Mariella, R., Jr. (2008). Sample preparation: the weak link in microfluidics-based biodetection. *Biomedical Microdevices* **10**(6): 777-784.

Martin, P. M. V and Martin-Granel, E (2006). 2,500-year Evolution of the Term Epidemic. *Emerging infectious diseases* **12**.

Martineau, F., F. J. Picard, Lansac, N. Ménard, C., Roy, P. H., Ouellette, M. and Bergeron, M. G. (2000). Correlation between the Resistance Genotype Determined by Multiplex PCR Assays and the Antibiotic Susceptibility Patterns of Staphylococcus aureus and Staphylococcus epidermidis. *Antimicrobial Agents and Chemotherapy* **44**(2): 231-238.

Martiny, D., Debaugnies, F., Gateff, D., Gérard, M., Aoun, M., Martin, C. Konopnicki, D., Loizidou, A., Georgala, A., Hainaut, M., Chantrenne, M., Dediste, A. Vandenberg, O. and Van Praet, S. (2013). Impact of rapid microbial identification directly from positive blood cultures using matrix-assisted laser desorption/ionization time-of-flight mass spectrometry on patient management. *Clinical Microbiology and Infection* **19**(12): E568-E581.

Matthews, K. R. R., Gillespie, B. E., Luther, D. A. and Oliver, S. P. (1997) Identification and differentiation of coagulase-negative Staphylococcus aureus by polymerase chain reaction. *Journal of food protection* **6**(3): 686-688.

McCreedy, T. (2000). Fabrication techniques and materials commonly used for the production of microreactors and micro total analytical systems. *TrAC Trends in Analytical Chemistry* **19**(6): 396-401.

McNeill, J. R. (2004) Yellow Jack and Geopolitics: Environment, Epidemics, and the Struggles for Empire in the American Tropics, 1650–1825. *OAH Magazine of History* **18**(3): 9-13.

Mediavilla, J. R., Chen, L., Mathema, B. and Kreiswirth, B. N. (2012) Global epidemiology of community-associated methicillin resistant Staphylococcus aureus (CA-MRSA). *Current Opinion in Microbiology* **15**(5): 588-595.

Melzak, K. A., Sherwood, C. S., Turner, R. F. B. and Haynes, C. A. (1996). Driving Forces for DNA Adsorption to Silica in Perchlorate Solutions. *Journal of Colloid and Interface Science* **181**(2): 635-644.

Mens, P. F., de Bes, H. M., Sondo, P., Laochan, N., Keereecharoen, L., van Amerongen, A,. Flint, J., Sak, J. R. S., Proux, S., Tinto, H., and Schallig, H. D. F. H. (2012) Direct Blood PCR in Combination with Nucleic Acid Lateral Flow

Immunoassay for Detection of Plasmodium Species in Settings Where Malaria Is Endemic. *Journal of Clinical Microbiology* **50**(11): 3520-3525.

Mens, P. F., van Amerongen, A., Sawa, P., Kager, P. A., Schallig, H. D. F. H. (2008) Molecular diagnosis of malaria in the field: development of a novel 1-step nucleic acid lateral flow immunoassay for the detection of all 4 human Plasmodium spp. and its evaluation in Mbita, Kenya. *Diagnostic microbiology and infectious disease* **61**(4): 421-427.

Merck (2013) Merck.com, Accessed January 2014.

Microtech (2014) Microtech.com, Accessed January 2014.

Misawa, Y., Yoshida, A., Saito, R., Yoshida, H., Okuzumi, K., Ito, N., Okada, M., Moriya, K and Koike, K. (2007) Application of loop-mediated isothermal amplification technique to rapid and direct detection of methicillin-resistant Staphylococcus aureus (MRSA) in blood cultures. *Journal of Infection and Chemotherapy* **13**(3): 134-140.

Moellering, R. C. (1995). Past, present, and future of antimicrobial agents. *The American journal of medicine* **99**(6): 11s-18s.

Muder, R. R., Brennen, C., Rihs, J. D., Wagener, M. M., Obman, A., Stout, J. E. and Yu, V. L. (2006) Isolation of Staphylococcus aureus from the Urinary Tract: Association of Isolation with Symptomatic Urinary Tract Infection and Subsequent Staphylococcal Bacteremia. *Clinical Infectious Diseases* **42**(1): 46-50.

Murrey, P., Rosenthal, K and Pfaller, M. (2013), Medical Microbiology.

Nakagawa, T., Tanaka, T., Niwa, D., Osaka, T., Takeyama, H. and Matsunaga, T. (2005). Fabrication of amino silane-coated microchip for DNA extraction from whole blood. *Journal of Biotechnology* **116**(2): 105-111.

Nakanishi, K. (1997). Pore Structure Control of Silica Gels Based on Phase Separation. *Journal of Porous Materials* **4**(2): 67-112.

Nawrocki, J. (1997) The silanol group and its role in liquid chromatography. *Journal of Chromatography* A **779**(1–2): 29-71.

Nerlich, A. G., Haas, C. J., Zink, A., Szeimies, U. and Hagedorn, H. G. (1997) Molecular evidence for tuberculosis in an ancient Egyptian mummy. *The Lancet* **350**(9088): 1404.

Nge, P. N., Rogers, C. I. and Woolley, A. T. (2013). Advances in Microfluidic Materials, Functions, Integration, and Applications. *Chemical Reviews* **113**(4): 2550-2583.

Niemz, A., Ferguson, T. M. and Boyle, D. S. (2011) Point-of-care nucleic acid testing for infectious diseases. *Trends in Biotechnology* **29**(5): 240-250.

Northrup, M. A., Benett, B., Hadley, D., Landre, P., Lehew, S., Richards, J. and Stratton, Paul. (1998) A Miniature Analytical Instrument for Nucleic Acids Based on Micromachined Silicon Reaction Chambers. *Analytical Chemistry* **70**(5): 918-922.

Oakley, J. A., Robinson, S., Dyer, C. E., Greenman, J., Greenway, G. M. and Haswell, S. J. (2009) Development of a gel-to-gel electro-kinetic pinched injection method for an integrated micro-fluidic based DNA analyser. *Analytica Chimica Acta* **652**(1–2): 239-244.

Oblath, E. A., Henley, W. H., Alarie, J. P. and Ramsey, J. M. (2013) A microfluidic chip integrating DNA extraction and real-time PCR for the detection of bacteria in saliva. *Lab on a Chip* **13**(7): 1325-1332.

Okada, J. (2005). Diagnostic tests: Clostridium difficile. Nippon rinsho. *Japanese journal of clinical medicine* **63 Suppl 7**: 210-213.

Ong, S., Zhang, S., Du, H. and Fu, Y. (2008) Fundamental principles and applications of microfluidic systems. *front biosci*: 2757-2773.

Orrling, K., Nilsson, P., Gullberg, M. and Larhed, M. (2004) An efficient method to perform milliliter-scale PCR utilizing highly controlled microwave thermocycling. *Chemical Communications*(7): 790-791.

Owusu-Edusei, K. J., Chesson, H. W., Gift, T. L., Tao, G., Mahajan, R., Ocfemia, M. C. and Kent, C. K. (2013) The estimated direct medical cost of selected sexually transmitted infections in the United States. *Sex Transm Dis* **40**(3): 197-201.

Papagrigorakis, M. J., Yapijakis, C., Synodinos, P. N. and Baziotopoulou-Valavani, E. (2006) DNA examination of ancient dental pulp incriminates typhoid fever as a probable cause of the Plague of Athens. *International Journal of Infectious Diseases* **10**(3): 206-214.

Parton, J., Birch, C., Kemp, C., Haswell, S. J., Pamme, N. and Shaw, K. J. (2012) Integrated DNA extraction and amplification using electrokinetic pumping in a microfluidic device. *Analytical Methods* **4**(1).

Peeling, R. W., Herring, A. and Hook. E. W. (2006). Why do we need quality-assured diagnostic tests for sexually transmitted infections?

Peeling, R. W. and A. Ronald (2009). Diagnostic challenges of sexually transmitted infections in resource-limited settings. *Future Microbiology* **4**(10): 1271-1282.

Poisson, S. D. (1837). Treatise (Ecole Polytechnique, Paris).

Posthuma-Trumpie, G., Korf, J. and Amerongen, A. (2009) Lateral flow (immuno)assay: its strengths, weaknesses, opportunities and threats. A literature survey. *Analytical and Bioanalytical Chemistry* **393**(2): 569-582.

Prakash, A. R., Amrein, M. and Kaler, K. V. I. S. (2008). Characteristics and impact of Taq enzyme adsorption on surfaces in microfluidic devices. *Microfluidics and Nanofluidics* **4**(4): 295-305.

Price, C. W., Leslie, D. C. and landers, J. P. (2009). Nucleic acid extraction techniques and application to the microchip. *Lab on a Chip* **9**(17): 2484-2494.

Pulcrano, G., Iula, D. V., Vollaro, A., Tucci, A., Cerullo, M., Esposito, M., Rossano, F. and Catania, M. R. (2013) Rapid and reliable MALDI-TOF mass spectrometry identification of Candida non-albicans isolates from bloodstream infections. *Journal of Microbiological Methods* **94**(3): 262-266.

Qiagen (2003) Qiagen, QIAamp® DNA Micro Handbook.

Qiu, X., Mauk, M. G., Chen, D., Liu, C. and Bau, H. H. (2010) A large volume, portable, real-time PCR reactor. *Lab on a Chip* **10**(22): 3170-3177.

Qu, Q. S., He,Y. Z., Gan, W. E., Deng, N. and Lin, X. Q. (2003) Electrochromatography with a 2.7 mm inner diameter monolithic column. *Journal of Chromatography* A **983**(1-2): 255-262.

Quinto-Su, P. A., Lai, H. -H., Yoon, H. H. Sims, C. E. Allbritton, N. L. and Venugopalan, V. (2008) Examination of laser microbeam cell lysis in a PDMS microfluidic channel using time-resolved imaging. *Lab on a Chip* **8**(3): 408-414.

Rasmussen, R. V., Fowler Jr, V. G., Skov, R. and Bruun, N. E. (2010) Future challenges and treatment of Staphylococcus aureus bacteremia with emphasis on MRSA. *Future Microbiology* **6**(1): 43-56.

Raygada, J. L. and Levine. D. P. (2009). Methicillin-resistant Staphylococcus aureus: A growing risk in the hospital and in the community. *American Health and Drug Benefits* **2**(2): 86-95.

Reedy, C. R., Bienvenue, J. M., Coletta, L. Strachan, B. C., Bhatri, N., Greenspoon, S. and Landers, J. P. (2010). Volume reduction solid phase extraction of DNA from dilute, large-volume biological samples. *Forensic Science International: Genetics* **4**(3): 206-212.

Reedy, C. R., Hagan, K. A., Strachan, B. C. Higginson, J. J. Bienvenue, J. M. Greenspoon, S. A. Ferrance, J. P. and Landers, J. P. (2010) Dual-Domain Microchip-Based Process for Volume Reduction Solid Phase Extraction of Nucleic Acids from Dilute, Large Volume Biological Samples. *Analytical Chemistry* **82**(13): 5669-5678.

Reedy, C. R., Price, C. W., Sniegowski, J. Ferrance, J. P., Begley, M. and Landers, J. P. (2011) Solid phase extraction of DNA from biological samples in a post-based, high surface area poly(methyl methacrylate) (PMMA) microdevice. *Lab on a Chip - Miniaturisation for Chemistry and Biology* **11**(9): 1603-1611.

Reid, M., Lachs, M. S. and Feinstein, A. R. (1995) Use of methodological standards in diagnostic test research: Getting better but still not good. *JAMA* **274**(8): 645-651.

Ren, K., Zhou, J and Wu H. (2012) Materials for Microfluidic Chip Fabrication. *Acc. chem. res* **46**(11): 2396-2406.

Rhie, W. and Higuchi, T (2010) Design and fabrication of a screw-driven multi-channel peristaltic pump for portable microfluidic devices. *J. Micromech. Microeng*. **20**(8).

Ripa, K. T. and Mårdh. P. A. (1977) Cultivation of Chlamydia trachomatis in cycloheximide-treated mccoy cells. *Journal of Clinical Microbiology* **6**(4): 328-331.

Ro, K. W., Liu, J. and Knapp, D. R. (2006). Plastic microchip liquid chromatography-matrix-assisted laser desorption/ionization mass spectrometry using monolithic columns. *Journal of Chromatography* A **1111**(1): 40-47.

Rohindra, D. R., Nand, A. V. and Khurma, J. R. (2004). Swelling properties of chitosan hydrogels. The South Pacific Journal of Natural and Applied Sciences **22**(1): 32-35.

Sack, D. A., Sack, R. B., Nair, G. B. and Siddique, A. K. (2004). Cholera. *The Lancet* **363**(9404): 223-233.

Sambrook, J. and Russell, D. (2001). Molecular cloning

Sawyer, W. H. and J. Puckridge (1973). The Dissociation of Proteins by Chaotropic Salts. *Journal of Biological Chemistry* **248**(24): 8429-8433.

Schaerli, Y., R. C. Wootton, Robinson, T., Stein, V., Dunsby, C., Neil, M. A. A., French, P, M. W. deMello, A. J. Abell, C. and Hollfelder, F. (2008) Continuous-Flow Polymerase Chain Reaction of Single-Copy DNA in Microfluidic Microdroplets. *Analytical Chemistry* **81**(1): 302-306.

Schlecht, C. A. and Maurer, J. A. (2011). Functionalization of glass substrates: mechanistic insights into the surface reaction of trialkoxysilanes. *RSC Advances* **1**(8): 1446-1448.

Seong, G. H., Heo, J Crooks, R. M. (2003). Measurement of Enzyme Kinetics Using a Continuous-Flow Microfluidic System. *Analytical Chemistry* **75**(13): 3161-3167.

Shaw, K. J. (2009). Integration of DNA purification and amplification on a microfluidic device.

Shaw, K. J., Docker, P. T., Yelland, J. V., Dyer, C. E., Greenman, J., Greenway, G. M. and Haswell, S. J. (2010) Rapid PCR amplification using a microfluidic device with integrated microwave heating and air impingement cooling. *Lab on a Chip* **10**(13): 1725-1728.

Shaw, K. J., Joyce, D, A., Docker, P. T., Dyer, C. E., Greenman, J. Greenway, G. M. and Haswell, Stephen J. (2009) Simple practical approach for sample loading prior to DNA extraction using a silica monolith in a microfluidic device. *Lab on a Chip* **9**(23): 3430-3432.

Shaw, K. J., Joyce, D. A., Docker, P. T., Dyer, C. E., Greenway, G. M. Greenman, J. and Haswell, S. J. (2011) Development of a real-world direct interface for integrated DNA extraction and amplification in a microfluidic device. *Lab on a Chip* **11**(3): 443-448.

Shaw, K. J., Thain, L., Docker, P. T. Dyer, C. E. Greenman, J. Greenway, G. M. and Haswell, S. J. (2009) The use of carrier RNA to enhance DNA extraction from microfluidic-based silica monoliths. *Anal Chim Acta* **652**(1-2): 231-233.

Shin, K. S., Song, H. G., Kim, H., Yoon, S., Hong, S. B., Koo, S. H., Kim, J., Kim, J., Roh, K. H. (2010) Direct detection of methicillin-resistant Staphylococcus aureus from blood cultures using an immunochromatographic immunoassay-based MRSA rapid kit for the detection of penicillin-binding protein 2a. *Diagnostic microbiology and infectious disease* **67**(3): 301-303.

Siegrist, J., Peytavi, R. and Madou. , M. (2009). Microfluidics for biological analysis: Triumphs and hurdles of CD platforms. *Current trends in science.*

Sing, K. S. W., Everett, D. H., Haul, R. A. W., Moscou, L., Pierotti, R. A., Rouquerol, J., Siemieniewska, T., (2008) Reporting Physisorption Data for Gas/Solid Systems. Handbook of Heterogeneous Catalysis, *Wiley-VCH Verlag GmbH & Co. KGaA.*

Singer, V. L., Jones, L. J., Yue, S. T. and Haugland, R. P. (1997) Characterization of PicoGreen Reagent and Development of a Fluorescence-Based Solution Assay for Double-Stranded DNA Quantitation. *Analytical Biochemistry* **249**(2): 228-238.

Skafte-Pedersen, P., Sabourin, D., Dufva, M. and Snakenborg, D. (2009) Multi-channel peristaltic pump for microfluidic applications featuring monolithic PDMS inlay. *Lab on a Chip* **9**(20): 3003-3006.

Snyder, K. (1997). "Peak tailing and resolution." *Chromatography online.*

Spanu, T., Posteraro, B., Fiori, B., D'Inzeo, T., Campoli, S., Ruggeri, A., Tumbarello, M., Canu, G., Trecarichi, E. M., Parisi, G., Tronci, M., Sanguinetti, M. and Fadda, G. (2012) Direct MALDI-TOF Mass Spectrometry Assay of Blood Culture Broths for Rapid Identification of Candida Species Causing Bloodstream Infections: an Observational Study in Two Large Microbiology Laboratories. *Journal of Clinical Microbiology* **50**(1): 176-179.

Stone . P. W. (2009). Economic burden of healthcare-associated infections: an American perspective. *Expert Rev Pharmacoecon Outcomes Res* **9**(5): 417-422.

Sur, K., McFall, S. M., Yeh, E. T., Jangam, S. R., Hayden, M. A., Stroupe, S. D. and

Kelso, D. M. (2010). Immiscible Phase Nucleic Acid Purification Eliminates PCR Inhibitors with a Single Pass of Paramagnetic Particles through a Hydrophobic Liquid. *The Journal of Molecular Diagnostics* **12**(5): 620-628.

Tabrizi, S. N., Unemo, M., Golparian, D., Twin, J., Limnios, A. E., Lahra, M. and Guy, R. (2013). Analytical Evaluation of GeneXpert CT/NG, the First Genetic Point-of-Care Assay for Simultaneous Detection of Neisseria gonorrhoeae and Chlamydia trachomatis. *Journal of Clinical Microbiology* **51**(6): 1945-1947.

Tewhey, R., Warner, J. B., Nakano, M., Libby, B., Medkova, M., David, P. H., Kotsopoulos, S., Samuels, M. L., Hutchison, J. B., Larson, J. W., Topol, E. J., Weiner, M. P., Harismendy, O., Olson, J., Link. D. R. and Frazer. K. A (2009). Microdroplet-based PCR enrichment for large-scale targeted sequencing. *Nature biotechnology* **27**: 1025-1031.

Tian, H., Hühmer, A. F. R and Landers, J. P. (2000) Evaluation of Silica Resins for Direct and Efficient Extraction of DNA from Complex Biological Matrices in a Miniaturized Format. *Analytical Biochemistry* **283**(2): 175-191.

Tsaloglou, M.-N., Bahi. M. M, Waugh, E. M., Morgan, H. and Mowlem, M. (2011) On-chip real-time nucleic acid sequence-based amplification for RNA detection and amplification. *Analytical Methods* **3**(9): 2127-2133.

Turkevich, J., Stevenson, P. C. and Hillier, J. (1951). A study of the nucleation and growth processes in the synthesis of colloidal gold. *Discussions of the Faraday Society* **11**: 55-75.

Valour, F., Blanc-Pattin, V., Freydière, A.-M., Bouaziz, A., Chanard, E., Lustig, S., Ferry, T., Laurent, F. (2013) Rapid detection of Staphylococcus aureus and methicillin resistance in bone and joint infection samples: evaluation of the GeneXpert MRSA/SA SSTI assay. *Diagnostic microbiology and infectious disease* **78**(3): 313-315.

Van Dyck, E., Ieven, M., Pattyn, S., Van Damme, L. and Laga, M. (2001). Detection of Chlamydia trachomatis and Neisseria gonorrhoeae by enzyme immunoassay, culture, and three nucleic acid amplification tests. *Journal of Clinical Microbiology* **39**(5): 1751-1756.

Walsh, P., Metzger, D. A and Higuchi R. (1991). Chelex 100 as a medium for simple extraction of DNA for PCR-based typing from forensic material. *Biotechniques* **54**(3): 134-139.

Warsa, U. C. (1996). Detection of tet(K) and tet(M) in Staphylococcus aureus of Asian Countries by the Polymerase Chain Reaction. *J Antibiot* **49**(11): 1127-1132.

Wathne, B., Hovelius B. and Mårdh, P. -A. (1987). Causes of Frequency and Dysuria in Women. *Scandinavian Journal of Infectious Diseases* **19**(2): 223-229.

Watson, J. (1953). Genetical Implications of the structure of Deoxyribonucleic Acid *Nature* **171**: 964-967.

Wavelengthelectronics (2013).

Wen, J., Guillo, C., Ferrance, J. P. and Landers, J. P. (2006). DNA extraction using a tetramethyl orthosilicate-grafted photopolymerized monolithic solid phase. *Analytical Chemistry* **78**(5): 1673-1681.

Whitesides, G. M. (2006). The origins and the future of microfluidics. *Nature* **442**(7101): 368-373.

Wisniewski, C. A., White, J. A., Michel, C.-E. C. Mahilurn-Tapay, L., Magbanua, J. P. V., Nadala, E. C. B., Barber, P. J. G, B. T. and Lee, H. H. (2008). Optimal method of collection of first-void urine for diagnosis of Chlamydia trachomatis infection in men. *Journal of Clinical Microbiology* **46**(4): 1466-1469.

Wolfe, K. A., Breadmore, M. C., Ferrance, J. P., Power, M. E., Conroy, J. F., Norris, P. M. and Landers, J. P. (2002). Toward a microchip-based solid-phase extraction method for isolation of nucleic acids. *Electrophoresis* **23**(5): 727-733.

Woolley, A. T., Hadley, D., Landre, P., deMello, A. J., Mathies, R. A. and Northrup, M. A. (1996) Functional Integration of PCR Amplification and Capillary Electrophoresis in a Microfabricated DNA Analysis Device. *Analytical Chemistry* **68**(23): 4081-4086.

Woolley, A. T. and R. A. Mathies. (1994) Ultra-high-speed DNA fragment separations using microfabricated capillary array electrophoresis chips. *Proceedings of the National Academy of Sciences of the United States of America* **91**(24): 11348-11352.

Wu, Q., Bienvenue, J. M., Hassan, B. J. Kwok, Y. C. Giordano, B. C. Norris, P. M., Landers, J. P. and Ferrance, J. P. (2006). Microchip-based macroporous silica sol-gel monolith for efficient isolation of DNA from clinical samples. *Analytical Chemistry* **78**(16): 5704-5710.

www.bd.com (2014). Accessed, January 2014

www.drdanglab.com (2014). Accessed, January 2014.

Xianbo, Q. and Jingqi,Y. (2005). Temperature Control for PCR Thermocyclers Based on Peltier-Effect Thermoelectric. *Engineering in Medicine and Biology Society, 2005. IEEE-EMBS 2005. 27th Annual International Conference.*

Yager, T. E., Fu, E., Helton, K., Nelson, K., Tam. M. R., and Weigl, B. H. (2006). Review Article Microfluidic diagnostic technologies for global public health. *Nature* **442**: 412-418.

Yang, Y. G., Kim, J. Y., Song, Y. -H and Kim, D. -S. (2007) A novel buffer system, AnyDirect, can improve polymerase chain reaction from whole blood without DNA isolation. *Clinica Chimica Acta* **380**(1–2): 112-117.

Yao, J. H., Elder, K. R., Guo, H. and Grant, M. (1992). Ostwald ripening in two and three dimensions. *Physical Review* B **45**(14): 8173-8176.

Younan, X. and Whitesides, G. M. (1998). Soft Lithography.

Zhang, Z., Zhang, L,. Chen, L., Chen, L. and Wan, Q. H. (2006) synthesis of Novel Porous Magnetic Silica Microspheres as Adsorbents for Isolation of Genomic DNA. *Biotechnol prog* **22**(2): 514-518.

Zhang, C., Xu, J., Ma, W. and Zheng, W. (2006) PCR microfluidic devices for DNA amplification. *Biotechnology Advances* **24**(3): 243-284.

Zhang, G., Guo, J. and Wang, X. (2009) Immunochromatographic Lateral Flow Strip Tests. Biosensors and Biodetection. *A. Rasooly and K. Herold, Humana Press.* **504:** 169-183.

Zhang, Y. and Ozdemir. P. (2009). Microfluidic DNA amplification—A review. *Analytica Chimica Acta* **638**(2): 115-125.

Zhu, Z., Jenkins, G., Zhang, W., Zhang, M., Guan, Z. and Yang, C. (2012) Single-molecule emulsion PCR in microfluidic droplets. *Analytical and Bioanalytical Chemistry* **403**(8): 2127-2143.

Ziolkowska, K., Jedrych, E., Kwapiszewski, R., Lopacinska, J., Skolimowski, M. and Chudy, M. (2010). PDMS/glass microfluidic cell culture system for cytotoxicity tests and cells passage. Sensors and Actuators B: Chemical **145**(1): 533-542.